PHYLODYNAMIC MODELLING OF FOOT-AND-MOUTH DISEASE VIRUS SEQUENCE DATA

Antonello Di Nardo

DVM, MSc, MRCVS

Submitted in fulfilment of the requirements for the Degree of Doctor of Philosophy

Institute of Biodiversity, Animal Health and Comparative Medicine

College of Medical, Veterinary and Life Sciences

University of Glasgow

5th September 2016

DECLARATION

I hereby declare that the research described within this thesis is my own work, unless otherwise stated, and certify that it has never been submitted for any other degree or professional qualification.

Antonello Di Nardo (*DVM, MSc, MRCVS*)
The Pirbright Institute
Ash Road
Pirbright, Woking
Surrey GU24 0NF

ACKNOWLEDGEMENT

Like Ulysses (or rather a Leopold Bloom), this journey starts back to a very beginning phase of the discovery of the field of epidemiology which, from that time, became my passion, my professional development and my pain. From Africa to Scotland, I have been very privileged to meet and share friendship and job collaboration with many interesting and peculiar characters, who have all contributed to my career development with their ideas, 'philosophies' and works.

I am deeply indebted to my academic promoter and supervisor, Dan, for his valuable guidance and critical analysis, motivating discussions (even with 'dozens' of beers), and inspiring supervision. He has been of invaluable help in the development of this project, of my thinking process, and of my career as a scientist. The very close collaboration with Glasgow also gave me the opportunity to work with some amazing and stimulating researchers, among all Paul and Richard. A much deserved price to the infinite patience of Don, my Pirbright supervisor, who gave me the opportunity to dive into this very challenging journey. I would also extend a special thanks to Nick who has been handing down to me the knowledge and very detailed history of FMD molecular epidemiology. I am also very lucky to have been working during the past 7 years in The Pirbright Institute, my colleagues which has contributed to make me feeling at home. I am grateful to Graham who has been behind the generation of the WGSs analysed in chapter 6. I also would like to acknowledge the fruitful discussion during the viva with my examiners, Rolf and Rowland.

I extend my gratitude to my family and friend both in Italy and London, I heartily thanks above all my mother Maria and my father Tonino that have been continuing kept faith, encourage, support and love.

ABSTRACT

The under-reporting of cases of infectious diseases is a substantial impediment to the control and management of infectious diseases in both epidemic and endemic contexts. Information about infectious disease dynamics can be recovered from sequence data using time-varying coalescent approaches, and phylodynamic models have been developed in order to reconstruct demographic changes of the numbers of infected hosts through time. In this study I have demonstrated the general concordance between empirically observed epidemiological incidence data and viral demography inferred through analysis of foot-and-mouth disease virus VP1 coding sequences belonging to the CATHAY topotype over large temporal and spatial scales. However a more precise and robust relationship between the effective population size (N_e) of a virus population and the number of infected hosts (or 'host units') (N) has proven elusive. The detailed epidemiological data from the exhaustively-sampled UK 2001 foot-and-mouth (FMD) epidemic combined with extensive amounts of whole genome sequence data from viral isolates from infected premises presents an excellent opportunity to study this relationship in more detail. Using a combination of real and simulated data from the outbreak I explored the relationship between N_e, as estimated through a Bayesian skyline analysis, and the empirical number of infected cases. I investigated the nature of this scaling defining prevalence according to different possible timings of FMD disease progression, and attempting to account for complex variability in the population structure. I demonstrated that the variability in the number of secondary cases per primary infection R_t and the population structure greatly impact on effective scaling of N_e. I further explored how the demographic signal carried by sequence data becomes imprecise and weaker when reducing the number of samples are described, including how the extent of the size and structure of the sampled dataset impact on the accuracy of a reconstructed viral demography at any level of the transmission process. Methods drawn from phylodynamic inference combine powerful epidemiological and population genetic tools which can provide valuable insights into the dynamics of viral disease. However, the strict and sensitive dependency of the majority of these models on their assumptions makes estimates very fragile when these assumptions are violated. It is therefore essential that for these

methods to be applied as reliable tools supporting control programs, more focused theoretical research is undertaken to model the epidemiological dynamics of infected populations using sequence data.

TABLE OF CONTENTS

LIST OF TABLES

LIST OF FIGURES

ABBREVIATIONS

ABC	Approximate Bayesian computation
BDM	Birth-death model
BEAST	Bayesian evolutionary analysis sampling trees
BF	Bayes factor
BIC	Bayesian information criterion
BSP	Bayesian skyline plot
BSSVS	Bayesian stochastic search variable selection
CI	Confidence interval
CID	Complexity invariant distance
CP	Contagious to infected premise
CTMC	Continuous time Markov chain
CV	Coefficient of variation
DC	Dangerous contact
DEFRA	Department for Environment, Food and Rural Affairs
DNA	Deoxyribonucleic acid
ERGM	Exponential-family random graph model
EU	European Union
FAO	Food and Agriculture Organization of the United Nations
FMD	Foot-and-mouth disease
FMDV	Foot-and-mouth disease virus
GMRF	Gaussian Markov random field
HPD	High posterior density
INLA	Integrated nested Laplace approximation
IP	Infected premise
IRES	Internal ribosome entry site
LTT	Lineage through time
NCBI	National Center for Biotechnology Information
NGS	Next generation sequencing
NMB	National movement ban
NSP	Non-structural protein

nt	Nucleotide
MAFF	Ministry of Agriculture, Fisheries and Food
MCC	Maximum clade credibility
MCMC	Markov chain Monte Carlo
MCP	Multiple change point
MRCA	Most recent common ancestor
NLFT	Number of lineages as a function of time
OIE	World Organisation for Animal Health
ORF	Open reading frame
PDF	Probability density function
PI	Percentile interval
pk	Posterior probability
PPS	Probability proportional to size
RMSD	Root-mean-square deviation
RNA	Ribonucleic acid
RT-PCR	Reverse transcription polymerase chain reaction
RTO	Regression through the origin
SAT	Southern African Territories
SEA	Southeast Asia
SEIR	Susceptible-Exposed-Infectious-Removed
SIR	Susceptible infectious recovered
SIS	Susceptible infectious susceptible
SMC	Sequential Monte Carlo
SRS	Simple random sampling
SSM	State-space model
ssRNA	Single-stranded ribonucleic acid
TMRCA	Time to most recent common ancestor
TN93	Tamura and Nei evolutionary model
UK	United Kingdom
UTR	Untranslated region
VP	Viral protein
WGS	Whole genome sequence
WRLFMD	World Reference Laboratory for Foot-and-Mouth Disease

to Giuseppina, Lucia and Mariarosa,

always there,

waiting for us…

CHAPTER 1

Foot-and-mouth disease and phylodynamics of infectious diseases

1.1 Foot-and-mouth disease

Foot-and-mouth disease (FMD) is an economically devastating viral disease of cloven-hoofed domestic and wild artiodactyls, causing an acute and highly contagious vesicular disease, which can progress into a persistent infection (Alexandersen et al., 2003). Vesicular lesions are mainly found in the epithelia of tongue, lips and feet but in some cases lesions also occur in snout, muzzle, teats, skin and rumen. The disease is characterised by a very short incubation period and high level of virus excretion, particularly in pigs. Animals exposed to the FMD virus (FMDV) usually develop a viraemia within 3 to 5 days of exposure, with clinical signs and lesions that usually last for 1 to 2 weeks post-infection (Kitching, 2002, Kitching and Alexandersen, 2002, Kitching and Hughes, 2002). However, hosts differ in susceptibility to infection and disease according to animal breed and productivity, farming system and environment, and the infecting virus strain (Rweyemamu et al., 2008). Although FMD does not usually cause high mortality in susceptible animals (high mortality may be seen in young animal due to acute fatal myocarditis) it decreases productivity, which in turn impacts on farmers' livelihoods. Since livestock constitute an important source of livelihood and tradable commodity in the agricultural based economies and social structure of many countries, FMD has a serious impact on food security, rural income generation, and the national economy by impairing livestock trade (Forman et al., 2009). The livestock sector has increased rapidly over the past decades, particularly in developing countries, where the growing demand has been driven by economic and population growth, rising per capita incomes and urbanisation (FAO, 2011). In addition, a wide range of traditional livestock management systems have evolved to optimise the use of resources, transformed by the implementation of more intensive farming units overlaid on the top of the traditional small-scale systems (*i.e.* pastoralist and/or smallholder production systems) (Di Nardo et al., 2011). However, the

increasing demand for livestock products and modernisation of management systems implies challenges in terms of efficient management of animal-health risks that have not always been considered as a priority in most developing countries. Therefore, in FMD endemic countries the lack of resources for an effective strategy to control disease through the restriction of animal movements makes FMD a continuous threat for its potential risk to spread at both the regional and global level. Nevertheless, the lack of baseline FMD information from several endemic countries with limited reporting of disease outbreaks provides less opportunity for the development of targeted policies and programs aimed at improving animal health and prevention of the disease. In recognising these constraints in endemic settings, in 2008 the Food and Agriculture Organization of the United Nations (FAO) launched a pathway for the progressive control of FMD which has been subsequently endorsed by the World Organisation for Animal Health (OIE) and it is nowadays one of the tools for the implementation of an integrated strategy for the global FMD control coordinated by the two Organisations (Sumption et al., 2012). Therefore, in specific regions of the world the implementation of regional roadmaps based on the circulating FMDV pools has greatly assisted in identifying hotspots which may be considered potential sources of lineages that pose a threat to neighbouring countries. Nevertheless, in the challenge of controlling FMD which, eventually, would work towards its eradication, new tools are warranted to enable a better characterisation on both molecular and epidemiological scales of the signal that drives the evolutionary history of FMDV and which underpin its transmission dynamics. Ultimately, a better understanding of the evolutionary dynamics of FMDV has the potential to inform intervention strategies and control policies to be risk-targeted.

1.1.1 Foot-and-mouth disease virus

FMDV is the prototypical member of the *Aphthovirus* genus, family *Picornaviridae*, which also comprises three other species *Bovine rhinitis A* virus, *Bovine rhinitis B* virus, and *Equine rhinitis A* virus (Knowles et al., 2011). The non-enveloped virion is characterised by a single-stranded positive-sense ribonucleic acid (RNA) (~8.4 kb in size), which is organised in: a 5' untranslated region (UTR) of ~1300 nt [which contains a number of structures, such as the S-fragment, a poly(C) tract, a series

of pseudoknots, a *cre* element and the internal ribosome entry site (IRES)]; the single open-reading frame (ORF) of ~7000 nt; a 3' UTR of ~90 nt [which contains the poly(A) tract] (Figure 1-1) (Mason et al., 2003). In an intact virion, the FMDV genome is surrounded by an icosahedral capsid of ~30nm in diameter composed of 60 copies of each of the four structural proteins (1A or VP4, 1B or VP2, 1C or VP2, and 1D or VP1), which possess determinants for infection and immunity (Jackson et al., 2003). Only VP1-3 proteins are exposed on the capsid surface, taking the form of similarly structured anti-parallel β-barrels. VPs are encoded by the P1 region, whereas the P2 and P3 regions encode nine non-structural proteins (NSPs) [2A, 2B and 2C from the P2 region; 3A, $3B^{VPg}$ (three copies, in tandem), $3C^{pro}$ and $3D^{pol}$ from the P3 region] responsible for genome processing (*i.e.* structural protein folding and assembly) and replication (Mason et al., 2003). Structural proteins accounts for approximately one-third of the polyprotein and are encoded towards the 5' end of the ORF, whereas the region encoding the NSPs comprises about two-thirds of the ORF. The P1 capsid is preceded by a Leader (L^{pro}) polypeptide which cleaves itself from the polyprotein. FMDV replicates via a negative sense RNA intermediate (Grubman and Baxt, 2004).

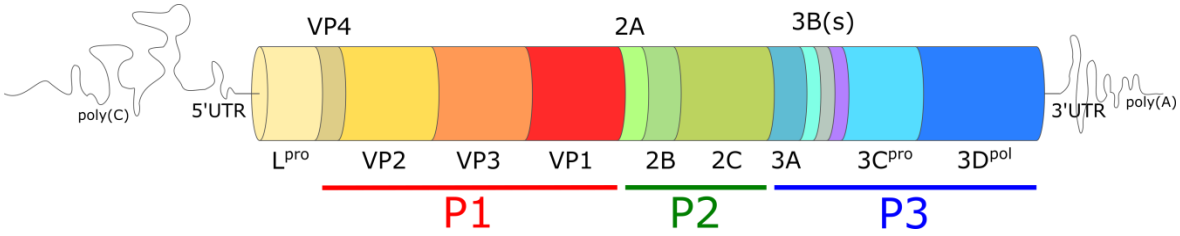

Figure 1-1. Schematic representation of the FMDV genome structure organisation showing the individual genomic regions described in text.

The high genetic variability of FMDV is reflected by the existence of seven immunologically distinct serotypes named O, A, C, Southern African Territories (SAT) 1, SAT 2, SAT 3, and Asia 1, which are further subdivided into topotypes based on the criterion of ~15-20% nt sequence difference in the VP1 coding region (Knowles and Samuel, 2003). Serotype C was last detected in Kenya and in Brazil during 2004; since then it appears to have become extinct (Roeder and Knowles, 2008). Within topotypes, lineages and even sub-lineages are defined (Knowles et al., 2010a). As a consequence of the high mutation and substitution rates of FMDV genomes, lineages quickly diverge as they replicate and spread into new areas. Therefore at a geographic level, FMDV is characterised by three continental epidemiological clusters in Africa, Asia and South America, which are further subdivided into seven distinct virus pools (Paton et al.,

2009) (Figure 1-2). Within each pool, multiple serotypes circulate and distinct patterns of viral evolution occur, with some countries sharing lineages belonging to different pools. To date, six out of the seven serotypes have been recorded in Africa (O, A, C, SAT 1, SAT 2, and SAT 3), while in the Middle East and Asia only four (O, A, C, and Asia 1) are normally present, although there have been sporadic incursions of exotic FMDV lineages from Africa into the Middle East, such as the reported SAT 1 outbreaks during 1962-65 and 1969-70, and the more recent introductions of SAT 2 in 2000, 2012 and 2015 (Bastos et al., 2003, Valdazo-González et al., 2012a, Knowles and Samuel, 2003, Knowles et al., 2015). Type Asia 1 lineages are generally confined to the Middle East and Asia, although historical outbreaks have been reported in Greece during 1984 and 2000. In the global picture of FMD distribution, FMDV populations might further acquire and mix genetic information by movements and/or immigrations of lineages from surrounding regions and, therefore, genetic variants accumulate rapidly in the field and co-circulate (Martinez et al., 1992, Pattnaik et al., 1998, Samuel et al., 1997).

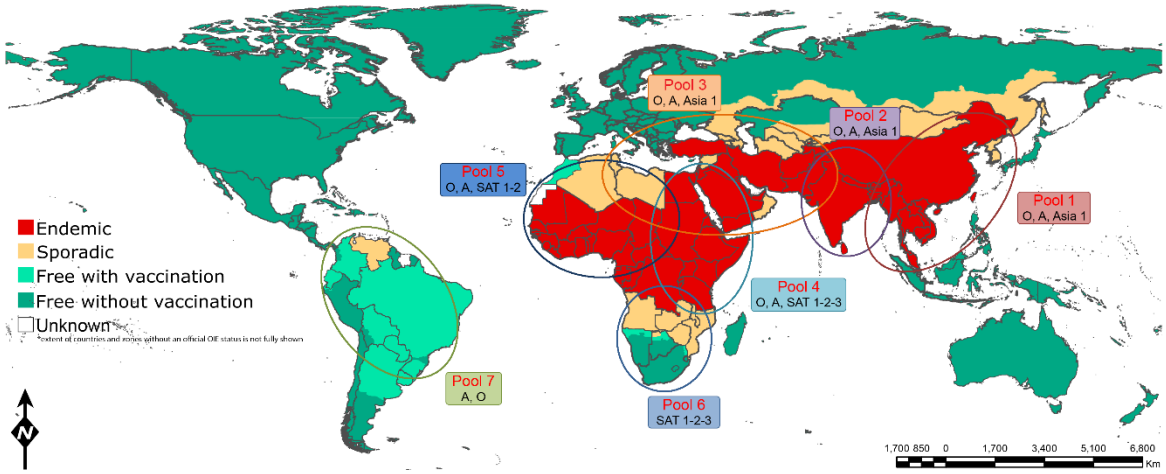

Figure 1-2. Conjectured FMD status in 2016 with seven regional FMDV pools and predominant serotype distribution at the global level.

Despite their worldwide distribution, FMDV serotypes show different properties, which contribute to their transmission competence. For example, some lineages belonging to serotype O, such as those of the CATHAY topotype, are restricted to specific hosts (Cheng et al., 2006, Knowles et al., 2001a), while others appear to lack species adaptation (*i.e.* the PanAsia lineage) (Knowles et al., 2005). Serotype A is the most antigenically variable serotype with differences in the VP1 coding region between continental topotypes reported to be of up to ~24% (Mohapatra et al., 2011), a characteristic that underpins the absence of cross-protection between some lineages

(Klein et al., 2006, Knowles et al., 2009, Jamal et al., 2011c). In addition, the SAT serotypes have been reported to have higher intraserotype nucleotide variation in comparison to serotype O (Bastos et al., 2001, Bastos et al., 2003). Differently, the type Asia 1 is considered to be the least diverse serotype both genetically and antigenically when compared to the other FMDV serotypes (Ansell et al., 1994), although reports highlight that field isolates belonging to the recently evolved Sindh-08 lineage causing outbreaks in livestock vaccinated with the established Asia-1/Shamir and Asia-1/Ind/8/79 vaccine strains (Jamal et al., 2011b). Therefore, FMDV populations can be seen as showing extensive genetic and antigenic heterogeneity at both molecular and geographic levels, driven by co-circulation of multiple lineages, heterogenic mixed host populations, extensive animal movements and trade patterns (Di Nardo et al., 2011).

1.1.1.1 FMDV evolutionary patterns

Similarly to other single-stranded RNA viruses, the genetic evolution of FMDV is mainly driven by the interplay of two mechanisms: 1) spontaneous mutation; 2) recombination. Due to the error-prone RNA-dependent RNA polymerase (3D in Figure 1-1), ssRNA viruses are characterised by high mutation rates (in a range of 10^{-5} to 10^{-3} nt misincorporations/site/replication cycle) (Drake, 1993, Duffy et al., 2008), which leads to evolution mainly through genetic drift (Domingo et al., 2005). At these rates of mutation, replicated FMDV genomes would differ on average from their parent genome by 0.1 to 10 base positions. A recent study reported that ssRNA are among those viruses showing the highest average genome mutation rates of the order of 0.66±0.42 substitutions/nt site/cell infection (Sanjuan, 2012). In a study of viruses belonging to the *Picornaviridae* family based on partial $3D^{pol}$ gene sequences, type A, O and C FMDV lineages were reported as evolving significantly more slowly than enteroviruses, with mean rate in the order of 1.45×10^{-3} nt substitutions/site/year estimated for type A and O lineages (Hicks and Duffy, 2011). Although constrained by the sequences available in Genbank, a review of evolutionary history based on VP1 coding sequences collected between 1932 and 2001 identified similar rates of nt substitution for all of the seven FMDV serotypes, with an average estimate of 2.48×10^{-3} nt substitutions/site/year (which resulted in a range of 1.07×10^{-3} nt substitutions/site/year for SAT 2 to 6.50×10^{3} nt substitutions/site/year for SAT 1) (Tully and Fares, 2008). However, the mutation

rate of FMDV is seen to vary according to the genome resolution and the transmission level at which it is expressed. An experimental study conducted both *in vivo* and *in vitro* and examining the whole-genome sequence (WGS) has shown that nt substitutions occur randomly across the FMDV genome, as might be expected at the finest scale in the absence of selection: within 20 serial passages only 2 nt substitutions out of 48 were recorded in the VP1 coding region recovered from infected pigs, and 4 out of 22 from cell cultures (Carrillo et al., 2007). Genome-wide mutation rate estimated from a within-host study system and employing next-generation sequencing (NGS) fixed the upper bound limit to 7.8×10^{-4} nt change/transcription event (Wright et al., 2011). In an endemic system, FMDV reveals a rate of nt change per year in a range of 4.5×10^{-4} to 4×10^{-2} based on VP1 coding sequences (Haydon et al., 2001, Bastos et al., 2003). In addition, estimates derived from a SAT 2 phylogenetic study of VP1 coding sequences, historically circulating in Africa and, more recently, in the Middle East reported an average molecular clock of 2.45×10^{-3} substitution/site/year (Hall et al., 2013). Enhancing the resolution of these analyses, WGSs of field samples collected during the 2001 United Kingdom (UK) epidemic estimated an average of nt changes per farm transfer at 4.3±2.1, with the substitution rate set at 2.37×10^{-5} nt/site/day [re-estimated from (Cottam et al., 2008a)], whilst the fully-resolved 2007 UK epidemic reported estimates ranging between 2.51×10^{-5} and 3.09×10^{-5} nt/site/day (Orton et al., 2013), with an average distance of 4.6 nt at source-to-recipient link levels (Valdazo-González et al., 2015). In addition, WGSs extracted from clinical samples collected during the 2011 Bulgaria epidemic revealed an evolutionary clock of 2.48×10^{-5} nt/site/day (Valdazo-González et al., 2012b). Table 1-1 presents a summary of the most recent publications reporting estimates of the FMDV molecular clock from sequence data based on either the WGS of the VP1 coding region and extracted from either an epidemic or endemic setting. Remarkably, very similar estimates of the FMDV evolutionary clock determined using WGS are reported, whilst a wider variability (although with the largest difference in the order of 4×10^{-3} nt/site/year) is found between estimates using VP1 data, with some results actually matching those of the WGS. This finding would thus contribute to the hypothesis that FMDV evolutionary dynamics are driven by a strict, stable and constant molecular clock.

Recombination is an important mechanism that contributes to the evolutionary patterns of RNA viruses. Although the extent to which recombination might play a role in the evolutionary dynamics of FMDV is not entirely understood, analysis of sequence

data indicates that these events do indeed occur (Heath et al., 2006, Jackson et al., 2007). Although rarely observed in the capsid proteins and more frequently in NSP coding regions, intertypic recombination has been reported in sites belonging to either the coding regions for NSPs (Domingo et al., 2003, Carrillo et al., 2005, Klein et al., 2007) or structural proteins (Tosh et al., 2002, Haydon et al., 2004), where NSP changes might lead to modification of the virulence (Klein et al., 2007). It is important to note that recombination events occur more frequently between FMDV lineages in regions where co-circulation of multiple serotypes and/or topotypes is present, therefore suggesting that co-infection drives the exchange of genetic material (Li et al., 2007, Lee et al., 2009, Wu et al., 2009, Balinda et al., 2010b, Jamal et al., 2011b, Chitray et al., 2014, Klein et al., 2007).

Table 1-1. Comparison of substitution rates between transmission chains estimated from FMDV sequence using a strict molecular evolutionary clock model. Genetic data were retrieved from either experimental, endemic or epidemic scenarios. †Values have been re-estimated from the original data.

Dataset	Scenario	Sequence Type	Substitution Rate		Reference
			(nt/site/day)	(nt/site/year)	
Cow-to-cow (chain A)	Experimental	WGS	2.27×10^{-5}	8.29×10^{-3}	(Juleff et al., 2013)
Cow-to-cow (chain B)	Experimental	WGS	2.86×10^{-5}	1.04×10^{-2}	(Juleff et al., 2013)
Herd-to-herd (1967)	Epidemic	WGS	2.39×10^{-5}	8.74×10^{-3}	(Wright et al., 2013)
Herd-to-herd (2001)	Epidemic	WGS	2.37×10^{-5}†	8.66×10^{-3}†	(Cottam et al., 2008a)
Herd-to-herd (2007)	Epidemic	WGS	2.51×10^{-5}	9.17×10^{-3}	(Cottam et al., 2008b)
Herd-to-herd	Epidemic	WGS	2.48×10^{-5}	9.05×10^{-3}	(Valdazo-González et al., 2012b)
Mixed (2007)	Epidemic	WGS	2.80×10^{-5}†	1.02×10^{-2}†	(Valdazo-González et al., 2015)
Isolate-to-isolate	Endemic	WGS	1.35×10^{-5}	4.94×10^{-3}	(Valdazo-González et al., 2013)
Isolate-to-isolate	Endemic	VP1	1.57×10^{-5}	5.74×10^{-3}	(Zhang et al., 2015)
Isolate-to-isolate	Endemic	VP1	7.56×10^{-5}	2.76×10^{-3}	(Balinda et al., 2010a)
Isolate-to-isolate	Endemic	VP1	6.79×10^{-6}	2.48×10^{-3}	(Tully and Fares, 2008)
Isolate-to-isolate	Endemic	VP1	6.71×10^{-6}	2.45×10^{-3}	(Hall et al., 2013)
Isolate-to-isolate	Endemic	VP1	4.87×10^{-6}	1.78×10^{-3}	(Mahapatra et al., 2015)
Isolate-to-isolate	Endemic	VP1	3.99×10^{-6}	1.46×10^{-3}	(Yoon et al., 2011b)
Isolate-to-isolate	Endemic	VP1	3.56×10^{-6}	1.30×10^{-3}	(Sangula et al., 2010)
Isolate-to-isolate	Endemic	VP1	3.01×10^{-5}	1.10×10^{-2}	(de Carvalho et al., 2013)
Isolate-to-isolate	Endemic	VP1	2.90×10^{-5}	1.06×10^{-2}	(Upadhyaya et al., 2014)
Isolate-to-isolate	Endemic	VP1	2.90×10^{-5}	1.06×10^{-2}	(Di Nardo et al., 2014)

1.1.2 FMDV genetic tracing

The increase in both VP1 and WGS data in the public domain reflects the increased application of genetic sequence data in FMDV research for molecular epidemiology and transmission tracing (Figure 1-3). Genome sequences of the VP1 coding region (approximately 639 nt in length) have been systematically and extensively used for reconstructing past FMD transmission events at both endemic and epidemic levels (Knowles and Samuel, 2003, Rweyemamu et al., 2008, Di Nardo et al., 2011, Valdazo-González et al., 2011, Cottam et al., 2006, Cottam et al., 2008b, Wright et al., 2013). Therefore, phylogenetic reconstruction of VP1 coding sequences generated

from FMDV isolates is a methodology routinely employed by the World Reference Laboratory for FMD (WRLFMD) to trace movements of FMDV lineages and identify the emergence of new lineages worldwide (Knowles et al., 2005, Knowles et al., 2009, Valarcher et al., 2009). Therefore, the use of VP1 coding sequences has been instrumental in the definition of transboundary movements of the different FMDV lineages and, thus, to greatly support FMD control policies at either country, regional or global level (Konig et al., 2007, Abdul-Hamid et al., 2011, Loth et al., 2011, Knowles et al., 2012, El-Shehawy et al., 2014). In addition, more complex studies involving a larger database of VP1 coding sequences have been able to reconstruct historical changes in FMDV population dynamics and retrospectively trace geographic movements of FMDV lineages across countries and regions (Yoon et al., 2011a, Di Nardo et al., 2014, Hall et al., 2013). Although containing important antigenic determinants and exhibiting frequent mutations, the VP1 coding sequence represents only ~8% of the FMDV genome and, therefore, the resolution provided is sometimes not adequate to fully capture the evolutionary dynamics of FMDV and/or to resolve transmission pathways of disease incursions. For example, the analysis of the 1982-83 FMD epidemic in Denmark using VP1 coding sequences alone did not provide enough variation to infer transmission between farms (Christensen et al., 2005). This observation was also true for the initial attempts to study the UK 2001 FMD outbreak and the FMDV type SAT 2 emergence in North African countries and the Middle East during 2012, which made only use of VP1 coding sequences (Knowles et al., 2001b, Ahmed et al., 2012).

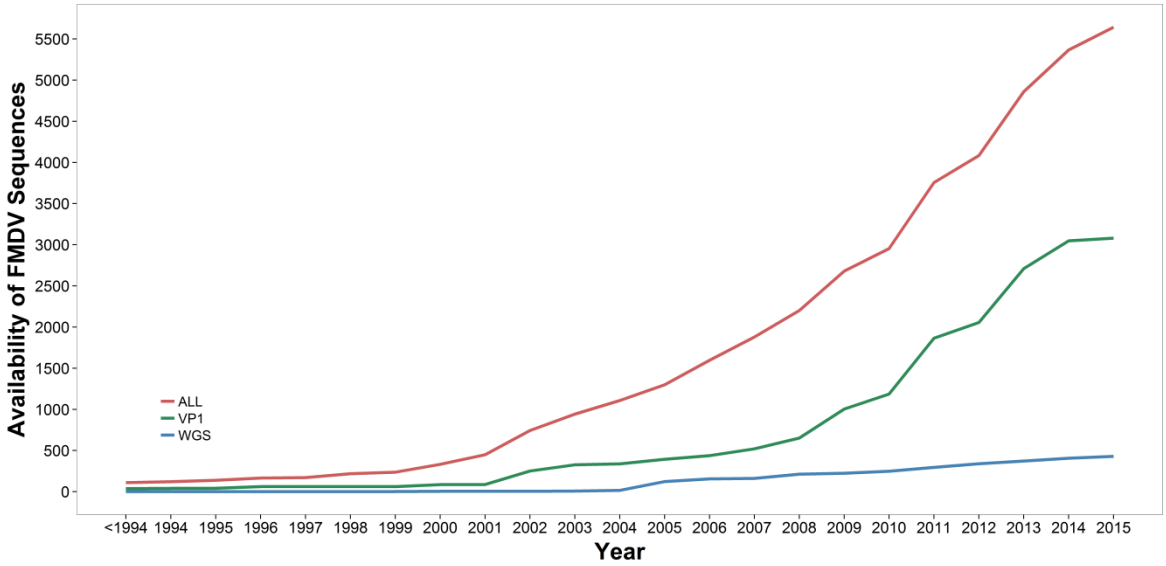

Figure 1-3. Number of FMDV sequences submitted to GenBank at NCBI since prior 1994. VP1 sequences includes all the sequences <700 nt belonging to the VP1 coding region; WGS includes all the sequences >7000 nt; ALL includes VP1, WGS and partial cds sequences.

More recently, efforts have been focussed on the use of FMDV WGS for undertaking forensic genetic tracing at the epidemic level, thus providing a far better resolution of the virus transmission chain (*i.e.* the reconstruction of '*who-infected-who*' transmission tree) (Cottam et al., 2006, Konig et al., 2009, Valdazo-González et al., 2012a, Wright et al., 2013, Cottam et al., 2008a). The use of WGS to fully-resolve the UK 2007 FMD epidemic has pioneered the application of forensic epidemiology and has provided a resource for the development of new molecular epidemiological methods based on model inferences {Morelli, 2012 #855;Ypma, 2013 #939}. In fact, real-time analyses of the samples collected during this series of outbreaks enabled the identification of undisclosed IPs prior to their detection by serosurveillance (Cottam et al., 2008b). The same approach was applied during the Bulgaria 2011 FMD outbreak, when 8 FMDV WGS were used to recognise undetected FMDV infection and, associated with other contemporary circulating viruses isolated from neighbouring countries, to understand the potential way that FMDV was introduced into Bulgaria (Valdazo-González et al., 2012b). These studies have highlighted the impact and feasibility of using WGS in real-time field outbreak investigation which, coupled with fully-resolved epidemiological information, provides an important tool for FMD control. Thus, early characterisation of the epidemiology and evolution of epidemics is essential for accurately reconstructing the transmission tree of viral dispersal and determining the most appropriate intervention strategies to be applied.

1.2 Phylodynamics of viral infectious diseases

Since the evolutionary rate of RNA viruses at nt level and their generation times are fast enough to be measured in a short timescale, they offer an excellent system for studying evolutionary processes that occur during transmission events (Drummond et al., 2003, Duffy et al., 2008). Accordingly, genetic mutations carried by RNA viral sequences enable the characterisation and reconstruction of on-going evolution (Felsenstein, 2004). Therefore, molecular epidemiology and phylogenetics provide the tools to understand the origin, evolutionary history, and transmission routes within epidemics. Genealogies, moreover, contain information about historical demography and processes that have acted to shape the diversity of populations. Given the same time-frame, ecological dynamics can be integrated within the phylogenetic inference to capture selective, ecological and demographic forces driving the evolution of pathogens (Grenfell et al., 2004). This analytical framework, described as phylodynamics, has the potential to bring together an estimation of genealogical relationships and inferences on population sizes, structures and migration patterns, thus enabling the reconstruction of detailed epidemiological dynamics and transmission routes of viral system.

1.2.1 Reconstructing the dynamics of viral epidemics

1.2.1.1 Coalescent theory

Statistical methods in molecular epidemiology have significantly contributed to the understanding of viral dynamics given the problem of data availability. One of the most important advances in population genetics which provides the foundation of phylodynamic inference is the formulation of the coalescent process first described by Kingman (Kingman, 1982b, Kingman, 1982a). The coalescent model is, essentially, a diffusion model of lines of descent which assumes a panmictic population governed by the Wright-Fisher neutral model of genetic variation (Fisher, 1930, Wright, 1931). Briefly, the Wright-Fisher model governs the evolution, at discrete time steps, of population (here assumed to be haploid, as is the case for many pathogens) with constant finite size, allowing each individual to randomly choose one parent from a

previous generation and, thus, to adopt its type. Given this specification, the assumptions constrained by the Wright-Fisher model are that the population is finite and constant, the generations are not overlapping, the reproduction is a random process, and no selection or recombination processes are allowed. With the coalescent model, the ancestral lineages are traced back in time to the most recent common ancestor (MRCA). The history of a sample of size n comprises $n-1$ coalescent events, with each of those decreasing the number of ancestral lineages by one. At each coalescent event two of the lineages fuse into one common-ancestral lineage, with the lineage remaining at the final coalescent event being the MRCA of the entire sample. The topology resulted from the coalescent process is a bifurcating tree (Figure 1-4).

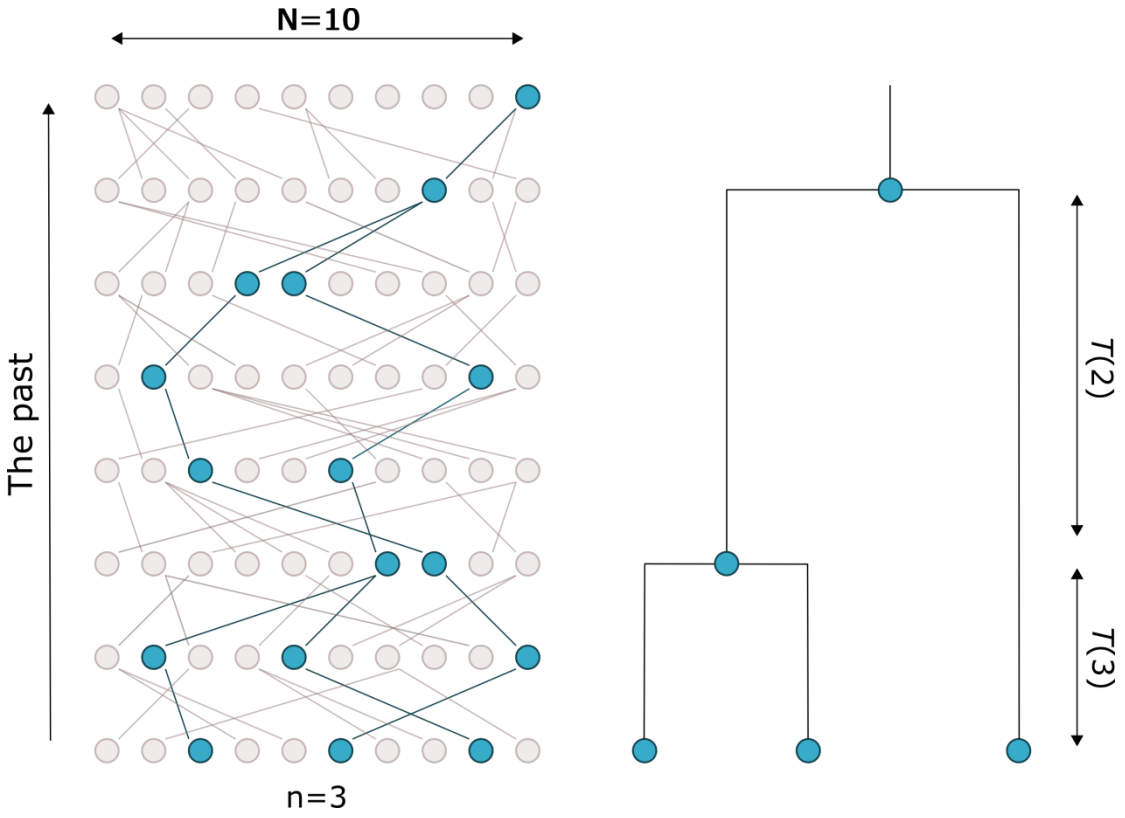

Figure 1-4. Schematic representation of the coalescent process. The genealogical relationships in an 8-generation realization of the Wright-Fisher model with population size *N* are shown on the left. The genealogy of a sample n is described in terms of its topology and branch lengths, which provide the waiting times between coalescence events (right).

The Kingman coalescent assumes that the population size *N* is large enough and the sample size n is much smaller, with a variance in the number of offspring not too large (Sjodin et al., 2005). To date, the most commonly used coalescent model is the Kingman derived variable population size model (Griffiths and Tavare, 1994a), which describes deterministic changes in the genealogical process according to relative size functions (such as exponential or logistic growth). This method has been further

extended to incorporate heterochronous sequences (Rodrigo and Felsenstein, 1999), to deal with stochastically fluctuating population size (Kaj and Krone, 2003) and even to apply the coalescent to spatially extended populations (Barton et al., 2002). In addition, a more exact coalescent framework than the Kingman approximation of the Wright-Fisher model has been recently developed, which enables the characterisation of exhaustive sampling (*i.e.* of matching the size of the Wright-Fisher population) and thus dealing with multiple coalescences at the same time (Fu, 2006).

1.2.1.2 Effective population size

Coalescence allows sampled sequences to be traced back in time within defined ancestral lineages that eventually converge on a single MRCA. Under the coalescent process, the shape and distribution of the phylogeny is reconstructed in terms of a demographic parameter called the effective population size N_e which corresponds to the ideal Wright-Fisher population size N (Charlesworth, 2009). The coalescent rate is, nevertheless, affected by several demographic parameters, such as the population structure and size, as well as genetic factors (*i.e.* reproductive forces) (Rosenberg and Nordborg, 2002). For example, the larger the number of lineages the faster is the rate; the larger the number of ancestors the slower is the rate. Moreover, the larger the population size, the more genetic variability can be seen in the population and, thus, the longer it takes for two lineages to coalesce. Therefore in its population genetic formulation, N_e provides an understanding of the observed extent and pattern of retrospective genetic variability of a population, and is a key parameter to explain the evolutionary mechanisms that drive the shape of variation in populations (Wang, 2005). From the initial theory of Wright (1931), the principle of N_e has been extended and applied to almost any evolutionary scenario, with several attempts to investigate the nature of N_e as an epidemiological measure in the field (Frost and Volz, 2010, Magiorkinis et al., 2013, Volz et al., 2009, Drummond et al., 2005, Volz, 2012). To date, studies have considered N_e as equivalent to the number of infected individuals (Kouyos et al., 2006). However, the direct relationship that exists between N_e and the actual number of infected individuals is not entirely clear, although this value is assumed to be invariably less than the true number of infected individuals and often this is attributed to heterogeneity in population structure (Luikart et al., 2010). In a recent

study, Volz et al. (2009) demonstrated the direct relationship of the coalescent rate with the transmission rate (*i.e.* incidence) but not with the measure of the number of infected individuals (*i.e.* prevalence), and showed how the prevalence might influence the shape of the phylogeny only through sampling effects. The authors reported the coalescent rate to be proportional to the epidemic incidence and inversely proportional to the square of the prevalence and, therefore, assuming that the rate is high when the prevalence is low and the incidence is relatively high (*i.e.* during the expansion phase of an epidemic). Frost and Volz (2010) further demonstrated that the pattern of coalescence for an infectious disease is dominated by the transmission rate, while the number of infected individuals is of secondary importance. Therefore, defining the coalescent rate as a measure of incidence, incidence and prevalence are expected to be out of phase, where peaks of incidence precede those of prevalence (Frost and Volz, 2010). This evolutionary feature has been observed in studying the phylodynamics of dengue virus serotype 4 in Puerto Rico, where fluctuating values of both N_e and case count over time were seen, although changes in N_e preceded changes in case count by months (Bennett et al., 2010). Since the timescale of the coalescent is defined as a function of both N_e and the generation time τ [here expressed with the definition of serial case interval τ_c (Frost and Volz, 2010)], correlations between increases in prevalence and corresponding increases in $N_e\tau_c$ might be seen in a neutral population showing absence of selection (Bedford et al., 2011). This has also been shown in a study of hepatitis C virus, where a clear correlation in relative size of N_e with the estimated number of infected individuals was reported (Magiorkinis et al., 2013). It should be noted that although the Wright-Fisher model assumes that every progeny is chosen at random from the parents according to a Poisson distribution, in nature and often in viral dynamics few cases produce the majority of infections. This variance in the number of progeny per parent can therefore increase the stochastic effect and thus affects the N_e estimate (Kouyos et al., 2006). The correlation between N_e and the variance in the number of progeny per parent (V_k) has been investigated for several formulations of the coalescent process, thus defining different N_e quantities such as the inbreeding effective number (N_{e_i}) and the variance effective number (N_{e_v}), which account for uneven progeny structures (Kimura and Crow, 1963). This leads to the assumption that N_e is connected with the census population size N and the variance (σ^2) in the reproductive success (Kingman, 1982b, Tavare et al., 1997) or, in a more epidemiological definition, the variance in the number of secondary infections per

primary infection [$var(R_t)$] (Koelle and Rasmussen, 2012). In addition, the ratio between the number of infected individuals, N, and the effective population size, N_e, (N/N_e) is formally described as being equal to the $var(R_t)$ when the genetic variability within virus strains has no effect on their infectious potential (Kingman, 1982b, Magiorkinis et al., 2013, Tavare et al., 1997).

Although the coalescent model is appropriate for making inferences about population dynamics, in the context of viral transmission it is mainly used for its simple mathematical formulation rather than its accuracy in defining the transmission process. For example, the coalescent model can provide estimations of change in population size but shows limitations as an estimator of epidemiological parameters. Furthermore, it does not make use of information on sampling time. Stadler *et al*. (2012) introduced the birth-death model (BDM) as an alternative to the coalescence for the tree-generating process. The birth-death process generates, forward in time and according to stochastic rates of birth and death, a tree with extinct and extant lineages (*i.e.* the 'complete tree'). The extinct and the not-sampled lineages are then deleted producing the reconstructed tree of only sampled extant lineages. As demonstrated, the BDM has the advantage of reflecting more accurately the process underlying the transmission dynamic and, moreover, to estimate the total number of infections caused by an individual over the course of the individuals infectious time (*i.e.* the basic reproductive number R_0). From their initial formulation, both the coalescent and BDMs have been extended to account for heterogeneous structured populations (Stadler and Bonhoeffer, 2013, Volz, 2012). In addition, several attempts have been recently made towards the implementation of stochastic demographic processes into a coalescent framework (Rasmussen et al., 2011, Rasmussen et al., 2014b)

1.2.1.3 Modelling the demography of viral populations

As presented in the previous section, the coalescent model defined by Kingman describes the relationship between coalescent times and the population size under the Wright-Fisher population model given a sampled genealogy. Given that $1/N_e$ is the probability, under the coalescent assumptions, that two lineages descend from a common ancestor at each generation and applying the derived probability distribution to a phylogenetic tree, it is possible to estimate the change in N_e throughout the history

of the population up to the MRCA. This feature of the coalescent enables quantification of the rate at which the population loses or enhances its genetic diversity and, therefore, the computation of historical patterns of viral population size provided by genomic data (de Silva et al., 2012). In the last decade, several methods have been developed for estimating the demography of populations from sequence data or an estimated genealogy. However, most of these approaches constrain the population history into continuous or piecewise parametric models, such as constant size, exponential growth, logistic growth, and expansion growth, and therefore do not fully capture the complex patterns of demographic changes (Kingman, 1982b, Slatkin and Hudson, 1991, Tavare et al., 1997, Wilson and Balding, 1998, Griffiths and Tavare, 1994a). In addition, an *a priori* assumption of a population size history is usually not possible and, therefore, simple population growth functions might not best describe the population history of interest.

Building up from this problem, Nee *et al*. (1995) introduced the lineage-through-time (LTT) plot that provides a graphical depiction of the accumulation of lineages in a time scale derived from a time-stamped phylogeny. However, the initial theoretical input of Pybus *et al*. (2000) with the introduction of the classic skyline plot provided the basis to derive more precise computation of demographic history reconstruction, thus giving rise to a family of so-called skyline plot methods (Table 1-2). Skyline reconstruction assumes that under the coalescent the mean population size for each coalescent interval can be estimated by the product of the interval size (γ_i) and $i(i-2)/2$, where i is the number of lineages in the interval (Figure 1-5) and, therefore, gives a non-parametric estimate of N_e based on a piecewise method. The limitation of the classical skyline plot is that it produces a noisy and stochastic reconstruction resulting from the lack of coalescent error assessment provided by the method, which is particularly evident when the genealogy contains a large number of short internal branches and, therefore, the phylogenetic error is substantial. To overcome this problem, the generalised skyline plot was developed (Strimmer and Pybus, 2001). The main difference between the classical and generalised skyline plots is that the latter overcomes the problem of the noisy estimates by grouping correlated coalescent events and, thus, sampling events into time intervals of a certain length ε. However, the genealogy is still assumed to be estimated without error and does not account for stochasticity in the coalescent process. Major improvements were implemented estimating N_e within a Bayesian Markov chain Monte Carlo (MCMC)

computation. Drummond *et al*. (2005) introduced the Bayesian skyline plot (BSP) that was implemented in a more comprehensive Bayesian framework, where genealogy, demography and substitution parameters are co-estimated within a single analysis (Drummond et al., 2002).

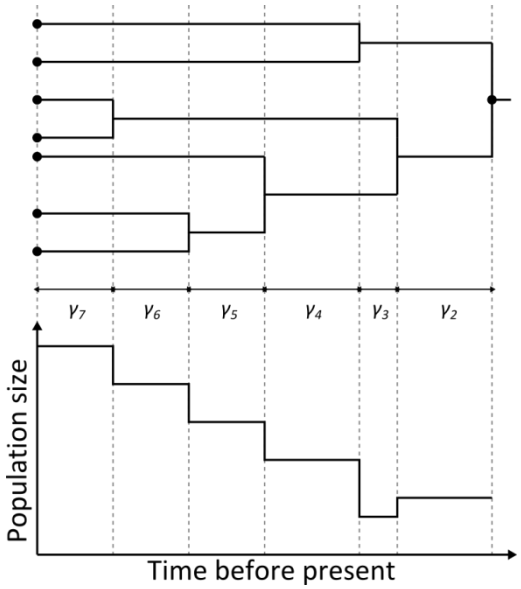

Figure 1-5. Inferring demographic history of virus population from a reconstructed phylogeny. Schematic representation of the skyline plot approach [sourced and adapted from (Ho and Shapiro, 2011)].

The BSP method employs a piecewise-constant model, grouping multiple correlated coalescent events into time steps. However, the BSP needs an *a priori* definition of the number of groups, which can lead to an increase in the estimation error when less informative data are analysed. Solutions are provided by averaging the demographic model using a reversible jump MCMC and assuming autocorrelation of population sizes over time – employed by the Bayesian Multiple Change Point (MCP) (Opgen-Rhein et al., 2005) – or deriving the demographic function directly from the data through a Bayesian stochastic search variable selection (BSSVS) method (Heled and Drummond, 2008). The latter model – the Extended Bayesian Skyline – further implements the analysis of multiple loci to increase the accuracy and resolution of the demographic reconstruction. Another alternative to the BSP is offered by the Bayesian Skyride (Minin et al., 2008). This method avoids the identification of an *a priori* number of coalescent groups using a prior based on a Gaussian Markov random field (GMRF) smoothing parameter that is directly informed by the data. Therefore, the difference in N_e between autocorrelated coalescent intervals is time-aware, penalised according to the lengths of the intervals and, therefore, assumes that the N_e changes gradually over time. A further development on the basis of the Skyride model but allowing the use of

multiple unlinked genetic loci, as featured in the Extended Bayesian Skyline, is the Bayesian Skygrid, which parameterises N_e as a piecewise constant function smoothing the trajectory by GMRF and allowing changes to the estimated trajectory at pre-specified fixed points in real time (*i.e.* grid points) (Gill et al., 2013). A method for calculating the N_e based on an approximate Bayesian computation (ABC) algorithm has also been proposed (Palacios and Minin, 2012). This method integrates Gaussian process-based Bayesian nonparametric approaches into integrated nested Laplace approximation (INLA) (Rue et al., 2009) without the need for complex MCMC computation and, therefore, speeding up the calculation and improving the efficiency.

Table 1-2. Model-based tools for reconstructing demographic history from both DNA and RNA virus sequence data (listed in chronological order of development).

Method	Estimate	Model	Type	Reference
LTT				(Nee et al., 1995)
Classic Skyline	Nonparametric	Piecewise-constant		(Pybus et al., 2000)
Generalized Skyline	Nonparametric	Piecewise-constant		(Strimmer and Pybus, 2001)
Bayesian MCP	Nonparametric	First-order spline	rjMCMC	(Opgen-Rhein et al., 2005)
Bayesian Skyline		Piecewise-constant		(Drummond et al., 2005)
Bayesian Skyride			GMRF	(Minin et al., 2008)
Extended Bayesian Skyline	Nonparametric	Piecewise-linear	BSSVS	(Heled and Drummond, 2008)
Nested Laplace Approx.	Nonparametric		ABC	(Palacios and Minin, 2012)
Bayesian Skygrid	Nonparametric	Piecewise-constant	GMRF	(Gill et al., 2013)

The emergence of demographic and skyline genealogy-based methods and their implementation into user-friendly software [*i.e.* the Bayesian Evolutionary Analysis Sampling Trees (BEAST)] has fostered the increase of phylodynamic studies in molecular ecology, biology and epidemiology, and the assessment of their validity and resolution power. Based on mitochondrial genome data, several studies have attempted to infer patterns of demographic variation in humans (Gignoux et al., 2011, O'Fallon and Fehren-Schmitz, 2011, Atkinson et al., 2009) and animal populations (Lippold et al., 2011, Finlay et al., 2007, Qu et al., 2011). Additionally, skyline reconstructions were employed to understand ecological and climatic factors affecting historical demographic dynamics of animal species (Koblmuller et al., 2012, de Bruyn et al., 2009, Hollatz et al., 2011, Amaral et al., 2012, Lorenzen et al., 2011) and the human population (Guillot et al., 2013). In the context of infectious disease, skyline analyses have been applied in both epidemic and endemic systems to understand the origin, expansion and/or decline of viral dynamics (Zehender et al., 2009, Pomeroy et al., 2008, Vijaykrishna et al., 2008, Carrington et al., 2005, Comas et al., 2013). In a recent study of human influenza A virus, BSP analysis revealed characteristic disease seasonality linked with temperate populations (Rambaut et al., 2008). In addition, a

three-stage process of host shift for rabies virus in bats was described for all different virus lineages (Streicker et al., 2012). The use of BSP to assess impact of control policies on viral diversity has been also applied in the context of hepatitis A virus with the introduction of vaccination in France related to the time of decline observed in the reconstructed skyline plot (Moratorio et al., 2007), whereas an exponential growth in the N_e of hepatitis C virus in Egypt was attributed to the introduction of parental antischistosomal treatments (Pybus et al., 2003). In a review of skyline plot methods, Ho and Shapiro (2011) tested five skyline models against two datasets generated via simulation. Beside the classic and generalised skyline, the BSP largely matched the trajectories of the simulated data although not full recovering the demography. Simulating epidemic and evolutionary dynamics of biannual measles outbreaks by a Time-Series SIR model, Stack *et al*. (2010) reported the failure of the BSP to reconstruct the full biennial dynamics of measles epidemics over different long-term sampling sets. This is relevant when populations undergo bottlenecks and the number of lineages is substantially reduced from one epidemic season to the next. In another study carried out with the aim of testing the BSP for reconstructing epidemic dynamics, data related to the early exponential phase of an influenza A virus H1N1 epidemic were simulated using a branching process model (de Silva et al., 2012). Results revealed biases in the skyline estimates, incorrectly inferring a decrease in the N_e in the last part of the epidemic phase when the population was still growing. This problem was related to the lack of genealogical information at later times, corresponding to the last coalescent event and the flattening of the LTT plot; therefore, the authors suggested truncating the BSP reconstruction behind the last coalescent event. In addition, some studies highlighted the limitations of the BSP for reconstructing viral demography due to its formulation being based on the coalescent, which approximates the population dynamics assuming a small sample of the entire population (Stadler et al., 2013).

1.2.1.4 Sampling genetic data

Making an inference on evolution and population structures for a given pathogen relies on adequate sampling which ideally should be based on knowledge of pattern and extent of genetic diversity at a given spatio-temporal scale. Therefore, two important questions might be raised in the context of sampling genetic data: 1) how

does the temporal distribution of the samples affect the estimation of the population size? and 2) can a sampling strategy be designed to optimise the reconstruction of population histories? For coalescent-based methods to work optimally, samples should be drawn from a well-defined scheme (Rosenberg and Nordborg, 2002) with individuals randomly sampled from a panmictic population. When heterochronous data are used, the random sampling is extended across geographical and temporal ranges; sampled sequences are assumed to be orthologous, non-recombining and neutrally evolving. It should be noted that, under the coalescent model, increasing the sample size does not extend the accuracy of the estimates, because of the existence of a single underlying genealogy (Rosenberg and Nordborg, 2002). However, sampling biases at the genetic level could result in strongly unbalanced trees, even in the case of a panmictic population (Mooers and Heard, 1997). Different opinions are expressed as to whether demographic history is best reconstructed from a local or a pooled sampling scheme when populations are geographically and genetically structured (St Onge et al., 2012). The effect of population subdivision and structure has been reported to impact on the reconstruction of population size changes (Peter et al., 2010, Chikhi et al., 2010). Stadler *et al*. (2009) suggested that a scattered sampling might result in a frequency polymorphism spectrum more similar to that expected in a neutral evolving population. However, St Onge *et al*. (2012) concluded that the effect of sampling on the site frequency spectrum is limited in many cases, such as populations that experience large demographic changes or when migration is unlimited. In the context of epidemics, using discrete-time simulations Stack *et al*. (2010) found that the bias in prevalence reconstruction using BSP depended largely on how samples were distributed over the course of the epidemic: the most reliable estimates could be obtained by sampling sequences towards the end of an epidemic. Therefore, a systematic approach based on serial sampling schemes should provide a broad view of the epidemic dynamic (Stack et al., 2010). For example, sampling a higher fraction of the infected population in a given time might result in trees with shorter terminal branches (Volz et al., 2009). In a phylodynamics study of norovirus GII.4, although the disease seasonality derived from the surveillance system was reconstructed using the BSP, re-performing the analysis using a subset of the polymerase dataset drastically reduced the resolution provided by the BSP, demonstrating that a high sampling density is required to analyse population dynamics of viruses characterised by seasonal variation interleaved by population bottlenecks (Siebenga et al., 2010). From

a different prospective, an extension of the BDM has been developed to account for incomplete sampling of the population (Stadler, 2010). The use of BDM has the advantage that it can be applied to different sampling scenarios (*i.e.* sparse or dense sampling schemes), since the sampling process is specified within the model (Stadler et al., 2012). In addition within this process, the sampling rates can be relaxed to vary through time by means of a step function (Stadler et al., 2013). However, one problem of the BDM is that it requires a specification of the sampling process and, therefore, if the testing system deviates from the theoretical formulation of the BDM the results obtained might be highly biased (Volz and Frost, 2014). This has been seen with the study of the recent Ebola virus epidemic in Sierra Leone (Stadler et al., 2014), where the assumption of a constant sampling rate of the BD exposed-infected model used for the analysis is violated by the sampling variability reported between collection periods (Volz and Pond, 2014).

1.2.2 Integrating epidemiology with phylogenetics

One of the most challenging tasks to fully understand the dynamics of pathogen dispersal is the integration of data based on epidemiological observations with phylogenetic inferences. In fact, although the transmission pathways can be reconstructed using either epidemiological (*i.e.* by the means of time, space or space-time data) or genetic data alone, inferences based on these approaches are generally biased and unreliable. Great robustness can be achieved by integrating these data types together. With the increasing affordability and speed with which genomic data can be generated, research on this topic has expanded in the last 5 years leading to a range of different methodological approaches to try to resolve the complex structure defined by the phylodynamic process (Grenfell et al., 2004). However, despite the increase in the application of coalescent-based methods in molecular epidemiology, difficulties arise when validating the obtained results through independent data. Biek et al. (2007) demonstrated the detailed information which can be extracted when integrating different types of data sources into the phylogenetic inference. In the context of viral dynamics, phylogenetic reconstruction has been used to understand the complex virus diversity within the inter-farm transmission dynamics of the H7N7 highly pathogenic avian influenza virus outbreak recorded in The Netherlands in 2003 (Bataille et al.,

2011). In addition, attempts to reconstruct the underlying transmission pathways of viral dynamics include the integration of spatial and temporal data within the phylogenetic reconstruction. Lemey *et al*. (2009a) provided the basis for an integrated Bayesian phylogeography framework built on a BSSVS model using discrete location states which helped in reconstructing the patterns of global spread of the H5N1 influenza A virus. This methodology was further tested analysing the process underlying the geographical migration of the initial spread of the H1N1 human influenza A virus pandemic (Lemey et al., 2009b). Further extensions enabled the use of continuous data, such as geographical coordinates, through the implementation of random walk diffusion models based on branch-specific variation in the dispersal rates (Lemey et al., 2010). In the FMD context, phylogeography has been used for characterising movement of lineages within a country (de Carvalho et al., 2013), within a continent and across different species (Hall et al., 2013), and from a whole topotype perspective (Di Nardo et al., 2014).

Differently, a set of studies were based on a previously developed parameter-free method for estimating the history of transmission events in the course of an epidemic, which reconstructs the temporal chain of transmission events (Haydon et al., 2003). However, accurate and unbiased reconstruction of the so-called transmission trees is likely to require a very good sampling of cases during an epidemic. Therefore, studies have been focused on the potential integration of genetic information with epidemiological data to enhance the resolution, which could be categorised into two distinct computational approaches: the 'transmission tree first' when the transmission tree is firstly reconstructed and then an evolutionary model is attached to the transmission model; and the 'phylogenetic first' where the genetic data are used to directly infer the transmission tree by augmenting some evolutionary model with epidemiological information. Cottam *et al*. (2008a) studied a cluster from the UK 2001 FMD epidemic and developed a transmission tree analysis based on estimating likely periods of infectiousness, constructing all plausible trees, and using genetic data to identify and exclude unlikely transmission trees. Following this approach, in a study of the H7N7 avian influenza A epidemic in The Netherlands in 2003 (Ypma et al., 2012), genetic, geographical and temporal data were integrated in one single likelihood function for estimating the infection events and the infectiousness of farms according to their size and type. Furthermore, this methodology appropriately handled missing data (*i.e.* cases for which no genetic data were available). A comprehensive analytical

framework is also proposed by Rasmussen *et al*. (2011), who integrated genealogies and time series data in a State-Space Model (SSM) parameter and population dynamics using a particle filtering MCMC method. A detailed spatial epidemiological model of transmission coupled with a simple evolutionary model has been proposed by Morelli et al. (2012), an approach that attempts simultaneous inferences to be made on epidemiological processes, the transmission chain and the mechanisms that shape the evolutionary process. The Bayesian framework proposed pioneered the further development of likelihood functions that integrated genetic distance and epidemiological models for analysing disease outbreaks and thus estimating transmission trees.

Moving from more classical phylogenetic approaches, Jombart *et al*. (2011) developed a method based on graph theory (Lieberman et al., 2005) that derives ancestries directly from the sampled isolates. This approach becomes relevant when the phylogeny includes both the ancestor and descendants, as in the case of an outbreak. Clearly, the structure of the contact network underlying epidemics impacts on the spread of a pathogen (Keeling, 2005), leaving detectable genetic signatures and providing evident correlations between genetic and epidemiological data (Welch et al., 2011). In a study of a nosocomial outbreak of hepatitis C (Spada et al., 2004), a Minimum Spanning Tree approach was used to reconstruct the transmission tree of the epidemic combined with information on the contact patterns of the hosts. Gordo and Campos (2007) studied the level and pattern of genetic diversity in viral populations developing a population genetic model incorporating epidemiological parameters based on SIS simulations on two different structures of the host contact network. The utility of integrating genetic data with epidemiology has been demonstrated by Lewis *et al*. (2008) who developed a Bayesian approach for reconstructing transmission network of HIV patients. The effect of contact network on phylogeny has been quantified in a recent study (Leventhal et al., 2012), where the authors reported significant variation of the Sackin index (*i.e.* a measure of the tree shape) according to different classes of contact structures tested.

A common assumption on which the relationship between transmission tree and phylogeny is founded is that transmission events and time of ancestry are equivalent and, therefore, transmission and phylogenetic trees are topologically equivalent (Pybus and Rambaut, 2009). However, this might not be correct when a substantial within-host (or even within-farm) evolutionary process potentially allows

several individual lineages to be transmitted from the same source (Kao et al., 2014). An initial attempt to include within-host genetic diversity linked a structured transmission tree with a within-host evolutionary process to resolve the full transmission history of epidemics (Ypma et al., 2013). However, problems arise since estimates based on either fixed phylogenetic or transmission tree topology are not able to fully capture the extent of the variability in the tree space (Vrancken et al., 2014). Didelot et al. (2014) explored this issue introducing a model based on a coalescent within-host evolutionary process, which accounted for uncertainty in the inferred phylogeny, in order to reconstruct disease transmission history in a densely sampled scenario and when multiple lineages might be passed to subsequent generations. Further developments on this approach have been recently put into a more theoretical framework (Hall and Rambaut, 2014). However, one limitation of all the above methods is that they require that all infected cases have been observed and, therefore, the trees should contain a tip from every case involved in the transmission chain. Although epidemiological data extracted from fully-resolved epidemics can be informative about unsampled genetic data, this would not always be the case in endemic settings where surveillance is unlikely to be exhaustive or when infections are characterised by a subclinical form. Studies have started to investigate space-time-genetic SEIR approaches (Mollentze et al., 2014, Soubeyrand, 2014) or a simpler discrete-time stochastic model (Jombart et al., 2014) that would enable the characterisation of missed or unsampled cases and the existence of polyphyletic systems. On a multi-scale perspective whether investigating small scale epidemics, disease spread at continental level or viral population structure (Figure 1-6), this highlights the important source of information that epidemiological data provides to the reliable reconstruction of transmission chains based on phylogenetic methods.

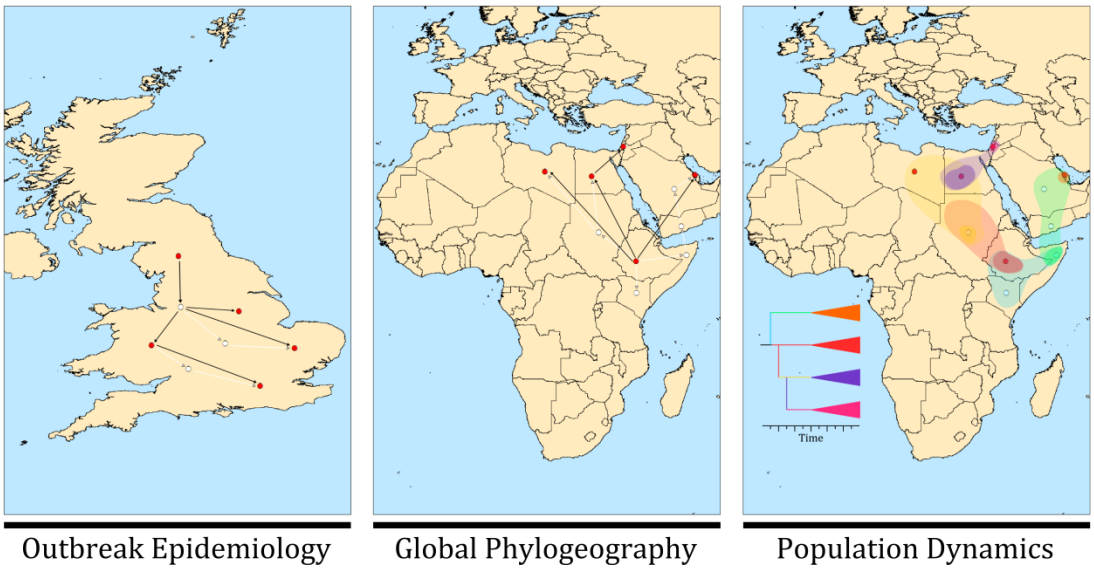

Figure 1-6. Schematic representation of multiple scale of virus evolution aimed at reconstructing pathways of pathogens transmission and their population dynamics.

1.3 Project rationale and scientific objectives

As previously described in §1.2.1, sequence data are commonly employed within well-established phylodynamic models for reconstructing demographic changes of infected populations through time (Drummond et al., 2005, Frost and Volz, 2010). However, some degrees of uncertainty still exist on how these methods perform for reproducing the real scale and size of disease outbreak trends as estimated through empirical epidemiological data. During the course of the UK 2001 FMD epidemic, epidemiological information on every conceivable element of the epidemic were collected through field investigations, thus enabling retrospective capture of the dynamics in space and time of the entire disease event (DEFRA, 2002). In addition, nearly one clinical sample from every reported infected premises (IPs) has been collected, from which FMDV isolates have been started to be sequenced (Cottam et al., 2006, Cottam et al., 2008a, Konig et al., 2009), and thus accurately documenting the extent of genetic variability within the whole epidemic. In this respect, the UK 2001 FMD epidemic, where prevalence, incidence and WGS data are fully known, provides an exceptionally suitable testing system for investigating the relationship between viral population dynamics reconstructed using both genetic and epidemiological data. The PhD project here presented made use of the epidemiological data collected during the UK 2001 FMD epidemic in order to investigate the correlation between the real

count of infected cases (derived from either prevalence or incidence data) and the viral demographic history inferred by sequence variability that is recorded from time-stamped WGSs extracted from the field isolates. At the time of starting this PhD research, the Epi-SEQ EMIDA-ERA NET funded project (www.episeq.eu/index_files/Page1077.htm) was focused on the genetic characterisation of the entire UK 2001 FMD collection of clinical samples stored at the WRLFMD, The Pirbright Institute - UK, which theoretically would have been sequenced within the timeframe of this PhD project. Unfortunately, delays have meant that some of the results obtained from this PhD project can only be validated sometime after its completion, when the full dataset of UK 2001 FMDV WGSs will be available. Therefore, the observations and research findings grounded on the results here presented were generated through an evolutionary simulation framework of the whole UK 2001 FMD epidemic, which has been informed by the space-time dynamics of the transmission events as reconstructed using the fully resolved epidemiological data. Hence, the overall aim of this PhD project was to test the hypothesis that inferences on the true number of infected cases can be drawn from patterns of mutation accumulating in sequence data recovered from observed cases, as estimated by transformations of the effective population size N_e. Accordingly, the work here presented attempts to disentangle some key questions in the field of phylodynamics of viral infectious disease, namely:

- ✓ Can the effective population size N_e derived from the BSP be scaled to some epidemiological relevant measure of prevalence?
- ✓ How does the sampling design affect the estimation of virus evolution and population demography?
- ✓ Can sequence data be used to infer unobserved disease events?

Results from this project may have particular relevance in FMD endemic settings where comprehensive sampling is not usually possible and official reporting of outbreaks limited. In this context, a clear understanding of the disease burden is therefore needed, which might be derived from the estimation of the viral population size as a proxy of disease prevalence. In addition, inferences about evolutionary changes on timescales enable the dating of epidemiologically important events and, therefore, independently validating against surveillance data to understand the impact of control measures imposed. Thus, reconstructing and predicting epidemiological dynamics and transmission routes during epidemic events or in an endemic setting

have the potential to inform intervention strategies and control policies In addition, the outcomes derived from this project have many potential and valuable applications not only for FMD but may also be generalised to other RNA viral diseases.

1.3.1 Thesis outline

The work produced in this thesis is structured into seven chapters, which are sequentially presented in a logical *consecutio*. Following this introductory chapter which reviews the studies published in the literature on the topics of FMD and phylodynamics of infectious diseases, Chapter 2 describes a practical example of the use of phylogenetic methods currently employed for reconstructing evolutionary history, demographic signal and the dispersal process of viruses. This study, based on the generation of new sequence data and analyses of 322 VP1 coding sequences, produced a comprehensive phylodynamics picture of the serotype O CATHAY FMDV topotype and its evolutionary adaptation into the Southeast Asia ecosystem. In addition, a detailed historical reconstruction of the FMDV epidemic events reported in the Philippines during 1994 and 2005 has been performed analysing the genetic signal carried by 112 VP1 coding sequences. Results generated from Chapter 2 have been already published in the peer-reviewed journal Veterinary Research (Di Nardo et al., 2014).

Chapter 3 presents the model framework that has been developed with the aim of reconstructing the transmission tree of the UK 2001 FMD epidemic and simulating the entire FMDV alignment of the epidemic, thus generating one WGS for each of the IPs reported to be infected during the outbreak. The metrics of the reconstructed epidemic are presented along with the estimation of its demographic size, as either prevalence or incidence estimation. In addition and as a preliminary attempt to validate the WGS simulation, the metrics of the simulated genetic data with the 39 already characterised WGS isolates (Cottam et al., 2006, Cottam et al., 2008a, Konig et al., 2009) have been compared.

Chapter 4 has been fully devoted to the relationship between the real number of infected cases (as estimated by prevalence or incidence data) and N_e. Using the WGS data derived from the simulation model presented in the previous chapter, the concept of the infection prevalence N^* has been explored to investigate a likely scaling

approach which could potentially link N_e with the real infected population size and, therefore, empowering the conceptualization of genetic data as a proxy for a prevalence measure. For this purpose, empirical prevalence and incidence data extracted from the UK 2001 FMD epidemic have been correlated with the demographic signal carried by the N_e and extracted from the BSP analysis of the WGS simulated data. In addition, further FMDV stationary demographic scenarios, simulated at different degree of population structure, have been tested in order to assess the impact of the variance in the population structure [*i.e.* $var(R_t)$] on the accuracy of the BSP-derived N_e estimates.

Chapter 5 examines the effect of sampling size on the reconstruction of viral demography further using the UK 2001 FMDV WGS simulated data and the N_e scaling formulations derived from Chapter 4. For this purpose, different sampling schemes have been tested from the simple realisation of a random process to more epidemiologically structured schemes, based on the probability proportional to size sampling theory. In addition, estimates extracted from the incomplete sampling BDM have been compared with their coalescent derivation.

Chapter 6 presents a preliminary characterisation of the whole UK 2001 FMD epidemic using an initial set of the WGS (n=154) that have been generated from the archive of clinical samples collected at the time of the outbreak (n=1404). These real data allow us to test the hypotheses derived from the results obtained from the analyses of the simulated data presented in Chapters 3 to 5 and, therefore, to initially validate their assumptions with a relatively small subset of the real WGS data (~11%). In addition, the results here presented attempt to draw the first *sensu scricto* phylodynamic inference from the fully-resolved epidemiological and genetic data of the UK 2001 FMD epidemic.

The final discussion and concluding remarks are then presented in Chapter 7.

CHAPTER 2

Di Nardo *et al. Veterinary Research* 2014, **45**:90
http://www.veterinaryresearch.org/content/45/1/90

VETERINARY RESEARCH

RESEARCH Open Access

Phylodynamic reconstruction of O CATHAY topotype foot-and-mouth disease virus epidemics in the Philippines

Antonello Di Nardo[1,2*], Nick J Knowles[2], Jemma Wadsworth[2], Daniel T Haydon[1] and Donald P King[2]

2.1 Abstract

Reconstructing the evolutionary history, demographic signal and dispersal processes from viral genome sequences contributes to our understanding of the epidemiological dynamics underlying epizootic events. In this study, a Bayesian phylogenetic framework was used to explore the phylodynamics and spatio-temporal dispersion of the O CATHAY topotype of foot-and-mouth disease virus (FMDV) that caused epidemics in the Philippines between 1994 and 2005. Sequences of the FMDV genome encoding the VP1 showed that the O CATHAY FMD epizootic in the Philippines resulted from a single introduction and was characterised by three main transmission hubs in Rizal, Bulacan and Manila Provinces. From a wider regional perspective, phylogenetic reconstruction of all available O CATHAY VP1 nucleotide sequences identified three distinct sub-lineages associated with country-based clusters originating in Hong Kong Special Administrative Region (SAR), the Philippines and Taiwan. The root of this phylogenetic tree was located in Hong Kong SAR, representing the most likely source for the introduction of this lineage into the Philippines and Taiwan. The reconstructed O CATHAY phylodynamics revealed three chronologically distinct evolutionary phases, culminating in a reduction in viral diversity over the final 10 years. The analysis suggests that viruses from the O CATHAY topotype have been continually maintained within swine industries close to Hong Kong SAR, following the extinction of virus lineages from the Philippines and the reduced number of FMD cases in Taiwan.

2.2 Introduction

Foot-and-mouth disease is an economically devastating transboundary disease of cloven-hoofed domestic and wild ruminants, causing an acute and highly contagious vesicular disease which can develop into a persistent infection. The aetiological agent is FMDV, a single-stranded RNA virus belonging to the *Aphthovirus* genus, family *Picornaviridae*. FMDV is characterised by high genetic variability and exists as seven different serotypes named as O, A, C, Asia 1, SAT 1, SAT 2, and SAT 3 (Knowles and Samuel, 2003). As a consequence of their high mutation rate, FMDV lineages quickly diverge as they replicate and spread into new areas. Therefore, transmission of the virus through space and time directly defines the evolutionary patterns observed between related FMDV strains (Knowles et al., 2010b). In addition to the accumulation of nucleotide substitutions through errors, large block of sequence changes can be mediated via recombination between different FMDV genomes, further expanding its evolutionary repertoire. In this context, FMDV populations often exhibit extensive genetic and antigenic heterogeneity at both the molecular and geographical level, driven by co-circulation of multiple lineages, heterogenic mixed host populations, extensive animal movements and trade patterns (Di Nardo et al., 2011). FMDV serotypes have evolved independently in different geographical regions to give rise to distinct genetic lineages, designated topotypes. Eleven topotypes have been defined for serotype O, based on phylogenetic relationships between available sequence data and a value of ~15% of nt sequence difference in the VP1 coding region (Knowles et al., 2010a, Samuel and Knowles, 2001).

2.2.1 The O CATHAY FMDV topotype

The first FMDV strain belonging to the O CATHAY topotype was isolated from Hong Kong SAR from pig samples collected during 1970 (HKN/21/70, GenBank accession no. AJ294911) and was characterised by a 93-102 nt deletion within the 3A coding region that is associated with the atypical porcinophilic phenotype of this FMDV lineage (Knowles et al., 2001a). Subsequently, O CATHAY isolates have been confirmed in several Southeast and East Asian countries (including Malaysia, the Philippines, Taiwan, Thailand and Vietnam), although since 1970, the majority of field cases due to

this topotype have been reported in Hong Kong SAR and China (Gleeson, 2002, Knowles et al., 2005, Cao et al., 2014). The O CATHAY FMD outbreak in Taiwan which began during 1997 resulted in the stamping-out of more than 4 million pigs and generated economic losses of over 6 billion US dollars (Yang et al., 1999). Outside of Asia, viruses belonging to the O CATHAY topotype have been responsible for isolated FMD outbreaks that occurred in Europe in 1981 (Thalheim, Austria), 1982 (Wuppertal, Germany) and 1995 (Moscow, Russia). In the last ten years, O CATHAY FMDV strains causing epizootics have been collected in Hong Kong SAR on a yearly basis, where the last reported outbreak occurred during March 2014. However, FMD viruses belonging to the type O CATHAY topotype are sampled on a more sporadic basis from countries in Southeast Asia, and it is currently unclear where this topotype is maintained and/or how it is dispersed.

2.2.2 FMDV in the Philippines

The introduction of FMD into the Philippines can be dated back to 1902 as a result of the importation of infected cattle from Hong Kong SAR to Manila. Following large epidemics reported in Sorsogon and Bukidnon Provinces in 1920, FMD became widespread in the entire Philippines. FMDV lineages belonging to serotypes A, O and C were identified in samples collected from outbreaks occurring in the Philippines during the period between 1954 and 2005. Major epidemics were caused by type O (from 1972 to 1991), type A (from 1975 to 1983) and type C (from 1976 to 1995) strains (Randolph et al., 2002). The O CATHAY topotype was first detected in August 1994 in a backyard piggery located in Rizal Province. More recently, this FMDV topotype has been the sole lineage responsible for epidemics in the Philippines until December 2005, when the last detected case was confirmed in Quezon Province. The majority of the cases due to O CATHAY were located on Luzon Island, from where FMD spread to 27 provinces. It has been estimated that wholesale market prices of both pork and even chicken in Central Luzon dropped significantly following the start of the epidemic in 1995, highlighting the economic impact of FMD across the entire supply chain (Abao et al., 2014). Since June 2011, the Philippines have been officially declared as FMD-free (without vaccination).

This study explored the phylodynamics of these O CATHAY outbreaks reconstructed through molecular epidemiological analyses of VP1 coding sequences (n = 112) collected between 1994 and 2005. In addition, a wider picture of the O CATHAY topotype phylogenetics was determined from a larger database of currently available VP1 coding sequences (n = 322) to enable the characterisation of geographical movements of this FMDV lineage across historically affected countries of Southeast and East Asia.

2.3 Materials and methods

2.3.1 Sample database

This study accessed archived vesicular fluid and/or epithelium samples (n = 112) from the FAO WRLFMD at The Pirbright Institute, UK, which had been stored at −20 °C in 0.04 M phosphate buffer (M25; disodium hydrogen phosphate, potassium dihydrogen phosphate, pH 7.5) and 50% (vol/vol) glycerol. This dataset represented clinical samples collected in the Philippines from 22 provinces in the period between 1994 and 2005 (Appendix 1). In addition, a further 210 VP1 coding region sequences and representing isolates collected from Austria, China, Germany, Hong Kong SAR, Malaysia, Russia, Taiwan, Thailand and Vietnam (Abdul-Hamid et al., 2011, Beard and Mason, 2000, Carrillo et al., 2005, Hui and Leung, 2012, Knowles et al., 2001b, Knowles et al., 2005, Tsai et al., 2000) were retrieved from both GenBank at NCBI (Benson et al., 2013) and the WRLFMD sequence archive and, then, integrated with the Philippines collection to comprise a total dataset of 322 VP1 coding sequences (Appendix 2) These VP1 coding region sequences have been submitted to GenBank and have been assigned the following accession numbers: KM243030-KM243172.

2.3.2 Viral RNA detection and sequencing

Clinical samples were processed in order to obtain the FMDV VP1 coding sequences (639 nt length, ~8% of the full genome length). Viral RNA for each sample was extracted from virus suspensions using the RNeasy® Mini Kit (QIAGEN® Ltd., UK),

according to the manufacturer's protocol. One-step Reverse Transcription Polymerase Chain Reaction (RT-PCR) to amplify the VP1 region of FMDV was carried out as previously described (Knowles et al., 2009). Primers used for the RT-PCR step were O-1C244F and O-1C272F for the forward, and EUR-2B52R for the reverse orientations (Table 2-1). PCR products were cleaned up using the Illustra GFX™ PCR DNA and Gel Band Purification Kit (GE Healthcare Ltd., UK), and were then cycle-sequenced using the BigDye® Terminator v3.1 Cycle Sequencing Kit (Applied Biosystems, UK). A set of forward and reverse primers was employed to ensure the complete coverage of the VP1 coding region (Table 2-1). Sequencing reactions were analysed using the ABI 3730 DNA Analyzer (Applied Biosystems, USA). Raw data files were assembled into a contig and edited using SeqMan Pro™ 12 (DNASTAR, Inc.), then aligned using Clustal Omega 1.2.0 (Sievers et al., 2011).

Table 2-1. Oligonucleotide primers used for either RT-PCR or cycle sequencing of the VP1 coding region from the FMDV isolates. Start and end locations have been mapped against the Kaufbeuren/FRG/66 type O FMDV isolate (GenBank accession no. X00871) (Forss et al., 1984).

Primer Designation	Primer Sequence (5′ to 3′)	Start - End
Reverse Primers		
NK72	GAAGGGCCCAGGGTTGGACTC	3558 – 3578
EUR-2B52R	GACATGTCCTCCTGCATCTGGTTGAT	3624 – 3649
O-1D487gR	TAATGGCACCRAAGTTGAA	3372 – 3390
O-1D628R	GTTGGGTTGGTGGTGTTGT	3181 – 3199
Forward Primers		
O-1C244F	GCAGCAAAACACATGTCAAACACCTT	2469 – 2494
O-1C272F	TBGCRGGNCTYGCCCAGTACTAC	2497 – 2519
O-1C283F	GCCCAGTACTACACACAGTACAG	2508 – 2530
O-1D296F	ACAACACCACCAACCCAAC	3181 – 3199
O-1C499F	TACGCGTACACCGCGTC	2724 – 2740
O-1C605hF	TGGCCAGTGCCGGTAAGGACTTTGAC	2830 – 2855
O-1C605nF	TGGCTAGTGCTGGCAAAGACTTTGAC	2830 – 2855

2.3.3 Phylogenetic analysis

Before performing the phylogenetic reconstruction, jModelTest 2.1.6 analysis (Darriba et al., 2012, Guindon and Gascuel, 2003) was undertaken to determine the best fitting nucleotide substitution model using the Bayesian Information Criterion (BIC) (Posada and Buckley, 2004). Statistical parsimony (Templeton et al., 1992) was used for reconstructing the genealogical networks as implemented in the TCS 1.21 program (Clement et al., 2000). The network generated was then edited and plotted in yEd Graph Editor 3.13.

A Bayesian analysis framework was employed for phylogenetic and demographic inferences using a MCMC method implemented in the BEAST 1.8.0 package (Drummond et al., 2012). The analysis was performed using the Hasegawa-Kishino-Yano substitution model plus gamma-distributed rates (HKY85+Γ4), and the relaxed uncorrelated lognormal molecular clock model (Drummond et al., 2006, Hasegawa et al., 1985). Demographic reconstruction was employed using the BSP (Drummond et al., 2005). Spatial patterns of FMDV dispersal were estimated through a probabilistic discrete asymmetric diffusion model using a continuous-time Markov chain process, adopting a BSSVS procedure to select among all possible migration pathways (Lemey et al., 2009a). Nonzero rates of virus movement between countries were judged to be supported when the associated Bayes Factor (BF) exceeded 3. The MCMCs were run for 150 million iterations, sub-sampling every 15 000 states. Convergence of the chain was assessed using Tracer 1.5 removing the initial 10% of the chain as burn-in. The Maximum Clade Credibility (MCC) tree was summarised using TreeAnnotator 1.8.0 and constructed using FigTree 1.4.1. Phylogeographic maps were constructed using ArcGIS 10.2.2 (Environmental Systems Research Institute, Inc.).

2.3.4 Statistical analysis

The epidemic curve was constructed using the Handistatus II data for the Philippines retrieved from the OIE website (OIE, 2014). Statistical computations were performed in R 3.1.1 (R Core Team, 2015) and graphs were plotted using the ggplot2 package for R (Wickham, 2009), whereas complex vector images were rendered using Inkscape 0.48.5. To determine the potential extent of recombination in the genetic structuring of the virus population, ratios of per-site recombination rate to the per-site mutation rate (*r*) were estimated using LAMARC 2.1.9 (Kuhner, 2006).

2.4 Results

2.4.1 O CATHAY FMDV country based phylodynamics: the Philippines

A FASTA search (McWilliam et al., 2013) of all publically available VP1 coding sequences was completed to identify a candidate for the most likely common ancestor for the Philippines lineage: the closest match was identified as a sequence from Hong Kong SAR with 99.2% nt identity (HKN/12/91, GenBank accession no. AJ294921). The observed evolutionary distances and total nt changes calculated from the root (HKN/12/91) increased linearly with time (R^2= 0.932; $F_{1,111}$ = 1528, p < 0.001) (Figure 2-1).

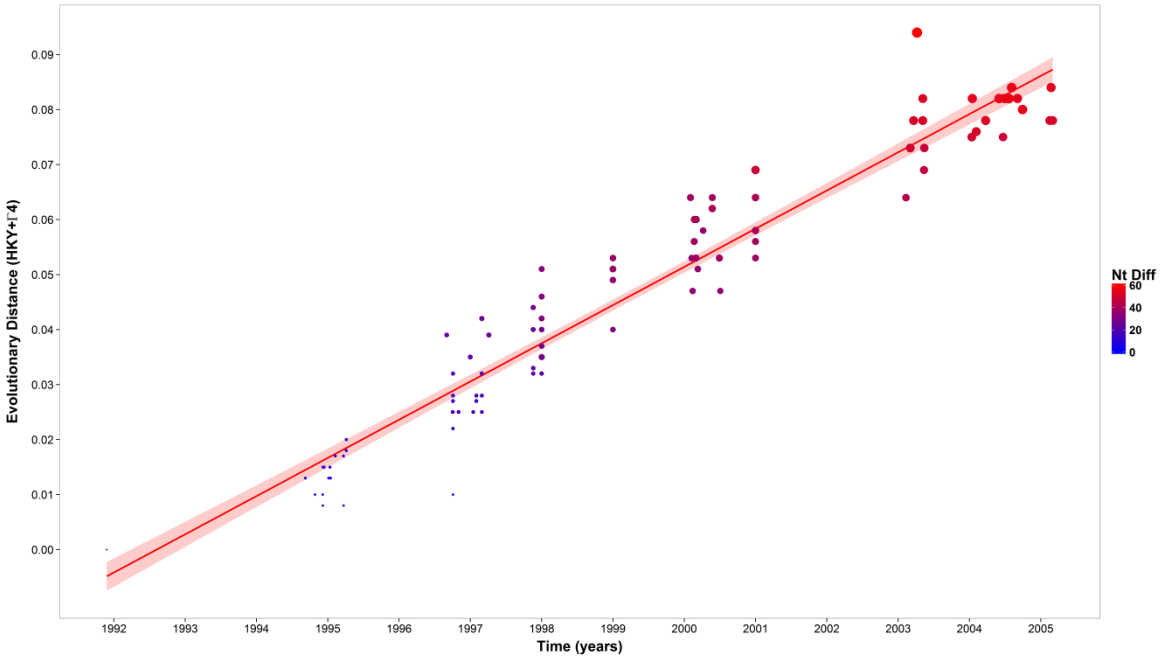

Figure 2-1 Accumulation of nucleotide differences calculated from the putative root (HKN/12/91 isolate) for the Philippines database with time expressed in years. Size of the points increases with increased number of nt substitutions. Shaded area represents 95% confidence intervals for the fitted line.

The number of nt substitutions in the VP1 coding sequences between the first O CATHAY isolate collected in the Philippines in 1994 and the last reported outbreak in 2005 was estimated to be 58, although the maximum number of nt substitutions was reported for the PHI/17/2003 isolate as 69 (maximum genetic distance 0.12 base substitution per site). No indels were found within the entire alignment. In addition, variability in the number of nt changes in samples collected within the same time

window (year) was observed. Average genetic divergences among year groups were estimated to be higher for 2000, 2001 and 2003, which deviate from the average value of 0.023±0.008 base substitutions per site per year (Table 2-2). Geographic distance was found to be significantly correlated with genetic distance ($F_{1,84}$ = 15.92, p < 0.001). A recombination rate (r) of 8.76×10^{-8} per site per generation (site/generation) was estimated for the Philippines indicative of an exceedingly low rate of recombination relative to mutation.

Table 2-2. Genetic, time and geographical pairwise distances (with corresponding standard deviation values) calculated for the within-year Philippines O CATHAY FMDV isolates groups and for each of the country based data from the earliest samples collected within the specific group. Genetic distances were estimated by the Hasegawa-Kishino-Yano substitution model plus gamma-distributed rates (HKY85+Γ4), whereas geographic distance were calculated using the Haversine formula (Sinnott, 1984). Genetic distance is expressed in base substitution per site, time distance is defined in years, whilst geographical distance is measured in kilometres.

Data	No of Samples	Genetic Distance	Time Distance	Geo Distance
Philippines				
1994	7	0.010±0.002	0.23±0.05	-
1995	8	0.013±0.006	0.63±0.77	124.72±95.81
1996	9	0.020±0.004	0.10±0.03	235.66±252.21
1997	14	0.016±0.013	0.38±0.38	119.65±117.12
1998	23	0.011±0.009	-	51.62±42.08
1999	5	0.011±0.002	-	146.83±222.79
2000	16	0.054±0.021	0.16±0.13	296.55±130.74
2001	7	0.057±0.008	-	14.22±4.28
2003	8	0.051±0.013	0.19±0.08	344.45±26.98
2004	12	0.010±0.004	0.41±0.23	322.32±38.83
2005	3	0.005±0.005	0.03±0.01	12.48±17.65
Global				
China	6	0.148±0.081	31.93±19.15	-
Hong Kong	138	0.157±0.022	32.95±7.24	-
Philippines	112	0.047±0.022	4.59±3.50	-
Taiwan	46	0.015±0.025	1.38±3.01	-
Vietnam	13	0.104±0.016	7.84±1.65	-

As estimated by the statistical parsimony network analysis, the MRCA of the Philippines O CATHAY taxon was identified as an unsampled virus 3 nt different from HKN/12/91 and 1-3 nt different from the earliest Philippines isolates collected between late 1994 and the start of 1995 (Figure 2-2). The diameter of the parsimony network between the MRCA and the most divergent FMDV isolate collected in 2004 (PHI/5/2004) was estimated to be 86 nt substitutions, of which 83 (96.51%) were synonymous and 3 (3.49%) non-synonymous. The average of number of nt substitutions incurred per year (nt/yr) of any isolate from its closest sampled ancestor was estimated to be 9.9±4.8, comprising an average of 8.8±4.2 synonymous and 1.0±0.9 non-synonymous changes, indicative of an average rate of change for VP1 sequences in the Philippines of approximately 1.5% per year. The average number of

changes for each isolate was 4.0±2.3 nt/yr, of which 3.4±2.1 and 0.6±0.5 were synonymous and non-synonymous substitutions, respectively.

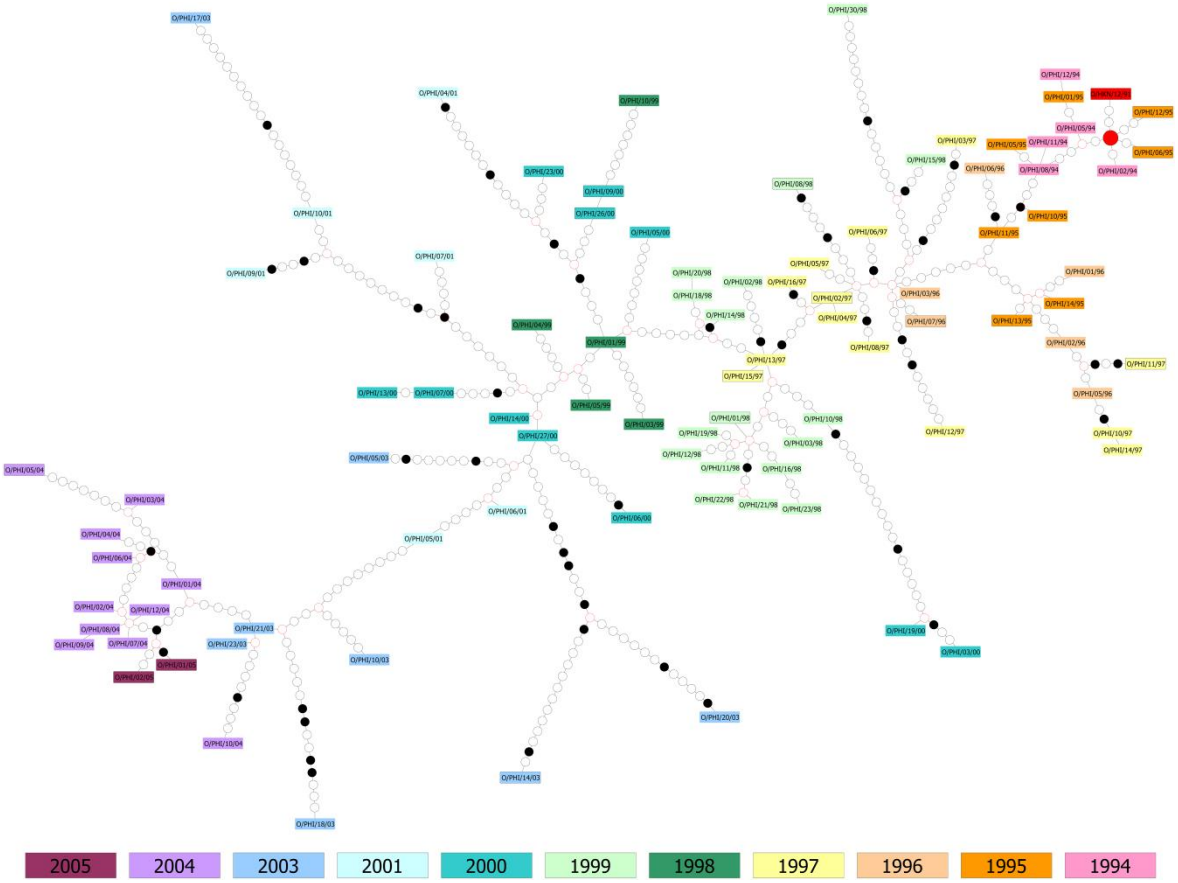

Figure 2-2 Network extracted from the statistical parsimony analysis performed in TCS for the Philippines isolates (n = 112). VP1 sequences are designated with their WRLFMD number and coloured by year of collection, where the outlier (HKN/12/91) is defined with a red box. The MRCA for the Philippines O CATHAY FMDV taxon is highlighted in a red ellipse. Black dots specify non-synonymous substitutions, whereas white dots represent synonymous substitutions. The year codes in the virus isolate labels have been abbreviated to the last two digits.

Most sequences clustered according to time across the network, although FMDV isolates collected in 2000 were assigned within three separate genetic lineages, resulting in three evolutionary pathways one of which was a dead-end. In addition, for some links more recently collected viruses were assigned earlier in time on the network. The case of PHI/12/94 which was found to be a descendant of PHI/1/95 can in part be explained by the short time distance which separates these two isolates (32 days) and it might be that both strains (or their ancestors) were co-circulating at time of sampling. The reconstructed phylogeny further defined these two viruses as being closely related (genetic distance of 0.002 base substitutions per site). Conversely, samples collected in March (PHI/9/2000) and June 2000 (PHI/26/2000) were determined to be the source of a virus collected in 1999 (PHI/10/99), although the 2000 isolates were direct descendants of a virus detected in January 1999 (PHI/1/99).

Looking in detail at this case, the phylogeny found descent of PHI/10/99, PHI/9/2000 and PHI/26/2000 from the same common ancestor. These samples were collected from the same region (Central Luzon) within an area of ~40 km of radius, potentially explaining the inconsistent result provided by the TCS analysis to have arisen from sampling bias. The discrete states analysis resolved the relationship of the PHI/10/99, PHI/9/2000 and PHI/26/2000 isolates rooting those from a common ancestor that descends in turn from an unsampled virus source both seeded from Bulacan Province, which includes the PHI/1/99 sample (Figure 2-3).

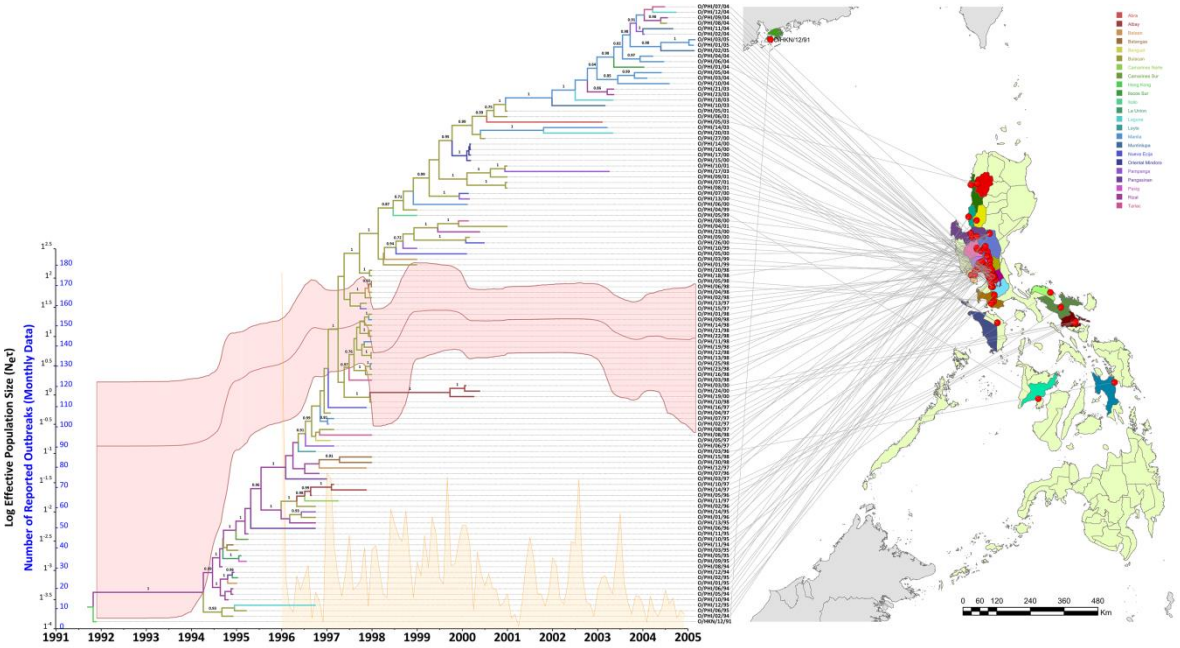

Figure 2-3 Phylodynamic reconstruction of the O CATHAY FMDV epidemics in the Philippines. Maximum clade credibility tree branches are coloured according to the most likely transmission source as reconstructed from the discrete states model. Nodes with a posterior probability value ≥0.7 are shown. FMDV demography is expressed by log Effective Population Size ($N_e\tau$) as estimated from the BSP along with the monthly epidemic curve reconstructed from the data retrieved from the OIE Handistatus II database (OIE, 2014).

The molecular clock for the O CATHAY Philippines lineage was estimated to be 1.25×10^{-2} nt/site/yr (95%HPD 9.47×10^{-3} to 1.57×10^{-2}) with a standard deviation of 0.70 (95%HPD 0.49 to 0.91). No evidence of autocorrelation of rates in the reconstructed phylogeny was provided by the covariance value of 2.65×10^{-3}. The introduction date, the TMRCA, of the type O CATHAY topotype FMDV lineage into the Philippines was calculated to be the 30th of March 1994 (95%HPD 07/08/1993 to 08/08/1994, a time interval which included the date of the first officially reported case).

The reconstructed FMDV population dynamics from the skyline plot (Figure 2-3) describes a demographic history characterised by three phases. In the first phase, after an initial exponential increase from mid-1994 until late 1997 at a rate that decreased from late 1996, a sudden and short period of decline was observed, resulting in a population bottleneck. Since genetic bottlenecks correspond to significant reductions in population size, these changes in the O CATHAY population dynamics in the Philippines probably link to the launch of an extensive control plan in 1996 that was successful in limiting the further spread of FMD and thereby reducing the number of outbreaks (Randolph et al., 2002). However, during 1999 a new FMD outbreak occurred within an already declared FMD-free zone, the Panay region. Therefore in the second phase, the skyline trajectory recorded a second rapidly increasing viral population size starting in mid-1998 and lasting up to the first months of 1999, which resulted in a diversification of viral lineages. In the third phase, the viral population size reached a plateau until late 2002, when further control policies resulted in a steady decline in FMD prevalence until eradication.

The epidemic curve drawn from the field epidemiological data from the OIE for the period 1995-2005 (OIE, 2014) described an oscillatory trend in the number of FMD outbreaks reported in the Philippines, with times of high epidemic peaks interleaved by low-level FMD circulation. The frequency of these oscillations was higher between 1997 and the beginning of 2000 (a monthly average of 37.9 FMD outbreaks), after which the number of FMD outbreaks started to decline following periods of low reporting (with a monthly average of 19.8 FMD outbreaks). However, the reported epidemic trend did not overlap with the skyline plot trajectory, although the epidemic window from mid-2000 to 2005 characterised by a reduced number of outbreaks could be evinced by the plateauing and subsequent decrease in the genetic diversity of the skyline plot. It should be noted that although more than 300 outbreaks were officially reported through OIE during 2002, no clinical samples (and thus genetic information) were collected within that time window.

According to the results obtained by the discrete states phylogeography analysis, the root of the Philippines taxon was found to be from Rizal Province, consistent with the location of the first officially reported cases of O CATHAY topotype in the Philippines during August 1994 (Figure 2-3). Three main epidemic hubs could be identified from the analysis: the first from the beginning of the epizootic up to mid-1996, where outbreaks were found to be seeded from Rizal Province; the second

lasting until 2001, where Bulacan Province was estimated to be the main source of FMD spread; and lastly, Manila Province as the last epidemic hub. The movement transitions between the three main epidemic hubs were supported by Bayes factor values of >24 [pk = 1.0] for movements from Rizal to Bulacan and from Bulacan to Manila, respectively.

2.4.2 Global and regional phylodynamics of O CATHAY topotype FMDV

The molecular clock rate for all the O CATHAY topotype VP1 data was estimated to be 1.06×10^{-2} nt/site/yr (95%HPD 8.99×10^{-3} to 1.23×10^{-2}), with a standard deviation of 0.81 (95%HPD 0.67 to 0.94). This value was comparable with the molecular clock rate reported for the Philippine isolates only. The MRCA for the O CATHAY topotype was estimated to have been present between 1955 and 1960. The r recombination parameter returned a value of 8.3×10^{-9} site/generation indicating a very low influence of recombination relative to mutation.

Three distinct sub-lineages were identified by the wider phylogenetic reconstruction that included the full database of O CATHAY VP1 coding sequences, which were clustered on a country level basis (Figure 2-4).

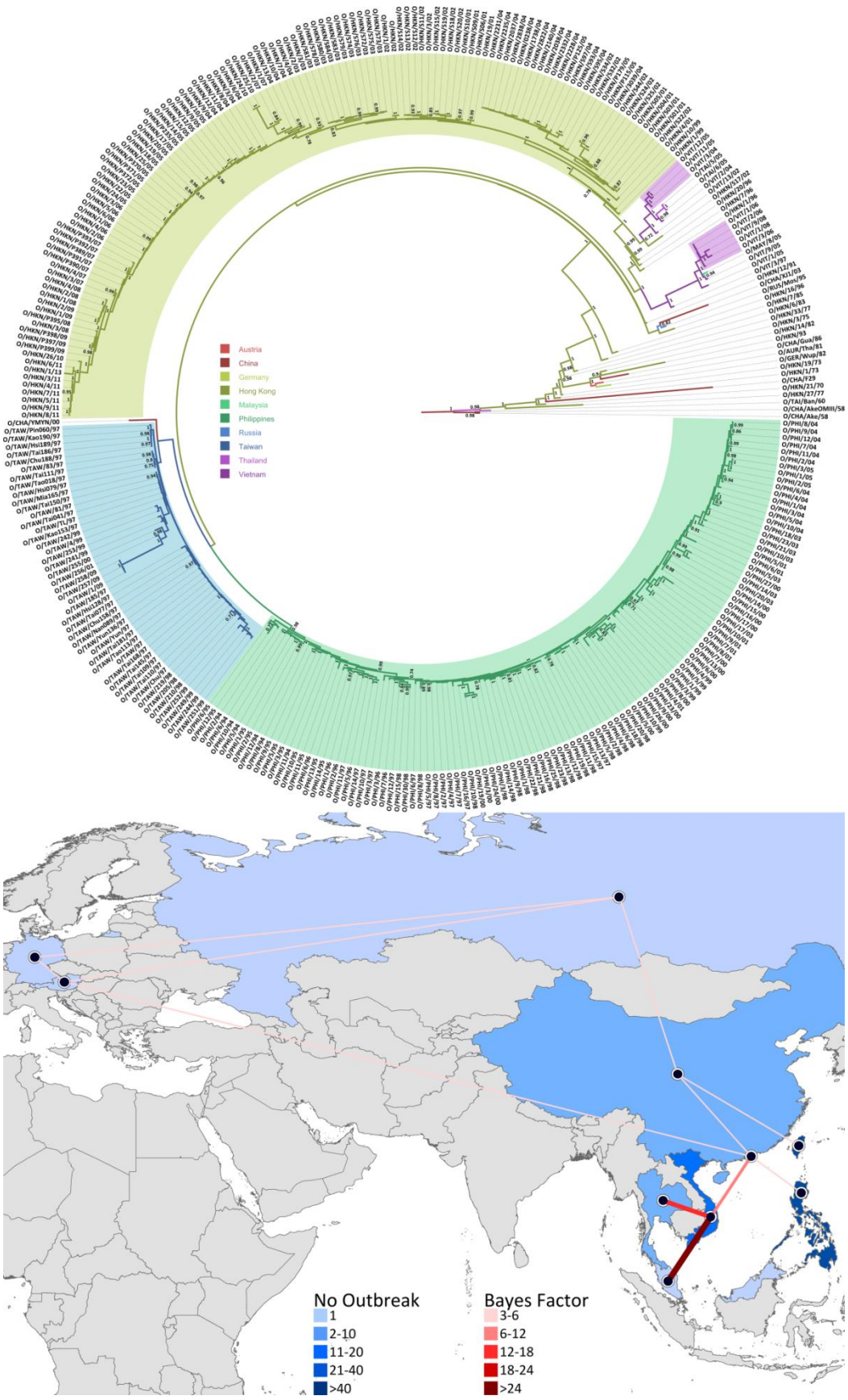

Figure 2-4 Maximum clade credibility tree for all the O CATHAY FMDV isolates sequenced (n = 322). Nodes with a posterior probability value ≥0.7 are shown. Branches are coloured according to the most probable country of the node from which they descended as estimated from the discrete state phylogeographic Bayesian model. Geographical links between countries identified by the BSSVS analysis are coloured by the corresponding BF value. The year codes in virus isolate labels have been abbreviated to the last two digits. The geographical locations are defined with the country centroid.

The FMDV strains circulating in the Philippines were found to have descended from a common ancestor that was shared with the Taiwanese isolates, in line with what was proposed to be the source of introduction of the O CATHAY virus into the Philippines in 1994 (Knowles et al., 2005). In turn, the Taiwanese cluster descended from an unsampled virus closely related to a FMDV isolate collected from China in 2000. The Hong Kong SAR isolates were defined in a separate phylogenetic cluster along with FMDV samples collected from countries in mainland Southeast Asia (Malaysia, Thailand and Vietnam). This finding is in contrast to that previously reported (Hui and Leung, 2012), which designated the Taiwanese lineages descending from a common ancestor with the Hong Kong SAR isolates, and identified the Philippines lineages as a distinct phylogenetic cluster. Hui and Leung (2012) inferred the phylogenetic relationship employing a Neighbor-joining method; nevertheless, estimating the phylogeny using a maximum-likelihood method (Guindon et al., 2010) did not alter the shape of the reconstructed phylogeny [data not shown]. The three phylogenetic clusters shared a common ancestor related to a FMDV strain collected in Hong Kong SAR in 1991 (HKN/12/91), which was in turn a descendent from other Hong Kong SAR isolates related to more recent samples obtained from Russia (1995), Hong Kong SAR (1996) and China (2003). FMDV isolates collected from countries of mainland Southeast Asia were phylogenetically grouped into two distinct clusters: the first (MRCA dated 1997) including the first O CATHAY virus isolate from Vietnam in 1997 from which viruses were collected in 2005-06 and 2008, and the only isolate from Malaysia (2005) was sourced; the second (MRCA dated 1998) associated with a later introduction of an O CATHAY strain in Vietnam in 2002, from which viruses isolated in 2004-05, and FMDV sequences from Thailand (2005) were related. The FMDV ancestor of the first mainland Southeast Asia sublineage was dated circa mid-1993, directly descending from the oldest MRCA of the Hong Kong SAR cluster, whereas the second sublineage was circulating in late 1998 and closely related to a virus collected in Hong Kong SAR in 2002. This phylogenetic picture supports two potential introductions of the O CATHAY FMDV lineage into Vietnam from Hong Kong SAR.

The MRCA shared between the Philippines and Taiwanese phylogenetic clusters was estimated to have been circulating in 1993 (95%HPD 1992 to 1994), whereas the origin of the MRCA for the more recent O CATHAY FMD epidemics in the Southeast and East Asia regions was dated 1991 (95%HPD 1990 to 1992). No other virus introduction or escape was ascribed to the Philippines O CATHAY FMD epidemic history, suggesting

the Philippines sub-lineage to be monophyletic. In contrast, Hui and Leung (2012) described two different FMDV introductions into the Philippines, assigning the PHI/5/95 isolates within the phylogenetic cluster which includes the Taiwanese isolates. However, the tree node that governed this inclusion had a bootstrap value of <70, suggesting uncertainty in the assignment of these descendants.

As estimated by the discrete phylogeography model, the root of the entire phylogenetic tree was reported to be in Hong Kong SAR and, therefore, representing a likely source for the introduction of the O CATHAY lineage into the Philippines and Taiwan. This is confirmed by the estimated BSSVS parameters, for which China and Hong Kong SAR were assessed as the main hubs of FMDV spread between countries (Figure 2-4): China was found to be the source for Hong Kong SAR (BF = 5.6, pk = 0.60), Taiwan (BF = 5.07, pk = 0.58) and Russia (BF = 4.33, pk = 0.54), whilst Hong Kong SAR was identified as the source of FMD transmission to Vietnam (BF = 6.75, pk = 0.65) and the Philippines (BF = 3.16, pk = 0.46). The link found between China and Russia reinforces the hypothesis that Chinese pork shipments were responsible for the introduction of the O CATHAY lineage into Moscow, Russia during 1995 [6]. Vietnam was estimated as a recipient of viruses moving from Malaysia (BF = 23.25, pk = 0.86), Thailand (BF = 12.55, pk = 0.77) and Hong Kong SAR (BF = 6.75, pk = 0.65). The most likely routes of chronological introduction of the FMDV O CATHAY lineage into Europe were identified to be from Hong Kong SAR to Austria (BF = 3.14, pk = 0.27). The virus movement within Europe has been identified from Austria to Germany (BF = 5.15, pk = 0.58). Thus supported by the Bayesian phylogenetic and BSSVS analyses, the historical movement of the FMDV type O CATHAY lineage across Asia might be temporally and spatially reconstructed as represented in Figure 2-6.

The historical phylodynamics of the FMDV O CATHAY lineage, as reconstructed by the skyline model using the full currently available VP1 coding sequences database (Figure 2-5), underwent three distinct and chronologically consequent evolutionary stages.

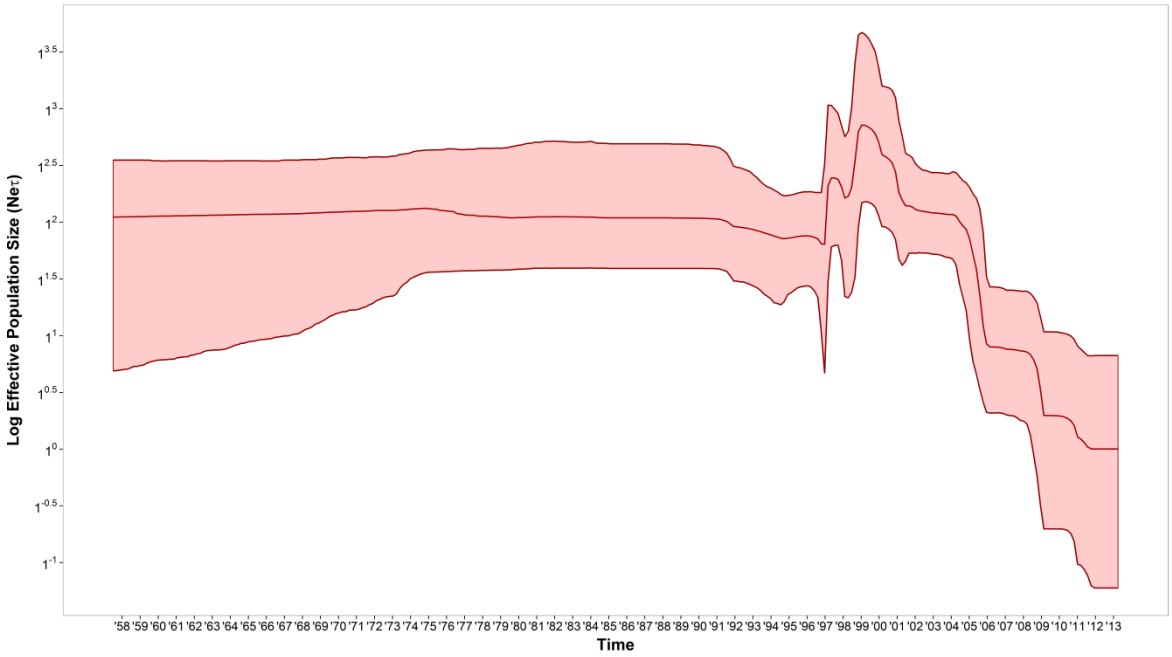

Figure 2-5 BSP of log effective population size ($N_e\tau$) against time in years estimated from the full O CATHAY FMDV database. Light red ribbon defines the 95% HPD interval area.

In the initial stage, the genetic diversity was roughly constant until 1997, after which there were two increasing phases within a period of 3 years from 1997 to 2000, with the highest peak in 1999. The last stage is characterised by four sequential declining phases, with a rapid sharp drop between 2004 and 2006. This triphasic phylodynamic feature might be associated with an oscillatory tendency of FMDV genetic diversity driven by a first expansion phase due to the introduction of the virus into Taiwan and Vietnam and the trigger of the Philippines epidemic, and a later contraction phase following steps taken to eradicate the disease from the Philippines and the decrease in the number of outbreaks reported from Taiwan, characterised by the period between 2001 and 2009 when few cases were reported. This assumes that the FMDV type O CATHAY topotype has been maintained constantly within the Hong Kong SAR livestock system.

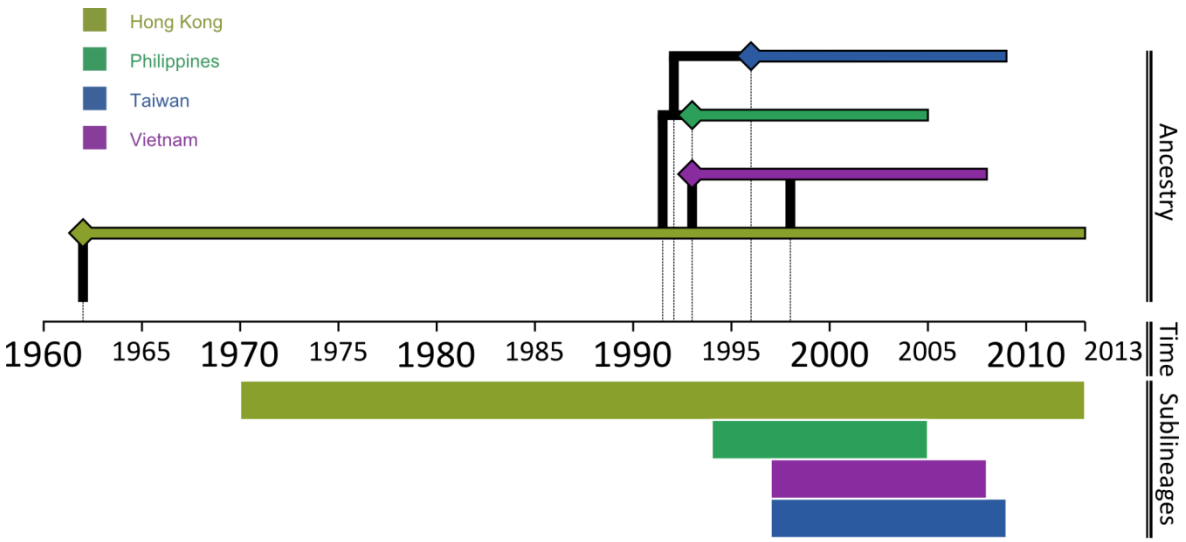

Figure 2-6 Chronological evolutionary trend and transmission ancestry of the O CATHAY FMDV topotype in Southeast Asia.

2.5 Discussion

The evolutionary dynamics of the O CATHAY topotype of FMDV have been analysed allowing the transmission dynamics to be reconstructed across countries in Southeast Asia that have been impacted by this lineage. The O CATHAY FMDV strains isolated from outbreaks reported in Hong Kong, Taiwan and Philippines were defined as belonging to three different sublineages, which were related by a shared common ancestry to an unsampled FMDV strain sourced from Hong Kong SAR. The O CATHAY FMD epizootic in the Philippines resulted from a single introduction and was characterised by three main transmission hubs in Rizal, Bulacan and Manila. Although the evolutionary dynamics of the O CATHAY FMDV lineage were described by three phases from the skyline reconstruction, this was not entirely consistent with the monthly epidemic curve (Figure 2-3). This could be either due to a spatio-temporal bias in the genetic information analysed or in the incompleteness of the outbreak reporting database used, or both.

The phylodynamics of FMDV reconstructed from the FMDV type O CATHAY VP1 coding sequences indicates a marked reduction in viral diversity in the last 10 years, corresponding to the eradication of FMD in the Philippines and the more limited disease events experienced in Taiwan. Furthermore, the introduction of the FMDV type O SEA topotype Mya-98 lineage into Hong Kong SAR during 2010 could have reduced the genetic diversity within O CATHAY lineages through direct competition with

available hosts, as well as the presence of cross-protective antibodies in convalescent animals. These findings indicate that the O CATHAY topotype is maintained in the Hong Kong SAR ecosystem and sporadically spread from there to other Southeast Asian countries, as would be the case for the Philippines in 1994 and Vietnam in 1997. However, few O CATHAY FMDV strains have been reported from mainland China, which has the largest swine production industry in the world (representing over 51% of the world's pig population). These few isolates were collected in 1986, 2000, 2001 and 2003, therefore sampling bias or underreporting of epidemic events occurring in China would likely have an impact on assessing the geographical movements of the FMDV type O CATHAY topotype. It is, nevertheless, clear from the analysis that a transmission link exists between China and Hong Kong SAR, thus indicating a historically southward movement of the O CATHAY FMDV lineage.

The molecular clock estimated here for the O CATHAY topotype is at the high end of evolutionary rate estimates for FMDV. Previously estimates reported an average evolutionary rate across all FMDV serotype of 2.48×10^{-3} nt/site/yr (Tully and Fares, 2008), while rates of 3.14×10^{-3}, 1.3×10^{-3} and 4.8×10^{-3} nt/site/yr were reported for serotype O (Tully and Fares, 2008, Yoon et al., 2011a, Jenkins et al., 2002). In addition, lineage-based FMDV molecular clock rates of 2.8×10^{-3}, 6.65×10^{-3}, 7.81×10^{-3} and 2.7×10^{-3} nt/site/yr were previously estimated for the O-PanAsia lineage in India, O-PanAsia-2 sublineage in Pakistan and Afghanistan, and type O in East Africa, respectively (Balinda et al., 2010a, Hemadri et al., 2002, Jamal et al., 2011a). The higher rate of FMDV evolution reported for the A Iran-05 FMDV lineage in Afghanistan and Pakistan (1.2×10^{-2} nt/site/yr) (Jamal et al., 2011c) was similar to the molecular clock for the O CATHAY topotype estimated by this study. Therefore, genotypically and regionally variable evolutionary rates may in fact reflect real differences in the epidemiological dynamics and host-interaction of FMDV.

Although using a large database of FMDV isolates and generating a comprehensive picture of the O CATHAY topotype evolutionary history, this study has some limitations largely derived from the nature of the genetic data used for the analysis. The VP1 coding region, although defining only ~8% (639 nt of length) of the complete FMDV genome, is the most variable section of the FMDV genome and is historically used for tracing the movement and spread of FMD globally (Knowles and Samuel, 2003, Samuel and Knowles, 2001) and, furthermore, provides the basis for FMDV genotype definition (Knowles et al., 2010a). Analysing a larger part of the FMDV

genome, such as the whole capsid region or the full-length genome, would produce results with a higher resolution (Cottam et al., 2006, Cottam et al., 2008b). However, it should be noted that recombination events seem to be more widespread in other part of the genome (Carrillo et al., 2005, Jackson et al., 2007, Wright et al., 2013), thus representing a limitation in interpreting results based on full-length genome analysis of large scale FMDV evolutionary studies. The ratio of per-site recombination to mutation rate here estimated from the full currently available FMDV type O CATHAY topotype VP1 coding sequences database is very low indicating that these results are not influenced by the process of recombination.

CHAPTER 3

A model framework for simulating space-time epidemiological and genetic data

3.1 Rationale

As reviewed in Chapter 1, an extensive literature has been devoted to the topic of phylodynamics for linking the population genetic concept of effective population size N_e with the evolutionary dynamics of virus transmission in space and time. However, studies published on this topic had rather limited focus on trying to disentangle the relationship of N_e with the actual number of infected cases. In addition, no studies have endeavoured to compare viral population dynamics derived from genetic sequences with empirical data observed from a completely sampled large epidemic where either prevalence or incidence are accurately observed through time. One exceptional example of a fully-resolved real disease epidemic is the UK 2001 FMD event, which is currently the largest and most completely sampled virus disease epidemic. To study the relationship between the dynamics as reconstructed from viral sequences and the actual count of infected cases over time, a thorough investigation of the fully-resolved UK 2001 FMD epidemic making use of the epidemiological data extracted at the time from the field outbreak investigation was undertaken. As discussed in §1.3, the genetic component of the epidemic was fully simulated for the entire epidemic using an evolutionary model parameterised from the 39 already characterised sequence data (Cottam et al., 2006, Cottam et al., 2008a, Konig et al., 2009). In order to generate a complete epidemiological and genetic dataset in which prevalence, incidence and WGS are linked to the fully-resolved transmission tree, a model framework has been built for:

- ✓ Reconstructing the transmission tree underlying the UK 2001 FMD epidemic using the epidemiological data and, therefore, providing a *who-infected-who* transmission network;

- ✓ Using the transmission tree as a backbone for simulating an FMDV WGS for each IP generated from a Markovian evolutionary model informed with data extracted from prior FMDV genetic analyses;
- ✓ Estimating the virus demographic history from the simulated WGS using the BSP and comparing this with the empirical prevalence and incidence data extracted from the UK 2001 FMD epidemiological data.

The model framework here described constitutes the mainstay algorithm for generating the WGS data that will be used in subsequent chapters for investigating in detail the influence of sampling and population structure in the relationship between reconstructed demographic history from sequence data and the actual count of infected cases, and its scaling formulations.

3.2 Model Framework

3.2.1 Data

The FMD epidemic affecting the UK in 2001, was caused by a virus belonging to the FMDV type O PanAsia lineage (Knowles et al., 2001b), and 2026 farms were confirmed at the time of the epidemic event as IPs. The introduction of FMDV into UK has been attributed to the illegal importation of infected or contaminated meat or meat products which were consumed as swill feed to pigs reared at Burnside Farm, Heddon-on-the-Wall (IP04) (DEFRA, 2002). The movement of the pigs from IP04 to the Essex abattoir (IP01) was the trigger and spread of the first phase of the epidemic in Essex and Kent, which started on the 19th of February (Gibbens et al., 2001). A second phase of the epidemic that was country wide was attributed to the airborne spread of FMDV from IP04 to sheep at Prestwick Hall Farm, Callerton (IP06), from where infected sheep were moved and sold in markets located in Hexham (Northumberland) and Longtown (Cumbria) thus resulting in the dissemination of the disease in multiple clusters throughout England and Wales (Gloster et al., 2005, Konig et al., 2009). In order to control the outbreak, a national ban on animal movements along with the culling of all susceptible animals on confirmed IPs and Direct Contacts (DCs) was introduced on the 23rd of February; thereafter, the control ('stamping out') measures were intensified

from the 31st of March and the so called 24/48 hour IP/CP culling policy (*i.e.* the culling of animals present in any contiguous premises to an infected IP within 48 hours) was adopted (Kao, 2002). The last case was reported the 30th of September in Cumbria.

3.2.1.1 Epidemiological data

Epidemiological data were retrieved from the original DEFRA database (Table 3-1), which consisted of information collected from each IP through paper forms during the veterinary field inspections (Taylor, 2012). The database was inspected for missing and/or illogical values and completed and/or corrected whenever possible.

Table 3-1. Description of observed epidemiological variables with associated symbols entered in the model.

Symbol	Details
ID	Index number of IP
K	Set of IPs
Y^{lon}	Longitude Y – decimal degree ($Y^{lon} = \{Y_k^{lon}: k = 1, \dots, K\}$)
X^{lat}	Latitude X – decimal degree ($X^{lat} = \{X_k^{lat}: k = 1, \dots, K\}$)
T^{les}	Time of oldest lesion (first observation of FMD) in IP ($\boldsymbol{T^{les}} = \{T_k^{les}: k = 1, \dots, K\}$)
T^{rep}	Time of report of IP ($T^{rep} = \{T_k^{rep}: k = 1, \dots, K\}$)
T^{sam}	Time of sample collection from IP ($T^{sam} = \{T_k^{sam}: k = 1, \dots, K\}$)
T^{rem}	Time of removal of IP ($T^{rem} = \{T_k^{rem}: k = 1, \dots, K\}$)
L^{age}	Age of oldest lesion – time from infectiousness to report – in IP ($\boldsymbol{L^{age}} = \{L_k^{age}: k = 1, \dots, K\}$)
N^{tot}	Total population of animals in IP ($N^{tot} = \{N_k^{tot}: k = 1, \dots, K\}$)
S^{rep}	Viral sequence sampled in IP at time T^{sam} ($S^{rep} = \{S_k^{rep}: k = 1, \dots, K\}$)

3.2.1.2 Genetic data

Genetic data were retrieved from the database of FMDV isolates collected during the UK 2001 FMD epidemic and previously sequenced by the WRLFMD, The Pirbright Institute - UK (Cottam et al., 2006, Cottam et al., 2008a, Konig et al., 2009), which consists of 39 FMDV WGSs (Appendix 3).

3.2.2 Transmission tree reconstruction

A transmission tree is a directed acyclic graph which describes the '*who-infected-who*' network topology (Figure 3-1). The model here developed for reconstructing the transmission tree between-premises was an individual-based

model of disease transmission, which provided a representation of the FMD infection dynamics that takes into account the timing and location of cases (Figure 3-1), and was constructed on a farm level (*i.e.* farms are considered as single epidemiological units), therefore omitting the potential impact of within-farm epidemic dynamics. Hence, for the purposes of these models it was assumed that FMD spread within a farm is instantaneous with all the animals that contribute to the transmission network becoming infected and subsequently infectious together. In addition, this model considered a single homogeneous virus population that was introduced on to each new farm and, following possible mutation, a single homogenous virus population transmitted onward. All but one premises started as susceptible, where the first infected premises is assumed to have been infected from an external source. FMD has a staged progression in time and, therefore, can be represented in a series of successive disease stages. These stages can be described as infected, infectious, reported and removed. Consider a set of K infected premises and let J be a function defining the transmission tree, a premise k at location (X_k^{lat}, Y_k^{lon}) is infected at time T_k^{exp} by a source i. Following a latency period T_k^{lat}, k becomes infectious at time T_k^{les} (the time at which the oldest lesion would have first become apparent), is reported at time T_k^{rep}, and is removed from the susceptible population at time T_k^{rem}. During the reporting of IP k, the interval between becoming infectious and reporting is assessed in the field by experts based on the ageing of the oldest clinical lesion L_k^{age} observed on the premise. The clinical sample is collected at time T_k^{sam}, thus, also defining the time a viral sequence S_k^{rep} is obtained.

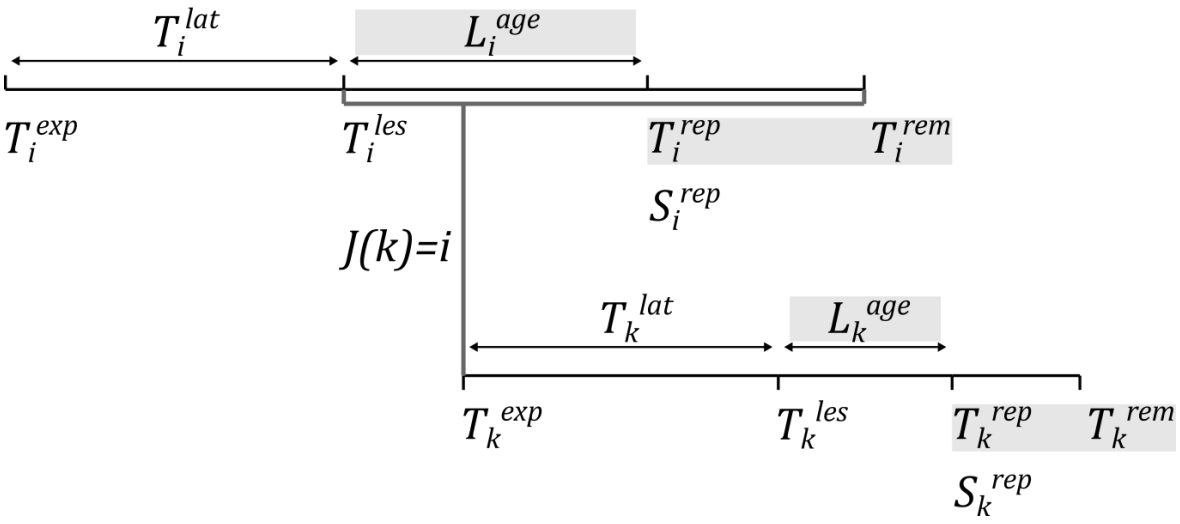

Figure 3-1. FMDV transmission between a parent IP *i* and a daughter IP *k*. Grey rectangles indicate observed variables.

The transmission tree J was estimated using the observed data recorded during the UK 2001 FMD epidemic (Table 3-1). The unobserved latency period T^{lat} for each IP was randomly sampled from a gamma distribution $\Gamma(\kappa, \theta)$ with shape and scale parameters set to be κ=22.12 and θ=0.22, respectively, which defines an interval with a mean of 4.87 and variance 1.07 (Figure 3-2) (Charleston et al., 2011, Mardones et al., 2010). The time to infection, T^{exp}, was assumed to be $T^{exp} = T^{les} - T^{lat}$. Time zero was assumed to be T_{IP4}^{exp} and IP4 to have been infected by an external source.

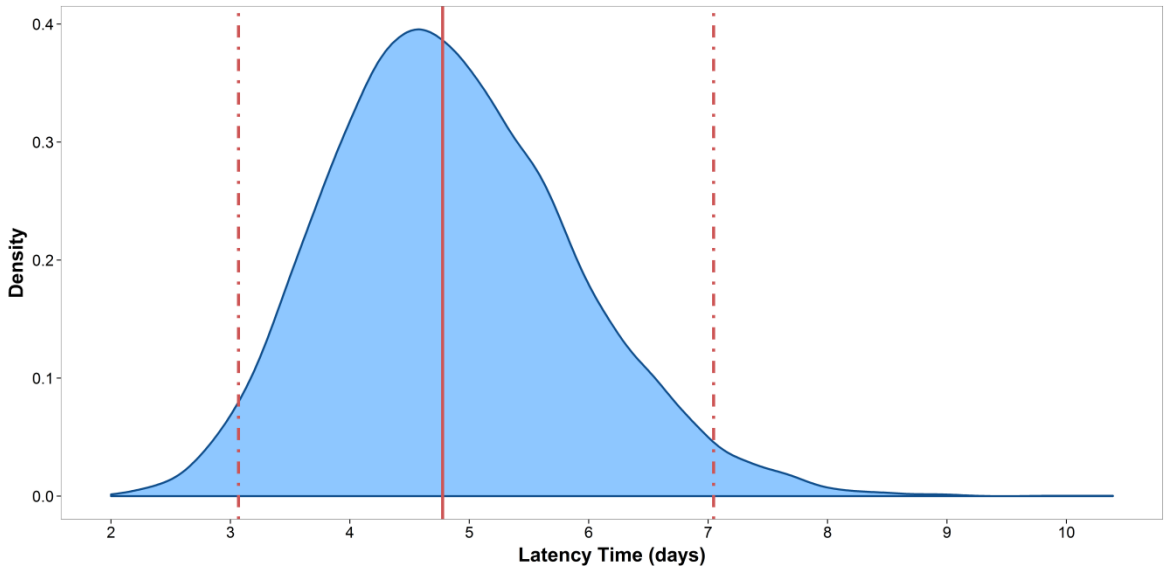

Figure 3-2. Gamma probability density function $\Gamma(\kappa, \theta)$ for the latency time variable. Solid line: median; dash-dotted lines: 0.025 and 0.975 quantiles.

3.2.2.1 Spatial transmission

FMD transmission between IPs was modelled using a kernel-based approach, similar to that used previously for avian influenza (Truscott et al., 2007), FMD (Chis Ster and Ferguson, 2007, Chis Ster et al., 2009) and bluetongue (de Koeijer et al., 2011). Accordingly, the force of infection λ experienced by a susceptible IP k from an infected IP i at time t was assumed to be:

$$\lambda_{ik} = \beta S_k K(d_{ik}) I_i(t)$$

where β was the transmission rate parameter (set as 5.8×10^{-5}) (Haydon et al., 1997); $S_k = sN_k^{tot}$ (s=15.2) and $T_i = tN_i^{tot}$ (t=4.3×10^{-7}) identify, respectively, the per-capita susceptibility and the per-capita transmissibility parameters for the total animal population N^{tot} on any given IP (Keeling et al., 2003). The distance kernel $Z(d_{ik})$ was implemented as a density-independent formulation and was given by:

$$Z(d_{ik}) = \frac{z(d_{ik})}{\sum_{k \neq i} z(d_{ik})}$$

where the geographical distance d between the IP locations was calculated using the Haversine formula (Sinnott, 1984). The spatial dispersion kernel $z(d_{ik})$ was implemented as a power-law function (Chis Ster and Ferguson, 2007) given by:

$$z(d_{ik}) = \left(1 + \frac{d_{ik}}{\alpha}\right)^{-\gamma}$$

The kernel offset (α) and power (γ) parameters were retrieved from the literature (Chis Ster and Ferguson, 2007, Chis Ster et al., 2009). The transmission probability from an infected IP i to a susceptible IP k at time t is then given by:

$$p_{ik} = 1 - e^{-\lambda_{ik}(t)}$$

The algorithm used to infer the most likely transmission tree (Figure 3-3) implemented a maximum-likelihood approach with a discrete time step (*i.e.* one day) for evaluating time dependencies between any source and recipient IP pairs given the transmission probability of link. The parent-daughter links were stochastically assigned using a multivariate trial based on their estimated likelihoods.

3.2.2.2 Prevalence and incidence estimation

Prevalence and incidence curves were based on three estimates, which corresponded to the time of three disease stages set for each IP and as described in

§3.2.2. The P^{exp} prevalence assumes infection to be defined over the interval from exposed to culled. The P^{les} assumes infection to be defined over the interval from the appearance of lesions to culled. The P^{rep} assumes infection is defined over the interval from reporting to culled, and in each case prevalence at any point is the number of farms infected when infection is defined by these different ways. The I^{exp} incidence estimates the number of new exposed IPs at each time (expressed in days) over the entire duration of the epidemic; the I^{les} incidence estimates the number of new IPs showing lesions at each day; I^{rep} incidence estimates the number of new IPs being reported each day over the entire course of the epidemic. These measures could be arbitrarily classified as exposure prevalence/incidence (*e.g.* P^{exp} prevalence), infectious prevalence/incidence (*e.g.* P^{les} prevalence) and reporting prevalence/incidence (*e.g.* P^{rep} prevalence).

3.2.2.3 Computing the generation time

Several definitions of generation time are present in the literature. The epidemiological generation time is the time interval between sequential cases, which is assumed to be equal to the duration of infectiousness (Fine, 2003, Svensson, 2007, Pomeroy et al., 2008, van Ballegooijen et al., 2009). However, Kenah et al. (2008) refer to the above epidemiological quantity as the generation interval, where the generation time is recognised to be the average duration of infection, which is longer than the generation interval during the exponential phase of an epidemic and shorter in the decline phase (Koelle and Rasmussen, 2012). Others studies describe the generation time as the prevalence-to-incidence ratio (Frost and Volz, 2013, White et al., 2006) or the expected time before an infected individual transmits the infection (Frost and Volz, 2010). Although in population biology a *plethora* of generation time definitions exist (Steiner et al., 2014), the common definition of intergeneration interval or time between two consecutive generations within a population (*i.e.* the parent-daughter interval) (Bienvenu and Legendre, 2015) would essentially overlap with the first epidemiological definition of generation time given above. In coalescent-based approaches, however, the generation time might be also described as the time between transmission events (Kuhnert et al., 2011). For the purpose of this study, three formulations of the generation time have been investigated.

Generation time τ

The first formulation defines the generation time with its common epidemiological definition of time interval between sequential cases (Fine, 2003, Svensson, 2007, Pomeroy et al., 2008, van Ballegooijen et al., 2009), which has been computed from the reconstructed UK 2001 transmission tree as $\tau = T_k^{exp} - T_i^{exp}$, where i is the parent IP and k is the daughter. This formulation will be referred in this text as the epidemiological generation time τ.

Generation time τ_c

The second formulation defines the generation time as the time interval between epidemiologically unrelated cases, or the serial cases interval (Frost and Volz, 2010). This parameterisation has been computed from the UK 2001 epidemiological data as $\tau_c = \sum_{t=0}^{T} \frac{C_t}{T}$, where C_t is the actual count of infected cases at time t. This definition of generation time will be referred in text as the serial case interval τ_c.

Generation time τ_p

The last formulation of the generation time is defined as the average time between infections at a given time at the population level. This has been computed using the inverse of the incidence-to-prevalence ratio (White et al., 2006, Frost and Volz, 2013). Thus it can be derived from the empirical epidemiological data at each time t of the UK 2001 FMD epidemic as $\frac{P_t^{exp}}{I_t^{exp}}$. This definition will be referred to in the text as the prevalence-to-incidence ratio τ_p.

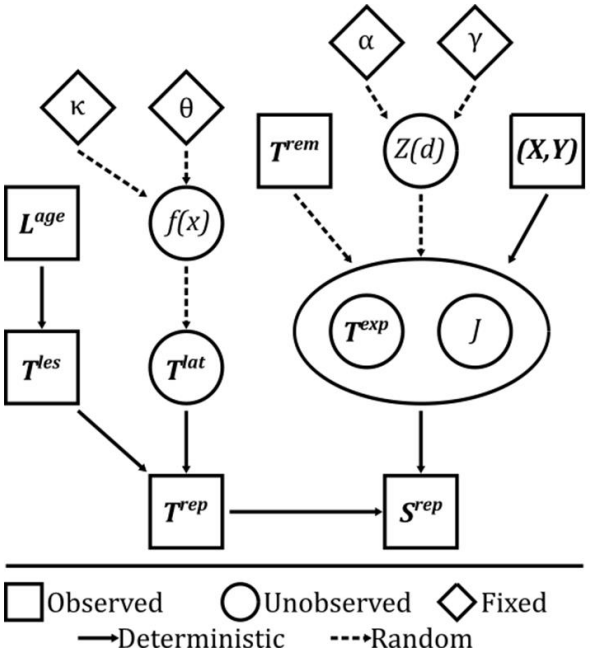


```
1.  For: treeStep in treeTime (min=lesT, max=remT)
2.    For: i in 1:IP
3.      If: treeStep!=lesT[i]
4.        next
5.      Else
6.        set source as IP[i]
7.        store index of IPs potentially susceptible of infection from IP[i] which(remT[i]<expT≤lesT[i])
8.        For: infectStep in infectTime (min=lesT[i], max=remT[i])
9.          For: k in 1:IP
10.           If: infectStep!=expT[k]
11.             next
12.           Else
13.             set recipient IP as IP[k]
14.             store index of IPs potentially source of infection for IP[k] which(remT<expT[k]≤lesT)
15.             If: length(likeSoulP>1)
16.               return transmission kernel for multiple sources
17.               return transmission probability for multiple sources
18.             Else
19.               return transmission kernel for single source
20.               return transmission probability for single source
21.             EndIfelse
22.           EndIfelse
23.         EndFor
24.       EndFor
25.     EndIfelse
26.   EndFor
27. EndFor
28. For: i in 1:IP
29.   set source as IP[i]
30.   store index of IPs potentially susceptible of infection from IP[i] which(remT[i]<expT≤lesT[i])
31.   For: k in 1:IP
32.     If: IP[k] has maximum transmission probability|list of likely IPs
33.       set transmission link between IP[i] and IP[k]=1
34.     Else
35.       set transmission link between IP[i] and IP[k]=0
36.     EndIfelse
37.   EndFor
38. EndFor
```

Figure 3-3. Transmission tree model scheme and algorithm. Direct acyclic graph illustrating dependencies in the model [bold symbols represent set of variables (*i.e.* $T^{exp} = \{T_1^{exp}, \dots, T_K^{exp}\}$)].

3.2.3 Genetic simulation

FMDV genetic sequences were simulated implementing the Tamura and Nei (1993) model of DNA sequence evolution, which defines the following nucleotide substitution rate matrix:

$$Q = \{q_{ik}\} = \begin{bmatrix} -(\alpha_1\pi_C + \beta\pi_R) & \alpha_1\pi_C & \beta\pi_A & \beta\pi_G \\ \alpha_1\pi_T & -(\alpha_1\pi_T + \beta\pi_R) & \beta\pi_A & \beta\pi_G \\ \beta\pi_T & \beta\pi_C & -(\alpha_2\pi_G + \beta\pi_Y) & \alpha_2\pi_G \\ \beta\pi_T & \beta\pi_C & \alpha_2\pi_A & -(\alpha_2\pi_A + \beta\pi_Y) \end{bmatrix}$$

where nucleotides are ordered T, C, A and G. The parameters used for the TN93 model are specified in Table 3-2. The TN93 model was selected for genetic simulations after performing jModelTest 2.1.7 analysis (Guindon and Gascuel, 2003, Darriba et al., 2012) using the 39 full-genome UK 2001 FMDV field isolates, which reported the TN93 as the best-fit model of nucleotide substitution.

Table 3-2. Description of parameters defined for the Tamura and Nei model of nucleotide substitution (Tamura and Nei, 1993).

Symbol	Details
$\pi_T, \pi_C, \pi_A, \pi_G$	Frequencies of nucleotide T, C, A, and G
π_Y, π_R	Frequencies of pyrimidines and purines
α_1, α_2	Rates of transitional changes between purines and between pirimidines
β	Rate of transversional changes

A previously sequenced FMDV isolate collected from the outbreak source IP (IP4) during the UK 2001 FMD epidemic (Appendix 3) was used for setting the initial virus genome from which the sequences of IPs were generated according to the previously reconstructed transmission tree network. FMDV was defined to evolve at a molecular clock rate μ equal to 2.37×10^{-5} nt/site/day (Orton et al., 2013), as parameterised using BEAST 1.8.0 (Drummond and Rambaut, 2007, Drummond et al., 2012). For each transmission link, the number of nucleotides by which a virus genome sampled on farm k differed from that on the farm from which it was infected (farm i) was randomly sampled from a Poisson distribution $Pois(\lambda)$ setting the mean to be $\lambda = \mu M \Delta t$, where M was the length of the FMDV complete genome [for the UK 2001 FMD epidemic M is equal to 8196 nucleotides, as estimated from the field isolates (Cottam et al., 2006)] and Δt is the evolutionary duration (the sum of the time intervals computed along the transmission tree – refer to 3.2.3.1). The algorithm used to simulate FMDV sequences implemented a discrete-time Markov chain model of first order (Rios Insua et al., 2012) to derive nucleotide changes in the recipient genome which depended on the nucleotide state of the source genome (Figure 3-5). In this inference scheme, the Markov transition probability matrix $P(t) = \{p_{ik}\} = e^{Q(t)}$ over time t estimated from the source genome using the TN93 model provided the probability of selecting any of the four nucleotides to be changed at the randomly selected site in the recipient genome determined chosen from a discrete uniform distribution $U(1, M)$. The $\alpha_1, \alpha_2, \beta$ parameters used to derive $P(t)$ were estimated from the available UK 2001 FMDV full-genome sequences (Appendix 3), resulting in values of 11.325, 23.281 and 3.7, respectively.

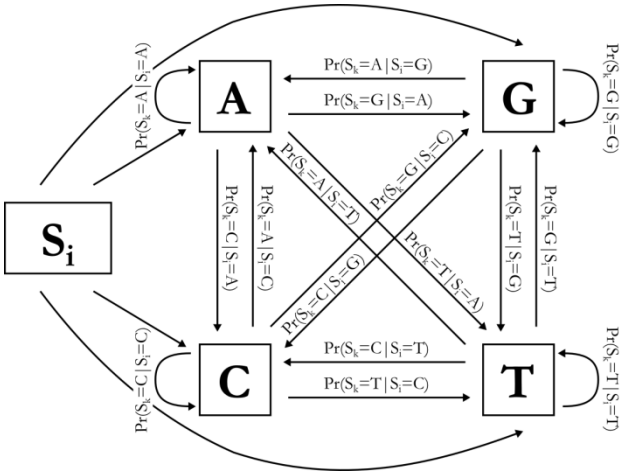

1. **For**: seqStep in seqTime (min=*repT*, max=*remT*)
2. **For**: *i* in 1:IP
3. **If**: seqStep!=*repT*[*i*] or genome[*i*] is not present
4. next
5. **Else**
6. set source as genome[*i*]
7. **For**: *k* in 1:IP
8. **If**: *k* in not linked with *i* (transTree=0) or genome[*k*] is present
9. next
10. **Else**
11. set recipient as genome[*k*]
12. return Δt and randomly return ntSubs from poisson distribution *f(x,μMΔt)*
13. randomly allocate change sites from uniform distribution *f(k,M)*|ntSubs
14. return nucleotide frequencies of genome[*i*]
15. return substitution rate matrix of genome[*i*]|TN93 model
16. return transition probability matrix of genome[*i*]|TN93 model
17. generate genome[*k*] through Markov-chain process
18. **For**: site in changeSites
19. return the state site nucleotide from genome[*i*]
20. return transition probabilities of recipient nucleotide|nucleotide[genome[*i*],site]
21. randomly sample nucleotide to change|transition probabilities
22. **EndFor**
23. copy conserved nucleotides from genome[*i*] to genome[*k*]
24. **EndIfelse**
25. **EndFor**
26. **EndIfelse**
27. **EndFor**
28. **EndFor**

Figure 3-4. Genetic simulation model scheme and algorithm. Nucleotide substitution probabilities set under the discrete-time Markov chain model of first order.

3.2.3.1 Simulation of genetic mutations along the transmission tree

The evolutionary duration Δt has been derived from the reconstructed transmission tree taking into account the dependency structure of sampled isolates. Briefly, a virus is introduced in an epidemiological system at coalescent time C_0 and evolves along a transmission tree structured as in Figure 3-5. Thus, the time length of the evolutionary duration of a sampled isolate S which evolved from a coalescent ancestor C is equal to:

$$\Delta t = (T_{C-1} - T_C) + (T_S - T_C)$$

As a result of the underlying tree structure, how time fixed mutations are passed to subsequent generations varies according to the numbers of lines of descent derived from a single coalescent ancestor. Virus lineages can evolve directly from a single coalescent ancestor and, therefore, they inherit the mutations of the genome sequences at the ancestor point (as being the case for S_1 and S_8 which are directly descending from C_0 and C_7). For example, the sampled virus isolate S_1, directly descended from the index virus C_0, shares common mutations with the intermediate lineage recovered at the coalescent time C_1 which are accumulated within the $T_{C_1} - T_{C_0}$ time interval, and has unique mutations accumulated during the $T_{S_1} - T_{C_1}$ time. Alternatively, multiple coalescent events are branched from the evolving virus lineage of a single coalescent ancestor: this lineage acquires genetic mutations forward in time which are then inherited and recovered at each subsequent coalescent point and, therefore, passed to descent sampled isolates. As an example of the latter case, the sampled virus isolate S_3 is descended from the evolving lineage derived from the coalescent ancestor C_1 but is directly originated from an intermediate lineage recovered at coalescent time C_4. Therefore, S_3 shares mutations which are chronologically accumulated by intermediate lineages recovered at coalescent times C_2 (within the $T_{C_2} - T_{C_1}$ time interval), C_3 (within the $T_{C_3} - T_{C_2}$ time interval) and C_4 (within the $T_{C_4} - T_{C_3}$ time interval), and is characterised by unique mutations accumulated during the $T_{S_3} - T_{C_4}$ time.

The above evolutionary structure defined for inheriting mutations between infector and infected farms enables the preservation of the dependencies of sampled lineages along the transmission tree which are recovered from the simulated sequences. In addition, in order to account for high within-farm genetic diversity in

systems where multiple animals are infected within a farm (as being the case for the UK 2001 FMD outbreak), the coalescent event for multiple evolving lineages was let to be early in infection, backward in time of the first related coalescent ancestor (*i.e.* the infection time of the infector farm rather than the infection time of the infected farm).

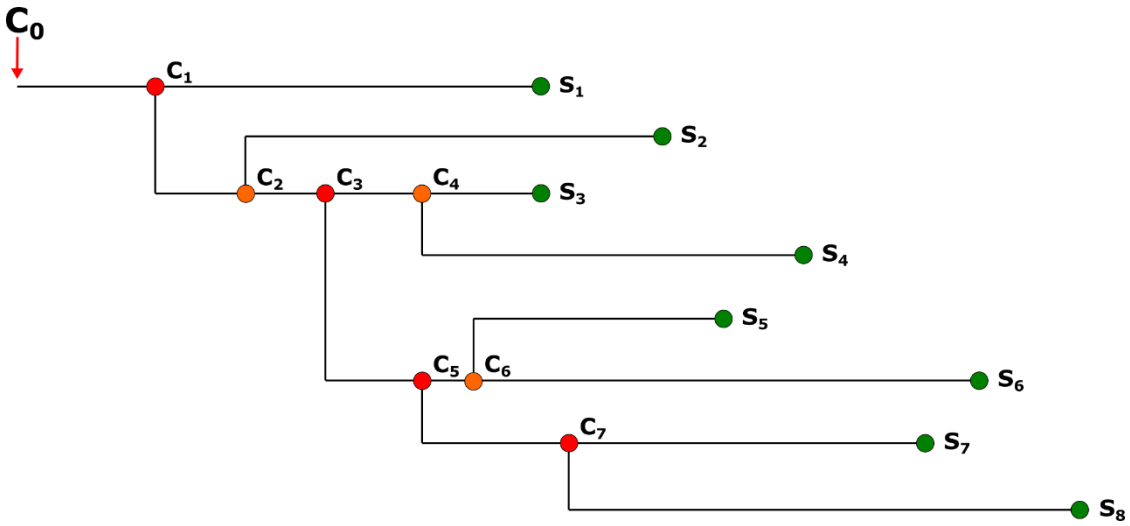

Figure 3-5. Evolutionary structure of the dependency between sampled lineages along a reconstructed transmission tree. Red nodes represent coalescent ancestors; orange nodes represent coalescent events of single lineages, whilst green tips represent sampled virus isolates.

3.2.3.2 Evolutionary analysis of the UK 2001 FMDV WGS simulated alignment

Evolutionary analyses were performed using BEAST 1.8.0 package (Drummond et al., 2012, Drummond and Rambaut, 2007). The analysis was executed with the TN93 substitution model and the strict clock evolutionary model, setting the molecular clock used for the simulation (2.30×10^{-5}) as the substitution rate defined by a gamma distribution $\Gamma(\kappa,\theta)$ prior of κ=0.0084 and θ=1000.0. A piecewise constant Bayesian skyline model with 10 groups was used as tree prior (Drummond et al., 2005). Other priors were set with the defaults parameters. Additional comparisons using only VP1 coding sequences were also undertaken.

3.2.4 Model implementation

The model was coded in the R programming language (R Core Team, 2015). Running the transmission tree reconstruction for the full UK 2001 FMD outbreak (2026 IPs) and simulating the corresponding genetic component took about 15 minutes using R 3.2.1 on an Intel i7 Quad Core processor with clock speed 3.40 GHz and 16 Gb of RAM memory.

3.3 Results

Three different epidemic datasets were constructed from the overall UK 2001 FMD database: the first, used the entire set of IPs described by DEFRA at the time of the epidemic (n=2026); the second excluded IPs that were at a later stage re-assessed as negative premises based on the laboratory analysis of collected samples, and those with missing results (n=1428); the third included only the confirmed IPs and those with missing results (n=1616) (Ferris et al., 2006, Taylor, 2012). For each of these datasets a transmission tree was estimated and corresponding WGSs simulated. All parameters are reported together with their standard deviations.

3.3.1 UK 2001 FMD transmission tree reconstruction

From the reconstructed transmission tree, epidemiological parameters were estimated according to two points in time of the UK 2001 FMD epidemic. These corresponded to the introduction of the national movement ban (NMB) (5th day from the start of the epidemic) and the subsequent 24/48 hour IP/CP culling policy (41st day from the start of the epidemic). The average number of secondary cases (R_t) generated from a single IP across the entire outbreak is constrained to be equal to $\frac{N-1}{N}$ (Figure 3-5). The R_t mean estimates were shown to increase for the period before the introduction of the NMB (5.5) and to decrease following the implementation of the 24/48 hour IP/CP culling policy (0.8).

The average value of the epidemiological generation time τ was estimated to be 7.2±2.7 days for the entire outbreak (Figure 3-6, Table 3-3). τ was found to be shorter for the period preceding the NMB (2.2±2.3), conversely estimates for the periods after the implementation of the two different control policies (NMB and the 24/48 hour IP/CP culling policy) were not significantly different from the average value obtained for the entire epidemic. The average serial case interval τ_c was estimated to be 8.7 days, and was 2.5±0.9 days before the NMB was implemented. The introduction of the NMB and the 24/48 hour IP/CP culling policies impacted on τ_c which lengthened to 13.7±5.9 and 14.3±4.4, respectively. The prevalence-to-incidence ratio τ_p was found to be on average 12.2±8.4, and lower for the period before the NMB was imposed (average value of 4.1±2.2), indicating an increasing generation time for new IPs following NMB. With the implementation of the NMB and the further 24/48 hour IP/CP culling policy τ_p increased to 9.2±3.2 and 13.5±8.9, respectively.

The culling time, defined by the time interval between exposure T^{exp} and the stamping-out of the animals present in the IP (T^{rem}), was estimated on average as 9.1±2.8 days. This interval was not found to be statistically different for the epidemic period preceding the NMB, proceeding the NMB and following the implementation of the 24/48 hour IP/CP culling policy (Appendix 4) (p>0.05).

The average geographical distance of parent-daughter transmission links was estimated to be 27.6±60.2 km. Before the implementation of the NMB control policy longer transmission links were reported (average value of 273.7±245.9 km), whilst more locally defined infection routes were estimated after the introduction of both the NMB and the 24/48 hour IP/CP culling policies (average value of 22.3±44.7 km and 30.5±62.5 km, respectively).

Similar results were obtained assessing the other UK 2001 FMD epidemic datasets (Appendix 4), with no statistical significant difference to report (p>0.05).

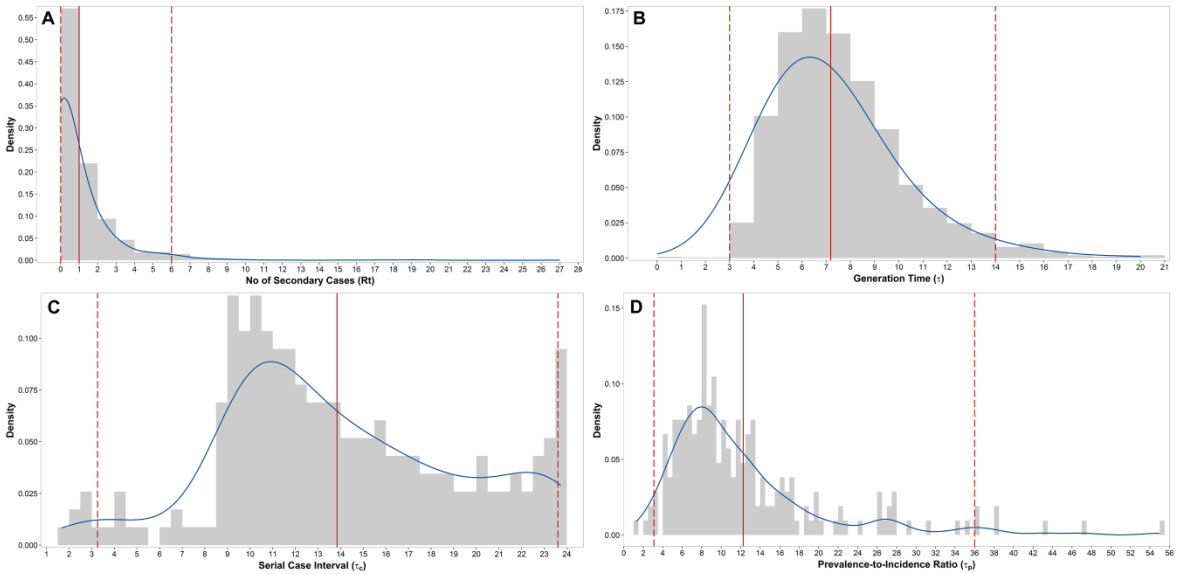

Figure 3-6. Number of secondary cases per primary infection (R_t, A) and epidemiological generation time (τ, B), serial case interval (τ_c, C) and prevalence-to-incidence ratio (τ_p, D) estimated for the UK 2001 FMD epidemic using the full IPs dataset (n=2026). Blue lines: kernel density estimates; solid lines: mean; dotted lines: 0.025 and 0.975 quantiles.

The reconstructed epidemic tree for the UK 2001 FMD epidemic is shown in Figure 3-7, along with the probabilities of transmission estimated for the established parent-daughter links. Visually inspecting the tree, the epidemic could be regarded as subdivided in 3 phases: a first exponentially growing phase lasting until ~50th day from the start of the epidemic, the initial decline phase lasting up to the ~80th day of the epidemic, and a prolonged 'tail-phase' until the end of the epidemic. These phases were found to overlap with the shape of the epidemic curve drawn from the incidence cases over time data, defining an upward slope with a peak at the 45th day (time frame 1st to 45th day), a downward slope until the 80th day (time frame 46th to 80th day) and the final tail-phase (time frame 81st to 232nd day). No substantial variations were observed in the tree topologies running the model using the three different epidemic datasets. The epidemic size (*i.e.* incidence cases over time) estimated from the reconstructed epidemic curve resulted in an average value of 8.9±11.5 IPs/day with a total number of 52 new IPs (I^{exp}) reported at the epidemic peak (Table 3-3). The data preceding, proceeding the NMB and following the 24/48 hour IP/CP culling policy were estimated as 4.1±2.8, 29.8±12.2 and 5.1±5.8 IPs/day, respectively (Appendix 5). At the time when the 24/48 hour IP/CP culling policy came into force, 57% (1149/2026) of IPs was reported to be already infected. No statistical differences (p>0.05) were reported between the incidences estimated using the different formulations defined in §3.2.2.2. Average disease prevalence for the entire epidemic was estimated as 88.3±113.88 IPs

using the P^{exp} formulation, with the prevalence size at epidemic peak of 442 IPs (Table 3-3). Average values of 18.3±15.4, 272.7±129.7 and 56.9±71.9 IPs were estimated from the data preceding, proceeding the NMB and following the 24/48 hour IP/CP culling policy (Appendix 5). Statistical differences were described between the three formulations of prevalence (P^{exp}, P^{les} and P^{rep}, defined in §3.2.2.2) (p<0.001), with an average multiplicative factor of ~2 between prevalences estimated at sequential disease stages.

The probability of transmission for the parent-daughter links (as estimated through the p_{ik} equation in §3.2.2.1) were generally indicative of one most likely link for both the initial and the ending phases of the outbreak (prob≥0.7), whereas some uncertainty was observed for evaluating the middle phase (time window between ~35 and ~50 days from the beginning of the epidemic). No significant differences were reported between the three different epidemic datasets (p>0.05).

Table 3-3. Empirical prevalence P, incidence I, epidemiological generation time τ, serial case interval τ_c, prevalence-to-incidence ratio τ_p and number of secondary cases per primary infection R_t with its variance $var(R_t)$ estimated from the reconstructed transmission tree according to each phase of the UK 2001 FMD epidemic.

		Epidemic Phase				
		Overall	*Exponential*	*Peak*	*Decline*	*Tail End*
Epidemiological τ		7.18±2.70	7.42±2.87	-	6.56±2.21	7.42±2.60
Serial case interval τ_c		8.73	9.33±6.06	21.30	22.06±1.15	12.67±2.90
Prevalence-to-incidence ratio τ_p		12.25±8.40	7.57±3.19	12.82	15.37±5.84	12.99±9.52
Number of secondary cases R_t		0.99±1.99	1.33±2.52	0.58±0.89	0.74±1.39	0.93±1.87
$var(R_t)$		3.95	6.37	0.79	1.94	3.51
Prevalence	P^{exp}	88.29±113.88	195.42±153.66	442.00	202.88±115.54	30.57±14.13
	P^{les}	46.18±60.81	96.40±81.70	230.00	144.00±64.42	15.89±7.45
	P^{rep}	20.36±30.71	48.38±44.15	127.00	50.06±20.90	5.33±3.47
Incidence	I^{exp}	8.88±11.50	22.33±15.44	52.00	15.43±10.72	3.12±2.22
	I^{les}	8.73±11.42	18.11±15.36	47.00	20.48±12.32	3.15±2.23
	I^{rep}	9.04±11.50	19.27±13.99	46.00	23.31±12.79	3.27±2.34

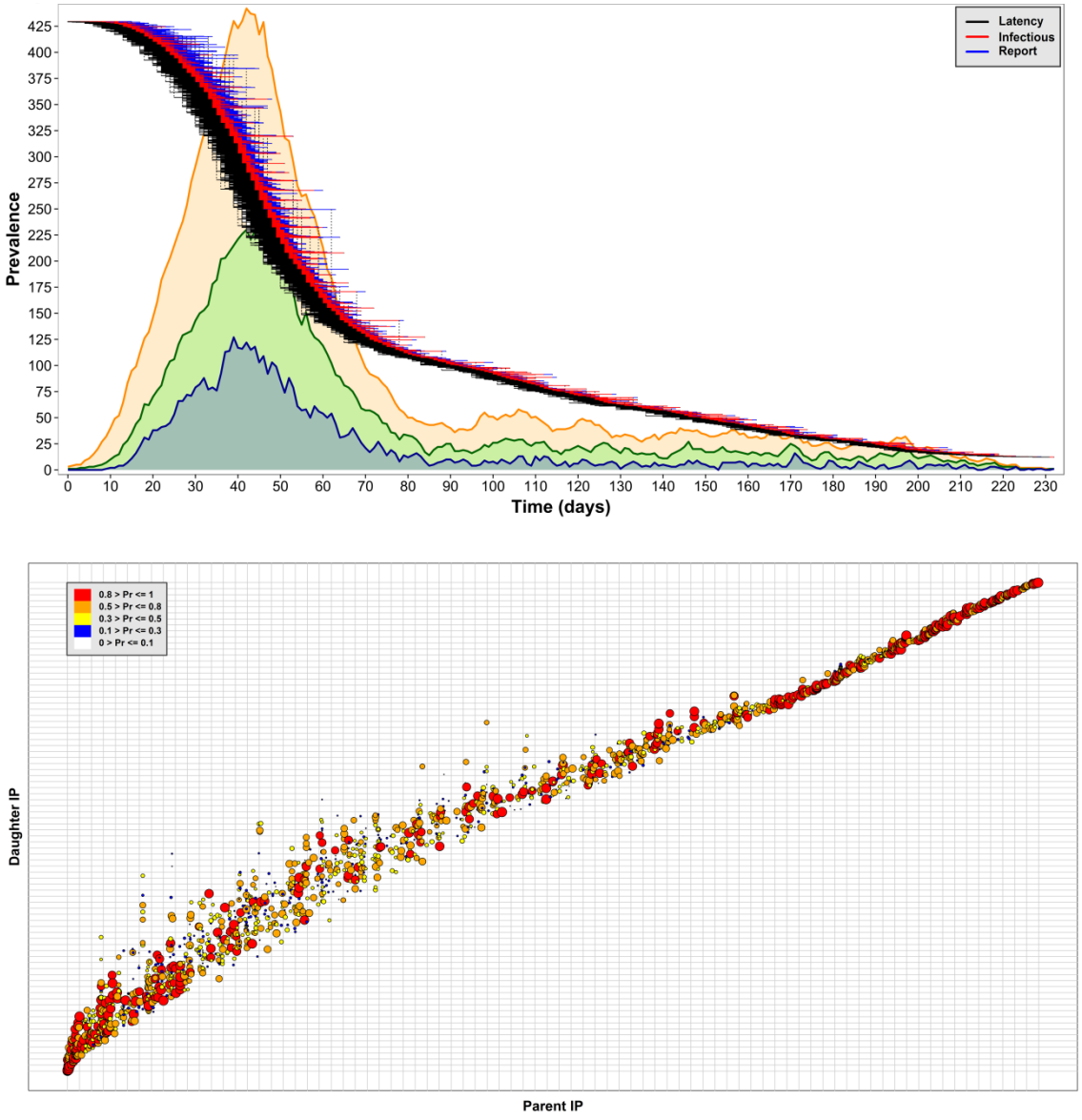

Figure 3-7. Transmission tree (top graph) and probability of parent-daughter established links (bottom graph) reconstructed using the full IPs dataset (n=2026). Colours for the transmission tree define the T^{exp} (black), T^{les} (red) and T^{rep} (blue) disease stages durations, respectively. Epidemic curves were estimated from the P^{exp} (orange), P^{les} (green) and P^{rep} (blue) prevalence data. Values of the estimated probability p_{ik} of the established transmission links are defined in the legend

3.3.2 UK 2001 FMDV genetic simulation

The nucleotide composition for the simulated FMDV genome sequences was represented by an average proportion of 0.215 (95PI 0.214 to 0.216), 0.279 (95PI 0.278 to 0.280), 0.247 (95PI 0.246 to 0.248) and 0.258 (95PI 0.256 to 0.259) T, C, A and G nucleotides, respectively. No differences were found (p>0.05) comparing the nucleotide composition of the simulated data with the WGS generated from the UK 2001 FMDV field isolates (n=39), the latter returning an average proportion of 0.215,

0.279, 0.248 and 0.258 for T, C, A and G nucleotides, respectively. The average number of nt substitutions per transmission link (Appendix 5) estimated from the full simulated data was 4.5±6.3. An average of 6.2±4.4, 6.1±8.3 and 3.3±4.26 nt substitutions/transmission link were estimated for the period preceding, proceeding the NMB and following the 24/48 hour IP/CP culling policy, respectively. No significant differences (p>0.05) in the estimated nt substitution/transmission link were reported for the 1616IPs and 1428 IPs datasets (Appendix 5). The observed evolutionary distance and total nt changes calculated from the index IP (IP4) were found to increase linearly with time (R^2=0.93; $F_{1,2025}$=27291) (Figure 3-8). The linearity in the nt change over time was also recovered from the 1616IPs and 1428 IPs.

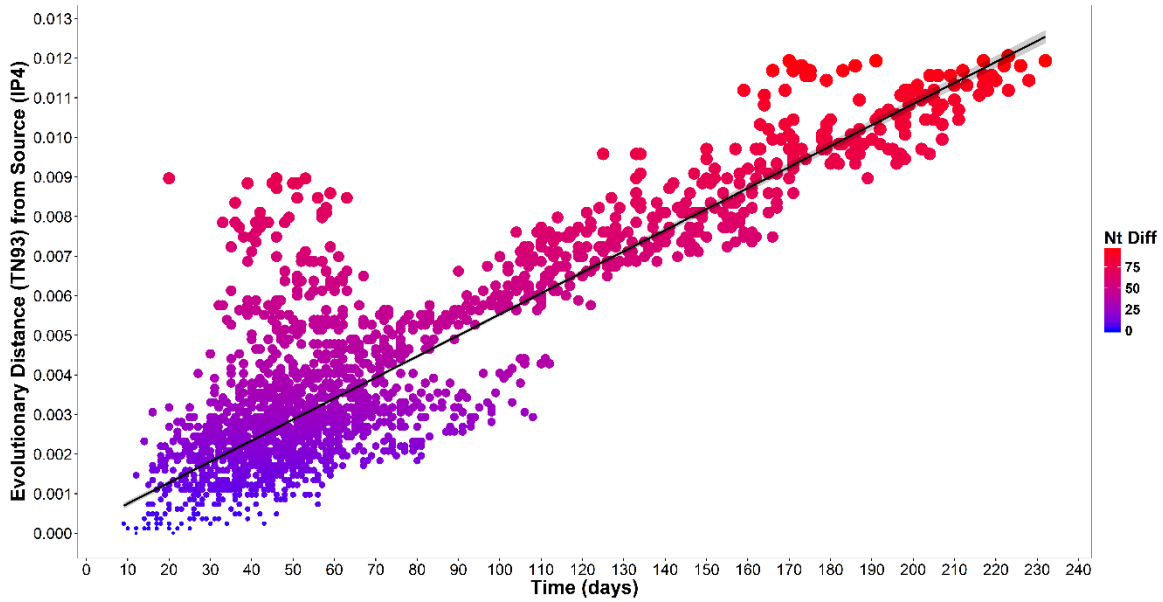

Figure 3-8. Accumulation of nucleotide differences estimated from the index IP (IP4) for the full IPs UK 2001 FMDV WGS simulated alignment (n=2026) with time expressed in days. Size of the points increases with increased number of nt substitutions. Shaded area represents 95% confidence intervals for the fitted line.

The phylogenetic trees reconstructed from the simulated data are shown in Figure 3-9. Although characterised by a high complexity due to the number of sequences, the phylogeny drawn from the simulated data defined five phylogenetic clusters, which were recognised in both the neighbor-joining tree and the time-stamped one generated from the BEAST analyses. No substantial variations were apparent from the topology of the phylogenetic trees reconstructed from the three different epidemic scenarios investigated. This 'ladder-like' topology of the trees might be due to strong continual selective pressure with a rapid turnover of lineages over time and strong temporal clustering (Gray et al., 2011, Grenfell et al., 2004).

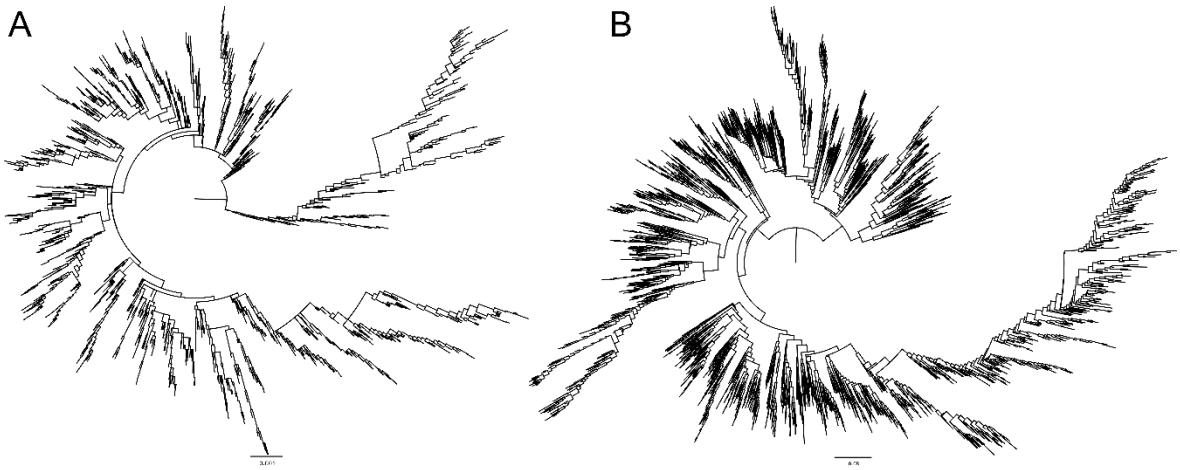

Figure 3-9. Tree phylogenies reconstructed using the FMDV WGS simulated from the full IPs dataset (n=2026). The phylogenetic trees were computed using the neighbor-joining method in MEGA 6.06 (A), and time-stamped from the BEAST analyses (B). All the trees were rooted from the outbreak source (IP4).

3.3.2.1 UK 2001 FMDV evolutionary analysis using WGS data

The average evolutionary duration (Δt) was estimated as 14.8±3.7 days for the full outbreak time window, with the periods preceding, proceeding the NMB and the 24/48 hour IP/CP culling policy were comparable with the average value estimated for the entire epidemic. No significant variation (p>0.5) in the Δt estimates were obtained running the simulation model for the three different epidemic datasets and for each of the time-period assessed (Appendix 5).

The molecular clock reconstructed from BEAST resulted in a value of 2.05×10^{-5} nt/site/day (95%HPD 1.97×10^{-5} to 2.14×10^{-5}), with no statistical difference observed for the other epidemic datasets (p>0.05). These results were comparable with those estimated from the 39 previously sequenced UK 2001 FMDV field isolates [2.26×10^{-5} nt/site/day, using a relaxed-exponential clock model (Cottam et al., 2006); 2.08×10^{-5} nt/site/day, using a relaxed-constant clock model (Cottam et al., 2008a); 2.33×10^{-5} nt/site/day here re-estimated using the same strict clock model assumed for simulating the WGSs].

3.3.2.2 UK 2001 FMDV evolutionary analysis using VP1 coding sequences

A molecular clock reconstructed from BEAST using the VP1 coding sequences extracted from the simulated data for the full epidemic dataset (n=2026) resulted in a value of 2.36×10^{-5} (95%HPD 1.94×10^{-5} to 2.54×10^{-5}), which was comparable with

those obtained from the WGS simulation and previously published data [see 3.3.2.1]. The average number of nt substitutions per transmission link estimated from the full simulated data of VP1 coding sequences was 0.44±1.13. An average of 0.80±0.84, 0.60±1.59 and 0.31±0.63 nt substitutions/transmission link were estimated for the period preceding, proceeding the NMB and following the 24/48 hour IP/CP culling policy, respectively. No significant differences (p>0.05) were reported when analysing the nt substitutions per transmission link using the 1616 IPs and 1428 IPs datasets.

3.3.3 Validating simulation with field isolates

To assess the validity of the simulation process, a subset of the fully simulated WGS database was extracted, which corresponded to the n=39 UK 2001 FMDV field isolates previously sequenced (Appendix 3). Phylogenetic reconstruction was conducted in both MEGA 6.06 (Tamura et al., 2013) using the neighbor-joining method and in BEAST using the same parameters as used for the full analysis (TN93, strict clock and BSP models). The average pairwise number of nt substitution was estimated to be 26.2±17.2 (95%PI 5 to 63, max=91) for the real data, and 44.8±27.4 (95%PI 6.5 to 96, min=0, max=109) for the simulated data, with an absolute difference between the real and simulated data of 18.6 nt. In addition, the total number of nt substitutions estimated between the source (IP4) and the latest reported IP with sequence (IP2027) (*i.e.* root-to-tip distance) was 50 and 85.5±7.0 for the field isolates and the simulated data, respectively (absolute difference of 24.5 nt). The molecular clock estimated from the UK 2001 FMDV field isolates returned a value of 2.33×10^{-5} (95%HPD 1.94×10^{-5} to 2.71×10^{-5}) nt/site/day, whereas a value of 3.47×10^{-5} (95%HPD 2.94×10^{-5} to 4.00×10^{-5}) nt/site/day was obtained from the simulated data. Again, these values were in line with those estimated from the full-simulated epidemic, the VP1 only analysis and with those retrieved from previously published studies [see 3.2.2.1].

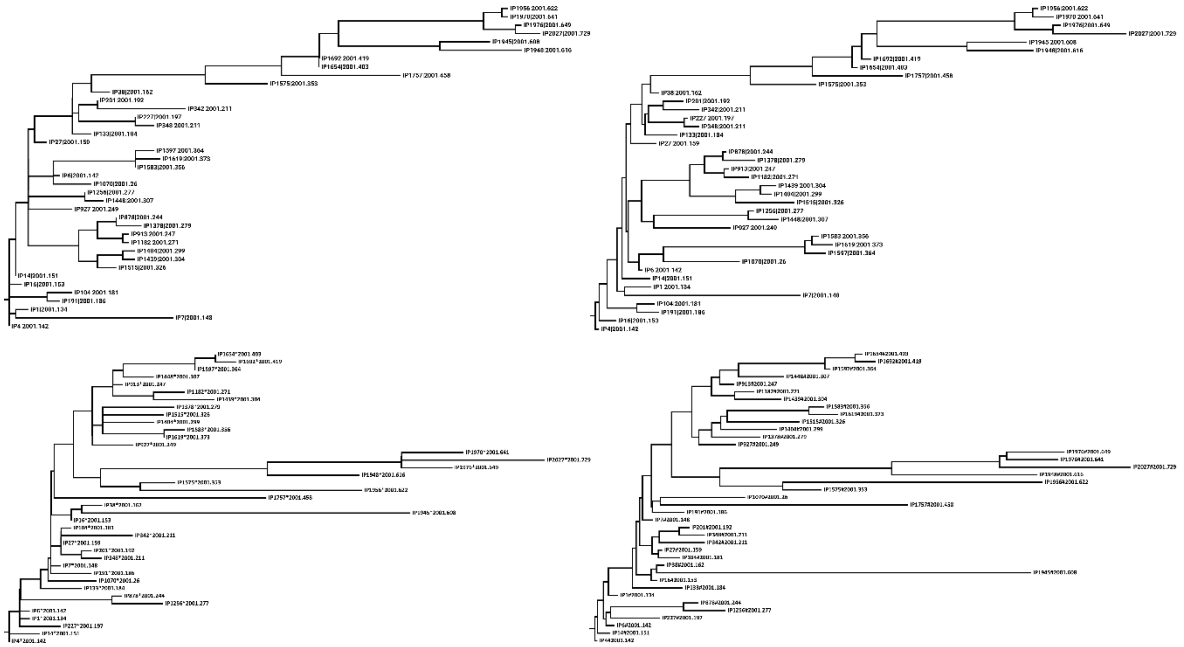

Figure 3-10. Phylogenetic reconstruction of the *n*=39 UK 2001 FMDV WGS generated from the field isolates (lower row) and simulated by the model (upper row). The left hand side trees were computed using the neighbor-joining method in MEGA 6.06, whilst the right hand side trees were reconstructed using BEAST. All the trees were rooted from the outbreak source (IP4).

The phylogenies obtained from both the UK 2001 FMDV isolates and the simulated data are shown in Figure 3-10. According to the structure of the tree, isolates were branching subsequently along the tree. In addition, phylogenetic links were in some cases established between different lineages, as observed for the field and simulated data.

3.4 Discussion

This chapter has been devoted to presenting the computational algorithm and methodological assumptions underlying the development of the transmission tree reconstruction and genetic simulation models applied to the UK 2001 FMD epidemic, in order to produce the first dataset of WGS data from a fully resolved transmission tree obtained from a real epidemic, from where the demography of the infected population (either expressed as prevalence or incidence) is fully known. This model framework is a key tool for testing the core hypothesis of this PhD project, that genetic sequences carry a demographic signal that can be eventually related in an epidemiological context with the prevalence of infected case. This will be the leading challenge addressed in Chapter 4, where the relationship between the effective

population size N_e derived from the BSP analysis and the actual number of infected cases estimated from either the empirical prevalence or incidence data will be investigated.

Although the transmission tree model here presented was a simplistic representation of the process underlying the transmission dynamics of FMD, it was not intended to be informative of the precise mechanisms of transmission but to capture the main features of transmission in time and space. Therefore, the objective of the algorithm developed for reconstructing the transmission tree was to provide a plausible transmission tree that captures the majority of the epidemic, defines the mainstay for the simulation process and provides a realistic framework for the simulation. Additionally, the model assumes that individual premises are not subject to multiple infections and, hence, the algorithm generates a single source-recipient link for each IP. However, given the relative rapidity with which culling policies were applied during the UK 2001 FMD epidemic, it could be assumed that multiple infections were unlikely to have played a major role in the epidemic.

The results generated from the reconstruction of the UK 2001 FMD transmission tree have characterised many of the primary features of the epidemic, and generated largely comparable data with those previously published (Chis Ster and Ferguson, 2007, Haydon et al., 2003, Gibbens et al., 2001, Cottam et al., 2008a). Examining the results generated using the parent-daughter transmission links established by the reconstructed transmission tree, the full epidemic curve of the entire UK 2001 FMD epidemic was characterised by phases of exponential growth, decline and tail end. These epidemic phases corresponded to different epidemiological features of the epidemic process with shorter serial case intervals, longer distance transmission links and large variance in the number of secondary cases per primary infection observed during the exponential phase, contrary to those for the decline and tail end phases. These findings match with the control policies imposed at the time of the outbreak, with no significant differences reported between the start of the NMB and the time when the 24/48 hour IP/CP culling policy came into force. This might lead to the suggestion of a relatively low impact of the 24/48 hour IP/CP culling policy on the further reduction of the transmission process subsequent to the implementation of the NMB and, moreover, when the epidemic was already starting to decline. In fact, the estimated prevalence-to-incidence ratio returned very similar values for the decline and tail end phases, suggesting that after the epidemic peak (which was earlier than

the beginning of the 24/48 hour IP/CP culling policy) new IPs are generated in direct proportion to the existing prevalence (*i.e.* R_t is constant and slightly less than 1).

The molecular clock recovered from the fully-simulated FMDV WGS data was found to be similar to the one estimated from the 39 WGS generated from the field isolates, which provides confidence around the robustness and validity of the simulation process. The differences observed in comparing the UK 2001 FMDV field isolates and the corresponding simulated lineages are likely to be mostly explained by the space-time process for generating the transmission tree which, as already discussed, might not be entirely accurate in establishing the actual transmission links observed during the UK 2001 FMD epidemic. However, this would likely have a limited influence on the simulation of the evolutionary process, and the reconstruction of the underlying phylogenetic trees. Similar results were obtained performing the analyses with only the VP1 coding region sequences, although with an expected greater degree of uncertainty given by the wider confidence intervals of the estimated parameters relative to those obtained using the WGS. This can be easily linked to the lower resolution provided by the VP1 coding region sequences, which represents only 8% of the complete FMDV genome.

The average number of nt substitutions per transmission links estimated from the WGS simulated alignment was very similar in comparison to that previously reported (Cottam et al., 2008a), even matching the difference reported between the mean number of substitutions per transmission link when partitioned into transmission events preceding and proceeding the NMB. However, comparing the extracted 39 simulated sequences with the corresponding field isolates, a relative difference was apparent between observed and simulated sequences for the average nt substitutions recovered over the root-to-tip distances, which were higher for the simulated WGS. It should be noted that the former estimate was established using only 20 WGSs generated from the Darlington cluster, which potentially might not be generalised to the evolutionary process underlying the full epidemic event. In a real epidemic, genetic change might acquire from within-farm evolutionary processes, for which multiple cycles of infection might be present on each IP. The process here developed for simulating the virus evolution does consider, although in a very crude form, the within-farm process, which contribute to the genetic diversity observed between the sequences recovered from each IP. For example, coalescent models assume that the transmission event is coincident with the coalescent event, which

might be not the case when significant variation is seen at the within-farm evolutionary scale. However, the impact of the within-farm evolutionary dynamics on the short timescale considered for an epidemic event could be regarded as limited and unlikely to add significant variation over and above that observed at consensus level (King *et al*., unpublished data).

CHAPTER 4

Reconstructing virus populations dynamics over time

4.1 Rationale

In population genetics, factors that cause differences between N_e and the census population size N have been well studied. As already reviewed in Chapter 1, N_e is defined as 'the size of an idealised population experiencing the same rate of random genetic change over time as the real population under consideration' (Wright, 1931, Wright, 1938), assuming that these two populations have the same properties under neutral selection (*i.e.* for the Wright-Fisher model $N_e \cong N$). However, violations of the assumptions underlying the Wright-Fisher model leads to a reduction in N_e relative to N, and the ratio $\frac{N_e}{N}$ assesses the departure from the assumption of the idealised model (Felsenstein, 1971, Kimura and Crow, 1963). N_e can be assumed to scale to the genetic diversity of the population as measured by the population genetic parameter θ, and by making various assumptions it is possible to identify additional scaling factors that relate N_e to the census population size N (Magiorkinis et al., 2013). The challenge in this chapter is to identify and empirically test the performance of different scaling factors that can be used to relate N_e to the census population size in an epidemiological context.

In epidemiology, the census population size relates to the actual numbers of infected cases measured as an estimate of prevalence, or possibly incidence. The correlation between N_e and the actual numbers of infected cases has been studied under the assumption of a time-varying coalescent model (Griffiths and Tavare, 1994a), and suggests that no simple relationship or clear transformation exists between these two quantities (Frost and Volz, 2010, Volz et al., 2009). The lack of a clear relationship between the effective and actual population size has been attributed to the variable nature of the serial case interval τ_c. The serial case interval will vary over the course of an epidemic (*e.g.* shortening during the exponential phase when the full population is susceptible and expanding when the susceptible population becomes

depleted – *i.e.* during the decline and/or tail end phases), causing variation in the relationship between transmission rate and the number of infected individuals. Bedford et al. (2011) found τ_c to be inversely proportional to the contact rate during the expansion phase of an epidemic, whilst τ_c was estimated to be inversely proportional to the rate of recovery when at equilibrium. However, during the exponential phase of an epidemic or within a steady endemic state where τ_c is roughly constant, a direct transformation might be found (Koelle and Rasmussen, 2012), hence N_e estimates would be proportional to the prevalence of infection (Frost and Volz, 2010). It should be noted that at steady state, prevalence is also proportional to incidence. The fact that the τ_c varies over the course of an epidemic implies that it might not be straightforward to estimate N_e at a given time (de Silva et al., 2012).

4.2 Methodological process for scaling N_e to the actual infected population size

This chapter reports studies of the viral population demography estimated from the genetic data simulated using the model described in Chapter 3. The aim is to investigate the relationship between N_e and the actual numbers of infected cases (cases here are defined as numbers of IPs) derived from the P^{exp} prevalence data, and estimated from a fully-resolved epidemic, the UK 2001 FMD epidemic. In order to investigate the correlation between estimates of N_e derived from the BSP and the real numbers of infected cases, three scaling formulations were examined, which also accounted for the variability in the generation time within the time frame of an epidemic. Account has also been taken of the definition of generation time provided in §3.2.2.3. The resulting prediction estimate from the $N_e$scaling should be considered as a proxy of prevalence measure, therefore it has been termed as the 'infection prevalence' N^*. The final derivation of the different scaling equations for estimating N^* is summarised in Table 4-1.

4.2.1 Reconstructing N_e changes through time from a Bayesian Skyline analysis

As detailed in §1.2.1 and §4.1, the parameter θ can be equated to the product $N_e\tau$ (Drummond et al., 2002). Rearranging for N_e, the latter equation results in $N_e = \frac{\theta}{\tau}$, that is the skyline-derived effective population size N_e. This value is easily computed using the BSP-derived θ and the generation time estimated from the UK 2001 FMD data, for which both the τ and τ_c definitions have been used (see §3.2.2.3). The above formulation has been referred to in the text as the 'scaled N_e formulation' and has been used for assessing the potential of using N_e estimates for predicting the actual demography of an infected population.

4.2.2 Deriving infection prevalence N^*

4.2.2.1 Reconstructing N^* assuming variance in the number of secondary cases per primary infection R_t

The ratio between the effective and actual population size $\frac{N_e}{N}$ has been related to the variance in the reproduction success σ^2 (Kingman, 1982b, Tavare et al., 1997) in the following way: $N_e = \frac{N}{\sigma^2}$. The variance in the reproduction success σ^2 in an epidemiological context is the variance in the number of secondary infections per primary infections [*i.e.* $var(R_t)$] or by the alternative form $\frac{var(R_t)}{E(R_t)^2} + 1$, which accounts for the fraction of the host population that is susceptible to infection (Koelle and Rasmussen, 2012)]. These two formulations lead to the following expressions for the derived infection prevalence: $N^* = \frac{\theta var(R_t)}{\tau}$ and $N^* = \frac{\theta(var(R_t)+E(R_t)^2)}{\tau E(R_t)^2}$. This scaling formulation has been termed the '$var(R_t)$ scaling formulation', referring to Tavare et al. (1997) or Koelle and Rasmussen (2012) for differentiating between the two $var(R_t)$ derivation forms. Both τ and τ_c definitions of generation time have been used within the context of the above scaling formulations (see §3.2.2.3).

4.2.2.2 Reconstructing N^* assuming the number of lineages as a function of time

A third formulation for deriving the infection prevalence N^* from N_e estimates has been investigated assuming that the population from which the observed data have been extracted is homogeneously mixing (Keeling and Rohani, 2008, Law et al., 2008). Assuming that the coalescent rate is equal to that of a haploid Wright-Fisher model and expressing the phylogenetic structure by the number of lineages as a function of time (NLFT), Frost and Volz (2013) derived a direct scaling formulation for the N_e estimate from the BSP analysis (considering for this case $N_e = \theta$) as $\theta = \frac{I\tau_p}{2}$, where I here denotes the number of infected individuals (originally termed in the study as the 'effective number of infections'). In this N_e scaling formulation the generation time has been strictly defined with the prevalence-to-incidence ratio τ_p definition (see §3.2.2.3). Thus rearranging for I and assuming $N^* \approx I$, the final scaling equation results in $N^* = \frac{2\theta}{\tau_p}$. This scaling formulation has been termed the 'NFLT scaling formulation'.

Table 4-1. Comparison of scaling equations of the effective population size N_e derived from time-varying coalescent based models for recovering the infection prevalence N^*. Parameters are defined as follow: τ = epidemiological generation time, τ_c= serial case interval, τ_p = prevalence-to-incidence ratio, σ^2 = variance in the reproductive success, $var(R_t)$ = variance in the number of secondary infections per primary infections, $E(R_t)$ = mean of the number of secondary infections per primary infections, θ = genetic diversity.

Generation Time	N_e/N	Scaling Factor Relating θ (BSP) and N_e	Final Derivation	Reference
τ	$N_e = \frac{N}{\sigma^2}$	$N_e = \frac{\theta}{\tau};\ \sigma^2 = var(R_t)$	$N^* = \frac{\theta var(R_t)}{\tau}$	(Kingman, 1982b) (Tavare et al., 1997) (Drummond et al., 2002) (Fine, 2003) (Svensson, 2007)
τ_c	$N_e = \frac{N}{\sigma^2}$	$N_e = \frac{\theta}{\tau_c};\ \sigma^2 = var(R_t)$	$N^* = \frac{\theta var(R_t)}{\tau_c}$	(Kingman, 1982b) (Tavare et al., 1997) (Drummond et al., 2002) (Frost and Volz, 2010)
τ	$N_e = \frac{N}{\sigma^2}$	$N_e = \frac{\theta}{\tau};\ \sigma^2 = \frac{var(R_t)}{E(R_t)^2} + 1$	$N^* = \frac{\theta(var(R_t) + E(R_t)^2)}{\tau E(R_t)^2}$	(Kingman, 1982b) (Tavare et al., 1997) (Drummond et al., 2002) (Fine, 2003) (Svensson, 2007) (Koelle and Rasmussen, 2012)
τ_c	$N_e = \frac{N}{\sigma^2}$	$N_e = \frac{\theta}{\tau_c};\ \sigma^2 = \frac{var(R_t)}{E(R_t)^2} + 1$	$N^* = \frac{\theta(var(R_t) + E(R_t)^2)}{\tau_c E(R_t)^2}$	(Kingman, 1982b) (Tavare et al., 1997) (Drummond et al., 2002) (Fine, 2003) (Svensson, 2007) (Koelle and Rasmussen, 2012)
τ_p	$N_e = \frac{I\tau_p}{2}$	$N_e = \theta$	$N^* = \frac{2\theta}{\tau_p}$	(Drummond et al., 2002) (White et al., 2006) (Frost and Volz, 2013)

4.2.2.3 Computation of infection prevalence N^* using the UK 2001 FMD simulated WGS

Twelve realisations of the UK 2001 FMD transmission tree reconstruction and genetic simulation generated full WGS datasets (n=2026 IPs) as detailed in §3.3. For each simulated alignment, BEAST 1.8.0 package (Drummond et al., 2012, Drummond and Rambaut, 2007) was employed to reconstruct the demography of the FMDV population from the simulated data using the BSP model (Drummond et al., 2005). The analysis was undertaken with the TN93 substitution model and the strict clock evolutionary model, the average rate of the fixed clock model as the one used for the simulation (2.33×10^{-5} nt/site/day) and defining a gamma distribution $\Gamma(\kappa, \theta)$ of κ=0.0084 and θ=1000.0 for the substitution rate prior. Other priors were set with the default values. Furthermore, epidemiological parameters used for formulating the scaling equations presented in Table 4-1 (*i.e.* τ, τ_c, τ_p, $var(R_t)$, $E(R_t)$) have been either estimated by averaging over the time course of the epidemic or estimated as changing through time, leading to two different scaling approaches, namely average and time-varying. Thus, the time-varying scaling approach takes into account the variability in time of the UK 2001 FMD epidemic and, therefore, of each epidemiological parameter used to derive the infection prevalence N^*. Natural splines (Harrell, 2001) were fitted to time-varying data and used to smooth and interpolate the required data for each time point. Fitting procedures have been performed in R 3.2.1 using the splines package (R Core Team, 2015). The τ_t generation time has not been smoothed since it can be easily estimated in continuous time from the UK 2001 FMD empirical data.

The root-mean-squared deviation (RMSD) was used for estimating the numerical departure of the recovered N^* from the empirical count of infected cases, expressed as prevalence. This statistical parameter is a scale-dependent accuracy measure based on the absolute squared error, which provides an indication of the difference between values predicted by a given model and the actual data (Hyndman and Koehler, 2006). For the scaling study, this can be estimated as $RMSD(N^*) = \sqrt{E((N_t^* - N_t)^2)}$, where N can denote prevalence or incidence estimated at time t. The RMSD returns a value of zero if the correlated time-series are perfectly matching $N^* \cong N = 0$.

4.2.3 Investigating the impact of changing $var(R_t)$ on the recovery of the infection prevalence N^*

To investigate the effect of $var(R_t)$ in estimating the infection prevalence N^* from a BSP-scaled N_e, a full simulation of a FMD stationary system was undertaken. The model structure was based on the scheme presented in Chapter 3, from which a monophyletic FMDV transmission scenario was generated using an individual-based non-spatial simulation of the transmission tree. This full simulation has been introduced to avoid potential secondary effects which might results by forcing high $var(R_t)$ at the transmission level structure of the UK 2001 FMD outbreak data. For the stationary system, the stages and, therefore, the timing of the FMD progression for an IP i were defined beginning with the infection time T_i^{exp}, at which a latency period D_i^{lat} commences. Following the incubation period, the IP becomes infectious at time T_i^{inf}, maintaining its infectivity for a period D_i^{inf} until the IP is removed from the system at time T_i^{rem}. The clinical sample is collected at time T_i^{sam}, which also defines the time a viral sequence S_i^{rep} is obtained (Figure 4-1). The duration of the latency period D^{lat} was randomly drawn from a gamma distribution $\Gamma(\kappa, \theta)$, which was defined by a shape and scale parameters of κ=22.12 and θ=0.22, respectively ($\bar{x}$=4.87 and σ^2=1.07) (Charleston et al., 2011, Mardones et al., 2010). The duration of infectious period D^{inf} was randomly sampled from a log-normal distribution $N(\ln x; \mu, \sigma)$ defined on a log-scale by a mean and standard deviation parameters of μ=1.15 and σ=0.38, respectively [modified from Charleston et al. (2011)].

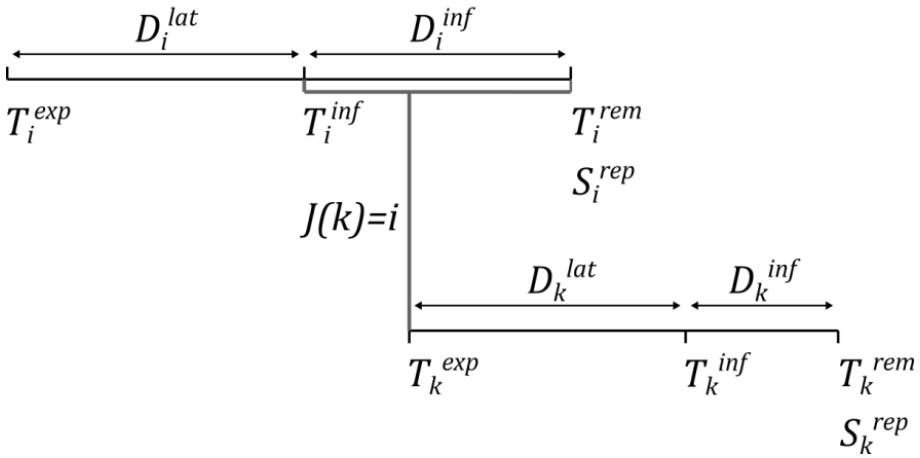

Figure 4-1. Dynamical model of FMDV transmission for a FMD stationary system between a parent IP i and a daughter IP k.

The negative binomial distribution has been previously used to model the variation in the number of progenies per individual parent. Low values of the dispersion parameter k describes the situation when only a small proportion of IPs go on to transmit the infection, whilst large values of the dispersion parameter indicates that the infected population contributes more uniformly to the future transmission (Lloyd-Smith, 2007, Lloyd-Smith et al., 2005, Garske and Rhodes, 2008). Following the methods provided by the above studies, the number of daughter IPs to be infected by each parent IP were randomly generated through a negative binomial distribution $NB(k, \mu)$ defined by a mean μ which was made dependent on the ratio of the required 'target' prevalence P at endemic equilibrium and the current simulated prevalence P_t^{exp} (μ=P/P_t^{exp}). The dispersion parameter k was set at different values (*i.e.* 0.01, 0.1, 0.5, 1, 10, 50, and 100) thus investigating the influence of varying $var(R_t)$ on N^*. The computational approach implemented allowed maintaining the R_t parameter constant throughout the simulation at an average value ~1 while varying its variance. The simulation of the genetic sequences sampled at time T^{sam} was processed under the Markovian evolutionary model presented in Chapter 3, where the Δt evolutionary duration was estimated along the simulated transmission tree according to the methodology described in §3.2.3.1.

The molecular clock for simulating FMDV WGS data was set at 2.33×10^{-5} nt/site/day, matching the one used for the UK 2001 FMD simulation. The simulation was run until 10000 IPs had been generated, but only a random sample of 1000 IPs and corresponding FMDV WGSs were extracted from the full dataset. This random sample was obtained only when the simulation reached its stationary prevalence equilibrium (*i.e.* at the predefined *P* value).

4.2.3.1 Computation of infection prevalence N^* from the simulated FMD stationary system

BEAST 1.8.0 analysis were performed for reconstructing the BSP plot (Drummond et al., 2005, Drummond et al., 2012) using the same settings previously described for the UK 2001 FMD epidemic: TN93 substitution model, strict clock evolutionary model and using the molecular clock inputted for the simulation as the substitution rate prior. Infected population size curves extracted from the prevalence

data of the entire simulated database (n=10000) (for the prevalence computation refer to §3.2.2.2) were compared with both the effective population size N_e and the recovered infection prevalence N^* derived from the BSP estimates using the average scaling approach as previously described in §4.2.2.3. The results obtained with this approach were analysed with the same methodology described above for the UK 2001 FMD epidemic reconstruction and using the scaling equations presented in Table 4-1

4.3 Results

4.3.1 Average scaling approach

From the infection prevalence N^* estimates derived from each of the scaling equations provided in Table 4-1, seven pairwise correlation analyses were undertaken for assessing the similarity between the N^* curves with the real epidemic curves obtained from the P^{exp} prevalence measure (as detailed in §3.2.2.2). The results produced for the 7 comparisons are presented in Table 4-2 and ranked in descending order from the best fit to the poorest one according to the RMSD parameters estimated. All parameters are reported together with their standard deviations.

Table 4-2. Statistical parameters estimated from the pairwise correlation between infection prevalence N^* and the empirical prevalence data extracted from the UK 2001 FMD epidemic using each of the three scaling equations. Data were ranked in descending order from the best fit. Prevalence data were estimated using the formulation defined in §3.2.2.2. Average scaling approach.

Rank	Scaling Equation	Generation Time	Prevalence	Empirical Peak	N^* Peak	RMSD	β	R^2
1	$N_e = \frac{\theta}{\tau}$	Epidemiological τ	P^{exp}	439.8±3.2	351.0±37.4	30.4±5.0	1.06±0.05	0.93±0.02
2	$N^* = \frac{2\theta}{\tau_p}$	Prevalence-to-incidence ratio τ_p	P^{exp}	439.8±3.2	419.6±47.6	35.3±7.1	0.88±0.05	0.93±0.02
3	$N_e = \frac{\theta}{\tau}$	Serial case interval τ_c	P^{exp}	439.8±3.2	291.2±28.7	41.9±4.4	1.27±0.05	0.93±0.02
4	$N^* = \frac{\theta(var(R_t)+E(R_t)^2)}{\tau E(R_t)^2}$	Serial case interval τ_c	P^{exp}	439.8±3.2	1132.9±120.8	291.1±20.5	0.33±0.01	0.93±0.02
5	$N^* = \frac{\theta var(R_t)}{\tau}$	Serial case interval τ_c	P^{exp}	439.8±3.2	1135.1±121.0	292.0±20.5	0.33±0.01	0.93±0.02
6	$N^* = \frac{\theta(var(R_t)+E(R_t)^2)}{\tau E(R_t)^2}$	Epidemiological τ	P^{exp}	439.8±3.2	1365.7±157.1	379.1±31.2	0.27±0.02	0.93±0.02
7	$N^* = \frac{\theta var(R_t)}{\tau}$	Epidemiological τ	P^{exp}	439.8±3.2	1368.8±157.5	380.3±31.2	0.27±0.02	0.93±0.02

Table 4-3. Statistical parameters estimated from the correlation between infection prevalence N^* and the empirical prevalence data extracted from the UK 2001 FMD epidemic using each of the three scaling equations. Data were ranked in descending order from the best fit. Prevalence data were estimated using the formulation defined in §3.2.2.2. Time-varying scaling approach.

Rank	Scaling Equation	Generation Time	Prevalence	Empirical Peak	N^* Peak	RMSD	β	R^2
1	$N_e = \frac{\theta}{\tau}$	Epidemiological τ	P^{exp}	439.8±3.2	310.0±29.8	37.9±4.3	1.20±0.05	0.93±0.01
2	$N^* = \frac{2\theta}{\tau_p}$	Prevalence-to-incidence ratio τ_p	P^{exp}	439.8±3.2	543.4±44.0	86.7±10.8	0.66±0.04	0.83±0.05
3	$N_e = \frac{\theta}{\tau}$	Serial case interval τ_c	P^{exp}	439.8±3.2	377.7±56.5	108.0±4.3	1.07±0.13	0.24±0.05
4	$N^* = \frac{\theta(var(R_t)+E(R_t)^2)}{\tau E(R_t)^2}$	Epidemiological τ	P^{exp}	439.8±3.2	2502.5±427.9	746.8±134.1	0.14±0.03	0.59±0.08
5	$N^* = \frac{\theta var(R_t)}{\tau}$	Epidemiological τ	P^{exp}	439.8±3.2	2596.8±489.8	777.8±151.2	0.14±0.03	0.58±0.08
6	$N^* = \frac{\theta(var(R_t)+E(R_t)^2)}{\tau E(R_t)^2}$	Serial case interval τ_c	P^{exp}	439.8±3.2	7399.5±1999.1	1250.4±270.7	0.04±0.01	0.03±0.01
7	$N^* = \frac{\theta var(R_t)}{\tau}$	Serial case interval τ_c	P^{exp}	439.8±3.2	7709.0±2269.6	1299.8±310.7	0.04±0.01	0.03±0.01

The best fit was obtained by the simple derivation of N_e from the BSP scaled using the epidemiological generation time τ (RMSD=30.4±5.0). The scaling formulation ranked second was the 'NLFT scaling formulation' (RMSD=35.3±7.1), which also produced the closest match with the empirical epidemic peak (average difference of 20.2 IPs). The third ranked N^* was obtained scaling the BSP using the serial case interval τ_c (RMSD=41.9±4.4). The results produced using the first two ranked scaling formulations and the one derived from the '$var(R_t)$ scaling formulation' [assuming the Koelle and Rasmussen (2012) derivation of $var(R_t)$ and the serial case interval τ_c] have been further analysed within this chapter, whilst N^* curves and analyses gathered from the remaining 4 pairwise comparisons are presented in Appendix 6. Incidence was found to be invariably lower than the infection prevalence N^* recovered from each of the 7 scaling correlation matrices, showing high deviance values and low similarity (RMSD>150). Therefore, this relationship has not been investigated further in the study.

4.3.1.1 Skyline scaled effective population size N_e

Assuming the generation time with its epidemiological definition (§3.2.2.3), the N_e curves derived using the skyline scaling formulation are shown in Figure 4-2. A high level of consistency was produced across the 12 realisations of the UK 2001 FMDV simulated WGS, with the shape and the structure of the N_e trajectory largely preserved. Visually inspecting the N_e curve generated from the n=2026 IPs dataset, the epidemic phases characterising the shape of the epidemic curve could be identified from the skyline trajectories, albeit some variabilities observed between runs. Dissecting the epidemic curve into the three subsequent phases (as define in §3.3.1) the correlation of the actual number of infected cases from P^{exp} and scaled N_e values are presented in Table 4-4. The correlation between N_e and P^{exp} was described to be highly linearly correlated (average R^2 value of 0.93±0.02), thus resulting in very low deviance (RMSD=30.4±5.0) estimate (Table 4-4). The average N_e estimated for the full epidemic dataset (n=2026) was found to be 77.7±3.5 cases/day, whilst the average data estimated for the exponential, peak, decline and tail end phases were 155.9±10.4, 351.0±37.4, 149.6±6.0 and 24.2±1.3 cases/day. To define the numerical size gap between N_e and prevalence, the count lag of the two quantities has been assessed

through a regression through the origin (RTO), reasonably assuming *a priori* that at time t=0 of the epidemic when no infection is generated both N_e and prevalence values are equal to 0 and, thus, no constant term would be defined for a linear model (in addition, the coalescent theory proposes that N is directly proportional to N_e). Lag estimates based on the slope of the regressor returned from the RTO (*i.e.* $N = \beta N_e$) found N_e values to be on average 1.06±0.05 times lower than the P^{exp} (p<0.001). The actual difference in the peak size between the empirical P^{exp} prevalence and the scaled N_e was estimated to be on average of 88.8±37.4 cases, whilst the absolute difference of cases across the entire UK 2001 FMD epidemic returned an average value of 10.7±3.5 IPs.

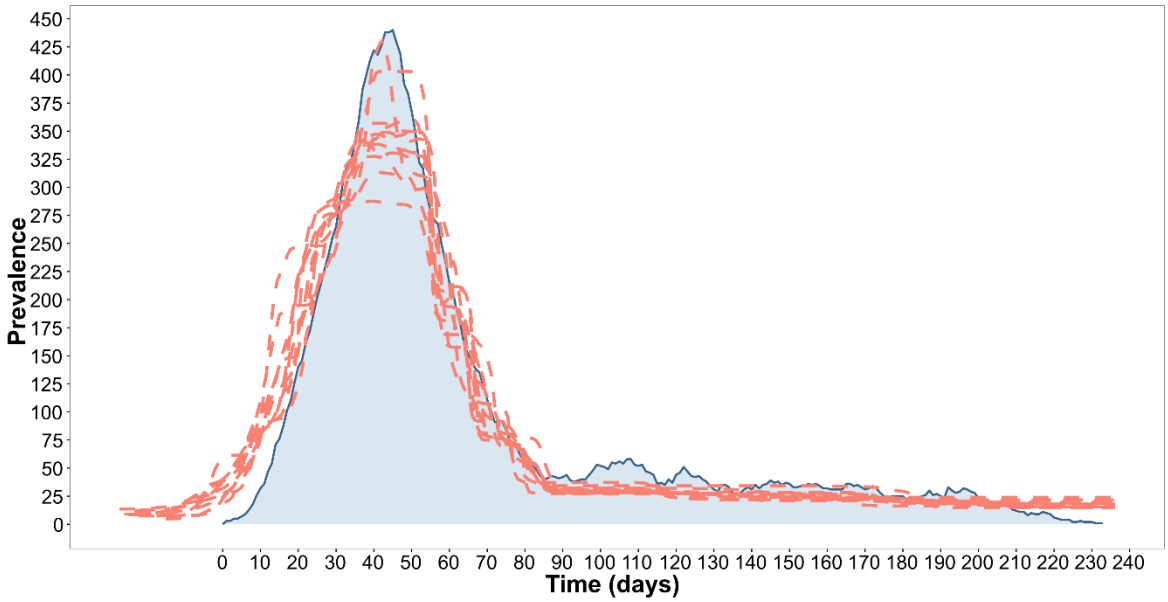

Figure 4-2. Scaled N_e estimated from 12 realisations of the UK 2001 FMDV simulated WGS data and reconstructed using the full IPs (n=2026) epidemic dataset. Epidemic curve was estimated from the P^{exp} (blue) prevalence data as defined in §3.2.2.2. Generation time is defined with the epidemiological τ formulation (§3.2.2.3).

Table 4-4. Overall and time specific number of infected cases estimated under 12 realisations of the UK 2001 FMD full IPs (n=2026) epidemic dataset from the empirical epidemiological data and the scaled N_e recovered from the BSP analysis. Generation time is defined with the epidemiological τ formulation.

		Epidemic Phase				
		Overall	*Exponential*	*Peak*	*Decline*	*Plateau*
Generation Time	τ	7.16±0.07	7.59±0.12	-	6.48±0.09	7.18±0.09
Prevalence	P^{exp}	88.42±0.32	195.01±2.15	439.83±3.19	203.17±0.83	30.62±0.04
Effective Population Size	N_e	77.69±3.50	145.17±9.34	351.03±37.41	182.77±9.40	24.75±1.34

4.3.1.2 Infection prevalence N^*estimated using the $var(R_t)$ scaling formulation

Computing the serial case interval τ_c and scaling the N_e estimates using the formulation of Koelle and Rasmussen (2012) which account for $var(R_t)$ in the infected population structure (§4.1.2.2), the recovered infection prevalence N^* curve is presented in Figure 4-3. Although the correlation between empirical and predicted prevalence was described as being highly linear (average R^2 value of 0.93±0.02), N^* estimates were reported to be higher than those extracted from the actual number of IPs recovered from the P^{exp}, on average of the order of 3.1±0.01 (p<0.001) (Table 4-2). In fact, the absolute difference in term of the size of the epidemic peak was estimated to be on average 693.0±120.8 IPs (Table 4-4), whilst across the entire UK 2001 FMD epidemic the average absolute difference was estimated to be 162.2±9.4 IPs. Deviance reported between the T^{exp} and the reconstructed infection prevalence N^* was, on average, 291.1±20.5 (Table 4-5).

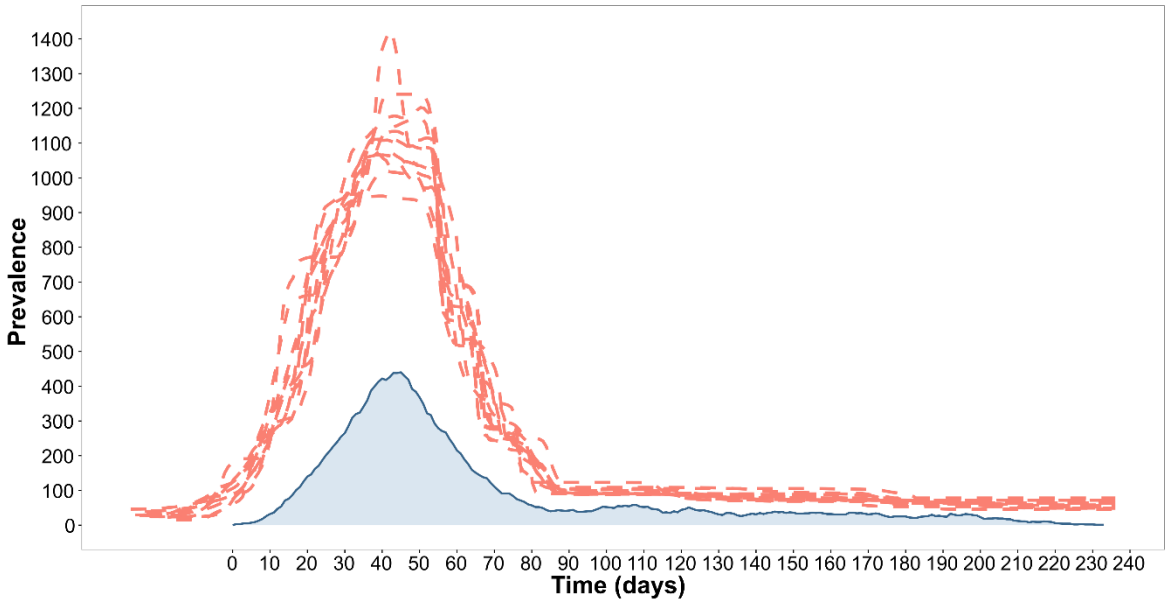

Figure 4-3. Infection prevalence N^* estimated from 12 realisations of the UK 2001 FMDV simulated WGS data and reconstructed using the full IPs (n=2026) epidemic dataset. The variance in the secondary cases per primary infection R_t was assumed the Koelle and Rasmussen (2012) formulation (§4.2.2.1). Generation time is defined with the serial case interval τ_c formulation (§3.2.2.3). Epidemic curve was estimated from the P^{exp} (blue) prevalence data as defined in §3.2.2.2.

Table 4-5. Overall and time specific number of infected cases estimated under 12 realisations for the UK 2001 FMD full IPs (n=2026) epidemic dataset from the empirical epidemiological data and the scaled infection prevalence N^* estimated under the assumption of variance in R_t [Koelle and Rasmussen (2012) parameterisation (§4.2.2.1)]. Generation time is defined with the serial case interval τ_c formulation (§3.2.2.3).

		Epidemic Phase				
		Overall	*Exponential*	*Peak*	*Decline*	*Plateau*
Serial Case Interval	τ_c	8.69±0.01	9.95±0.29	22.16±0.46	22.09±0.01	12.68±0.01
Prevalence	P^{exp}	88.42±0.32	195.01±2.15	439.83±3.19	203.17±0.83	30.62±0.04
Infection Prevalence	N^*	251.18±9.44	469.08±22.00	1135.15±121.01	590.85±24.23	80.04±4.50

4.3.1.3 Infection prevalence N^* estimated using the NLFT scaling formulation

Expressing the phylogenetic structure by NLFT, the generation time used for estimating the infection prevalence N^* has been defined as the prevalence-to-incidence ratio τ_p (Frost and Volz, 2013). Visually evaluating the N^* trajectories resulting from the 12 realisations of the UK 2001 FMD simulation model (Figure 4-4), a substantial overlap with the epidemic curve estimated from the P^{exp} prevalence was observed, with the prevalence found to be 1.1±0.05 times lower than the predicted infection prevalence N^* values. The average absolute difference over the entire epidemic was found to be of only 4.4±5.1 IPs, with the difference at the epidemic peak of 20.2±47.6 IPs (Table 4-5). The close fit between actual and predicted data was further described by the lowest deviation (RMSD=35.3±7.1). In addition, the infection prevalence N^* and the actual number of infected showed a strong linear correlation (R^2=0.93±0.02).

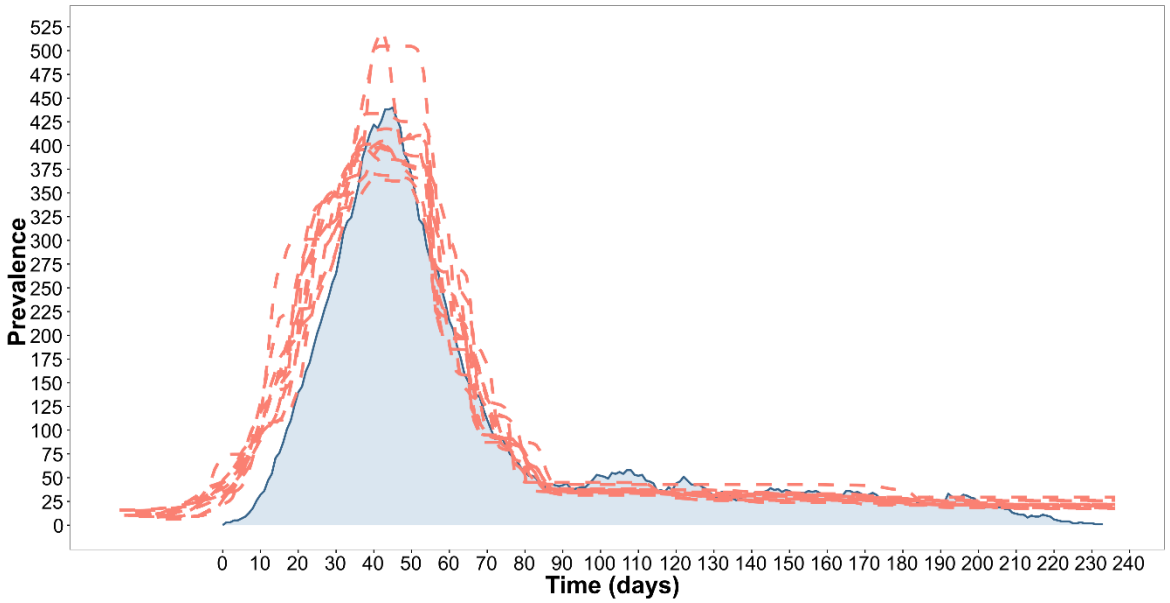

Figure 4-4. Infection prevalence N^* estimated from 12 realisations of the UK 2001 FMDV simulated WGS data and reconstructed using the full IPs (n=2026) epidemic dataset. Generation time is parameterised as the prevalence-to-incidence ratio τ_p (Frost and Volz, 2013) (§3.2.2.3, §4.2.2.2). Epidemic curve was estimated from the P^{exp} (blue) prevalence data as defined in §3.2.2.2.

Table 4-6. Overall and time specific number of infected cases estimated under 12 realisations for the UK 2001 FMD full IPs (n=2026) epidemic dataset from the empirical epidemiological data and the scaled infection prevalence N^* estimated by expressing the phylogenetic structure by NLFT. Generation time is defined with the prevalence-to-incidence ratio τ_p formulation (§3.2.2.3, §4.2.2.2).

		Epidemic Phase				
		Overall	*Exponential*	*Peak*	*Decline*	*Plateau*
Prevalence-to-Incidence Ratio	τ_p	12.15±0.40	7.81±1.15	11.85±2.71	15.33±0.97	12.82±0.52
Prevalence	P^{exp}	88.42±0.32	195.01±2.15	439.83±3.19	203.17±0.83	30.62±0.04
Infection Prevalence	N^*	92.87±5.14	173.53±12.55	419.61±47.58	218.50±13.66	29.58±1.93

4.3.2 Time-varying scaling approach

As detailed in the material and methods section (§4.2.2.3), with the time-varying approach the parameters used within each of the scaling formulation were estimated as discrete-time values using interpolated spline curves on the empirical UK 2001 FMD epidemiological data. Figure 4-6 shows the splines fit for each of the epidemiological generation time τ, the prevalence-to-incidence ratio τ_p, the R_t average value and the variance in R_t, whilst in Table 4-7 the estimates generated for each of the above parameters, and the serial case interval τ_c, are reported. Differently from the decline and plateau phases, a substantial departure from the overall average estimates were reported for the exponential phase of the UK 2001 FMD epidemic, where a large $var(R_t)$ and a low τ_p were recorded (Table 4-7), with $var(R_t)$ producing very high values within the first 10 days from the beginning of the epidemic. As per the serial case interval τ_c, estimates were found to increase with time, where lower values were reported for the exponential phase as opposed to the later epidemic phases.

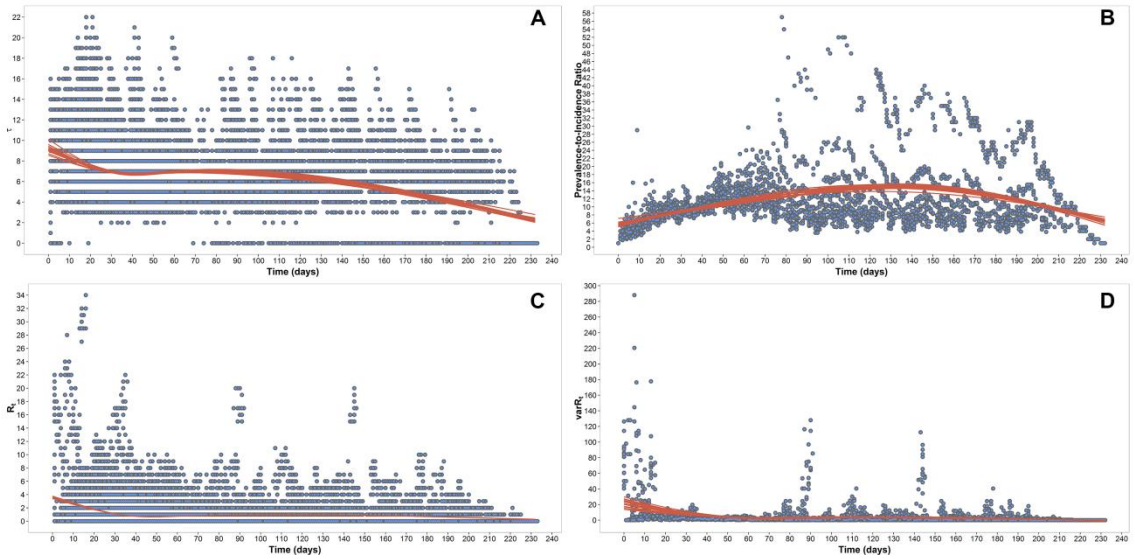

Figure 4-5. Natural splines interpolation for time-varying epidemiological parameters estimated from the empirical UK 2001 FMD epidemic data. Generation time τ (A), prevalence-to-incidence ratio τ_p (B), average number of secondary cases per primary infection R_t (C), variance in the number of secondary cases per primary infection $var(R_t)$.

Table 4-7. Epidemiological parameters estimated following natural spline interpolations of the 12 realisations of the reconstructed UK 2001 FMD transmission tree.

	Epidemic Phase				
	Overall	*Exponential*	*Peak*	*Decline*	*Plateau*
Epidemiological Generation Time (τ)	5.91±0.10	7.57±0.11	5.91±0.10	6.93±0.07	5.35±0.67
Serial Case Interval (τ_c)	8.73	9.42±0.38	21.40±0.68	22.06±0.05	12.68±0.01
Prevalence-to-Incidence Ratio (τ_p)	11.63±0.21	8.07±0.21	11.64±0.21	11.71±0.4	12.70±0.26
R_t Variance	4.28±0.45	12.18±2.25	4.28±0.45	2.75±0.52	2.23±0.19
R_t Mean	0.99±0.04	2.04±0.26	1.16±0.07	1.09±0.05	0.98±0.04

Similarly to that reported for the average scaling approach, spline fitted values were then used to investigate the effect of the time-varying scaling approach for deriving the N_e estimates and, thus, the infection prevalence N^* curve. Therefore, twenty one pairwise correlation analyses were also undertaken between the N^* estimates derived by using the time-varying parameter estimates for each of the scaling equations provided in Table 4-1 and the P^{exp} prevalence estimate (as detailed in §3.2.2.2). The results produced are presented in Table 4-3 and ranked in descending order from the best fit to the poorest according to the RMSD estimates. The full details of the results generated from each of the scaling formulation are presented in Appendix 7.

As observed with the average scaling approach, the best fit was still obtained with the scaling formulation consisting of the simple derivation of N_e from the BSP scaled using the serial case interval τ, although returning relatively higher deviance estimates (RMSD=37.9±4.3) (Table 4-3). With the time-varying scaling approach, the absolute difference in size of the entire epidemic between predicted and actual data

was estimated as 9.5±2.7 IPs, although with a larger distance between epidemic peaks (129.8±29.8 IPs) from what estimated using the average scaling approach (Figure 4-6). Overall, the scaled N_e was found to be 1.2±0.05 times lower than the actual number of infected IPs derived from the P^{exp} prevalence. Predicted and empirical data were described as highly linear correlated (R^2=0.93±0.01) (Table 4-3).

The infection prevalence N^* derived using the 'NLFT scaling formulation' was ranked second similar to the average scaling approach, but here reporting lower similarity with the shape and trajectory of the empirical data (RMSD=86.7±10.8) (Table 4-3). On visual inspection, the N^* curve was found to reach the peak of the epidemic earlier in time than the one obtained from the average scaling approach (~34th day), thus shifting the N^* curve to the left. The distance estimated between the epidemic peaks recovered from predicted and actual data was higher (103.6±44.0 IPs) (Figure 4-6). In addition, the difference between P^{exp} and N^* at the exponential phase was very large, with an average of 199.5±24.1 more predicted cases. The ratio between empirical and predicted data was estimated as 0.66±0.04. The linear correlation was found to be lower than that obtained using the average scaling approach (R^2=0.83±0.05) (Table 4-3).

The correlation between N^* derived from the '$var(R_t)$ scaling formulation' [assuming the Koelle and Rasmussen (2012) derivation of $var(R_t)$ and the serial case interval τ_c] and P^{exp}, produced incorrect results by implementing the time-varying scaling approach, with very low similarity observed between the empirical and predicted prevalence curves (RMSD=1250.4±270.7) (Table 4-3). Visually the infection prevalence N^* curves were conspicuously noisy with the epidemic peak shifted earlier in time (~10th day) (Figure 4-6). The difference in size between predicted and empirical data was reported to be on average 418.4±90.3 IPs, with a peak difference of 6959.7±1999.1 cases. Overall, the infection prevalence N^* was found to be 25 times higher than the empirical P^{exp} prevalence, returning a very low linear correlation (R^2=0.03±0.01) (Table 4-3).

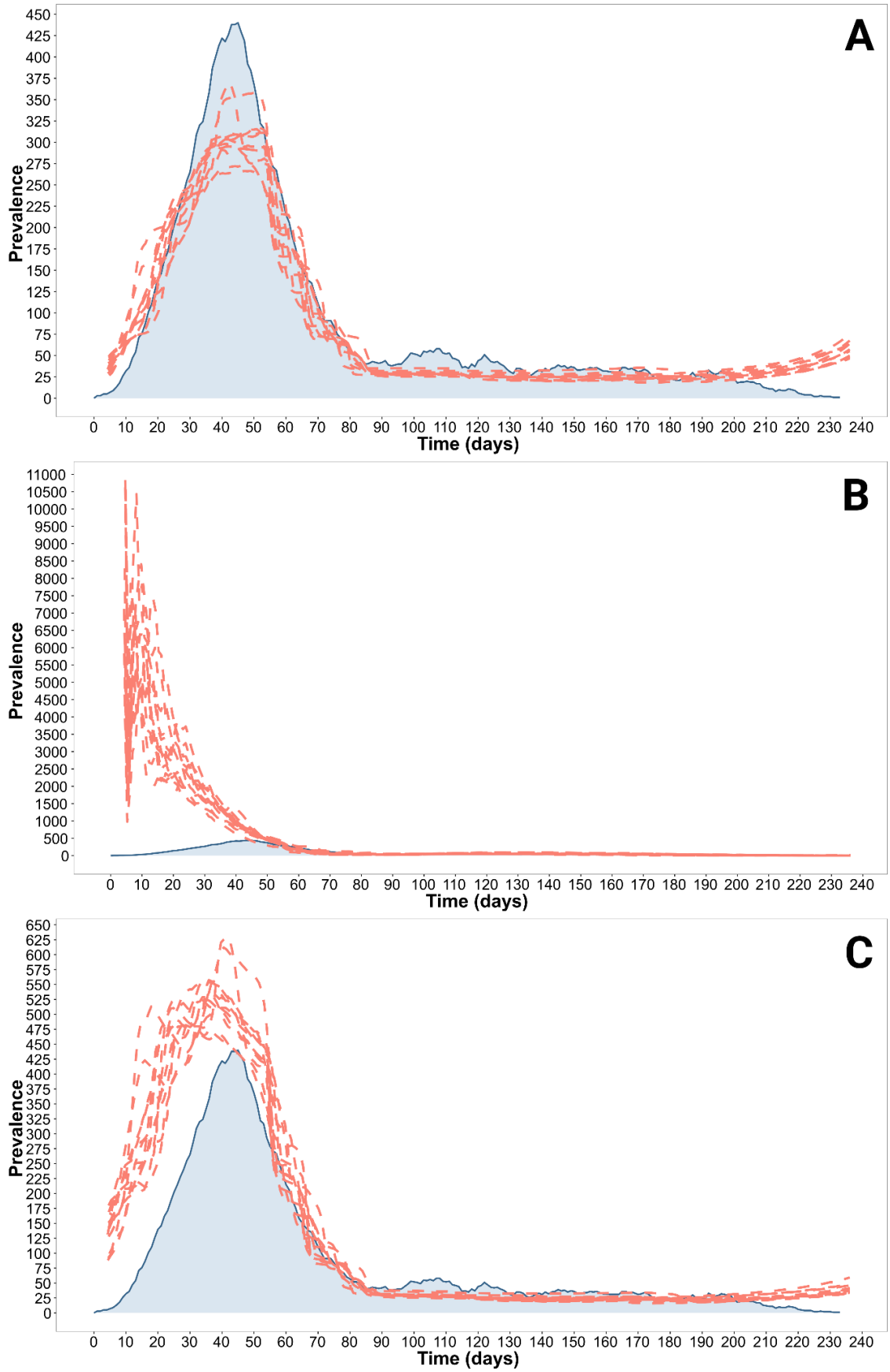

Figure 4-6. Infection prevalence N^* estimated from 12 realisations of the UK 2001 FMDV simulated WGS data and reconstructed using the full IPs (n=2026) epidemic dataset using the time-varying scaling approach. N^* derived with the: NLFT formulation (A), N_e formulation (B) and $var(R_t)$ formulation assumed as the Koelle and Rasmussen (2012) form (C) (§4.2.1 and §4.2.2). Epidemic curve was estimated from the P^{exp} (blue) prevalence data as defined in §3.2.2.2.

4.3.3 Viral demography reconstruction through simulations of a FMD stationary system

A full simulation of an FMD stationary system was undertaken to investigate the effect of varying $var(R_t)$ on the prediction of the actual number of infected case from an infection prevalence N^* estimate. For this purpose, different infected population structures using different values of $var(R_t)$ (generated through changing the dispersion parameter k) were tested using the three highest ranked scaling formulation resulting from §4.3.1 and using the average scaling approach. Table 4-8 reports the epidemiological parameters estimated from each of the simulations using a range of dispersion parameters for generating the number of IP daughters for each parent IP. The epidemiological generation time τ was maintained constant across each of the simulations while varying k, with values corresponding to that estimated from the UK 2001 FMD epidemic. It was interesting to find that the serial case interval τ_c was not substantially affected by varying $var(R_t)$, returning a very similar value (average value of 39.12±5.3) for all the 8 different k parameterisations (although with relatively higher standard deviation estimated for $k \leq 0.1$). The number of secondary case per primary infection R_t was also very similar while varying $var(R_t)$, but reporting higher standard deviation estimates when small dispersion parameter k was inputted in the simulation (*i.e.* mainly at 0.01 and 0.1 values), which thus resulted in a high $var(R_t)$ as expected. As shown in Figure 4-7 to 4-9, the prevalence curves estimated from the simulated FMD stationary systems clearly fluctuated less through time when k was large, thus generating a more stable system and resulting in low $var(R_t)$ estimates. The epidemiological parameters derived with $1<k<0.5$ were those that corresponded to those estimated from the UK 2001 FMD epidemic, although the serial case interval was much higher. Clock rates estimated from BEAST were closely matched with the one used for simulating the FMDV WGS, although higher rates were obtained with dispersion parameters set at $0.01<k<0.1$. The 95%HPD intervals were found to be wider for the scenarios characterised by high $var(R_t)$ [data not shown].

Table 4-8. Epidemiological parameters estimated from the stationary FMD simulation and using different dispersion parameters for generating the number of IP daughters for each parent IP.

	$NB(k,p)$ Dispersion Parameter							
	0.01	*0.1*	*0.5*	*1*	*10*	*50*	*100*	*1000*
Generation Time (τ)	7.21±1.52	7.09±1.74	7.13±1.66	7.03±1.63	7.07±1.65	7.09±1.66	7.08±1.64	7.07±1.62
Serial Case Interval (τ_c)	46.15±9.50	39.15±19.46	37.45±26.87	42.14±23.18	27.70±21.04	41.09±22.73	40.40±22.69	38.85±20.88
R_t Variance	109.93	11.55	3.91	2.59	1.26	1.21	1.18	1.13
R_t Mean	1.00±10.48	1.04±3.40	1.07±1.99	1.06±1.61	1.06±1.12	1.06±1.10	1.07±1.09	1.06±1.11
Prev-to-Inc Ratio (τ_p)	23.79±44.38	11.61±13.40	10.73±9.15	10.33±6.56	10.41±7.07	10.33±6.42	10.14±5.58	10.51±8.08
Clock Rate (nt/site/day)	5.24×10^{-5}	2.96×10^{-5}	2.17×10^{-5}	2.07×10^{-5}	1.91×10^{-5}	1.95×10^{-5}	1.94×10^{-5}	1.94×10^{-5}

4.3.3.1 Skyline scaled effective population size N_e

The effective population size N_e scaled from the BSP estimates of the FMDV WGS simulated under the stationary system, and derived using the epidemiological formulation of the generation time τ, are plotted in Figure 4-7 along with the reconstructed epidemic curve drawn from the P^{exp} prevalence data. It is clear from a visual inspection that the decrease in the k dispersion parameter used for simulating the population dynamics [thus increasing the $var(R_t)$], was correlated with the increase in the N_e predicted infected population size. Starting from a value of 10 used for the dispersion parameter k, N_e was found to be reaching the size of the empirical prevalence estimated from the P^{exp} data. The difference in size was described with the prevalence data being 1.2 times higher than the N_e values (RMSD=228.5) (Table 4-9). No significant variation between simulations ran using k values in the 50 to 1000 range were observed (p>0.05). At values of the dispersion parameter 10>k>1 (a scenario that is close to the UK 2001 FMD epidemic), the N^* curve was found to be lower than the actual P^{exp} prevalence, although closely reconstructing the empirical prevalence trajectory. For this case, the P^{exp} estimates were 1.8 and 1.2 times higher than the predicted infection prevalence N^* for k=1 and k=10, respectively.

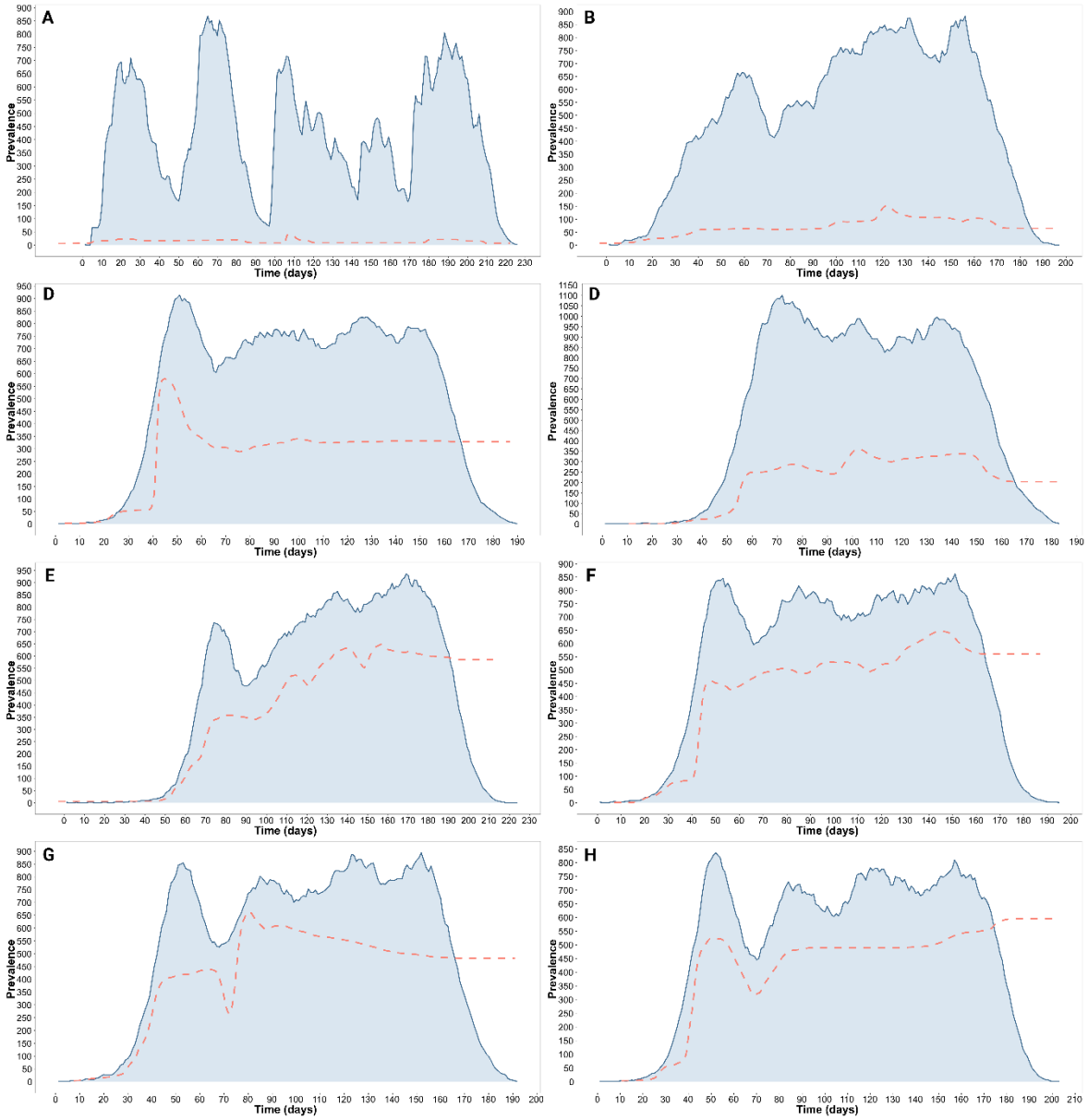

Figure 4-7. Scaled N_e estimated using the BSP from the WGS generated by the stationary FMD simulation. $NB(k,p)$ dispersion parameter set as 0.01 (A), 0.1 (B), 0.5 (C), 1 (D), 10 (E), 50 (F) 100 (G), and 1000 (H). Epidemic curve was estimated from the P^{exp} (blue) prevalence data. Generation time is defined with the epidemiological τ formulation. Average scaling implementation.

Table 4-9. Statistical parameters estimated from the correlation between scaled N_e values based on the BSP and the empirical prevalence data extracted from the simulated FMD stationary system under different parameterisations of the dispersion parameter k. Generation time is defined with epidemiological τ formulation. Average scaling implementation.

	$NB(k,p)$ Dispersion Parameter							
	0.01	*0.1*	*0.5*	*1*	*10*	*50*	*100*	*1000*
RMSD	471.7	492.0	475.5	345.5	228.5	247.9	248.7	255.1
β	28.19	7.01	2.77	1.85	1.23	1.22	1.27	1.14
R^2	0.85	0.92	0.91	0.87	0.88	0.87	0.88	0.82

4.3.3.2 Infection prevalence N^*estimated using the $var(R_t)$ scaling formulation

Including the $var(R_t)$ of the Koelle and Rasmussen (2012) form and the serial case interval τ_c as scaling parameters for recovering the infection prevalence N^* using the estimates obtained from the BSP analysis, the N^* curves reconstructed for each of the simulation scenarios of the FMD stationary system are presented in Figure 4-8. The recovered N^* estimates were found to be directly proportional with the decrease in the $var(R_t)$ produced by larger dispersion parameter k used for sampling from the negative binomial distribution. At k=0.01 [$var(R_t)$=109.9], the P^{exp} prevalence was estimated on average 1.6 times higher than N^*, with a relatively higher deviance (RMSD=254.8) (Tables 4-10). In addition, the oscillatory structure of the empirical prevalence was not fully reproduced by the predicted N^* trajectory. With a decrease step in k [value of 0.1, $var(R_t)$=13.9], the infection prevalence N^* was found to be further decreasing its correlation with the P^{exp} prevalence (RMSD=402.4), thus indicating a drop in the number of infected cases recovered by N^* with the decrease in the $var(R_t)$ of the system. A further increase of the dispersion parameter k for simulating a decrease in the $var(R_t)$ of the system produced a further drop in the N^* estimates. On average with k≥10, the P^{rem} prevalence was found to be 4.6±0.90 times higher than N^* , with predicted and empirical data being reported as highly linearly related (average R^2 value of 0.86±0.03) (Table 4-10). For the scenario corresponding to the UK 2001 FMD (10<k<1), N^* was found largely lower than the P^{exp} prevalence, with the latter being 3.5±0.4 times higher than the N^* estimates.

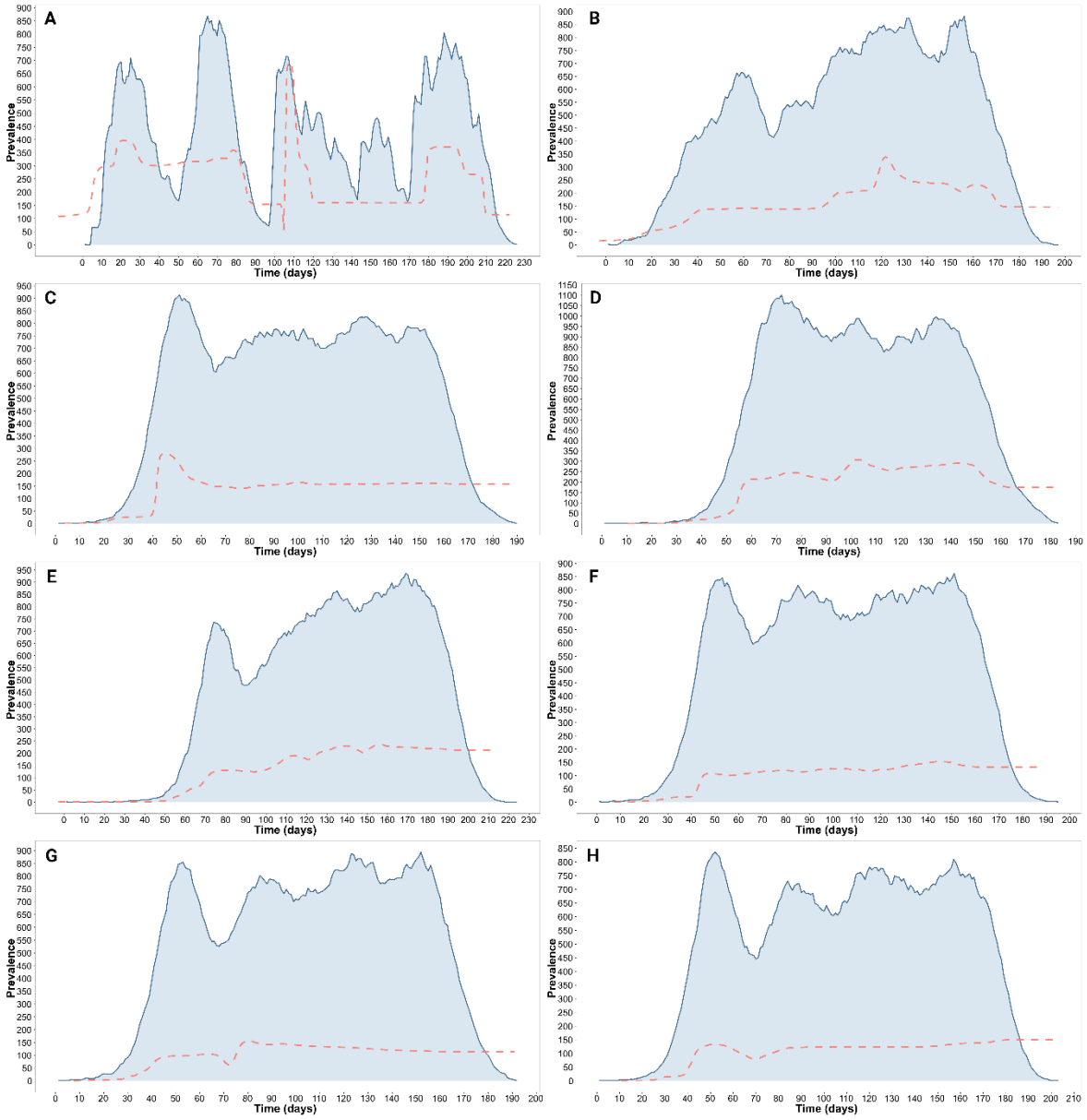

Figure 4-8. Infection prevalence N^* estimated from the WGS generated by the stationary FMD simulation. The variance in the secondary cases per primary infection R_t for the scaling equation has been assumed as the Koelle and Rasmussen (2012) formulation. Generation time is defined with the serial case interval τ_c formulation. $NB(k,p)$ dispersion parameter set as 0.01 (A), 0.1 (B), 0.5 (C), 1 (D), 10 (E), 50 (F) 100 (G), and 1000 (H). Epidemic curve was estimated from the P^{exp} (blue) prevalence data.

Table 4-10. Statistical parameters estimated for the relationship between infection prevalence N^* estimated under the assumption of variance in R_t [Koelle and Rasmussen (2012) parameterisation] and the empirical prevalence data extracted from the simulated stationary system under different parameterisations of the dispersion parameter k. Generation time is defined with the serial case interval τ_c formulation. Average scaling implementation.

	$NB(k,p)$ Dispersion Parameter							
	0.01	*0.1*	*0.5*	*1*	*10*	*50*	*100*	*1000*
RMSD	254.8	402.4	506.9	479.7	435.1	521.2	524.4	479.5
β	1.62	3.12	3.23	3.84	3.39	5.18	5.38	4.53
R^2	0.85	0.92	0.91	0.87	0.88	0.87	0.88	0.82

4.3.3.3 Infection prevalence N^* estimated using the NLFT scaling formulation

Expressing the phylogenetic structure by NLFT and using the prevalence-to-incidence ratio τ_p for recovering the infection prevalence N^*, the effect of the different values of the dispersion parameter k [and thus the $var(R_t)$] used for simulating the FMD stationary system is presented in Figure 4-9. As observed from the reconstructed N^* curves, the decrease in the dispersion parameter k used for the negative binomial distribution and, therefore, the increase of in the $var(R_t)$ value was correlated with a decrease in N^*, although constantly providing a fair degree of precision in reconstructing the shape and trajectory of the prevalence curve. At higher $var(R_t)$ (109.9 and 11.5, derived using k=0.01 and 0.1, respectively), no clear correlation between the recovered N^* and prevalence was reported, with very low deviances from P^{rem} estimated (RMSD=477.4 for k=0.01, and RMSD=475.8 for k=0.1) (Table 4-11). Increasing the dispersion parameter k at values of 0.5 and 1 [$var(R_t)$ equal to 3.9 and 2.6, respectively], N^* predicted estimates started to increase, although producing high deviances from the prevalence data extracted from the P^{exp} time (RMSD=405.7 for k=0.5, and RMSD=269.4 for k=1) (Table 4-11). Empirical P^{exp} prevalence was found to be of the order of 2.1 (k=0.5) and 1.4 (k=1) times higher than the infection prevalence N^*, respectively . With a further increase in the dispersion parameter k (between 10 and 100) and thus a decrease in the $var(R_t)$ (estimated on average as 1.2±0.04), a more evident correlation between the recovered N^* and the P^{exp} prevalence was observed. On average, RMSD deviance estimates was reported to be 222.9±12.7 (Table 4-11), with N^* values to be 1.09±0.01 times lower than the P^{exp}. This difference was not found to be statistically significant (p>0.05). For values of k corresponding to the UK 2001 FMD epidemic (10<k<1), N^* was again observed to be highly correlated with the P^{exp} prevalence, although being on average 1.1±0.3 higher than the empirical data, with the shape of the N^* trajectory closely matching the empirical P^{exp} curve.

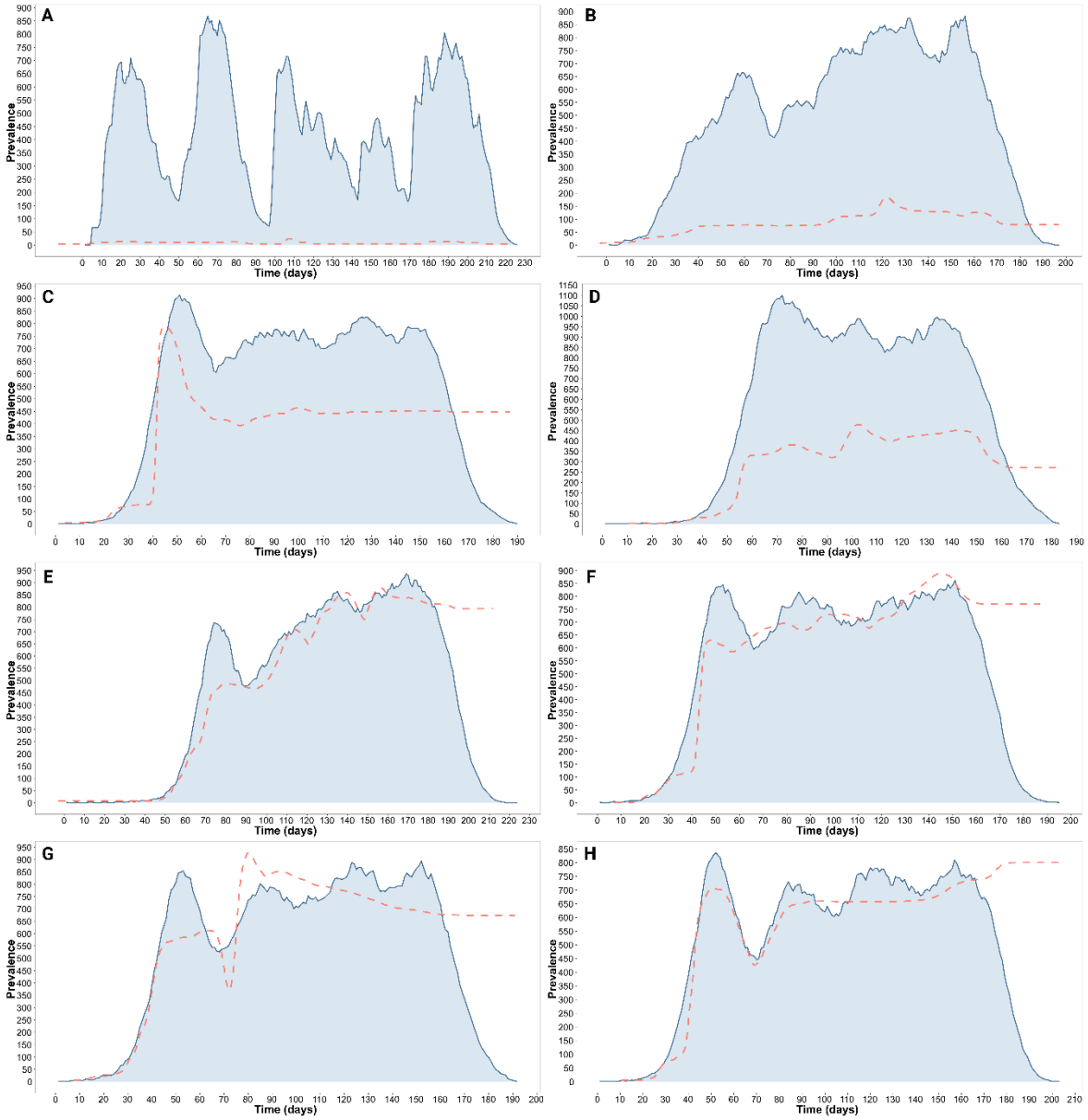

Figure 4-9. Infection prevalence N^* estimated from the WGS generated by the stationary FMD simulation. Generation time is parameterised as the prevalence-to-incidence ratio τ_p (Frost and Volz, 2013) (§3.2.2.3, §4.2.2.2). $NB(k,p)$ dispersion parameter set as 0.01 (A), 0.1 (B), 0.5 (C), 1 (D), 10 (E), 50 (F) 100 (G), and 1000 (H). Epidemic curve was estimated from the P^{exp} (blue) prevalence data.

Table 4-11. Statistical parameters estimated for the relationship between infection prevalence N^* estimated by expressing the phylogenetic structure by NLFT and the empirical prevalence data extracted from the simulated stationary system under different parameterisations of the dispersion parameter k. Generation time is defined with the prevalence-to-incidence ratio τ_p formulation (§3.2.2.3, §4.2.2.2). Average scaling implementation.

	$NB(k,p)$ Dispersion Parameter							
	0.01	*0.1*	*0.5*	*1*	*10*	*50*	*100*	*1000*
RMSD	477.4	475.8	405.7	269.4	210.3	235.8	222.8	264.0
β	46.02	5.73	2.08	1.36	0.91	0.89	0.91	0.85
R^2	0.85	0.92	0.91	0.87	0.88	0.87	0.88	0.82

4.4 Discussion

In this chapter, a thorough investigation of the relationship that exists between the effective population size N_e extracted from the BSP and the actual number of infected cases has been presented. The aim was to attempt to identify a valid formulation which can be used to scale N_e to a proxy measure of empirical prevalence data, here termed the infection prevalence N^*. Three formulations derived from $\frac{N_e}{N}$ equations (as in Table 4-1) were tested with two different scaling approaches, namely average and time-varying, describing the potential epidemiological and/or evolutionary factors associated with the relationship of these two quantities, from a simple linear scaling of generation time to the account of complex variabilities in the population structure under study. The uniqueness of this study relies in the data which, albeit simulated for its genetic component, have been obtained from a single exhaustive and fully-resolved epidemic (*i.e.* the UK 2001 FMD epidemic) where the demography of the infected population is fully known, thus enabling measurement of a direct correlation in time between the real epidemic size and the recovered infection prevalence N^*.

Although the shape and trajectory of the scaled N^* curve followed with precision the epidemic curve generated from the prevalence data and a strong linear relationship has been established (R^2 value of up to 0.93), the exact match varied considerably according to the scaling formulation used. Thus, defining prevalence data according to the timing of the FMD disease progression (as previously described in §3.2.2.2), different correlations exist between the infection prevalence N^* and the prevalence data extracted from each of the time-related FMD stages. It is evident that, using N_e estimated directly from the BSP and scaling this quantity using the epidemiological definition of generation time τ, a clear correlation with the prevalence extracted from the P^{exp} is observed. Expressing the phylogenetic structure by NLFT and using the prevalence-to-incidence ratio τ_p for deriving the infection prevalence N^*, this quantity effectively resolves the shape and trajectory of the prevalence computed from the P^{exp} data. On the other hand, accounting for the variability in the number of progeny per single IP generated across the different phases of the epidemic and using the Koelle and Rasmussen (2012) form of $var(R_t)$ along with the serial case interval τ_c for recovering N^*, estimates were observed to not correlate with the infected

population size derived from the P^{exp} prevalence data, where the predicted N^* was found to be considerably higher than the empirical prevalence. This finding indicates that, for correctly scaling an estimate of N_e to the actual number of infected cases (expressed as prevalence), the generation time should be measured by as the prevalence to incidence ratio τ_p, and scaling should express the phylogenetic structure by the number of lineages as a function of time.

Investigating the effect of the $var(R_t)$ on the estimation of the infected population demography and examining the results obtained from the analysis of the stationary FMD simulation, it is evident that the variability in the number of secondary cases per primary infection R_t greatly impacts on the BSP reconstruction of the actual number of infected cases and, although accurately describing the shape of the demographic curve and its trajectory, the increase in the stochastic reproduction of the infected population [*i.e.* $var(R_t)$] significantly reduces the BSP accuracy. This outcome has been consistently observed for every formulation used to scale the BSP estimates to either the effective population size N_e or the infection prevalence N^*, even those that include the variance in the number of secondary cases per primary infection explicitly in the formulation of the scaling equation. On the other hand when $var(R_t)$ is reduced by increasing the dispersion parameter k, the infection prevalence N^* matches the P^{exp} prevalence, although the precise relationship varies according to the formulation used for scaling the BSP data and, therefore, the model assumptions. For example, the fit from the scaling equation that considers the phylogenetic structure by NLFT suggests that in a more homogeneous FMD system [i.e. with $k \geq 10$ and $var(R_t) \approx 1$] the predicted infection prevalence N^* is a good approximation to the empirical IP count (P^{exp} derived). This means that every IP in the system has the same chance of transmitting infection to subsequent generations and, therefore, the average time between infections is the only possible scaling factor and is constant.

Assuming a more stochastic disease system in which the presence of 'superspreaders' is not solely driving the transmission process [*i.e.* $0.5 < k < 10$ and $2 \lesssim var(R_t) \lesssim 3$], estimates of infection prevalence N^* provided by the scaling transformation of N_e which account for $var(R_t)$, closely match with the empirical infected population size (P^{rep} derived), maintaining or even increasing its accuracy when the system is structured as being more homogeneous [i.e. with $k \geq 10$ and $var(R_t) \approx 1$]. When $10 < k < 1$, the FMD stationary system returns very similar estimates of epidemiological parameters (*i.e.* τ_e, $var(R_t)$, $E(R_t)$, τ_p) to those obtained from the

UK 2001 FMD empirical data, with a further similarity on the correlation between the infection prevalence N^* recovered using the NLFT scaling formulation and the P^{exp} prevalence data. The β parameters extracted from the two analyses were also very close (0.88 and 0.91 for the UK 2001 FMD epidemic and the FMD stationary system, respectively). However, the effect of the serial case interval τ_c within the FMD stationary system on recovering the empirical prevalence using the N^* estimator needs to be further clarified.

Magiorkinis et al. (2013) describe how the N/N_e ratio (*i.e.* the prevalence to the effective number of infections ratio) is equal to $var(R_t)$ when the genetic variability between strains has a negligible effect on their infection potential, with the $var(R_t)/\tau$ being termed the phylodynamic transmission parameter (PTP). Theoretically, the PTP is assessed through linearly correlating N with N_e and obtaining the estimates from the slope β of the regressor (*i.e.* $N = \beta N_e$). The results provided by the UK 2001 FMD epidemic (using the epidemiological generation time τ corresponding to the definition the authors described in their study) do not support this hypothesis, since the β is calculated to be 1.1±0.05 whilst the $var(R_t)$ extracted from the epidemiological data is estimated to be 3.9±0.1. This relationship does not converge even when recovering the N_e using the serial case interval τ_c (β=1.3±0.05). Looking at the results generated from the FMD stationary system, the recovery of the $var(R_t)$ from β estimates seems to be possible with large values used for the dispersion parameter of the negative binomial distribution (for $k \geq 10$), which thus defines systems with lower variability in the population structure (*i.e.* where all the IPs are contributing on average equally to the transmission process and no 'superspreaders' would be defined). This finding would indicate that the recovery of the infection prevalence N^* from a simple linear relationship between the real infected population size N and the effective population size N_e in a really complex system would be in some way difficult. Nevertheless, it has been demonstrated here that in a more homogeneous epidemiological system, such as the UK 2001 FMD epidemic, the empirical prevalence P^{exp} and the infection prevalence N^* are very closely related in relative size.

It is interesting to note that although the number of infected cases estimated by the UK 2001 FMD epidemic or the simulated FMD stationary systems are dying out in the tail end phase, and thus leading to the end of the infection, the BSP still continue to record infections. For example, at day 232 from the start of the UK 2001 FMD epidemic (*i.e.* the last day of the epidemic) the N_e estimated by the BSP still recorded an average

of 17 active cases, whilst the prevalence is equal to 1 and the incidence is zero. The BSP issue in the estimation of the last phase of *a datum* system has been already reported as due to a lack of genealogical information at later times (de Silva et al., 2012). Although this would not be an issue while retrospectively analysing viral disease demography though generally biasing the results, it might lead to incorrect forecasts if using the BSP to monitor the infection trend in real time during an epidemic.

CHAPTER 5

Optimal structure of incompletely sampled datasets

5.1 Rationale

In Chapter 4, it was demonstrated that the infection prevalence N^* scaled from N_e estimated from genetic data collected from a fully resolved epidemic system might be equated to the actual number of infected cases, although there was inherited complexity and variability in matching a single prevalence estimate. It was also observed that when expressing the phylogenetic structure by NLFT and scaling N_e using the prevalence-to-incidence ratio τ_p, the correlation between the predicted N^* and the empirical infected population size is close to P^{exp}. This finding was been also reproduced at a simulated steady state, when the variance in the reproductive number of the IPs is set equal to that of the UK 2001 FMD epidemic. It should be noted that the N^* demographic signal recovered from the UK 2001 FMD epidemic resulted from a large and fully observed and sequenced outbreak (albeit simulated), whilst the simulated steady state was derived from a more poorly sampled but relatively large population. However, in more common epidemic or endemic scenarios, it would often be the case that representative field samples would not be collected from all of the reported IPs. Therefore, the actual sampling rate would vary and this could directly impact on the accuracy of reconstructed population dynamics.

The coalescent model, from which the BSP is derived, assumes that the samples are randomly collected from a homogeneous population (Griffiths and Tavare, 1994b), a criterion which in a real scenario would not be always satisfied. Most importantly, increasing the sample size s does not improve the accuracy of estimates in a manner that is typically observed in conventional statistical analysis. For example, in the standard coalescent model the variance of estimators of the scaled mutation rate $\theta = 4Nu$ decreases at a rate $1/\log s$, rather than $1/s$ (Rosenberg and Nordborg, 2002). Sampling bias represents an important issue for coalescent-based demographic reconstruction methods. In recent years, there has been a substantial expansion in the

volume of genetic data within surveillance programs and larger multi-gene and WGSs are now becoming routine for disease monitoring. Despite this, very few studies have attempted to understand the effect of reduced sampling rates, bias or structure of the sampling protocol on the reconstructed population dynamics given by analysis of the BSP. Although focussing on investigating the accuracy of BSP estimates on complex acute RNA virus dynamics, Stack et al. (2010) provided an indication of how bias in the structure of sequenced samples renders BSP estimates less reliable. In addition, it has been considered that samples taken at a single time point would not provide enough resolution for reconstructing past population dynamics (Rambaut et al., 2008, Stack et al., 2010). However, no studies have made use of fully-resolved epidemic data to capture the impact of sampling bias in the estimation of viral population history.

In this chapter by sub-sampling from a full (simulated) UK 2001 FMDV WGS dataset, the effect of the sampling rate on the efficiency of the BSP-derived N_e to reconstruct the epidemic demography has been explored. Different sampling protocols have been employed, from a simple random assumption of sampling sequence data to a more structured and stratified protocols. As already reported, the scaling formulation which expressed the phylogenetic structure by NLFT, making use of the prevalence-to-incidence ratio for scaling the effective population size N_e, provided the best fit for recovering empirical prevalence from the predicted infection prevalence N^*. Therefore, this scaling formulation has been further used for performing the analyses of this chapter. The methodology used for estimating the effective population size N_e from a BSP analysis was that used in chapter 4 (§4.2.2.3).

5.2 Simple random sampling of genetic data

Twelve simulation runs of the UK 2001 FMD epidemic were used to assess the variability of the reconstructed FMDV population dynamics from data drawn using a simple random sampling (SRS) protocol. FMDV WGS were sampled at a decreasing sampling proportion s at 0.25 intervals from the database of the full epidemic dataset (n=2026 IPs) using the common definition of SRS without replacement and disregarding the order of the sample (Lohr, 2010, Tille, 2006). The molecular clock rate (estimated from BEAST) recovered from these sampled datasets are shown in Figure 5-1. When sampling represented 50% or more of the total WGS, the molecular clock

rate was more accurately estimated (average value of 2.17×10^{-5} nt/site/day) with narrow 95%CIs and low deviance between model runs (CV=0.08), whilst when using less than 50% of the full WGS dataset higher clock values (average value of and 3.28×10^{-5} nt/site/day) and wider 95%CIs were reported.

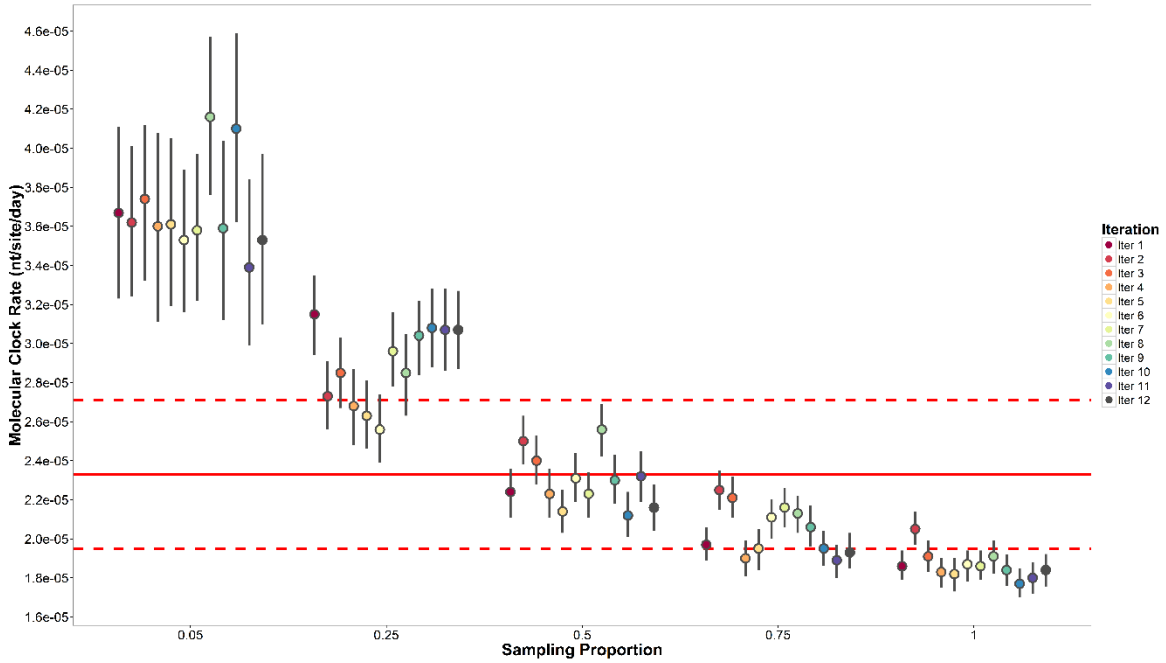

Figure 5-1. Molecular clock rate (nt/site/day) estimated using BEAST 1.8.0 under the assumption of a strict clock evolutionary model from 12 realisations of the full UK 2001 FMDV WGS simulated database (n=2026) and from each of the resampled datasets at a decreasing sampling proportion rate s of 0.25. The red line defines the molecular clock rate estimated from empirical sequence data (n=39 WGS) collected from the UK 2001 field samples (with estimated clock of 2.33×10^{-5}), whilst the red dashed lines define its 95%CI region (1.95×10^{-5} to 2.4×10^{-5}). Sampled datasets drawn under the SRS scheme.

Relating the effective population size N_e to the infection prevalence N^* using the NLFT scaling formulation, a direct correlation was observed between a decreased sampling rate and an increase in the noise derived from the reduced genetic signal, although this was observed most strongly for sampled datasets comprising less than 50% of the total samples (Figure 5-2). On visual inspection, the epidemic curves recovered from the infection prevalence N^* were largely matching the prevalence recovered from the P^{exp} data when s>50%. For example at s=0.75, the absolute difference between sampled and full WGS data was on average 36.4±14.9 IPs. On the other hand, the accuracy in matching the P^{exp} prevalence was reduced when sampling at lower rate, recording an average absolute difference of 132.9±15.0 IPs from the full WGS data at s=0.25. The same regression through the origin (RTO) procedure used in Chapter 4 has been performed here in order to correlate the infection prevalence N^* estimated from sampled data and that recovered from the full WGS dataset. As shown

in Table 5-1, the β parameter was found to be close to 1 with very low variability between model runs when sampling 75% of the total number of WGS data (CV=0. 07), whilst sampling less than 25% of the data produced less accurate and noisier results (average β value of 2.38±0.57; CV=0.15±0.03). At s=0.25 the predicted N^* was reported to be close to the half of the empirical prevalence P^{exp} (β=1.98±0.26). The accuracy was found to reduce linearly with decreasing sampling rate (R^2=0.89). The observed decay in the accuracy derived from reducing the sampling rate was reflected in the difference in the infection prevalence N^* between the sampled and the full data.

Considering the N^* estimates extracted from each of the epidemic phases, an absolute difference of 277.6 IPs (CV=0.09) between the sampling database comprising 5% of the total data and the full WGS dataset was reported for the epidemic peak, whilst a difference of 142.1 IPs (CV=0.12) was estimated for the decline phase. Conversely, a lower size difference was observed for the exponential and plateau phases, although decreasing the amount of data used for generating the N^* curve increased the extent of the variability between estimates produced using different model runs (average CV value for s≤0.25 of 0.30±0.19).

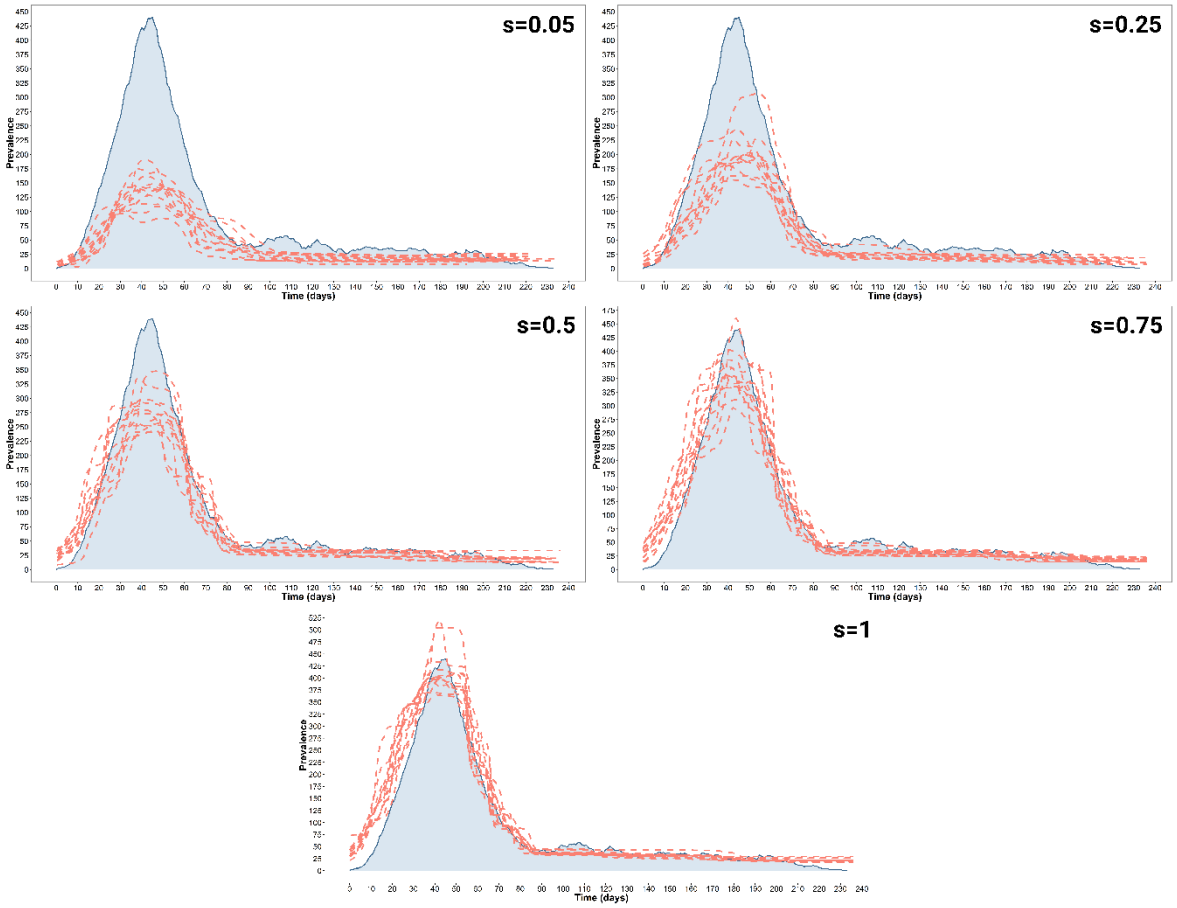

Figure 5-2. Infection prevalence N^* estimated from 12 realisations of the full UK 2001 FMDV WGS simulated database (n=2026) and resampled datasets at a decreasing sampling proportion rate s of 0.25. Epidemic curve was estimated from the P^{exp} (blue) prevalence data as defined in §3.2.2.2. Datasets were sampled under the SRS scheme.

Table 5-1. Time specific number of infected cases recovered from the infection prevalence N^* estimated from 12 realisations of the UK 2001 FMD full IPs (n=2026) epidemic scenario and resampled datasets at a decreasing sampling proportion s of 0.25. β parameter designates the slope of the regressor of the RTO analysis. Datasets were sampled under the SRS scheme.

		Epidemic Phase			
Sample proportion	*β*	*Exponential*	*Peak*	*Decline*	*Plateau*
P^{exp}		195.01±2.15	439.83±3.19	203.17±0.83	30.62±0.04
1 (n=2026)	Ref.	173.53±12.55	419.61±47.58	218.50±13.66	29.58±1.93
0.75 (n=1519)	1.16±0.08	162.19±19.28	364.81±43.26	156.70±13.82	26.94±3.54
0.5 (n=1013)	1.42±0.09	137.06±16.12	281.72±33.55	134.48±14.53	26.42±4.39
0.25 (n=506)	1.98±0.26	98.05±14.02	207.80±40.21	109.09±19.55	19.51±4.00
0.05 (n=101)	2.78±0.48	71.86±10.52	141.95±26.60	76.34±17.64	19.61±5.36

5.3 'Probability proportional to size' sampling of genetic data

To account for the structure of the genetic signal carried by WGS data within a partially sampled scenario, a 'probability proportional to size' (PPS) sampling scheme (Lohr, 2010) was applied to sample from the simulated UK 2001 FMDV WGS full

dataset (n=2026 IPs). First, it is necessary to establish strata of the data – here termed elements, M_i. The probability of sampling from the ith element, p_i, is proportional to the relative size of the M_i, thus $p_i = \frac{|M_i|}{\sum_{i \in U} |M_i|}$ (where U is the union of all indices). For continuous variables (such as genetic distance, evolutionary duration, epidemiological generation time τ , and spatial transmission distance), the empirical probability density function for the variable was estimated from the reconstructed UK 2001 transmission tree using a kernel density approach and partitioned in to 3 elements: the lower 2.5th percentile, the $\bar{x}$±SD and the upper 97.5th percentile regions (Figure 5-3). For discrete variables (such as spatial region, month and week of reporting), each ith element denoted each of the discrete values. The general PPS algorithm for sampling within each of the above defined M_i elements was then used (Cochran, 1977). For the PPS trial, datasets that were sampled at a decreasing rate s of 0.25 from the full WGS database were constructed for each of the epidemiological and genetic variables assessed, where the genetic sequence from the index IP (IP4) was always included.

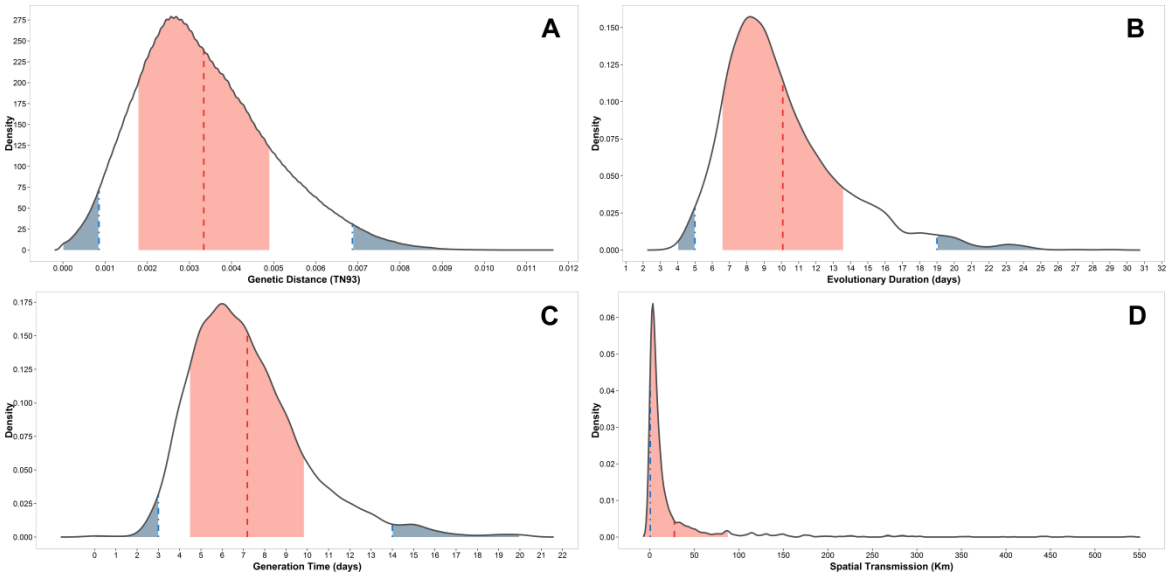

Figure 5-3. Empirical probability density functions of epidemiological and genetic parameters estimated from the UK 2001 FMD epidemic using a kernel density approach for sampling WGS data by a PPS scheme. (A) genetic distance estimated using the TN93 substitution model (Tamura and Nei, 1993), (B) evolutionary duration Δt, (C) generation time with the epidemiological definition of τ, (D) spatial transmission distance estimated between parent-daughter transmission link. Blue areas define the lower 2.5th percentile and 97.5th percentile regions, whilst the red area denotes the $\bar{x}$±SD region.

5.3.1 Sampling within genetic strata

5.3.1.1 Evolutionary duration Δt

The M_i elements of the probability density function estimated from the evolutionary duration Δt data extracted from the reconstructed UK 2001 transmission tree returned were defined as follows: <2.5th percentile, 4 to 5 days; $\bar{x}$±SD, 10.1±3.5 days; >97.5th percentile, 19 to 29 days (Figure 5-3). As shown in Figure 5-4, the reconstructed N^* curve tended to largely deviate from the estimates derived from the full WGS data at a sampling rate s<0.5 (epidemic peak difference of 153.7 IPs), although at s=0.75 the absolute difference was found to be 50.3±14.8 IPs. Using only 5% of the full WGS data, the epidemic peak was estimated at only less than half of the empirical size (absolute difference of 288.0±24.3 IPs). In addition, large deviance values were estimated from different sampled datasets (average CV value of 0.27±0.22), even with sampling rates of more than 50% of the total WGS data (CV=0.38±0.25), indicating lower precision in the estimate of the infection prevalence N^* by the PPS scheme than using a simple SRS (Table 5-2). In addition, the β parameter increased linearly with the reduction in the sampling rate (R^2=0.90), with β values estimated at s≤0.5 higher than that obtained using the SRS scheme (2.14±0.71 vs 2.06±0.69).

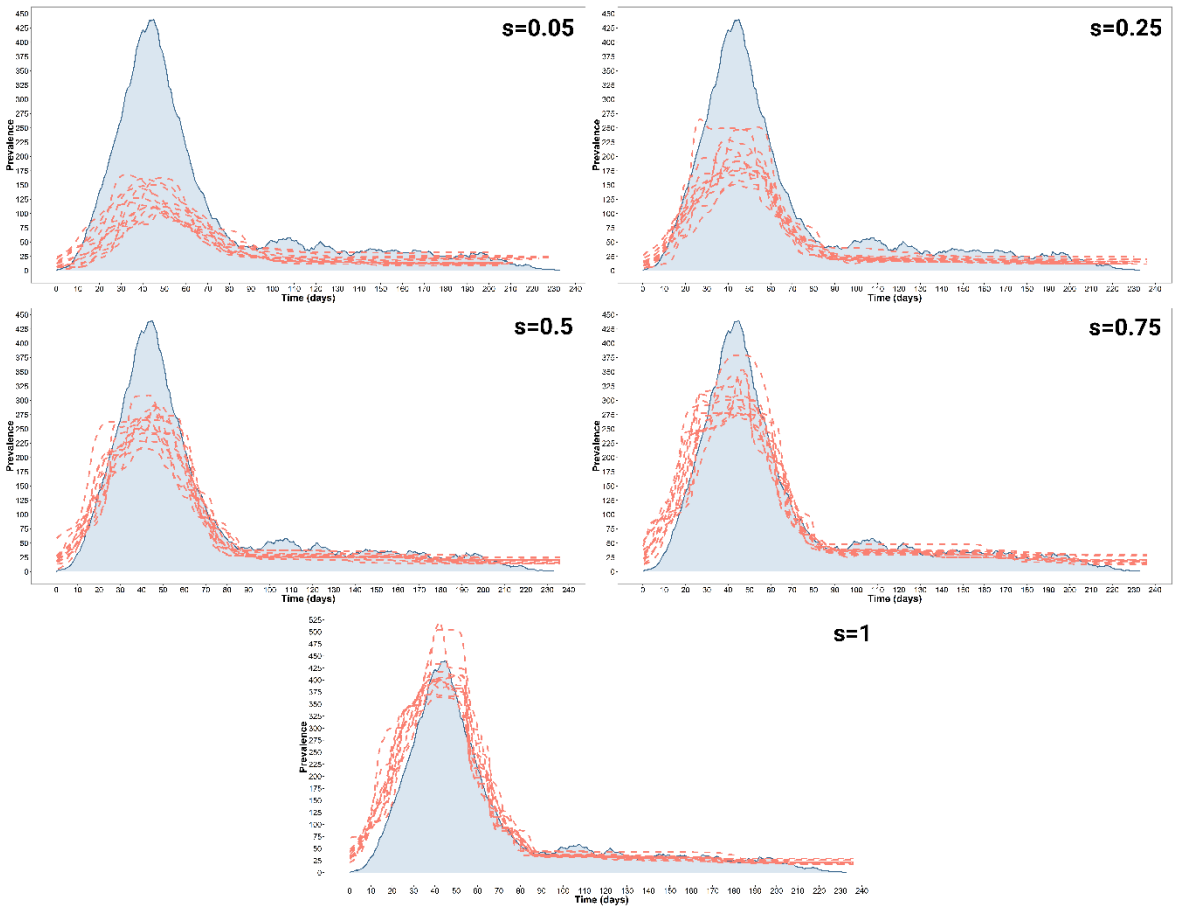

Figure 5-4. Infection prevalence N^* estimated from 12 realisations of the full UK 2001 FMDV WGS simulated database (n=2026) and resampled datasets at a decreasing sampling proportion rate s of 0.25. Epidemic curve was estimated from the P^{exp} (blue) prevalence data as defined in §3.2.2.2. Datasets were sampled under the PPS scheme using the evolutionary duration Δt genetic variable.

Table 5-2. Time specific number of infected cases recovered from the infection prevalence N^* estimated from 12 realisations of the UK 2001 FMD full IPs (n=2026) epidemic scenario and resampled datasets at a decreasing sampling proportion s of 0.25. β parameter designates the slope of the regressor of the RTO analysis. Datasets were sampled under the PPS scheme using the evolutionary duration Δt genetic variable.

		Epidemic Phase			
Sample proportion	*β*	*Exponential*	*Peak*	*Decline*	*Plateau*
P^{exp}		195.01±2.15	439.83±3.19	203.17±0.83	30.62±0.04
1 (n=2026)	Ref.	173.53±12.55	419.61±47.58	218.50±13.66	29.58±1.93
0.75 (n=1519)	1.25±0.05	151.62±18.20	314.10±33.73	150.03±10.28	28.95±2.88
0.5 (n=1013)	1.51±0.10	124.03±15.68	265.93±27.50	128.97±12.26	23.96±2.81
0.25 (n=506)	2.03±0.27	96.30±12.28	202.11±34.51	98.59±8.87	19.15±3.62
0.05 (n=101)	2.91±0.47	66.83±12.50	131.60±24.32	74.15±9.33	20.41±5.27

5.3.1.2 Epidemiological generation time τ

The M_i elements of the probability density function estimated from the epidemiological generation time τ, were demarcated as follows: <2.5th percentile, 0 to 3 days; $\bar{x}$±SD, 7.2±2.7 days; >97.5th percentile, 14 to 20 days (Figure 5-3). As shown in Figure 5-5, as the sampling rate decreases, a corresponding decrease in the accuracy of reproducing the infection prevalence N^* curve derived from the full WGS dataset

(R^2=0.88) is observed At s≥0.5 the size and shape of the empirical epidemic curve was largely recovered, estimating an average absolute difference of 53.1±16.7 IPs, with a difference in the epidemic peak size of 81.2±30.0 IPs at s=0.75. In addition, the precision between different sampled datasets was found to be similar to that of a simple SRS scheme, estimating an average CV value of 0.43±0.10 for the PPS in comparison with the 0.45±0.06 returned for the SRS. The absolute difference between the 25% sample and the full WGS data was estimated as 103.7±16.6 IPs, whilst using less data (5% of the total WGS) did not significantly reduce the infection prevalence N^* estimates (absolute difference of 134.1±18.8 IPs) (Table 5-3). However, at s=0.05 estimates were less precise that that obtained using a simple SRS (CV of 0.27 vs 0.17).

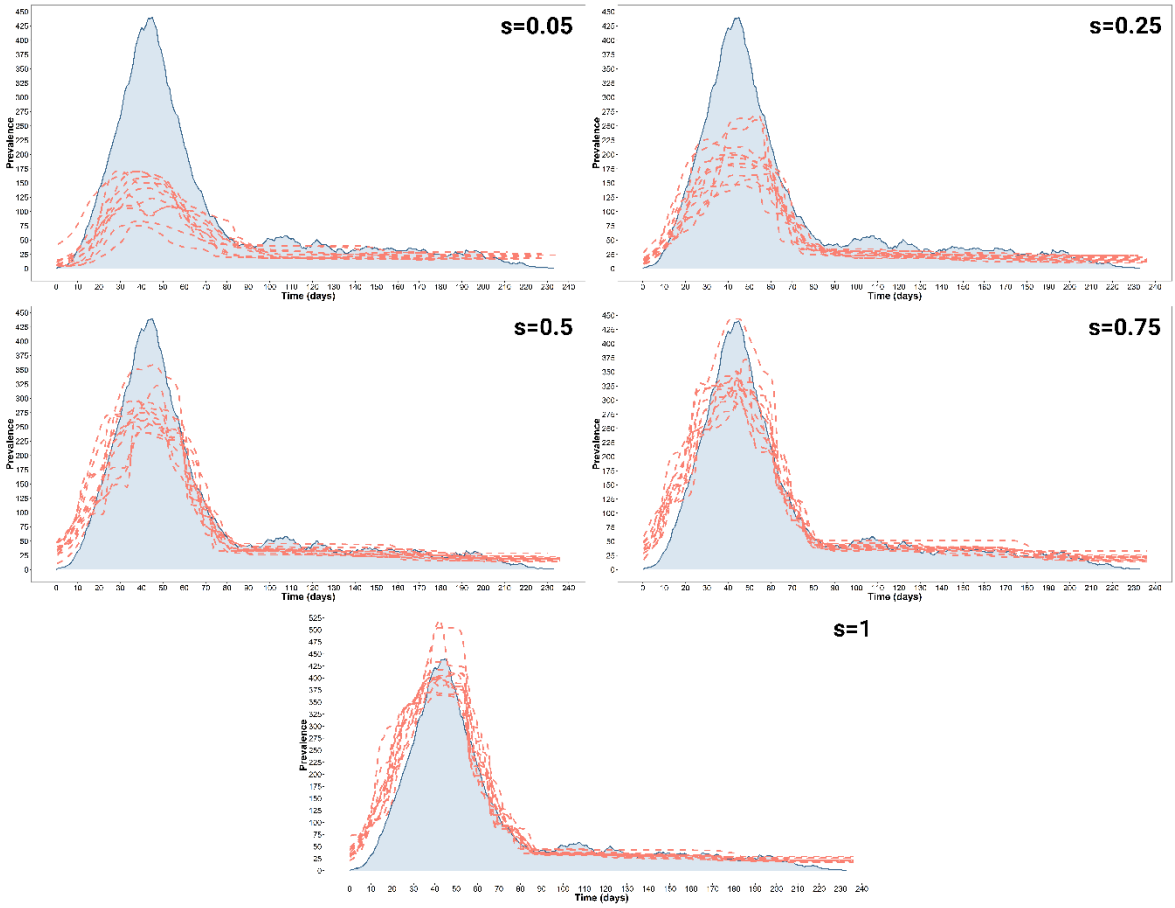

Figure 5-5. Infection prevalence N^* estimated from 12 realisations of the full UK 2001 FMDV WGS simulated database (n=2026) and resampled datasets at a decreasing sampling proportion rate s of 0.25. Epidemic curve was estimated from the P^{exp} (blue) prevalence data as defined in §3.2.2.2. Datasets were sampled under the PPS scheme using the epidemiological generation time τ variable.

Table 5-3. Time specific number of infected cases recovered from the infection prevalence N^* estimated from 12 realisations of the UK 2001 FMD full IPs (n=2026) epidemic scenario and resampled datasets at a decreasing sampling proportion s of 0.25. β parameter designates the slope of the regressor of the RTO analysis. Datasets were sampled under the PPS scheme using the epidemiological generation time $\boldsymbol{\tau}$ variable.

		Epidemic Phase			
Sample proportion	*β*	*Exponential*	*Peak*	*Decline*	*Plateau*
P^{exp}		195.01±2.15	439.83±3.19	203.17±0.83	30.62±0.04
1 (n=2026)	Ref.	173.53±12.55	419.61±47.58	218.50±13.66	29.58±1.93
0.75 (n=1519)	1.17±0.05	159.29±18.92	342.58±37.30	157.28±14.78	32.20±2.99
0.5 (n=1013)	1.40±0.12	138.66±16.24	283.02±32.45	134.10±10.76	27.01±3.54
0.25 (n=506)	1.96±0.18	101.41±14.02	201.17±37.33	102.63±12.19	21.17±2.95
0.05 (n=101)	2.81±0.75	71.98±19.89	134.90±33.95	75.17±17.67	23.05±4.71

5.3.1.3 TN93 genetic distance

The M_i elements of the probability density function estimated from the TN93 genetic distance data extracted from the UK 2001 FMDV WGS simulated under the full epidemic scenario were defined as follows: <2.5th percentile, 0 to 0.0008 base substitutions/site; $\bar{x}$±SD, 0.003±0.001 base substitutions/site; >97.5th percentile, 0.007 to 0.01 base substitutions/site (Figure 5-3). Although the decrease in the accuracy produced by reducing the sampling rate according to the PPS scheme defined using the TN93 genetic distance values was found to be highly linearly related (R^2=0.95), the absolute difference in terms of infection prevalence N^* between the full WGSs data and each of the sampled datasets was not substantial (average value of 54.6±19.9 IPs for 0.5≤s≤0.75) (Table 5-4). This was reflected in the shape of the reconstructed N^* curves, which were reduced in size according to the reduced number of samples present in the dataset, with the structure of each epidemic phase largely preserved (Figure 5-6). Absolute differences for the exponential, peak, decline and plateau phases were 27.1±14.9, 106.9±49.3, 76.5±13.0 and 7.8±2.8 IPs, respectively. In addition, the relative variability between sampled datasets was found to be equal when sampling at different rates s (average CV value of 0.13±0.17 and 0.14±0.17 for 0.5≤s≤0.75 and s=0.25, respectively). The β parameters estimated at lower sampling rate (s≤0.25) were lower than the corresponding values obtained from the simple SRS scheme (2.16±0.36 vs 2.38±0.57). However, the epidemic peak size predicted with a sampling rate of s=0.05 was largely biased and poorly matching the empirical size, with an absolute difference of 255.7±45.4 IPs and a relatively low accuracy between datasets (CV=0.46).

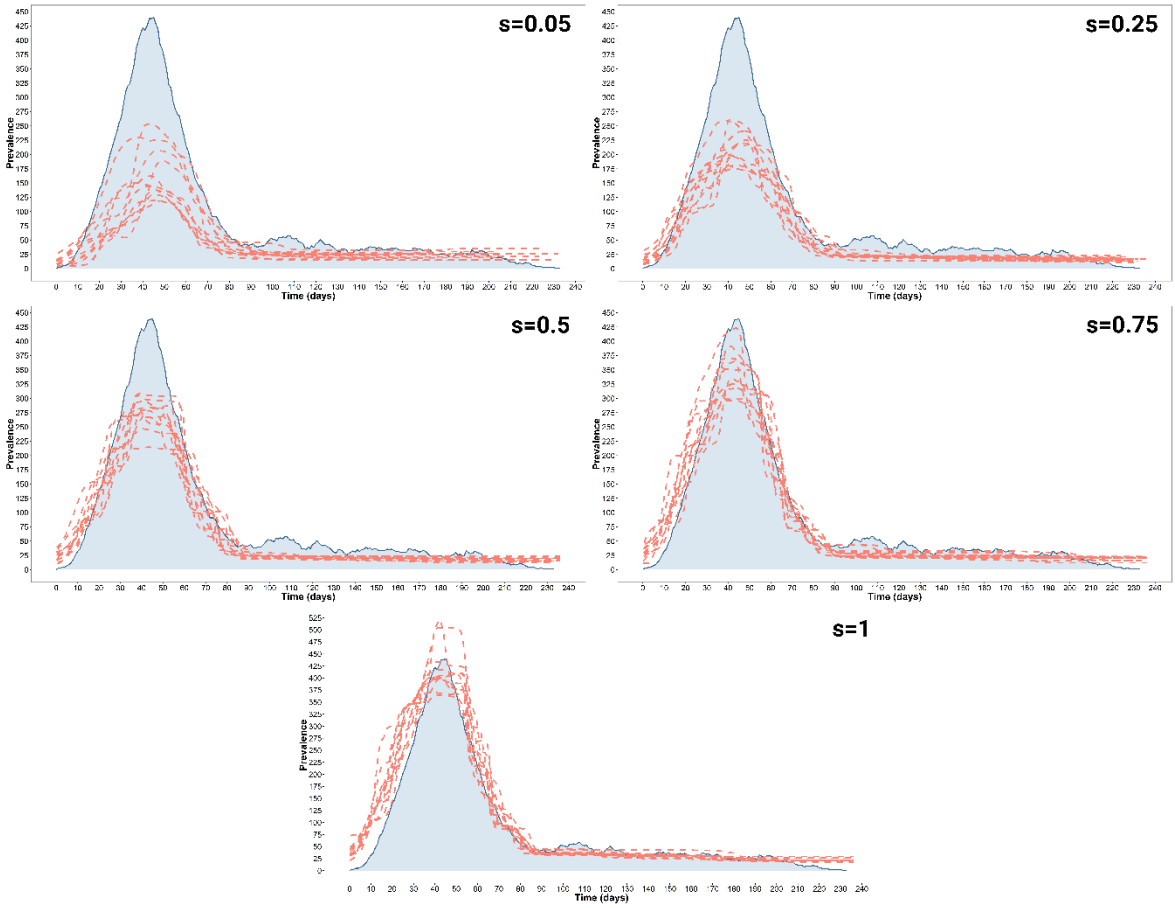

Figure 5-6. Infection prevalence N^* estimated from 12 realisations of the full UK 2001 FMDV WGS simulated database (n=2026) and from each of the resampled datasets at a decreasing sampling proportion rate s of 0.25. Epidemic curve was estimated from the P^{exp} (blue) prevalence data as defined in §3.2.2.2. Datasets were sampled under the PPS scheme using the TN93 genetic distance variable.

Table 5-4. Time specific number of infected cases recovered from the infection prevalence N^* estimated from 12 realisations of the UK 2001 FMD full IPs (n=2026) epidemic scenario and resampled datasets at a decreasing sampling proportion s of 0.25. β parameter designates the slope of the regressor of the RTO analysis. Datasets were sampled under the PPS scheme using the TN93 genetic distance variable.

		Epidemic Phase			
Sample proportion	*β*	*Exponential*	*Peak*	*Decline*	*Plateau*
P^{exp}		195.01±2.15	439.83±3.19	203.17±0.83	30.62±0.04
1 (n=2026)	Ref.	173.53±12.55	419.61±47.58	218.50±13.66	29.58±1.93
0.75 (n=1519)	1.21±0.07	158.91±12.70	348.12±38.22	151.18±9.00	23.79±2.87
0.5 (n=1013)	1.47±0.08	135.88±12.85	277.78±25.95	132.82±7.59	19.83±2.18
0.25 (n=506)	1.91±0. 21	104.37±12.43	212.28±30.34	106.66±12.15	19.61±2.66
0.05 (n=101)	2.42±0.60	74.34±16.45	163.87±45.43	86.48±24.12	28.76±16.88

5.3.2 Sampling within spatial strata

5.3.2.1 Regional division

A regional stratum was defined as a single UK County which reported FMD cases during the 2001 FMD epidemic and, from which, an FMDV isolate was collected. Thus, the full WGS data (n=2026) was subdivided into M_i elements to which the PPS

sampling scheme has been applied. This spatial allocation was based on the spatial connections between the geographical coordinates of each reported IPs and the spatial UK county layer, which defines the county borders (according to 2009 boundaries) (Figure 5-7).

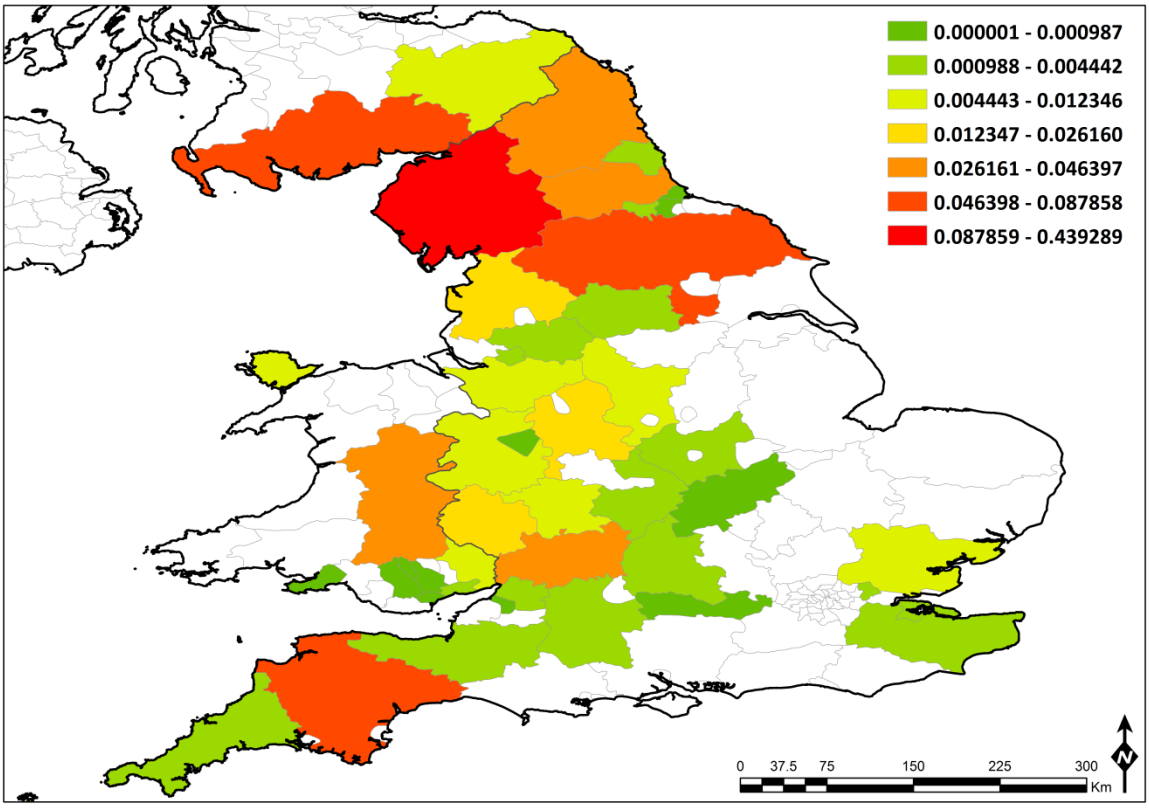

Figure 5-7. Spatial proportion of IPs according to the affected UK counties as reported during the UK 2001 FMD epidemic. The spatial layer defines the UK counties based on the 2009 boundaries.

Results for the estimated infection prevalence N^* curves are shown in Figure 5-8. Although the relative variability between sampled datasets was reported to produce no substantial difference at higher and lower rates of s (average CV value of 0.11±0.01 and 0.18±0.06 for $0.5 \leq s \leq 0.75$ and $0.05 \leq s \leq 0.25$, respectively), reducing the sample size greatly impacted on the accuracy of matching the estimates obtained with the full WGS data. Using only 5% of the total data, an absolute difference of 102.6±18.6, 272.1±42.4 and 139.0±14.3 IPs was estimated for the exponential, peak and decline phases, respectively, whilst averages of 24.8±12.2, 95.8±34.0 and 74.6±16.7 IPs were calculated with datasets sampled at a rate of $0.5 \leq s \leq 0.75$ (Table 5-5). However, the reduced accuracy of the PPS at a sampling rate s=0.05 was similar to the estimates obtained using a simple SRS scheme (absolute difference values of 0.9, 5.6 and 3.1 IPs for the exponential, peak and decline phases, respectively). The β parameter estimated

for the spatial region PPS was found to linearly decrease with the reduced sampling rate s (R^2=0.89), with no statistical difference with the SRS scheme (p>0.05).

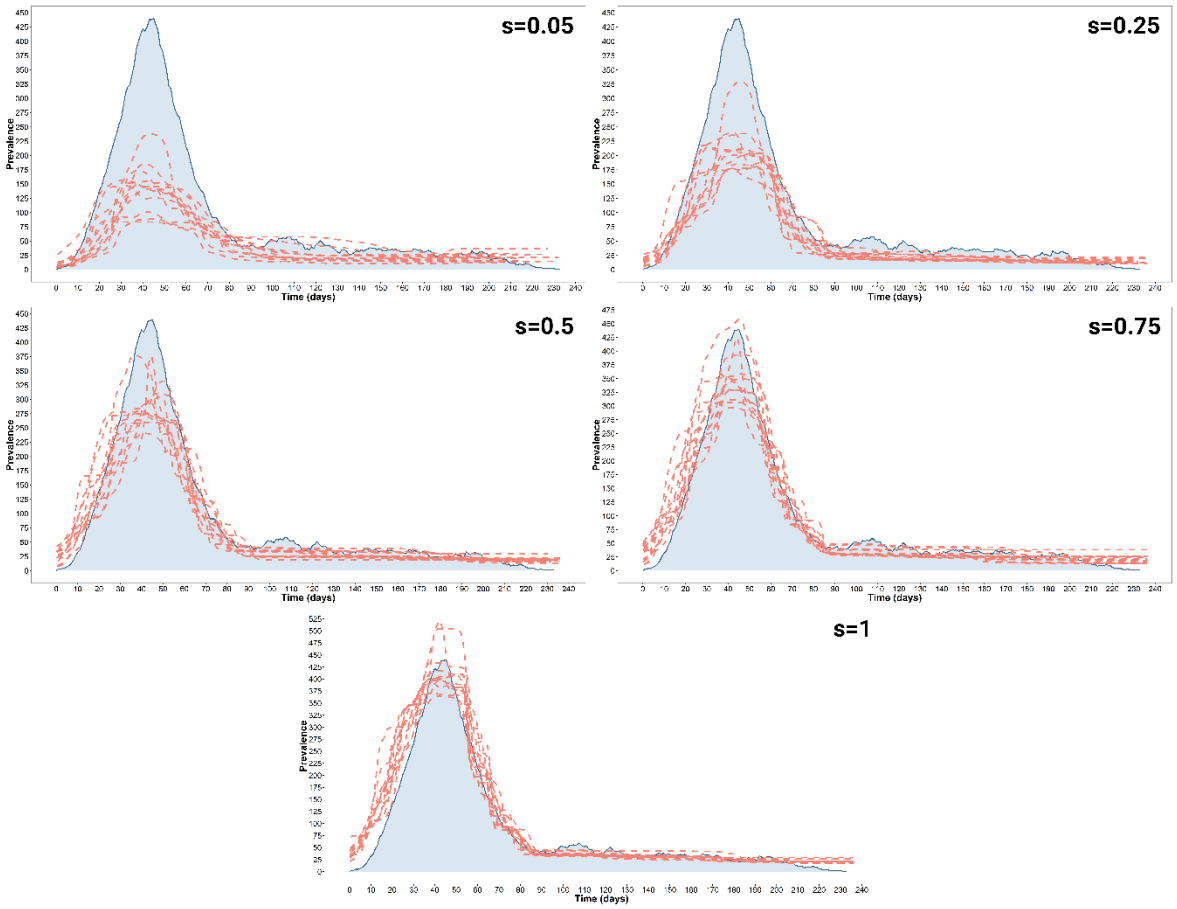

Figure 5-8 Infection prevalence N^* estimated from 12 realisations of the full UK 2001 FMDV WGS simulated database (n=2026) and resampled datasets at a decreasing sampling proportion rate s of 0.25. Epidemic curve was estimated from the P^{exp} (blue) prevalence data as defined in §3.2.2.2. Datasets were sampled under the PPS scheme using the spatial region discrete variable.

Table 5-5. Time specific number of infected cases recovered from the infection prevalence N^* estimated from 12 realisations of the UK 2001 FMD full IPs (n=2026) epidemic scenario and resampled datasets at a decreasing sampling proportion s of 0.25. β parameter designates the slope of the regressor of the RTO analysis. Datasets were sampled under the PPS scheme using the spatial region discrete variable.

		Epidemic Phase			
Sample proportion	*β*	*Exponential*	*Peak*	*Decline*	*Plateau*
P^{exp}		195.01±2.15	439.83±3.19	203.17±0.83	30.62±0.04
1 (n=2026)	Ref.	173.53±12.55	419.61±47.58	218.50±13.66	29.58±1.93
0.75 (n=1519)	1.17±0.07	165.31±16.85	355.17±48.65	155.72±10.06	27.41±6.07
0.5 (n=1013)	1.41±0.13	140.10±12.98	299.72±43.30	132.04±12.94	25.58±4.05
0.25 (n=506)	1.90±0.22	104.56±16.69	215.37±41.75	109.81±11.23	18.96±3.01
0.05 (n=101)	2.64±0.51	70.90±18.57	147.54±42.46	79.45±14.29	23.82±7.88

5.3.2.2 Spatial transmission distance

The M_i areas of the probability density function estimated from the spatial distance of parent-daughter transmission links that were extracted from the

reconstructed UK 2001 FMD transmission tree were defined as follows: <2.5th percentile, 0 to 0.6 km; $\bar{x}$±SD, 27.6±6.2 km; >97.5th percentile, 218.3 to 543.2 km (Figure 5-3). Looking at the results provided by the infection prevalence N^* (Figure 5-9), the decrease in accuracy driven by the reduced sampling rate s was again found to be linearly described (R^2=0.89), returning an average β parameter of 1.31±0.20 for sampled datasets drawn with 0.5≤s≤0.75. Accordingly, the absolute difference between the size of the infected population derived from the full WGS data and the sampled datasets was small at s=0.75 and s=0.5, with average estimates of 30.9±15.6 66.9±16.5 IPs, respectively (Table 5-6). Estimates of the β parameter at s=0.75 was found to be lower than the one obtained using a simple SRS scheme (1.13±0.09 vs 1.16±0.08). However, when only 25% of the total WGS data was sampled, the accuracy in the estimate of the epidemic peak was reduced (absolute difference of 198.8±33.5 IPs) and was characterised by a substantial relative variability between different sampled datasets (CV=0.17). At s=0.05, the predicted size at epidemic peak was further reduced, with an absolute difference value of 279.9±31.7. The overall relative variability between datasets determined by the PPS sampling approach was found to be similar to that of a simple SRS scheme (average CV of 0.10±0.07 and 0.11±0.05 for PPS and SRS, respectively).

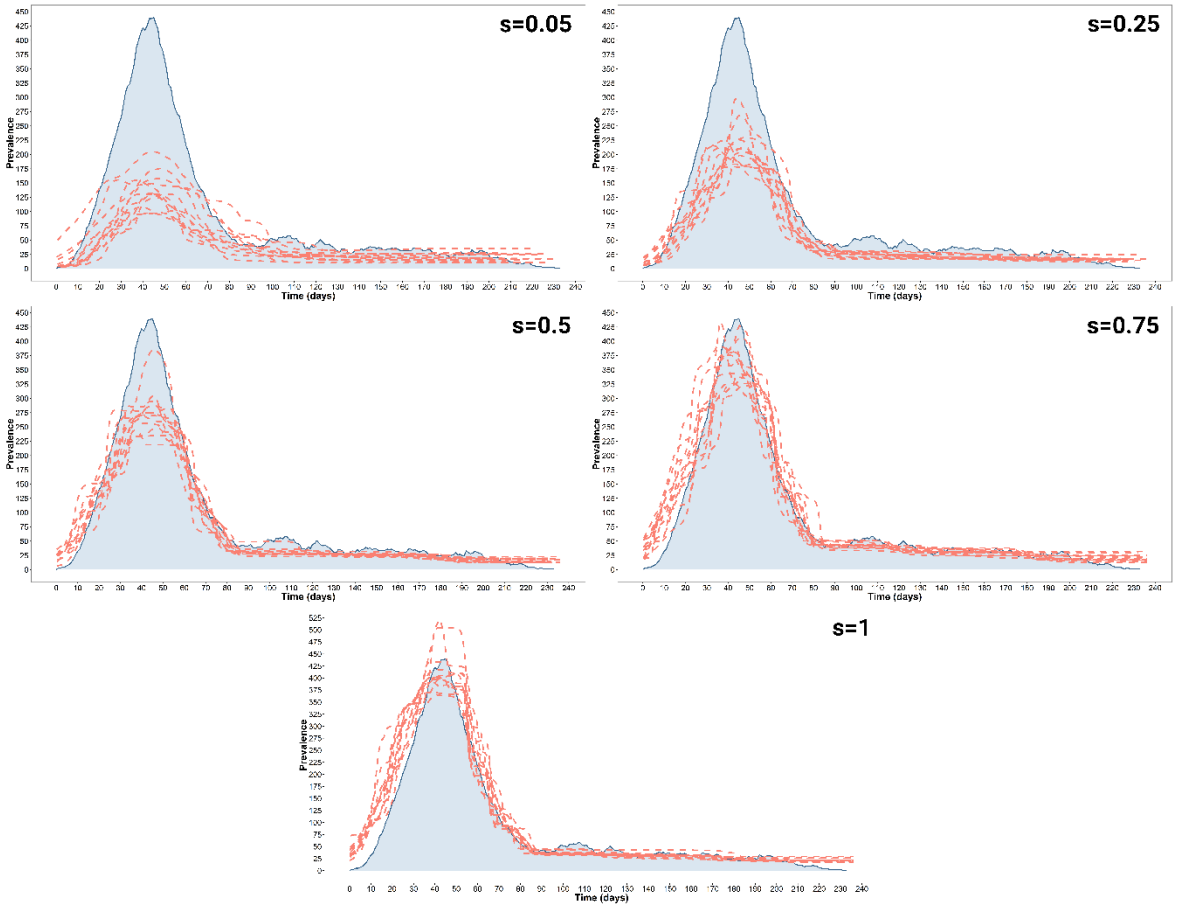

Figure 5-9. Infection prevalence N^* estimated from 12 realisations of the full UK 2001 FMDV WGS simulated database (n=2026) and resampled datasets at a decreasing sampling proportion rate s of 0.25. Epidemic curve was estimated from the P^{exp} (blue) prevalence data as defined in §3.2.2.2. Datasets were sampled under the PPS scheme using the spatial transmission distance epidemiological variable.

Table 5-6. Time specific number of infected cases recovered from the infection prevalence N^* estimated from 12 realisations of the UK 2001 FMD full IPs (n=2026) epidemic scenario and resampled datasets at a decreasing sampling proportion s of 0.25. β parameter designates the slope of the regressor of the RTO analysis. Datasets were sampled under the PPS scheme using the spatial transmission distance epidemiological variable.

		Epidemic Phase			
Sample proportion	*β*	*Exponential*	*Peak*	*Decline*	*Plateau*
P^{exp}		195.01±2.15	439.83±3.19	203.17±0.83	30.62±0.04
1 (n=2026)	Ref.	173.53±12.55	419.61±47.58	218.50±13.66	29.58±1.93
0.75 (n=1519)	1.13±0.06	161.66±14.02	370.81±39.62	163.75±15.18	30.37±2.62
0.5 (n=1013)	1.45±0.08	134.21±12.48	280.22±39.54	135.295±12.32	23.90±1.74
0.25 (n=506)	1.93±0.17	98.57±13.97	220.77±33.50	107.07±12.60	20.22±2.99
0.05 (n=101)	2.77±0.60	71.92±12.66	139.69±31.67	81.75±26.69	22.31±8.32

5.3.3 Sampling within temporal strata

5.3.3.1 Month timing

The strata for the PPS sampling scheme using the month of IP reporting were estimated from the UK 2001 FMD epidemic records, which returned a total of 8 *M*

elements equivalent to the timing in month of the epidemic described from February to September 2001 (Figure 5-10).

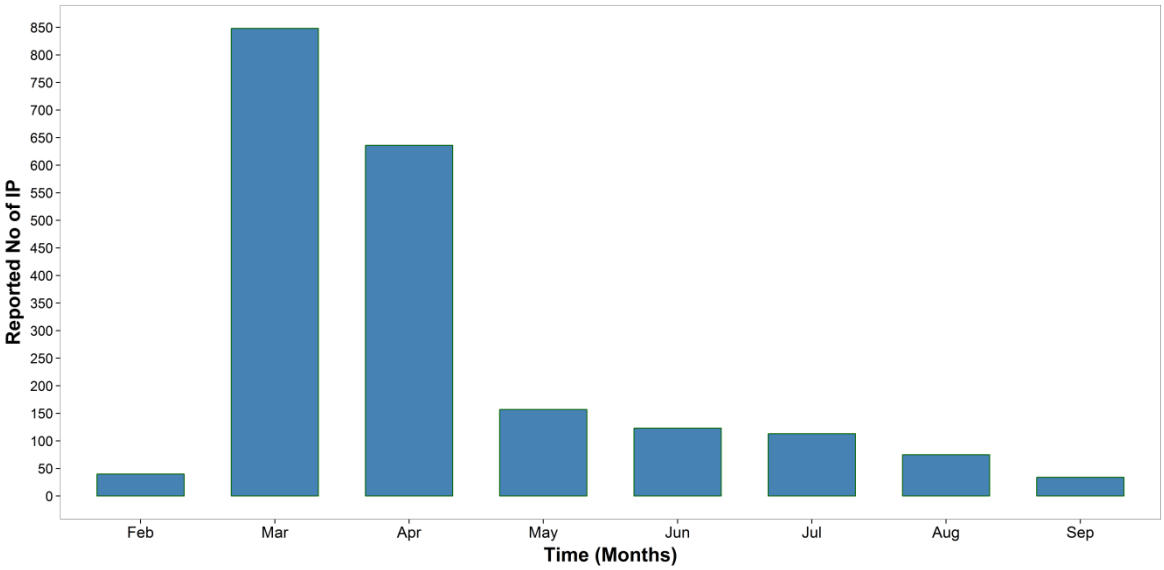

Figure 5-10. Total number of IP reported to be infected by FMDV during the UK 2001 FMD epidemic by month of reporting.

On a visual inspection, the N^* curves derived from the PPS datasets sampled at a rate of $s \leq 0.25$ were found to be slightly inhomogeneous in terms of shape and trajectory, whilst these were relatively similar between sampled datasets at sampling rates of 0.5 and 0.75 (Figure 5-11). The decrease in the accuracy of the reconstructed N^* curves derived from sampling WGS at a decreasing rate s was linearly described (R^2=0.93), although the absolute difference estimated between the full WGS data and the sampled datasets both drawn using s=0.25 and s=0.05 were roughly equal (average values of 100.4±16.6 and 128.1±17.1 IPs, respectively) (Table 5-7). Similar to the simple SRS scheme, the estimated size of the epidemic peak obtained using the s=0.25 sampled datasets was almost half of that obtained using the full WGS data (absolute differences of 207.5±35.3 IPs), which is defined by a β value of 1.93±0.24.At s=0.05, the epidemic peak size was further reduced by ~30% (absolute difference of 264.4±35.1).

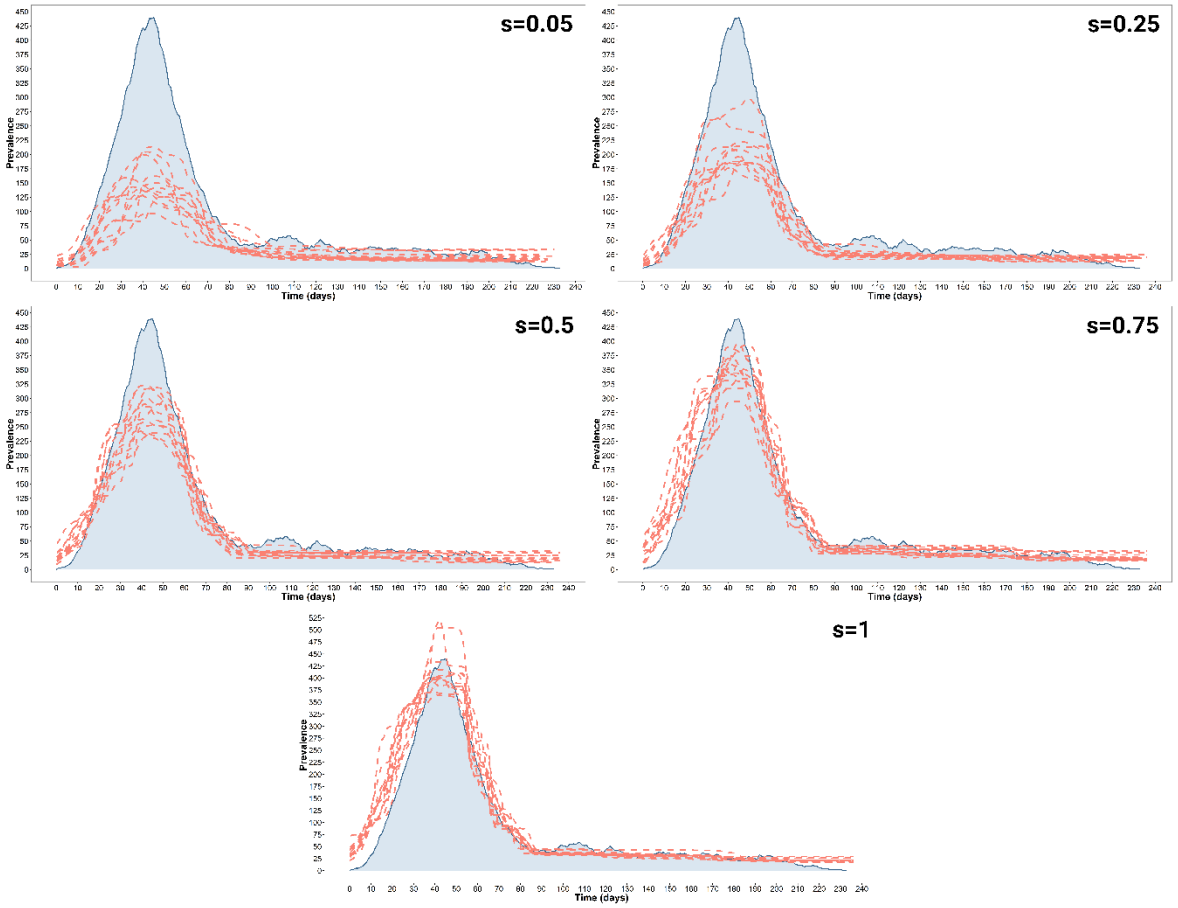

Figure 5-11. Infection prevalence N^* estimated from 12 realisations of the full UK 2001 FMDV WGS simulated database (n=2026) and resampled datasets at a decreasing sampling proportion rate s of 0.25. Epidemic curve was estimated from the P^{exp} (blue) prevalence data as defined in §3.2.2.2. Datasets were sampled under the PPS scheme using the month of reporting time discrete variable.

Table 5-7. Time specific number of infected cases recovered from the infection prevalence N^* estimated from 12 realisations of the UK 2001 FMD full IPs (n=2026) epidemic scenario and resampled datasets at a decreasing sampling proportion s of 0.25. β parameter designates the slope of the regressor of the RTO analysis. Datasets were sampled under the PPS scheme using the month of reporting time discrete variable.

		Epidemic Phase			
Sample proportion	*β*	*Exponential*	*Peak*	*Decline*	*Plateau*
P^{exp}		195.01±2.15	439.83±3.19	203.17±0.83	30.62±0.04
1 (n=2026)	Ref.	173.53±12.55	419.61±47.58	218.50±13.66	29.58±1.93
0.75 (n=1519)	1.17±0.09	161.79±13.93	353.65±31.26	157.38±10.75	27.96±4.82
0.5 (n=1013)	1.45±0.11	132.56±15.54	280.16±31.49	134.79±9.73	24.01±4.85
0.25 (n=506)	1.93±0.24	101.37±14.23	212.09±35.32	105.45±13.54	20.66±3.23
0.05 (n=101)	2.52±0.38	69.32±14.78	155.22±35.07	83.33±14.66	22.23±6.38

5.3.3.2 Week timing

Similarly to the PPS month sampling approach, the strata for the PPS sampling scheme using the week of FMD case reporting were estimated from the UK 2001 FMD epidemic records, which returned a total of 32 M elements corresponding to the timing of the epidemic in week, starting from the 3rd week of February (8th week of the year) to the 4th of September 2001 (41st week of the year) (Figure 5-12).

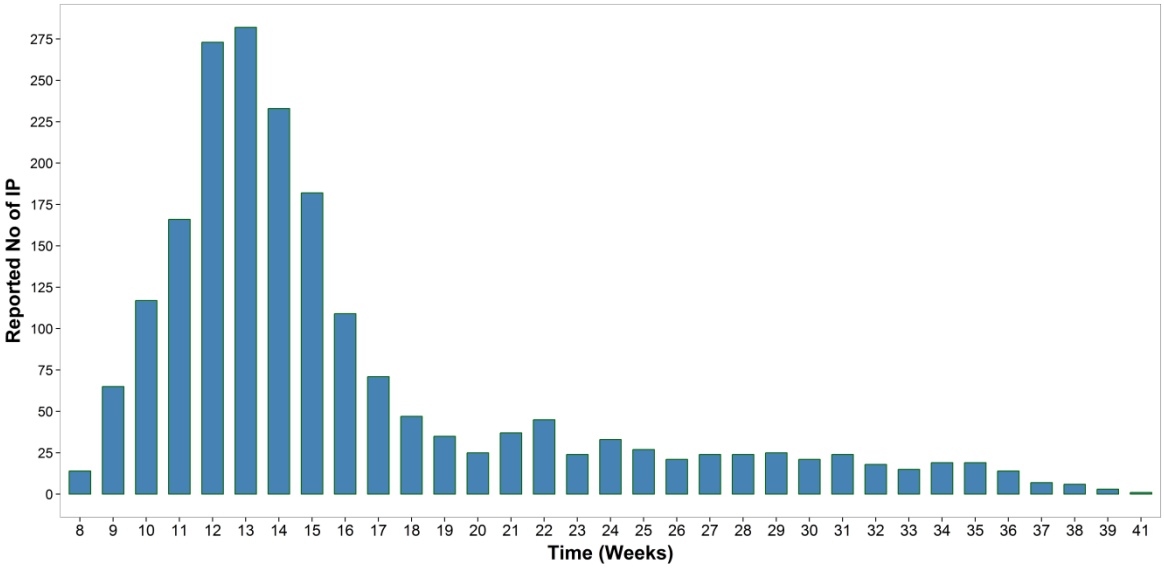

Figure 5-12. Total number of IP reported to be infected by FMDV during the UK 2001 FMD epidemic by week of reporting.

Decreasing the rate s at which samples were drawn from the full WGS data was linearly correlated with a decrease in the accuracy of reconstructing the size of the infected population through time as derived by the infection prevalence N^* estimates (R^2=0.85). This was supported, on a visual inspection (Figure 5-13), by the flattening of the epidemic peak size with the decrease in the amount of WGS present in the sampled dataset (absolute difference of 213.7±27.9 and 281.3±29.6 IPs for s=0.25 and s=0.05, respectively) (Table 5-8). Despite the reduced accuracy provided by the reduced genetic data, the relative variability between sampled datasets was relatively low at $0.25 \leq s \leq 0.05$ (average CV of 0.14±0.07). This finding was observed to be even lower at $0.75 \leq s \leq 0.5$ (average CV values of 0.07±0.01), with higher precision than what obtained using a simple SRS scheme (average CV value of 0.11±0.01). At s=0.75 the predicted epidemic peak was very close to the one derived from WGS data, and estimated to be of 62.9±38.5 IPs (β=1.15).

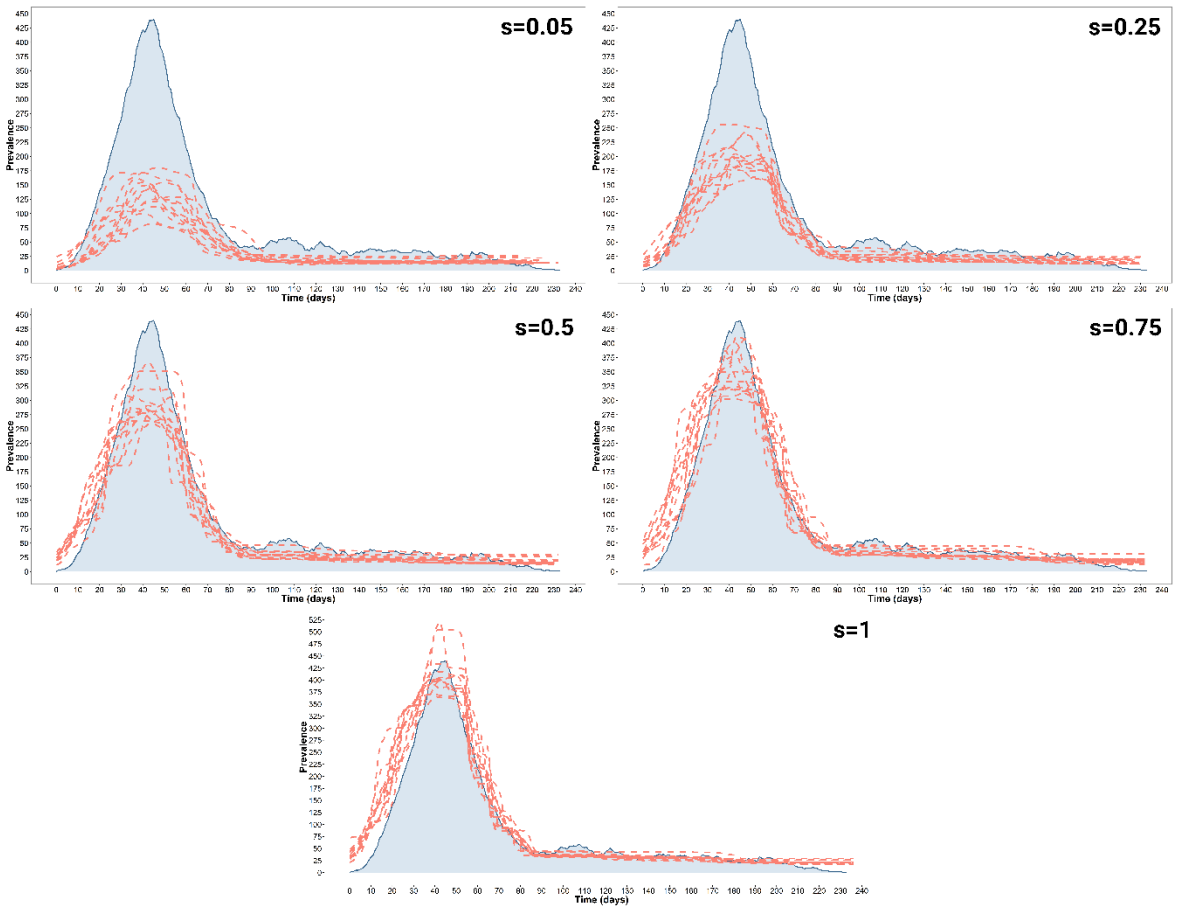

Figure 5-13. Infection prevalence N^* estimated from 12 realisations of the full UK 2001 FMDV WGS simulated database (n=2026) and resampled datasets at a decreasing sampling proportion rate s of 0.25. Epidemic curve was estimated from the P^{exp} (blue) prevalence data as defined in §3.2.2.2. Datasets were sampled under the PPS scheme using the week of reporting time discrete variable.

Table 5-8. Time specific number of infected cases recovered from the infection prevalence N^* estimated from 12 realisations of the UK 2001 FMD full IPs (n=2026) epidemic scenario and resampled datasets at a decreasing sampling proportion s of 0.25. β parameter designates the slope of the regressor of the RTO analysis. Datasets were sampled under the PPS scheme using the week of reporting time discrete variable.

		Epidemic Phase			
Sample proportion	*β*	*Exponential*	*Peak*	*Decline*	*Plateau*
P^{exp}		195.01±2.15	439.83±3.19	203.17±0.83	30.62±0.04
1 (n=2026)	Ref.	173.53±12.55	419.61±47.58	218.50±13.66	29.58±1.93
0.75 (n=1519)	1.15±0.09	166.00±14.18	356.68±38.58	159.19±10.75	28.12±4.98
0.5 (n=1013)	1.37±0.09	141.45±14.71	300.68±32.20	132.19±10.97	23.85±4.79
0.25 (n=506)	1.95±0.20	97.84±13.06	205.85±27.93	106.28±10.26	20.68±3.92
0.05 (n=101)	2.94±0.58	70.83±16.35	138.34±29.59	74.80±18.77	18.29±4.44

5.4 Sampling within epidemic phases

In the previous sections, the impact of sampling WGSs at reduced rates s on the accuracy of reconstructed population sizes as estimated by the full WGS data was evaluated, either considering a simple random or a more structured sampling scheme. With these methods WGSs have been sampled from the entire time frame of the UK 2001 FMD epidemic, therefore providing a more homogeneous sampling which is less

biased in the diversity of the genetic signal carried by the selected WGSs. To account for a more biased and unstructured sampling, a SRS scheme with a low sampling rate s≈0.03 has been applied to each of the UK 2001 FMD epidemic phases (*i.e.* exponential, decline and tail end), where the index IP (IP4) was included in each of the sampled datasets. For this assessment, to recover the prevalence, the three scaling formulations for the infection prevalence N^*, as ranked in §4.3.1, were used for scaling N_e obtained from the BSP. In addition and to explore a model which include sampling uncertainty in its mathematical formulation, the Birth-Death model (BDM) which accounted for incomplete sampling (Stadler, 2009) has been used to assess the sample probability ρ predicted by this method using the very same sampled WGSs. The BDM is implemented in BEAST 1.8.0 (Drummond et al., 2012).

5.4.1 Exponential phase

The infection prevalence N^* curves predicted for the exponential phase of the UK 2001 epidemic were characterised, on a visual inspection (Figure 5-14), by large relative variability between sampled datasets (CV=0.47±0.01), which was reported for all of the scaling formulations applied (Table 5-10). Although the relative shape and trajectory of the epidemic phase was preserved, the accuracy in matching the actual infected population size, as estimated using the full WGS data, was found to be reduced on average by 65.4% and 58.4% when using the N_e scaled by the epidemiological generation time τ and assuming N^* scaled using the NLFT formulation, respectively. Predicted estimates were found to differ on average of 67.5±19.2 and 81.1±24.7 to those obtained using the full WGS data for the scaled-N_e and the NLFT scaling formulations, respectively (Table 5-10). A high variability was reported when scaling the N^* using the $var(R_t)$ formulation (CV=0.30). The sample probability estimated using the BDM (ρ=0.10±0.03) was reasonably matching the empirical value of the sample proportion (n=60, s=0.06) given the actual number of infected cases reported within the time frame of the exponential phase (Table 5-11).

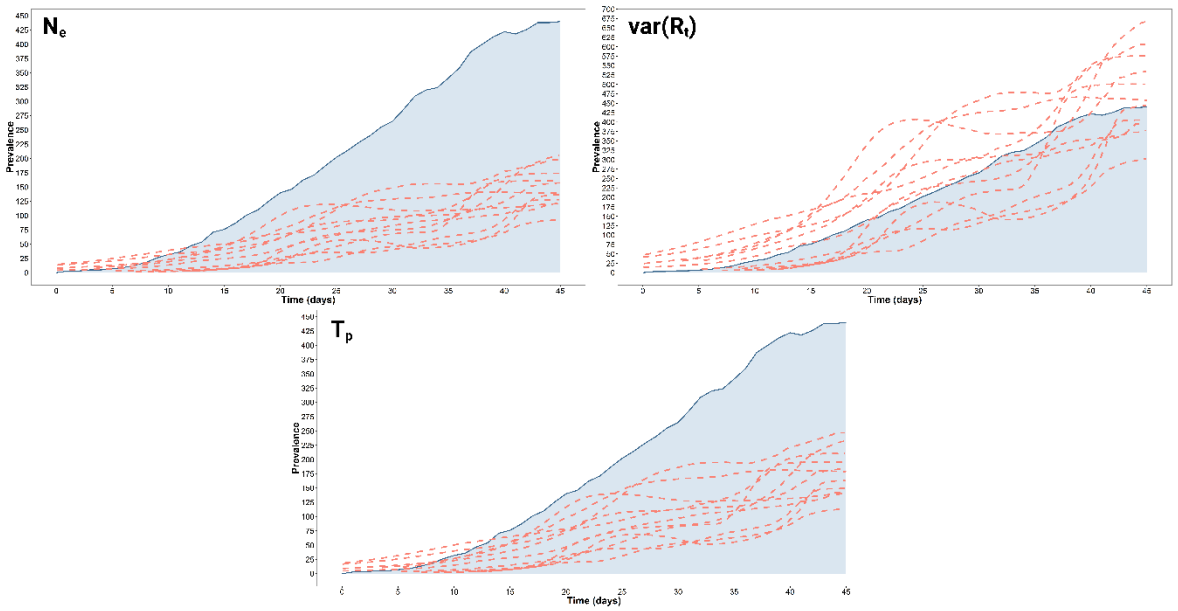

Figure 5-14. Epidemic size of the UK 2001 FMD exponential phase estimated from 12 realisations of FMDV WGS simulated database (n=2026) resampled at a rate s≈0.03. The three plots shows the scaled N_e, the infection prevalence N^* derived by the $var(R_t)$ scaling formulation using the Koelle and Rasmussen (2012) form, and the infection prevalence N^* derived from the NLFT scaling formulation using the prevalence-to-incidence ratio τ_p. Epidemic curve was estimated from the P^{exp} (blue) prevalence data as defined in §3.2.2.2. Datasets were sampled under the SRS scheme.

Table 5-9. Time specific number of infected cases estimated from 12 realisations of FMDV WGS simulated database (n=2026) and at a sampling rate s≈0.03. β parameter designates the slope of the regressor of the RTO analysis. The infection prevalence N^* was scaled by the $var(R_t)$ scaling formulation using the Koelle and Rasmussen (2012) form, and by the NLFT scaling formulation using the prevalence-to-incidence ratio τ_p. Datasets were sampled under the SRS scheme.

		Infection Prevalence N^*		
	Epidemic Phase	N_e	$var(R_t)$	τ_p
Exponential	Prevalence	195.01±2.15	195.01±2.15	195.01±2.15
	WGS full data	145.17±9.34	469.08±22.00	173.53±12.55
	SRS (n=60, s≈0.03)	67.48±19.23	217.89±63.25	81.14±24.69
	β	4.14±1.64	1.29±0.51	3.49±1.38
Decline	Prevalence	203.17±0.83	203.17±0.83	203.17±0.83
	WGS full data	182.77±9.40	590.85±24.23	218.50±13.66
	SRS (n=60, s≈0.03)	120.34±53.41	391.82±175.13	144.38±65.08
	β	2.05±0.78	0.63±0.24	1.72 ±0.66
Plateau	Prevalence	30.62±0.04	30.62±0.04	30.62±0.04
	WGS full data	24.75±1.34	80.04±4.50	29.58±1.93
	SRS (n=60, s≈0.03)	15.14±4.02	48.77±12.42	8.19±5.28
	β	2.07±0.48	0.64±0.14	1.74±0.43

Table 5-10. Comparison of the empirical proportion s of IPs reported during the UK 2001 FMD epidemic according to each epidemic phase and the corresponding sample probability ρ obtained using 12 realisations of the BDM (Stadler, 2009).

	Empirical			**BDM**
Epidemic Phase	n	N	s	ρ
Exponential	60	1037	0.06	0.10±0.03
Decline	60	537	0.11	0.39±0.08
Plateau	60	457	0.13	0.63±0.05

5.4.2 Decline phase

The prevalence data by time estimated using the sampled datasets with all the three different scaling formulation was not able to recover the true shape and trajectory of the true UK 2001 FMD decline phase, thus visually appeared as a flat line (Figure 5-15). For the scaled N_e data and the NLFT formulations, estimates were found to be lower than the values obtained with the full WGS data (absolute difference of 85.0±49.4 IPs and 76.8±38.9), whilst the infection prevalence N^* derived using the $var(R_t)$ formulation was estimated as higher than the full WGS data (absolute difference of 192.9±169.9 IPs) (Table 5-9). All of the scaling formulations returned a large variability between estimates extracted from different realisations of the model (average CV values of 0.44±0.01). The BDM estimated that the data were drawn from ~20% more samples (ρ=0.39±0.08) than the real sample proportion (n=60, s=0.11) (Table 5-10).

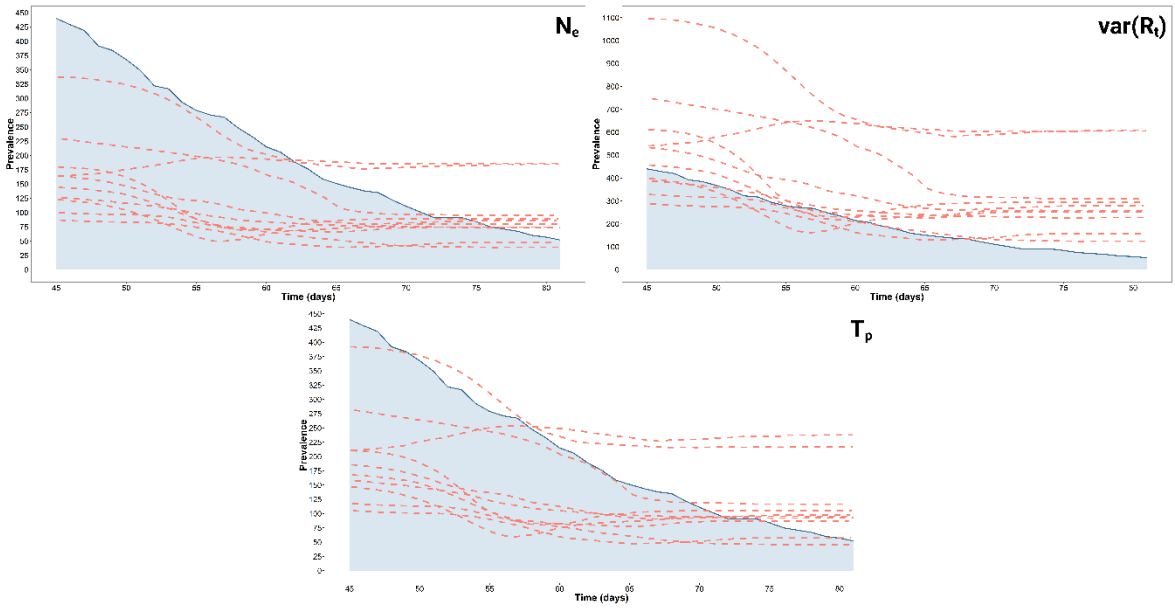

Figure 5-15. Epidemic size of the UK 2001 FMD decline phase estimated from 12 realisations of FMDV WGS simulated database (n=2026) resampled at a rate s≈0.03. The three plots shows the scaled N_e, the infection prevalence N^* derived by the $var(R_t)$ scaling formulation using the Koelle and Rasmussen (2012) form, and the infection prevalence N^* derived from the NLFT scaling formulation using the prevalence-to-incidence ratio τ_p. Epidemic curve was estimated from the P^{exp} (blue) prevalence data as defined in §3.2.2.2. Datasets were sampled under the SRS scheme.

5.4.3 Tail end phase

Evaluating the infected population size estimates obtained by sampling at a low rate from the cases reported during the tail end phase (Figure 5-16), a low absolute

difference between the sampled datasets and the full WGS estimates was described for all the scaling formulations (average value of 15.3±2.9), with the WGS data being higher than the scaled N_e data and the freely mixing formulations. However, a high relative variability between datasets was observed, estimated in an average CV value of 0.27±0.02 (Table 5-9). It should be noted that, as already described in Chapter 4, the BSP reported an increased number of infected cases in the last weeks, failing to describe the actual fading out of the epidemic. The BDM analysis returned a sample probability ρ of 0.63±0.05 (Table 5-10), which was higher than the real sample proportion drawn from the list of reported cases within the time frame of the tail end phase (n=60, s=0.13).

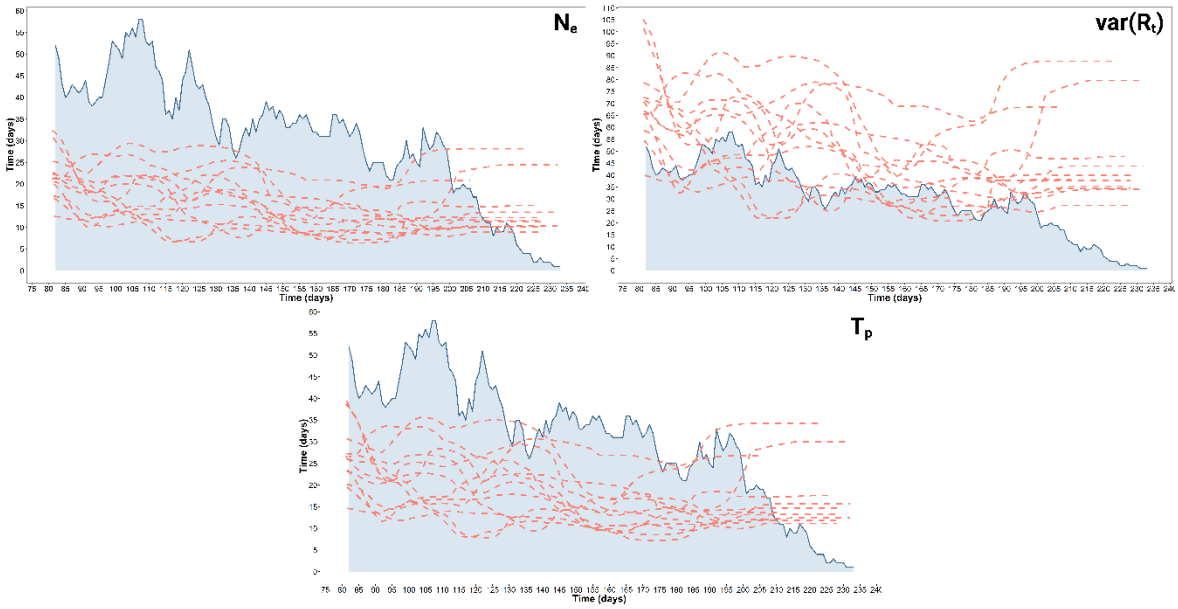

Figure 5-16. Epidemic size of the UK 2001 FMD tail end phase estimated from 12 realisations of FMDV WGS simulated database (n=2026) resampled at a rate s≈0.03. The three plots shows the scaled N_e, the infection prevalence N^* derived by the $var(R_t)$ scaling formulation using the Koelle and Rasmussen (2012) form, and the infection prevalence N^* derived from the NLFT scaling formulation using the prevalence-to-incidence ratio τ_p. Epidemic curve was estimated from the P^{exp} (blue) prevalence data as defined in §3.2.2.2. Datasets were sampled under the SRS scheme.

5.5 Conclusion

This chapter analysed the impact of the size and structure of the sampled dataset on the accuracy of the reconstructed viral demographies. The results generated should provide information on how the demographic signal carried by sequence data becomes imprecise and weaker when reducing the number of samples. Using a simple random sampling protocol (SRS scheme) to generate WGS sub-datasets from the

complete simulated dataset from the UK 2001 epidemic, an approximately linear decay in the accuracy in the reconstruction of the actual infected population size was observed, which was particularly pronounced for datasets containing less than 50% of the full WGS data. In contrast, for a highly sampled dataset, the estimated absolute difference with the full WGS data was found to be relatively low, with average values of 8.0±6.6 IPs for s=0.75. At a lower sampling rate (s=0.25) this value became larger, estimated to be on average 36.3±8.5 IPs, whilst the accuracy was reduced by more than 50% when sampling only 5% of the total infected population. This was also reflected by the shape and trajectory of the epidemic curve reconstructed by scaling N_e to the infection prevalence N^*: at a rate s≤0.05 the epidemic peak was found to be flatter, therefore providing less accurate information on the total size of the epidemic event. It is interesting to note that at s=0.25 the size of the predicted infected population size was found to be half of the empirical prevalence (β=1.98±0.26). The majority of the reduced accuracy at lower sampling rates was focussed on the peak and decline phases of the epidemic, whilst at both the exponential and the tail end phases, the recovered N^* size reconstructed from the sampled datasets was similar to the estimates obtained using the full WGS data.

As suggested by the results obtained using the PPS sampling scheme, a correlation might be described between the type of variable used to select the samples and the accuracy in the reconstruction of the size of the infection prevalence N^* when analysing datasets constructed at lower sampling rates. For example, when PPS sampling from the PDF the TN93 genetic distance variable the accuracy of the infected population size estimated at s=0.25 was higher in comparison with the SRS scheme (reduced accuracy of 39.0% and 41.1% for PPS and SRS schemes, respectively. This finding would indicate that the structure of the genetic data and, therefore, the demographic signal is more preserved when sampling using the PPS scheme thus producing more precise results. As a confirmation, when using the PDF of the genetic distance variable, accounting for the extent of the genetic signal of the full WGS data for sampling via the PPS, the reduced accuracy at s=0.05 was estimated to be 43.4%, in contrast with a value of 53.5% obtained using the simple SRS scheme. In addition, the β parameters estimated by PPS sampling were found to be lower than the values obtained using the SRS scheme. Accounting for the spatial and temporal structure of the epidemic process within the PPS sampling protocol did not significantly improve on the accuracy of the estimated population size as opposed to the SRS scheme, with

the reconstructed epidemic peak largely flattening at low sampling rates. At s=0.05, the accuracy was reduced on average by 49.8±11.5%, 50.7±13.5%, 50.7±0.06% and 55.4±10.0% for the regional, spatial transmission, month and week samplings, respectively, also reporting larger β estimates. In addition, as already observed for the continuous genetic variables, the precision of the population size estimates between different sampled datasets were higher in comparison to the SRS scheme (CV=0.15±0.03), returning average CV values of 0.26, 0.24, 0.21 and 0.20 for the regional, spatial transmission, month and week samplings, respectively.

Analysis of each UK 2001 FMD epidemic phases when using very small (s≈0.03) and relatively biased sampled datasets confirmed what was already observed with a larger sample size. For the exponential phase, the population size estimates produced using the SRS sampled data were reported to be relatively inaccurate, with a reduced accuracy of 53.2±14.2% estimated using the NLFT scaling formulation, and producing nosier (CV=0.27) curves compared with the full WGS data (CV=0.18). The infection prevalence N^* curve obtained for the decline phase using the sampling data was akin to a flat line, thus not capturing the real trend of the prevalence data extracted from the empirical infected population size, a feature that was also described for the tail end phase analysis, although the latter produced the oscillatory trend observed during the last three months of the epidemic fadeout. These findings were unexpected considering that a constant linear transformation between scaled N_e estimates and the real infected population size during an exponential epidemic phase, or a steady endemic state has been previously described (Koelle and Rasmussen, 2012, Magiorkinis et al., 2013), assuming that the generation time τ is constant through time. Although this holds true, visually inspecting and comparing both the reconstructed and the empirical epidemic curves, it is not valid when comparing the size of both the N_e or the infection prevalence N^* with the real number of infected cases. It should be noted that, as already described in Chapter 4, the BSP reported an increased number of infected cases in the last weeks of the tail end epidemic phase, failing to describe the actual fading out of the epidemic.

The BDM computed for estimating the sample probability ρ was able to detect, albeit slightly higher, the number of IPs reported only for the exponential phase (ρ=0.10±0.03, s=0.06), whilst was failing to recover the true data for both the decline and the tail end phases. When sampling 50% of the full WGS data regardless of the epidemic phase, the BDM estimated a ρ=0.32, lower than the empirical value although it was included within the 95% confidence interval (95%HPD 0.07 to 0.54). In addition,

estimates of the sampling probability ρ obtained using the BD Skyline model (Stadler et al., 2013) or the BDSIR model implemented in BEAST 2.3.0 software (Bouckaert et al., 2014) were not significantly different from those presented here [data not shown]. Although it would be difficult to detect deviation of the sampling process from the BDM form in a real world scenario, one of the assumptions of the BDM is that the sampling rate should be constant through time (Boskova et al., 2014), which should hold true in the case of the SRS scheme here adopted for homogeneous sampling from each phase of the UK 2001 FMD epidemic. Therefore, as previously demonstrated and the results here confirmed (Stadler et al., 2015), the BDM correctly reflects the real sampled proportion of infected population only during an exponential growing phase with a constant sampling rate, whilst for other scenario its estimates might be largely biased by the misspecification of the sampling process formulated by the BDM (Volz and Frost, 2014).

Lastly, comparing the coalescent-based method (*i.e.* scaled N_e estimated obtained using the BSP plot) with the BDM for reconstructing the real infected population size from partially sampled sequence data, pro and cons of both methods might be perceived. Although the accuracy and precision of the BDM estimate was largely high when investigating the exponential phase of an epidemic when the coalescent-based approach failed to provide an accurate picture, the coalescent approach performed better in assessing the real infected population size of the entire epidemic (as evaluated using the SRS scheme). It has been observed that epidemiological dynamics reconstructed using both the coalescent-based approach and BDM might be largely biased when assessing epidemic with R_0 value close to 1 or with small effective susceptible populations (Popinga et al., 2015), which might be the case for the UK 2001 FMD epidemic.

CHAPTER 6

Phylodynamics of the UK 2001 FMD epidemic using available WGS data: a preliminary analysis

6.1 Rationale

Throughout the studies presented in this thesis, the research focus has been on investigating the relationship between the empirical epidemic size and the corresponding predicted infection prevalence N^* recovered solely from genetic data. It has been also observed how this relationship might be less accurately established when improperly structured samples of genetic data are used. The complex relationship between the empirical epidemic size and the predicted infection prevalence N^* has been studied *in silico* from the UK 2001 FMD epidemic where the demography of the infected population is well understood. An evolutionary simulation framework of the whole UK 2001 FMD epidemic has been developed, which has been informed by the space-time dynamics of the transmission events as reconstructed using the fully resolved epidemiological data. However, some of the results obtained from this project can only be validated sometime after its completion, when the full dataset of UK 2001 FMDV WGSs will be available. At the time of writing, an initial set of the WGS (n=154) is available that have been generated from the archive of clinical samples collected at the time of the outbreak (n=1404) by the Epi-SEQ EMIDA-ERA NET funded project (www.episeq.eu/index_files/Page1077.htm). Accordingly, this chapter presents a preliminary characterisation of the UK 2001 FMD epidemic based on these real data, enabling testing of the hypotheses suggested by the results obtained from the analyses of the simulated data presented in Chapters 4 and 5 and, therefore, to initially validate their assumptions with a relatively small subset of the real WGS data [~11% of the total clinical samples collected at the time of the outbreak (n=1404), ~8% of the total number of reported IPs (n=2026)]. In addition, a random subset of the simulated data representative of the sample of the n=154 real WGSs was obtained to compare the population dynamics recovered from the real data with that derived *in silico*.

6.1.1 Brief description of the UK 2001 FMD epidemic event

Between February and September 2001, a total of 2026 IPs were reported to be infected by FMD in UK, defining the largest FMD epidemic recorded following the eradication of the disease from Europe. It has been estimated that during the seven months of the epidemic almost 6.5 million animals were culled to control the outbreak, with a total financial cost of about £8 billion shared between the private and public sectors (Donaldson et al., 2006). On 19th February 2001 suspect cases of FMD were reported to the MAFF (later re-organised as DEFRA) from an official veterinary inspection at an abattoir in Essex (IP01), southeast England. The causative agent was confirmed as type O PanAsia FMDV strain by the WRLFMD at the Institute for Animal Health, Pirbright, on the 20th of February (Gibbens et al., 2001, Knowles et al., 2001b). Infected pigs were delivered to the abattoir from farms in southeast and northern England. Forensic tracing and inspecting farms which supplied livestock to the Essex abattoir found clinical signs of FMD in pigs fed unprocessed waste food (swill) at the index premise in Heddon-on-the-Wall (IP04), Newcastle-upon-Tyne, northeast England (DEFRA, 2002). It has been allegedly attributed that illegal import of FMDV contaminated pork products from Asia has been the likely way by which FMD was introduced into UK, although tests performed failed to recover the virus. The initial expansion phase of the epidemic was driven by three main events: the infection via airborne route to Prestwick Hall Farm, Callerton, (IP06) 5km away from the index case (Gloster et al., 2003); the movement of infected sheep from IP06 to the Hexham livestock auction market in Northumberland; the movement of infected sheep bought at the Hexham market to Longtown market in Cumbria before entering into the national sheep marketing system. It has been reconstructed through epidemiological investigations that the sheep moved from Longtown market were disseminated to 10 of the 12 geographical IP clusters that were identified during the epidemic before the first case was reported the 19th of February (Gibbens et al., 2001, Mansley et al., 2003). The trigger of the exponential phase of the epidemic was thus mainly due to the dissemination of infected sheep through the marketing network across the country and then to local spread across clusters of IPs within each affected geographical area (Mansley et al., 2011). Within the first 10 weeks from the beginning of the epidemic ~1600 IPs were reported, reaching a peak between the 27th and 29th of March. In the 20 weeks of the tail end phase of the epidemic (from May to September), 400 farms

were reported as infected, with the last case confirmed on the 30th of September in Cumbria. These last cases were identified in previously unaffected and widely separated areas and mainly characterised by local spread (Mansley et al., 2011). Although the overall picture of the UK 2001 FMD epidemic has been largely reconstructed through epidemiological analysis of data generated through field investigations, the source for the majority of the IPs remains unidentified.

6.2 Materials and methods

6.2.1 Generating the UK 2001 FMDV WGS

The 154 FMDV WGSs analysed in this study were partially obtained from the WRLFMD database of already published WGS of the UK 2001 FMD epidemic (n=39) (Cottam et al., 2006, Cottam et al., 2008a, Konig et al., 2009), with further 115 WGS newly generated from the Epi-SEQ EMIDA-ERA NET funded project (www.episeq.eu/index files/Page1077.htm), which is focused on the genetic characterisation of the entire UK 2001 FMD collection of clinical samples stored at the WRLFMD, The Pirbright Institute – UK. For the samples, sequencing was performed on an Illumina MiSeq NGS sequencer using a 12.5pM pool in a 2×250-2×300 cycle sequencing reaction using a 600 cycle v.3 cartridge. The protocol that has been used for generating the consensus level sequences from FMDV clinical samples has been previously published (Logan et al., 2014). The geographical locations and frequency of the time of collection for the 154 WGSs used in this study are detailed in Figure 6-1.

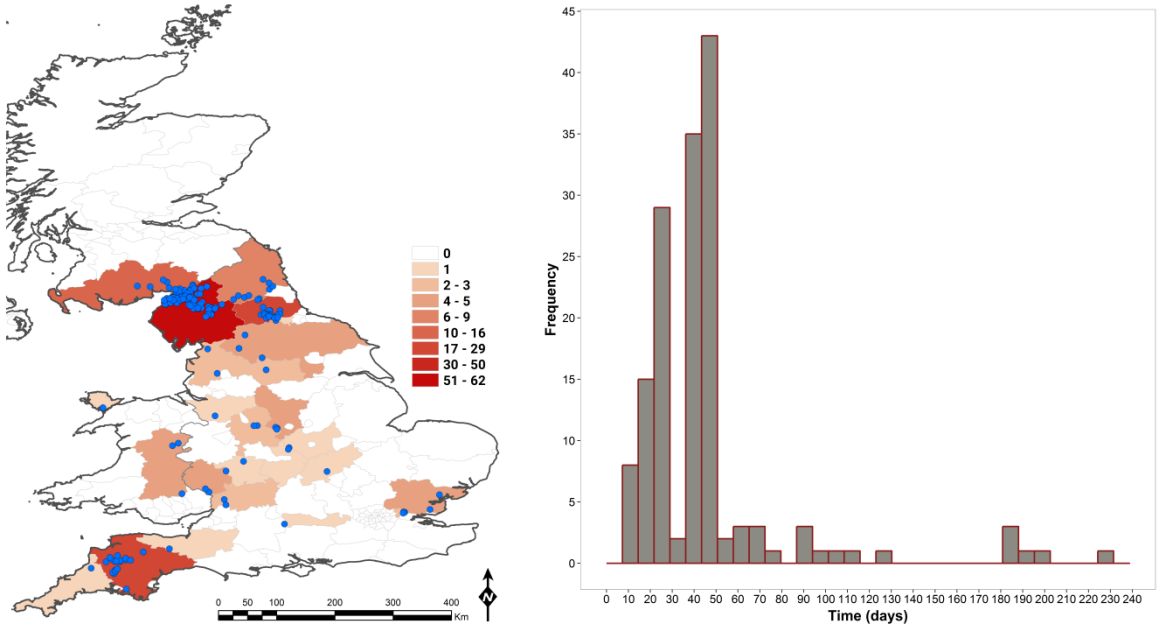

Figure 6-1. Geographical location and frequency in time of the n=154 WGS generated from the samples collected during the UK 2001 FMD epidemic and analysed in this study. Counties are coloured according to the total number of samples present.

6.2.2 Data analysis

6.2.2.1 Recovery the evolutionary and demographic signal

BEAST 1.8.0 package (Drummond et al., 2012, Drummond and Rambaut, 2007) was employed to estimate the evolutionary clock rate of the UK 2001 FMD epidemic and to reconstruct the demography of the infected population. The analysis was undertaken with the TN93 substitution model and testing both the strict and random local clock evolutionary models (Drummond and Suchard, 2010). The average rate of the clock model was fixed as the one previously estimated from the n=39 already published FMDV WGS (2.33×10^{-5} nt/site/day) and defining a gamma distribution $\Gamma(\kappa,\theta)$ of κ=0.0086 and θ=1000.0 for the substitution rate prior. A piecewise constant Bayesian skyline model with 10 groups was used as tree prior (Drummond et al., 2005). Other priors were set with the defaults parameters. The MCMC chain was run for 100 million iterations, sub-sampling every 10000 states. Convergence of the chain was assessed using Tracer 1.5 removing the initial 10% of the chain as burn-in. The MCC tree was summarised using TreeAnnotator 1.8.0 and constructed using FigTree 1.4.2. To reconstruct the demography of the FMDV population from the real 154 FMDV WGSs data, the scaling formulations previously tested and which produced the highest fit (as

reported in §4.3.1) were here used to recover the infection prevalence N^* from the N_e estimated from the BSP. These were the scaled N_e formulation, the $var(R_t)$ formulation using the Koelle and Rasmussen (2012) form, and the one assuming a freely mixing population (Frost and Volz, 2013). This methodology was used for both the real and simulated WGSs.

6.3 Results

6.3.1 Evolutionary patterns

The observed evolutionary distances and total nt changes calculated from the root (IP04) increased linearly with time (R^2=0.93; $F_{1,153}$=1993, p<0.001) (Figure 6-2). The root-to-tip distance of substitutions between the index IP04 and the latest reported IP2027 was estimated to be 50 nt, although the maximum number of nt substitutions across all the WGSs was 78 nt between IP1945 and IP2027 (maximum genetic distance 0.01 base substitution per site). It is interesting to note that these two IPs were located in two separate geographical clusters and phylogenetically not related (IP1945 collected in Powys, Wales, and IP2027 in Cumbria), thus defined within two different evolutionary chains. In addition, two pairs of identical sequences were observed, namely IP28/IP536 and IP44/IP96.

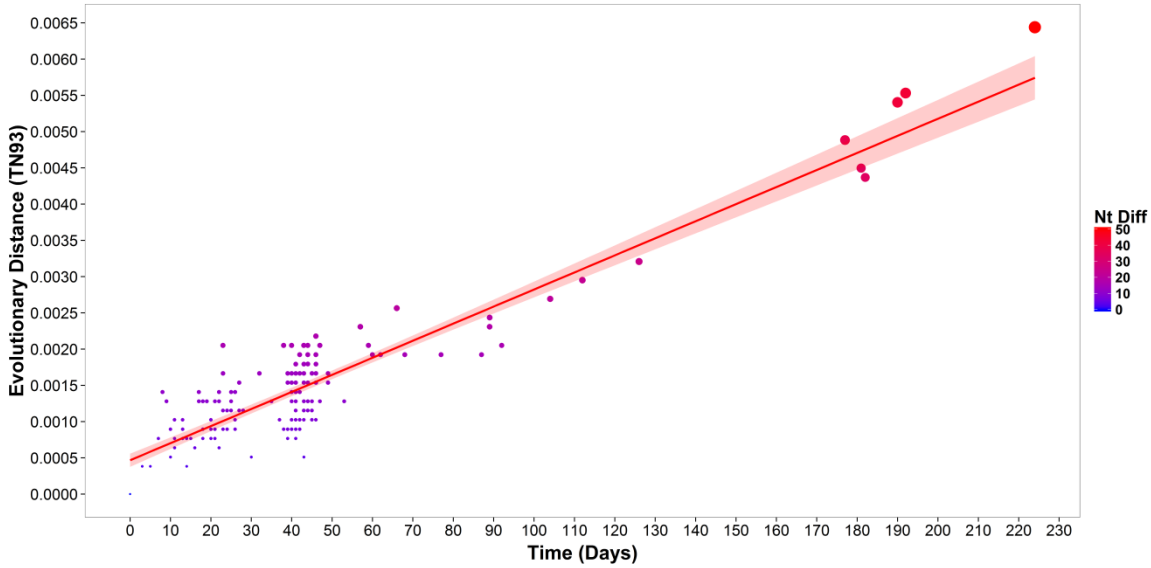

Figure 6-2. Accumulation of nucleotide differences estimated from the index IP (IP4) for the FMDV WGS alignment (*n*=154) generated from the clinical field samples collected during the UK 2001 FMD epidemic. Size of the points increases with increased number of nt substitutions. Shaded area represents 95% confidence intervals for the fitted line.

Nucleotide changes were reported in a total of 567 sites across the FMDV genome, of which 86 sites found within the noncoding regions at the 5' and 3' ends and 481 sites were identified within the ORF. Of these substitution sites in the ORF, 58 were detected within the VP1 coding region (12.1% of the total coding sites). The molecular clock estimated from BEAST returned a value of 2.18×10^{-5} nt/site/day (95%HPD 1.87×10^{-5} to 2.48×10^{-5}). This result was comparable with those estimated from previously published studies [2.26×10^{-5} nt/site/day, using a relaxed-exponential clock model with 23 WGSs (Cottam et al., 2006); 2.08×10^{-5} nt/site/day, using a relaxed-constant clock model with 22 WGSs (Cottam et al., 2008a); 2.37×10^{-5} nt/site/day here re-estimated using the same strict clock model with 39 WGSs (§3.3.2.1)].

6.3.2 Demographic change of infected population size over time

The reconstructed viral infection demography of the UK 2001 FMD epidemic estimated from the BSP and scaled to the infection prevalence N^* is presented in Figure 6-3, along with the empirical epidemic curves produced using the prevalence data defined in §3.2.2.2. On a visual inspection, the shape and trajectory of the N^* curve matched the real epidemic curve, although the recovered epidemic peak (39th day) was found to be shifted earlier in time than the reported (43rd-46th day). In addition, the

end of the decline phase (~50th day) was again earlier than the reported (~80th day). The skyline scaled N_e was found to follow the exponential size of the P^{exp} prevalence (absolute difference of 47.2 IPs), although describing an earlier and lower in size epidemic peak (absolute difference of 101.6 IPs) (Table 6-1). The tail end phase was higher in size than the actual number of IPs reported during that phase (absolute difference of 33.6 IPs). The N^* estimates derived using the $var(R_t)$ scaling formulation of the Koelle and Rasmussen (2012) form were reported to be largely higher than any empirical prevalence data, with an absolute difference of the epidemic peak size of 645.9 IPs from the P^{exp}. Differently, the N^* recovered from the BSP estimates and derived using the NLFT scaling formulation closely matched the empirical epidemic curve estimated from the P^{exp} prevalence at its exponential and peak phases (absolute difference of 19.8 and 39.1 IPs, respectively). However as already described, the decline phase was found to end ~30 days before the empirical estimated date and the final tail end phase was characterised by a relatively higher average number of reported IPs (absolute difference of 45.5 IPs).

Table 6-1. Time specific number of infected cases estimated using the infection prevalence N^* recovered from the BSP analysis of the n=154 WGSs generated from the clinical samples collected during the UK 2001 FMD epidemic. Predicted number of infected cases were estimated using the scaled N_e (A), the infection prevalence N^* derived by the $var(R_t)$ scaling formulation using the Koelle and Rasmussen (2012) form (B), and the infection prevalence N^* derived from the NLFT scaling formulation using the prevalence-to-incidence ratio τ_p (C). P^{exp} prevalence data was estimated as defined in §3.2.2.2.

		Epidemic Phase				
		Overall	*Exponential*	*Peak*	*Decline*	*Tail End*
Prevalence	P^{exp}	88.42±0.32	195.01±2.15	439.83±3.19	203.17±0.83	30.62±0.04
Effective Population Size	N_e	86.79	147.85	338.19	98.64	64.24
Infection Prevalence [$var(R_t)$, τ_c]	N^*	278.64	474.66	1085.70	316.66	206.23
Infection Prevalence (τ_p)	N^*	102.84	175.18	400.70	116.87	76.11

Extracting the simulated WGSs from the same premises from which the real n=154 sequences were generated and reconstructing the population dynamics of the UK 2001 FMD epidemic from this simulated sample generated, the infection prevalence N^* curves along with the scaled N_e presented in Figure 6-4. Although the shape and trajectory match that of the empirical epidemic curve, the exponential phase was characterised by two incremental steps with the epidemic peak roughly matching that of the empirical prevalence (at around the 42-43th day from the start of the epidemic), followed by a sudden drop of the decline phase ending at the ~50th day. This matched the findings observed from the real data, although the biphasic exponential growth is more marked in the simulated data. However, results of the simulation were describing N_e and N^* derived using the NLFT scaling formulation to be lower in size than the

empirical prevalence (absolute difference at the peak of 320.4 and 297, respectively), whilst the N^* estimates derived using the $var(R_t)$ scaling formulation of the Koelle and Rasmussen (2012) form largely recovering the P^{exp} (absolute difference at the peak of 55.6). This differed from the identified relationship between empirical prevalence and N^* for each of the scaling formulation applied to the real data. In addition, the molecular clock rate estimated was relatively higher than the one derived from the real n=154 WGSs, returning a value of 3.12×10^{-5} nt/site/day (95%HPD 2.81×10^{-5} to 3.44×10^{-5}), with the HPD interval of which did not contain the clock rate used for the simulation and was not overlapped with the HPD of the real data.

Table 6-2. Time specific number of infected cases estimated using the infection prevalence N^* recovered from the BSP analysis of the simulated n=154 WGSs. Predicted number of infected cases were estimated using the scaled N_e (A), the infection prevalence N^* derived by the $var(R_t)$ scaling formulation using the Koelle and Rasmussen (2012) form (B), and the infection prevalence N^* derived from the NLFT scaling formulation using the prevalence-to-incidence ratio τ_p (C). P^{exp} prevalence data was estimated as defined in §3.2.2.2.

		Epidemic Phase				
		Overall	*Exponential*	*Peak*	*Decline*	*Tail End*
Prevalence	P^{exp}	88.42±0.32	195.01±2.15	439.83±3.19	203.17±0.83	30.62±0.04
Effective Population Size	N_e	27.99±4.83	63.25±10.78	119.40±20.91	29.78±8.66	14.79±4.25
Infection Prevalence [$var(R_t), \tau_c$]	N^*	90.05±13.37	203.55±30.47	384.18±58.40	95.60±26.04	47.53±12.75
Infection Prevalence (τ_p)	N^*	33.49±5.95	76.54±12.71	142.83±25.70	35.75±10.95	17.70±5.17

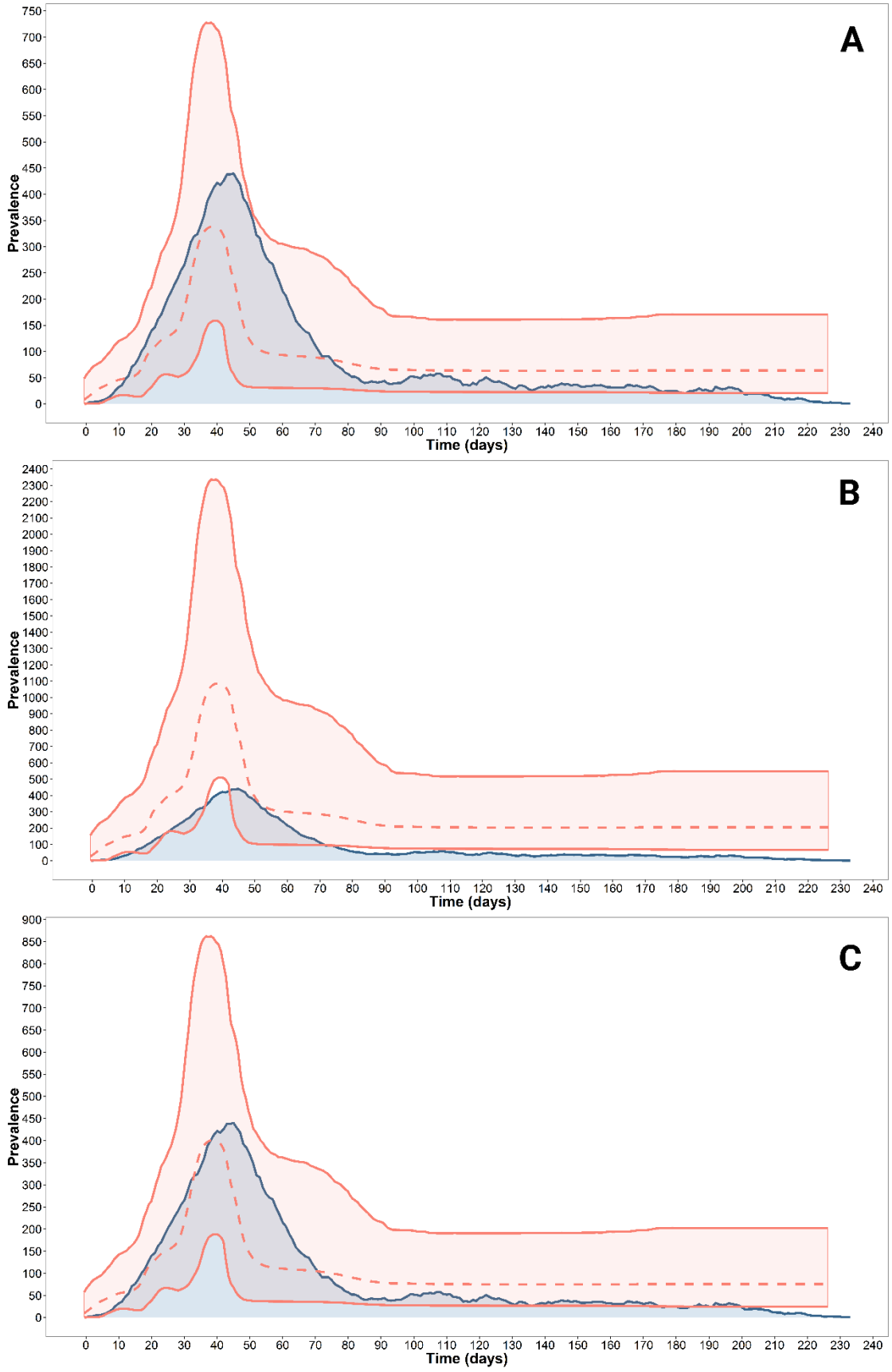

Figure 6-3. Demography of the UK 2001 infected viral population estimated from the BSP and recovered using the infection prevalence N^* scaling formulations defined in §4.3.1. The three plots shows the scaled N_e (A), the infection prevalence N^* derived by the $var(R_t)$ scaling formulation using the Koelle and Rasmussen (2012) form (B), and the infection prevalence N^* derived from the NLFT scaling formulation using the prevalence-to-incidence ratio τ_p (C). Epidemic curve was estimated from the P^{exp} (blue) prevalence data as defined in §3.2.2.2.

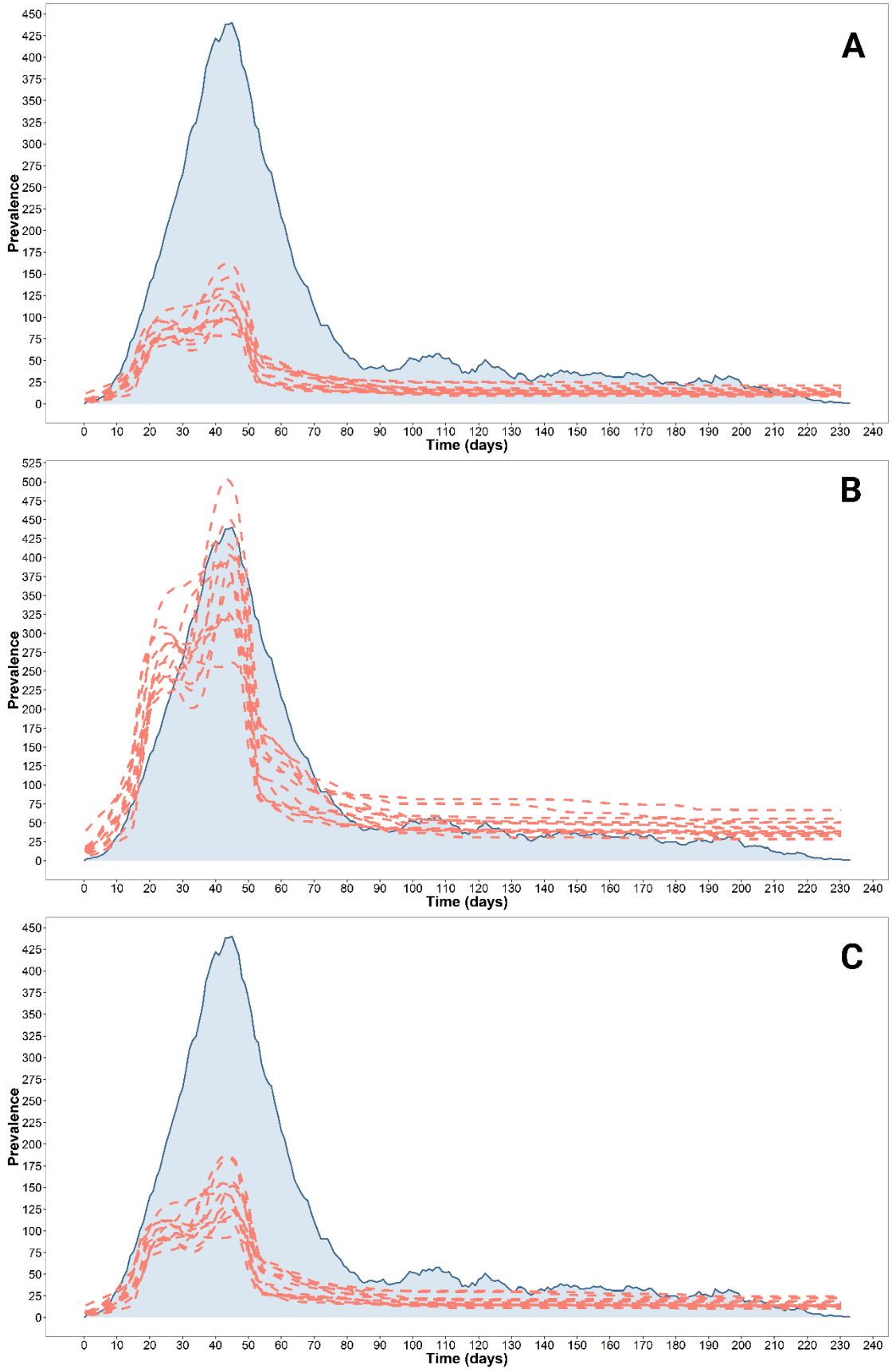

Figure 6-4. Demography of the UK 2001 infected viral population estimated from the simulated data and recovered using the infection prevalence N^* scaling formulations defined in §4.3.1. The three plots shows the scaled N_e (A), the infection prevalence N^* derived by the $var(R_t)$ scaling formulation using the Koelle and Rasmussen (2012) form (B), and the infection prevalence N^* derived from the NLFT scaling formulation using the prevalence-to-incidence ratio τ_p (C). Epidemic curve was estimated from the P^{exp} (blue) prevalence data as defined in §3.2.2.2.

6.4 Discussion

This chapter undertakes preliminary analyses to combining epidemiological and genetic data to recover the phylodynamics of the UK 2001 FMD epidemic. Previously, studies have investigated the temporal and spatial dispersal of FMDV across the UK 2001 FMD epidemic using WGSs generated from the clinical samples collected from each IPs, although only focusing on dissecting the evolutionary patterns of the virus (Cottam et al., 2006), and investigating transmission links within epidemiologically isolated clusters (Cottam et al., 2008a, Konig et al., 2009). However, these studies used less than ~2% of the total number of reported IPs, which limits generalisation to the full epidemic event. In this study a larger database of WGSs (n=154, ~8% of the total number of reported IPs, and ~11% of the collected clinical samples) have been used, with the aim of recovering the infected population dynamics of the UK 2001 FMD epidemic. This has been achieved by employing a phylodynamic method (the BSP) and using those scaling formulations identified from chapter 4 to be effective in recovering the empirical prevalence. It should be noted that this initial dataset was primarily extracted from the full collection of clinical samples of the UK 2001 FMD epidemic with the main purpose of testing and validating the protocol for generating the consensus level sequence from NGS reads, providing confidence in the accuracy of the sequences. Therefore, samples were not selected for sequencing at random, and this is likely to bias the demographic signal derived from the sequence data.

The reconstruction in time of the infected population demography using the N_e estimated from the BSP produced results different to those anticipated and based on studies reported in chapter 4. Every scaling formulation used for recovering the infection prevalence N^* produced results that differed from those reconstructed from the simulated WGSs. The highest ranked scaling formulation derived from §4.3.1 (which expresses the phylogenetic structure by NLFT and use the prevalence-to-incidence ratio τ_p) was found using the real data to closely match the prevalence estimated from the P^{exp} data. However, it is visually clear that this relationship is almost perfectly observed for the exponential phase of the epidemic, whilst the infected population size of the later phases was not recovered. The N^* curve drops more rapidly after the peak than that reported form the empirical prevalence data,

producing an earlier tail end phase which was also overestimated in size. This behaviour of the N^* curve has been also recovered from the simulated data, and therefore could be due to the structure of the sample dataset thus biasing the estimates obtained from both the real and the simulated datasets. As previously described, the sampled dataset here used for analysing the UK 2001 FMD epidemic has not been randomly selected. In fact, 85% of the total WGSs were from IPs reported between the first two months (February and March) of the epidemic, which might substantially bias the genetic diversity recovered over time. As observed from chapter 5, reducing the amount of samples and biasing the collection in time and space could substantially affect the estimates produced by the BSP analysis and, thus, the recovered infection prevalence N^* by any scaling formulation.

A more speculative and critical discussion should be devoted to questioning the reason for the lack of fit between the simulated and real data. It might be argued that the genetic mutations (estimated as root-to-tip distance) raised from the simulation are produced with an error. However, 50 and 84.5±7.5 nt changes at the root-to-tip level (from IP04 to IP2027) have been estimated for the field isolates and the simulated data, respectively (absolute difference of 14.5±7.5 nt). Therefore, the higher number of changes obtained from the simulation would have led to increased genetic diversity, differently to what reported. This comment might be also valid to explain the observed difference in the clock rate recovered from the real and simulated data, estimated at values of 2.18×10^{-5} and 3.12×10^{-5} nt/site/day, respectively.

As already discussed in chapter 3, the substantially different behaviour observed between the real and simulated data might be due to the effect of within-farm evolutionary processes. In a real epidemic, genetic change might accrue from within-farm evolutionary processes, for which multiple cycles of infection might be present on each IP. Genetic diversity derived from the swarm of unsampled genome at the within-farm level might contribute to the size of the 'effective population', although at consensus level this variability could not be recovered. However, the process developed for simulating the virus evolution does consider, although using a very simplified algorithmic implementation, the characterisation of the within-farm dynamics, which might contribute to the genetic diversity observed between the sequences recovered from each IP. On this line, it would be interesting to see if the observed nt change per farm transfer estimated from the real data (if the real

transmission tree would ever be resolved) would match with the value obtained from the simulated data.

Another explanation could be that the reconstruction of the transmission tree that has been used as a backbone for the Markovian evolutionary simulation differed importantly from the real one. However very similar results were obtained running different realisations of the transmission tree reconstruction model (as could be evinced from §4.3) and, in addition, the bias in the structure of the n=154 in estimating the real shape of the epidemic curve (peak and decline phase) have been observed similarly with the simulated data, thus suggesting that the underling transmission tree has been largely recovered. It is, thus, clear that despite attempts in explaining this unresolved and unexpected behaviour, it merits further investigations.

The effective control of FMD, and any other infectious disease, relies on a close epidemiological investigation of the spatio-temporal dynamics of pathogen dispersal, along with the understanding of the evolutionary drives which contributes to the transmission process. Although this initial investigation made use of a small and not uniformly structured dataset, it can preliminarily define the potential resolution which the UK 2001 FMD epidemic might provide for contributing to seminal works on the development of new epidemiological tools which can be used to further enhance our ability in predicting and controlling future outbreaks.

CHAPTER 7

Final Discussion and Concluding Remarks

With the development of the discipline of 'phylodynamics' (Grenfell et al., 2004), seminal studies from several research groups have contributed to our understanding of how epidemiological dynamics can be recovered from an estimated phylogeny (Drummond et al., 2002, Lemey et al., 2009a, Stadler et al., 2012). Population genetic models have also provided the substrate to augment the information derived from the ancestral relationship of sampled lineages with population dynamics inference, to derive a more detailed representation of how the genetic diversity (and the corresponding concept of 'effective population size' N_e) leaves imprints in genetic sequences about past population dynamics. This theory reminds us how epidemiological and evolutionary forces act within the same time frame, and why genetic data sampled from infected hosts can reveal the dynamics of disease spread (Drummond and Rambaut, 2007, Frost and Volz, 2010, Kuhnert et al., 2014). Scholars have shown how the demographic history of infectious disease reconstructed from genome sequences follow in relative size the observed disease dynamics (Rambaut et al., 2008). However, evolutionary dynamics accruing from high population complexity, which is often the case for infectious disease of viral origin, could challenge the ability of analytical approaches used in phylodynamic inference to produce robust estimates (Bennett et al., 2010, Siebenga et al., 2010, Rasmussen et al., 2014a). Degrees of uncertainty still exist on how these methods perform for reproducing the real scale and size of disease outbreak trends as estimated through empirical epidemiological data. Our ability to genetically characterise pathogens has increased exponentially in the last ten years, driven by the advance in high-throughput sequencing technology and the ability to rapidly generate WGSs at low costs, enabling genetic sequences to be provided from each individual in an infected population and thus leading to really large-scale and high resolution population genetic studies for the first time.

In this thesis the exhaustively-sampled UK 2001 FMD epidemic has been used to investigate how established phylodynamic methods based on a coalescent model [*i.e.* the Bayesian skyline plot (Drummond et al., 2005)] perform to recover the demographic history estimated from time series of case reports, thus enabling capture

of the real dynamic of the infected population. Although in viral systems N_e has often been interpreted in an epidemiological sense as the effective size of an infected population, previously it has been shown that coalescent rates are governed by both incidence and prevalence, so that BSP estimates might not accurately be used to infer prevalence alone (Frost and Volz, 2010, Volz 2012). The aim of this study was to attempt to identify a valid formulation which can be used to scale the population genetics parameter N_e (derived from the BSP) to a measure of empirical prevalence data, here termed the infection prevalence N^*. This theoretical relation has been investigated defining prevalence data according to the timing of FMD disease progression, and attempting to account for complex variabilities in the population structure under study. I conclude, that different relationships can be established between the infection prevalence N^* and the prevalence data. The best fit between N^* and the empirical prevalence was found by expressing the phylogenetic structure by the number of lineages as a function of time and using the prevalence-to-incidence ratio τ_p (Frost and Volz, 2013). I here demonstrated, albeit *in silico*, how this quantity effectively resolves the shape and trajectory of the prevalence computed from the P^{exp} prevalence data, where infected cases are defined to exist over the time interval from exposed to being culled. This result provides further insights in how the relationship between N_e and prevalence can be defined in a closed viral epidemic system, although this might be not so straightforward. In fact, it has also been established here that the variability in the number of secondary cases per primary infection R_t greatly impacts on the ability of the BSP to recover the real number of infected cases: increasing the variance in the reproduction number of the infected population [*i.e.* $var(R_t)$] significantly impacts on the accuracy of the estimator. This is in line with the theoretical definition of the BSP model, which assumes that viral lineages are sampled from a single, freely mixing population. Therefore it is clear that this assumption can always be violated in practice and, thus, be invalid in complex epidemiological systems. Thus, accounting for the effect of the variance in the reproductive success [*i.e.* $var(R_t)$] in scaling N_e, N^* estimates were observed to correlate with the infected population size derived from the P^{exp} prevalence data at a very high level of population structure (*i.e.* in a system with a high value of $var(R_t)$ and presence of 'super-spreaders'). In addition, the fit from the scaling equation, that expresses the phylogenetic structure by the number of lineages as a function of time, suggests that in a more homogeneous FMD system [*i.e.* when $var(R_t)\approx 1$] the predicted infection prevalence N^* is a good

approximation to the empirical IP count (P^{exp} derived). This stands as a demonstration that because every IP in a homogenous system has the same chance of transmitting infection to subsequent generations and, therefore, the average time between infections (*i.e.* the serial case interval) is the only possible scaling factor that is maintained constant through the system. It is therefore clear that the results generated provide further supporting evidence that the population structure greatly impacts on estimation of demographic dynamics (Frost and Volz, 2010, Frost and Volz, 2013, Rasmussen et al., 2014a, Pybus et al., 2012). Although structured coalescent models define population structures within its model definition, current phylogenetic implementation (Vaughan et al., 2014) might not be able to fully capture heterogeneity in contacts and transmission among infected individuals. It might be, therefore, essential to account for variability in the infected population structure within the model specification for population size estimates to be more accurate.

A unique feature of the evolutionary process implemented here for generating the genetic variability of the UK 2001 FMD simulated epidemic is that the virus is constrained to evolve along a well-reconstructed transmission tree, thus enabling the preservation of the dependencies of sampled lineages along the transmission tree which are then recovered from the simulated sequences. In addition, in order to account for high within-farm genetic diversity, the coalescent event was set to be early in infection, backward in time of the first related coalescent ancestor (*i.e.* the infection time of the infector farm rather than the infection time of the infected farm). Most phylodynamic models assume that the timing of coalescent events in the phylogeny coincides with the timing of the transmission events. This is obviously not the case when a significant genetic variation exists at the within-host and/or within-farm level as, for examples, in the case of highly population structured infectious disease epidemics. It has been previously reported how the within-farm genetic diversity can contribute to the genetic diversity observed between sampled sequences (Ypma et al., 2013) and, therefore, ignoring this aspect could have led to false estimates of the population size.

Traditionally, methods used for measuring, quantitatively and qualitatively, the burden of pathogen spread within populations rely on surveillance data collected through either disease monitoring programs or during epidemics. As already discussed, in recent years there has been a substantial expansion in the volume of genetic data generated within surveillance programs and larger multi-gene sequences

and WGS are now becoming routine for disease monitoring. Therefore, the potential utility of using molecular methods for estimating infected population dynamics is to support surveillance programs or more conventional control practices. Although in practice this would require less field effort than conventional serosurveillance studies and the deployment of fewer economic resources, sensitivity of the analyses generated through the use of phylodynamics tools to non-random sampling is a widely recognised problem (St Onge et al., 2012, Stack et al., 2010, Volz and Frost, 2014). It is often the case that collected samples would not be representative of the entire infected population, introducing on in the efficacy by which population-level information is extracted and, thus, impacting on the accuracy of reconstructed population dynamics. This might be more relevant when considering endemic disease affecting developing countries with poor health infrastructure. In these setting the availability of less-intensive and more error prone sampled data challenges the evaluation of the health status and, thus, the design of effective control policies. Considering FMD as an example, analysis of sequence data based on the VP1 coding regions collected from Southeast Asian countries revealed the potential impact of undisclosed cases (and potentially misreported disease events) on the maintenance of the disease within an endemic setting (Knowles et al., 2012). This leads to the inability of the FMD research community to capture the real burden of the disease and, thus, to generate the necessary resources to control FMD in these ecosystems.

The effect of sampling strategies on phylodynamic inferences and, thus, on the reconstructed temporal dynamics of viral populations has not been exhaustively explored and, moreover, no attempts have been put forward the assessment of the impact of population structures in an infectious disease context (Chikhi et al. 2010, Stack et al., 2010, de Silva, Ferguson and Fraser, 2012). Results reported within this thesis provides further information on how the demographic signal carried by sequence data becomes imprecise and weaker when reducing the number of samples. In order to address this research question, scenarios from the UK 2001 FMD simulation were intended to represent sampling for the population of an epidemic virus across multiple spatial, temporal and genetic structures. It has been shown that, when sampling at a rate of less than 50% of the total infected population, the N^* curve was reported to generate underestimates of the infectious prevalence and, more understandably, more variable estimates with greater standard errors. In addition, with a sample of only 25% of the total infected population the predicted infection

prevalence N^* was found to be half of the empirical prevalence. It has been also observed how accounting for the spatial and temporal structure of the transmission process within the sampling protocol does not significantly improve the accuracy of the estimated population size at very low sampling rates, in contrast to more evolutionary based sampling approaches which represent the extent of the genetic signal (*i.e.* accounting for the length of the evolutionary process generated between serial cases or the observed genetic distance between sequences). It should be further noted from the analysis of these results that sampling methods designed in a more biased and unstructured fashion (*i.e.* strictly sampling from some infected populations and not others) can falsely suggest population dynamics trends (spurious temporal variation in the BSP reconstruction as, for example, population declines), which would in fact be entirely sampling artefacts and, therefore, not truly reflecting the real demography of the infected population. This leads to the conclusion that the impact of the size and structure of the sampled dataset on the accuracy of the reconstructed viral demographies is relevant at any scale of the transmission process and, therefore, the results derived from this study can provide relevant material to be used in order to inform sampling strategies designed to investigate disease dynamics at endemic level. For example, undisclosed (*i.e.* unsampled) cases maintain endemicity at a fixed level, which could be difficult to account for when the structure of the sampled population is biased. As already discussed, the coalescent model, from which the BSP is derived, assumes that the samples are randomly collected from a homogeneous population (Griffiths and Tavare, 1994b), a criterion which in a real scenario would not be always satisfied. In addition, the BSP model does not specifically account for the sampling process, resulting in more biased estimates when the population is not randomly sampled (Popinga et al., 2015). Therefore, estimates of population dynamics based on coalescent based methods would benefit from the further integration of surveillance information for the specification of the sampling process, which would lead to reduction in the bias of the inference methods. In fact, time series of sequence data can be effectively used for recovering the population size through time if the sampling process can be correctly specified (Volz and Frost, 2014).

It has been already demonstrated how genetic data carries signal on evolutionary forces, demographic size and structure of populations. However, the challenge here lies in how to rigorously make these estimations accurate and unbiased. A further unresolved question is how genome sequences must be examined for

epidemiological characterisation. Methods drawn from phylodynamic inference combine powerful epidemiological and population genetics tools that can provide valuable insights into the dynamics of viral disease. However, the sensitivity of the majority of these models on their assumptions makes estimates less reliable when these are violated, as it has been here reported. Therefore, to be applied as reliable tools supporting control programs, more focused theoretical research is required to model with much more details the processes driving the evolutionary shape of a natural population. This could take into account the structural inhomogeneity of the infected population, the non-random effect derived from partial sampling, the evolutionary interplay driven by coexisting lineages (as in the FMD case) within an ecosystem and the sample size at which the phylodynamic inference starts to be reliable. The further development of phylodynamics methods which integrate inferences of both genetic and epidemiological processes would thus likely provide a promising framework to address these challenges.

APPENDICES

Appendix 1

FMDV type O CATHAY VP1 Philippines sequences database. Designation and origin of the FMDV clinical samples (*n* = 112) collected from the Philippines between 1994 and 2005 and processed in this study. †Date received by the WRLFMD was used where exact collection date was missing.

Virus Designation	Tree Code	Region	Location	Date of Collection†	Species	GenBank No	Reference
O/PHI/2/94	O/PHI/2/94	-	-	06/12/1994†	Porcine	KM243034	(Di Nardo et al., 2014)
O/PHI/5/94	O/PHI/5/94	-	-	06/12/1994†	Porcine	KM243035	(Di Nardo et al., 2014)
O/PHI/6/94	O/PHI/6/94	-	-	06/12/1994†	Porcine	KM243036	(Di Nardo et al., 2014)
O/PHI/8/94	O/PHI/8/94	Calabarzon	Bagong Nayon	08/09/1994	Porcine	KM243037	(Di Nardo et al., 2014)
O/PHI/10/94	O/PHI/10/94	Calabarzon	San Isidro	28/10/1994	Porcine	KM243038	(Di Nardo et al., 2014)
O/PHI/11/94	O/PHI/11/94	Calabarzon	-	07/12/1994	Porcine	KM243039	(Di Nardo et al., 2014)
O/PHI/12/94	O/PHI/12/94	Ilocos	-	13/12/1994	Porcine	KM243040	(Di Nardo et al., 2014)
O/PHI/1/95	O/PHI/1/95	Central Luzon	Tenejero	05/01/1995	Porcine	KM243041	(Di Nardo et al., 2014)
O/PHI/2/95	O/PHI/2/95	Ilocos	-	12/01/1995	Porcine	KM243042	(Di Nardo et al., 2014)
O/PHI/3/95	O/PHI/3/95	Central Luzon	-	15/01/1995	Porcine	KM243043	(Di Nardo et al., 2014)
O/PHI/5/95	O/PHI/5/95	Ilocos	-	09/02/1995	Porcine	DQ164946	(Knowles et al., 2005)
O/PHI/6/95	O/PHI/6/95	Central Luzon	Santa Ines	23/03/1995	Porcine	KM243044	(Di Nardo et al., 2014)
O/PHI/9/95	O/PHI/9/95	NCR	-	23/03/1995	Porcine	KM243045	(Di Nardo et al., 2014)
O/PHI/10/95	O/PHI/10/95	Bicol	-	06/04/1995	Porcine	KM243046	(Di Nardo et al., 2014)
O/PHI/11/95	O/PHI/11/95	NCR	-	06/04/1995	Porcine	KM243047	(Di Nardo et al., 2014)
O/PHI/12/95	O/PHI/12/95	Calabarzon	Calabuso	03/10/1996†	Porcine	KM243048	(Di Nardo et al., 2014)
O/PHI/13/95	O/PHI/13/95	Calabarzon	Ampid	03/10/1996†	Porcine	KM243049	(Di Nardo et al., 2014)
O/PHI/14/95	O/PHI/14/95	Central Luzon	-	03/10/1996†	Porcine	KM243050	(Di Nardo et al., 2014)
O/PHI/1/96	O/PHI/1/96	Central Luzon	-	03/10/1996†	Porcine	KM243053	(Di Nardo et al., 2014)
O/PHI/2/96	O/PHI/2/96	Central Luzon	-	03/10/1996†	Porcine	KM243054	(Di Nardo et al., 2014)
O/PHI/3/96	O/PHI/3/96	Eastern Visayas	-	03/10/1996†	Porcine	KM243055	(Di Nardo et al., 2014)
O/PHI/5/96	O/PHI/5/96	Bicol	-	01/09/1996	Porcine	KM243056	(Di Nardo et al., 2014)

O/PHI/6/96	O/PHI/6/96	Ilocos	Aliaga	01/10/1996	Porcine	KM243057	(Di Nardo et al., 2014)
O/PHI/7/96	O/PHI/7/96	Calabarzon	Mahabang Parang	01/11/1996	Porcine	KM243058	(Di Nardo et al., 2014)
O/PHI/2/97	O/PHI/2/97	NCR	-	16/01/1997	Porcine	KM243059	(Di Nardo et al., 2014)
O/PHI/3/97	O/PHI/3/97	Ilocos	-	01/01/1997	Porcine	KM243060	(Di Nardo et al., 2014)
O/PHI/4/97	O/PHI/4/97	Central Luzon	Poblacion	01/02/1997	Porcine	KM243061	(Di Nardo et al., 2014)
O/PHI/5/97	O/PHI/5/97	CAR	Guisad	01/02/1997	Porcine	KM243062	(Di Nardo et al., 2014)
O/PHI/6/97	O/PHI/6/97	Central Luzon	-	01/03/1997	Porcine	KM243063	(Di Nardo et al., 2014)
O/PHI/7/97	O/PHI/7/97	NCR	Payatas	01/03/1997	Porcine	KM243064	(Di Nardo et al., 2014)
O/PHI/8/97	O/PHI/8/97	Central Luzon	Malibong Bata	01/03/1997	Porcine	KM243065	(Di Nardo et al., 2014)
O/PHI/10/97	O/PHI/10/97	Bicol	Cabangan	01/03/1997	Porcine	KM243066	(Di Nardo et al., 2014)
O/PHI/11/97	O/PHI/11/97	Bicol	-	06/04/1997	Porcine	KM243067	(Di Nardo et al., 2014)
O/PHI/12/97	O/PHI/12/97	Central Luzon	-	19/11/1997†	Porcine	KM243070	(Di Nardo et al., 2014)
O/PHI/13/97	O/PHI/13/97	Central Luzon	Balatong	19/11/1997†	Porcine	KM243071	(Di Nardo et al., 2014)
O/PHI/14/97	O/PHI/14/97	Bicol	-	19/11/1997†	Porcine	KM243072	(Di Nardo et al., 2014)
O/PHI/15/97	O/PHI/15/97	Central Luzon	Sampaga	19/11/1997†	Porcine	KM243073	(Di Nardo et al., 2014)
O/PHI/16/97	O/PHI/16/97	Central Luzon	-	19/11/1997†	Porcine	KM243074	(Di Nardo et al., 2014)
O/PHI/1/98	O/PHI/1/98	Central Luzon	-	01/01/1998	-	KM243075	(Di Nardo et al., 2014)
O/PHI/2/98	O/PHI/2/98	Central Luzon	-	01/01/1998	-	KM243076	(Di Nardo et al., 2014)
O/PHI/3/98	O/PHI/3/98	Central Luzon	Matatalaib	01/01/1998	-	KM243077	(Di Nardo et al., 2014)
O/PHI/4/98	O/PHI/4/98	Central Luzon	-	01/01/1998	-	KM243078	(Di Nardo et al., 2014)
O/PHI/5/98	O/PHI/5/98	Calabarzon	-	01/01/1998	-	KM243079	(Di Nardo et al., 2014)
O/PHI/6/98	O/PHI/6/98	Calabarzon	-	01/01/1998	-	KM243080	(Di Nardo et al., 2014)
O/PHI/8/98	O/PHI/8/98	Central Luzon	-	01/01/1998	-	KM243081	(Di Nardo et al., 2014)
O/PHI/9/98	O/PHI/9/98	NCR	Nepomuceno	01/01/1998	-	KM243082	(Di Nardo et al., 2014)
O/PHI/10/98	O/PHI/10/98	-	-	01/01/1998	-	KM243083	(Di Nardo et al., 2014)
O/PHI/11/98	O/PHI/11/98	NCR	Malinta	01/01/1998	-	KM243084	(Di Nardo et al., 2014)
O/PHI/12/98	O/PHI/12/98	-	-	01/01/1998	Porcine	KM243085	(Di Nardo et al., 2014)
O/PHI/13/98	O/PHI/13/98	-	-	01/01/1998	Porcine	KM243086	(Di Nardo et al., 2014)
O/PHI/14/98	O/PHI/14/98	-	-	01/01/1998	Porcine	KM243087	(Di Nardo et al., 2014)
O/PHI/15/98	O/PHI/15/98	-	-	01/01/1998	Porcine	KM243088	(Di Nardo et al., 2014)
O/PHI/16/98	O/PHI/16/98	-	-	01/01/1998	Buffalo	KM243089	(Di Nardo et al., 2014)
O/PHI/18/98	O/PHI/18/98	-	-	01/01/1998	Porcine	KM243090	(Di Nardo et al., 2014)
O/PHI/19/98	O/PHI/19/98	Central Luzon	-	01/01/1998	Porcine	KM243091	(Di Nardo et al., 2014)
O/PHI/20/98	O/PHI/20/98	Central Luzon	-	01/01/1998	-	KM243092	(Di Nardo et al., 2014)
O/PHI/21/98	O/PHI/21/98	Central Luzon	-	01/01/1998	Porcine	KM243093	(Di Nardo et al., 2014)
O/PHI/22/98	O/PHI/22/98	Central Luzon	-	01/01/1998	Porcine	KM243094	(Di Nardo et al., 2014)
O/PHI/23/98	O/PHI/23/98	Central Luzon	-	01/01/1998	Porcine	KM243095	(Di Nardo et al., 2014)
O/PHI/25/98	O/PHI/25/98	NCR	Nepomuceno	01/01/1998	Porcine	KM243096	(Di Nardo et al., 2014)
O/PHI/30/98	O/PHI/30/98	Calabarzon	-	01/01/1998	Porcine	KM243097	(Di Nardo et al., 2014)
O/PHI/1/99	O/PHI/1/99	Central Luzon	-	01/01/1999	Porcine	KM243098	(Di Nardo et al., 2014)

O/PHI/3/99	O/PHI/3/99	Central Luzon	Cupang West	01/01/1999	Porcine	KM243099	(Di Nardo et al., 2014)
O/PHI/4/99	O/PHI/4/99	Central Luzon	Tungkong Mangga	01/01/1999	Porcine	KM243100	(Di Nardo et al., 2014)
O/PHI/5/99	O/PHI/5/99	Western Visayas	-	01/01/1999	Porcine	KM243101	(Di Nardo et al., 2014)
O/PHI/10/99	O/PHI/10/99	Central Luzon	-	01/01/1999	Porcine	KM243102	(Di Nardo et al., 2014)
O/PHI/3/2000	O/PHI/3/00	Bicol	Tagas	02/02/2000	Porcine	KM243103	(Di Nardo et al., 2014)
O/PHI/5/2000	O/PHI/5/00	Central Luzon	Santa Rosa	08/02/2000	Porcine	DQ164947	(Knowles et al., 2005)
O/PHI/6/2000	O/PHI/6/00	NCR	Fairview	13/02/2000	Porcine	KM243104	(Di Nardo et al., 2014)
O/PHI/7/2000	O/PHI/7/00	Central Luzon	Santo Rosario	21/02/2000	Porcine	KM243105	(Di Nardo et al., 2014)
O/PHI/8/2000	O/PHI/8/00	Central Luzon	Santa Cruz	22/02/2000	Porcine	KM243106	(Di Nardo et al., 2014)
O/PHI/9/2000	O/PHI/9/00	Central Luzon	Pritil	01/03/2000	Porcine	KM243107	(Di Nardo et al., 2014)
O/PHI/13/2000	O/PHI/13/00	Central Luzon	Santiago	02/03/2000	Porcine	DQ164948	(Knowles et al., 2005)
O/PHI/14/2000	O/PHI/14/00	Mimaropa	-	11/03/2000	Porcine	DQ164949	(Knowles et al., 2005)
O/PHI/15/2000	O/PHI/15/00	Mimaropa	-	11/03/2000	Porcine	KM243108	(Di Nardo et al., 2014)
O/PHI/16/2000	O/PHI/16/00	Mimaropa	-	11/03/2000	Porcine	KM243109	(Di Nardo et al., 2014)
O/PHI/17/2000	O/PHI/17/00	Mimaropa	-	11/03/2000	Porcine	KM243110	(Di Nardo et al., 2014)
O/PHI/19/2000	O/PHI/19/00	Bicol	-	07/04/2000	Porcine	KM243111	(Di Nardo et al., 2014)
O/PHI/23/2000	O/PHI/23/00	Calabarzon	San Andres	24/05/2000	Porcine	KM243112	(Di Nardo et al., 2014)
O/PHI/24/2000	O/PHI/24/00	Bicol	Rawis	24/05/2000	Porcine	KM243113	(Di Nardo et al., 2014)
O/PHI/26/2000	O/PHI/26/00	Central Luzon	Tabon	29/06/2000	Porcine	KM243114	(Di Nardo et al., 2014)
O/PHI/27/2000	O/PHI/27/00	Central Luzon	-	04/07/2000	Porcine	KM243115	(Di Nardo et al., 2014)
O/PHI/4/2001	O/PHI/4/01	Central Luzon	-	01/01/2001	Porcine	KM243116	(Di Nardo et al., 2014)
O/PHI/5/2001	O/PHI/5/01	Central Luzon	-	01/01/2001	Porcine	KM243117	(Di Nardo et al., 2014)
O/PHI/6/2001	O/PHI/6/01	Central Luzon	Dulong Bayan	01/01/2001	Porcine	KM243118	(Di Nardo et al., 2014)
O/PHI/7/2001	O/PHI/7/01	Central Luzon	Dulong Bayan	01/01/2001	Porcine	KM243119	(Di Nardo et al., 2014)
O/PHI/8/2001	O/PHI/8/01	Central Luzon	Poblacion	01/01/2001	Porcine	KM243120	(Di Nardo et al., 2014)
O/PHI/9/2001	O/PHI/9/01	Central Luzon	Santo Cristo	01/01/2001	Porcine	KM243121	(Di Nardo et al., 2014)
O/PHI/10/2001	O/PHI/10/01	Central Luzon	Partida	01/01/2001	Porcine	KM243122	(Di Nardo et al., 2014)
O/PHI/5/2003	O/PHI/5/03	CAR	-	10/02/2003	Porcine	DQ164950	(Knowles et al., 2005)
O/PHI/10/2003	O/PHI/10/03	NCR	-	04/03/2003	Porcine	DQ164951	(Knowles et al., 2005)
O/PHI/14/2003	O/PHI/14/03	NCR	Dian	21/03/2003	Porcine	KM243123	(Di Nardo et al., 2014)
O/PHI/17/2003	O/PHI/17/03	Central Luzon	Santa Filomena	08/04/2003	Porcine	DQ164952	(Knowles et al., 2005)
O/PHI/18/2003	O/PHI/18/03	Calabarzon	Balibago	07/05/2003	Porcine	KM243124	(Di Nardo et al., 2014)
O/PHI/20/2003	O/PHI/20/03	Calabarzon	Balibago	07/05/2003	Porcine	KM243125	(Di Nardo et al., 2014)
O/PHI/21/2003	O/PHI/21/03	Calabarzon	Pagrai	13/05/2003	Porcine	DQ164953	(Knowles et al., 2005)
O/PHI/23/2003	O/PHI/23/03	Calabarzon	-	15/05/2003	Porcine	DQ164954	(Knowles et al., 2005)
O/PHI/1/2004	O/PHI/1/04	Ilocos	Cabaroan Daya	13/01/2004	Porcine	DQ164955	(Knowles et al., 2005)
O/PHI/2/2004	O/PHI/2/04	Central Luzon	-	16/01/2004	Porcine	DQ164956	(Knowles et al., 2005)
O/PHI/3/2004	O/PHI/3/04	NCR	Kamuning	05/02/2004	Porcine	DQ164957	(Knowles et al., 2005)
O/PHI/4/2004	O/PHI/4/04	NCR	Nepomuceno	24/03/2004	Porcine	DQ164958	(Knowles et al., 2005)
O/PHI/5/2004	O/PHI/5/04	NCR	Pinagbuhatan	01/06/2004	Porcine	DQ164959	(Knowles et al., 2005)

O/PHI/6/2004	O/PHI/6/04	NCR	Dagat-Dagatan	21/06/2004	Porcine	DQ164960	(Knowles et al., 2005)
O/PHI/7/2004	O/PHI/7/04	Central Luzon	Ayson	29/06/2004	Porcine	DQ164961	(Knowles et al., 2005)
O/PHI/8/2004	O/PHI/8/04	Central Luzon	-	14/07/2004	Porcine	DQ164962	(Knowles et al., 2005)
O/PHI/9/2004	O/PHI/9/04	Calabarzon	Mayamot	21/07/2004	Porcine	DQ164963	(Knowles et al., 2005)
O/PHI/10/2004	O/PHI/10/04	NCR	Project 8	04/08/2004	Porcine	DQ164964	(Knowles et al., 2005)
O/PHI/11/2004	O/PHI/11/04	NCR	-	03/09/2004	Porcine	DQ164965	(Knowles et al., 2005)
O/PHI/12/2004	O/PHI/12/04	Calabarzon	Calabuso	29/09/2004	Porcine	DQ164966	(Knowles et al., 2005)
O/PHI/1/2005	O/PHI/1/05	NCR	La Loma	16/02/2005	Porcine	KM243127	(Di Nardo et al., 2014)
O/PHI/2/2005	O/PHI/2/05	NCR	-	23/02/2005	Porcine	KM243128	(Di Nardo et al., 2014)
O/PHI/3/2005	O/PHI/3/05	NCR	La Loma	03/03/2005	Porcine	KM243131	(Di Nardo et al., 2014)

Appendix 2

FMDV type O CATHAY VP1 sequences database. Designation and origin of the VP1 sequences (n = 210) retrieved from either GenBank or the WRLFMD databases and belonging to the O CATHAY topotype. †Date received by WRLFMD, year of collection or GenBank submission date were used where exact collection date was missing.

Virus Designation	Tree Code	Country	Location	Date of Collection	Species	GenBank No	Reference
O/CHA/Akesu/58	O/CHA/Ake/58	China	Akesu	01/01/1958†	Bovine	AJ131469	(Zhao et al., unpublished data)
O/CHA/Akesu-MIII/58	O/CHA/AkeOMIII/58	China	Akesu	01/01/1958†	-	AY359854	(Wang et al., unpublished data)
O/TAI/Ban/60	O/TAI/Ban/60	Thailand	Bangkok	01/01/1960†	Porcine	KM243030	(Di Nardo et al., 2014)
O/HKN/21/70	O/HKN/21/70	Hong Kong	Hang Tau	13/03/1970	Porcine	AJ294911	(Knowles et al., 2001a)
O/HKN/1/73	O/HKN/01/73	Hong Kong	Lantau Island	01/01/1973	Porcine	AJ294912	(Knowles et al., 2001a)
O/HKN/19/73	O/HKN/19/73	Hong Kong	Ha Cheung Sha	19/06/1973	Bovine	AJ294913	(Knowles et al., 2001a)
O/HKN/3/75	O/HKN/03/75	Hong Kong	Ping Shan	23/12/1974	Porcine	AJ294915	(Knowles et al., 2001a)
O/HKN/27/77	O/HKN/27/77	Hong Kong	-	01/01/1977	Porcine	KM243031	(Di Nardo et al., 2014)
O/HKN/33/77	O/HKN/33/77	Hong Kong	Tin Ping Shan	01/01/1977	Porcine	AJ294916	(Knowles et al., 2001a)
O/AUR/Tha/81	O/AUR/Tha/81	Austria	Thalheim	18/03/1981†	Porcine	KM243032	(Di Nardo et al., 2014)
O/HKN/14/82	O/HKN/14/82	Hong Kong	Hei Ling Chau	25/02/1982	Porcine	AJ294917	(Knowles et al., 2001a)
O/GER/Wup/82	O/GER/Wup/82	Germany	Wuppertal	16/06/1982†	Porcine	KM243033	(Di Nardo et al., 2014)
O/HKN/6/83	O/HKN/06/83	Hong Kong	Pok Fu Lam	18/12/1982	Bovine	AJ294919	(Knowles et al., 2001a)
O/HKN/7/85	O/HKN/07/85	Hong Kong	Ma On Kong	25/01/1985	Porcine	AJ294920	(Knowles et al., 2001a)
O/CHA/Gua/86	O/CHA/Gua/86	China	Guangdong	01/01/1986†	Porcine	AJ131468	(Zhao et al., unpublished data)
O/HKN/12/91	O/HKN/12/91	Hong Kong	Shek Kwu Chau	26/11/1991	Porcine	AJ294921	(Knowles et al., 2001a)
O/HKN/93	O/HKN/93	Hong Kong	-	01/01/1993†	Porcine	AJ131470	(Zhao et al., unpublished data)
O/1685/RUS/95	O/RUS/Mos/95	Russia	Moscow	16/06/1995	Porcine	AJ004680	(Sherbakov et al., unpublished data)
O/HKN/1/96	O/HKN/01/96	Hong Kong	Lau Fau Shan	16/01/1996	Porcine	KM243051	(Di Nardo et al., 2014)
O/HKN/7/96	O/HKN/07/96	Hong Kong	-	06/02/1996	Bovine	AJ294922	(Knowles et al., 2001a)
O/HKN/16/96	O/HKN/16/96	Hong Kong	Lei Uk	29/03/1996	Porcine	KM243052	(Di Nardo et al., 2014)
O/HKN/20/96	O/HKN/20/96	Hong Kong	-	17/04/1996	Bovine	AJ294924	(Knowles et al., 2001a)
O/TAW/97	O/TAW/97	Taiwan	-	01/04/1997†	Porcine	AY593835	(Carrillo et al., 2005)
O/TAW/Yun/97	O/TAW/Yun/97	Taiwan	Yunlin	01/04/1997†	Porcine	AF308157	(Beard and Mason, 2000)
O/TAW/Chu/97	O/TAW/Chu/97	Taiwan	Chu-Pei	01/04/1997†	-	AF026168	(Tsai et al., 2000)
O/TAW/TL/97	O/TAW/TL/97	Taiwan	-	01/04/1997†	Porcine	AF030259	(Lai et al., unpublished data)
O/TAW/Tao018/97	O/TAW/Tao018/97	Taiwan	Taoyuan	01/04/1997†	Porcine	AF095863	(Tsai et al., 2000)

O/TAW/Tai041/97	O/TAW/Tai041/97	Taiwan	Tainan	01/04/1997†	Porcine	AF095864	(Tsai et al., 2000)
O/TAW/Pin060/97	O/TAW/Pin060/97	Taiwan	Pingtun	01/04/1997†	Porcine	AF095865	(Tsai et al., 2000)
O/TAW/Tai077/97	O/TAW/Tai077/97	Taiwan	Taichung	01/04/1997†	Porcine	AF095866	(Tsai et al., 2000)
O/TAW/Hsi079/97	O/TAW/Hsi079/97	Taiwan	Hsinchu	01/04/1997†	Porcine	AF095867	(Tsai et al., 2000)
O/TAW/Nan089/97	O/TAW/Nan089/97	Taiwan	Nantou	01/04/1997†	Porcine	AF095868	(Tsai et al., 2000)
O/TAW/Tai109/97	O/TAW/Tai109/97	Taiwan	Taipei	01/04/1997†	Porcine	AF095869	(Tsai et al., 2000)
O/TAW/Tai110/97	O/TAW/Tai110/97	Taiwan	Taipei	01/04/1997†	Porcine	AF095870	(Tsai et al., 2000)
O/TAW/Tai111/97	O/TAW/Tai111/97	Taiwan	Taitung	01/04/1997†	Porcine	AF095871	(Tsai et al., 2000)
O/TAW/Tao113/97	O/TAW/Tao113/97	Taiwan	Taoyuan	01/04/1997†	Porcine	AF095872	(Tsai et al., 2000)
O/TAW/Hsi128/97	O/TAW/Hsi128/97	Taiwan	Hsinchu	01/04/1997†	Porcine	AF095873	(Tsai et al., 2000)
O/TAW/Yun136/97	O/TAW/Yun136/97	Taiwan	Yunlin	01/04/1997†	Porcine	AF095874	(Tsai et al., 2000)
O/TAW/Tai145/97	O/TAW/Tai145/97	Taiwan	Taipei	01/04/1997†	Porcine	AF095875	(Tsai et al., 2000)
O/TAW/Tai150/97	O/TAW/Tai150/97	Taiwan	Taipei	01/04/1997†	Porcine	AF095876	(Tsai et al., 2000)
O/TAW/Kao153/97	O/TAW/Kao153/97	Taiwan	Kaohsiung	01/04/1997†	Porcine	AF095877	(Tsai et al., 2000)
O/TAW/Chu158/97	O/TAW/Chu158/97	Taiwan	Chunhwa	01/04/1997†	Porcine	AF095879	(Tsai et al., 2000)
O/TAW/Mia165/97	O/TAW/Mia165/97	Taiwan	Miaoli	01/04/1997†	Porcine	AF095879	(Tsai et al., 2000)
O/TAW/Tai168/97	O/TAW/Tai168/97	Taiwan	Tainan	01/04/1997†	Porcine	AF095880	(Tsai et al., 2000)
O/TAW/Tai181/97	O/TAW/Tai181/97	Taiwan	Tainan	01/04/1997†	Porcine	AF095881	(Tsai et al., 2000)
O/TAW/Tai186/97	O/TAW/Tai186/97	Taiwan	Taichung	01/04/1997†	Porcine	AF095882	(Tsai et al., 2000)
O/TAW/Chu188/97	O/TAW/Chu188/97	Taiwan	Chunhwa	01/04/1997†	Porcine	AF095883	(Tsai et al., 2000)
O/TAW/Hsi189/97	O/TAW/Hsi189/97	Taiwan	Hsinchu	01/04/1997†	Porcine	AF095884	(Tsai et al., 2000)
O/TAW/Kao190/97	O/TAW/Kao190/97	Taiwan	Kaohsiung	01/04/1997†	Porcine	AF095885	(Tsai et al., 2000)
O/TAW/81/97	O/TAW/81/97	Taiwan	Yilan	17/04/1997	Porcine	KM243068	(Di Nardo et al., 2014)
O/TAW/83/97	O/TAW/83/97	Taiwan	Taitung	24/04/1997	Porcine	KM243069	(Di Nardo et al., 2014)
O/VIT/3/97	O/VIT/03/97	Vietnam	-	26/08/1997†	Porcine	AJ294930	(Knowles et al., 2001a)
O-TW-185-97	O/TAW/185/97	Taiwan	-	07/12/1997	Porcine	GQ292726	(Lin et al., 2010)
O-TW-205-98	O/TAW/205/98	Taiwan	Tainan	07/01/1998	Porcine	GQ292727	(Lin et al., 2010)
O-TW-210-98	O/TAW/210/98	Taiwan	Yunlin	23/01/1998	Porcine	GQ292728	(Lin et al., 2010)
O-TW-219-98	O/TAW/219/98	Taiwan	Tainan	07/04/1998	Porcine	GQ292729	(Lin et al., 2010)
O/HKN/1/99	O/HKN/01/99	Hong Kong	Mong Tseng Tsuen	05/01/1999	Porcine	AJ294925	(Knowles et al., 2001a)
O/TAW/4/99	O/TAW/04/99	Taiwan	Penghu	01/02/1999	Porcine	AJ294928	(Knowles et al., 2001a)
O-TW-241-99	O/TAW/241/99	Taiwan	Yunlin	14/02/1999	Porcine	GQ292730	(Lin et al., 2010)
O-TW-242-99	O/TAW/242/99	Taiwan	Yunlin	20/02/1999	Porcine	GQ292731	(Lin et al., 2010)
O-TW-244-99	O/TAW/244/99	Taiwan	Penghu	23/02/1999	Porcine	GQ292732	(Lin et al., 2010)
O/HKN/10/99	O/HKN/10/99	Hong Kong	Pak Sha Tsuen	19/03/1999	Porcine	AJ318836	(Knowles et al., unpublished data)
O-TW-249-99	O/TAW/249/99	Taiwan	Pingtun	15/04/1999	Porcine	GQ292733	(Lin et al., 2010)
O-TW-251-99	O/TAW/251/99	Taiwan	Kaohsiung	20/04/1999	Porcine	GQ292734	(Lin et al., 2010)
O-TW-252-99	O/TAW/252/99	Taiwan	Tainan	21/04/1999	Porcine	GQ292735	(Lin et al., 2010)
O-TW-253-99	O/TAW/253/99	Taiwan	Hsinchu	29/04/1999	Porcine	GQ292736	(Lin et al., 2010)
O-TW-255-2000	O/TAW/255/00	Taiwan	Taoyuan	22/10/2000	Porcine	GQ292737	(Lin et al., 2010)

O/CHA/YM/YN/2000	O/CHA/YMYN/00	China	Yunnan	18/12/2000	Porcine	HQ412603	(Xin et al., unpublished data)
O/CHA/F29	O/CHA/F29	China	-	01/01/2001†	Porcine	AF403048	(Lou and Du, unpublished data)
O/HKN/4/2001	O/HKN/04/01	Hong Kong	-	01/01/2001	Porcine	DQ164875	(Knowles et al., 2005)
O-TW-256-2001	O/TAW/256/01	Taiwan	Taipei	25/02/2001	Porcine	GQ292738	(Lin et al., 2010)
O/HKN/S01/2001	O/HKN/S01/01	Hong Kong	-	01/07/2001	Porcine	JF968125	(Hui and Leung, 2012)
O/HKN/S03/2001	O/HKN/S03/01	Hong Kong	-	01/07/2001	Porcine	JF968126	(Hui and Leung, 2012)
O/HKN/S04/2001	O/HKN/S04/01	Hong Kong	-	01/07/2001	Porcine	JF968127	(Hui and Leung, 2012)
O/HKN/S05/2001	O/HKN/S05/01	Hong Kong	-	01/07/2001	Porcine	JF968128	(Hui and Leung, 2012)
O/HKN/19/2001	O/HKN/19/01	Hong Kong	Sheung Shui	28/09/2001	Porcine	DQ164876	(Knowles et al., 2005)
O/HKN/S06/2001	O/HKN/S06/01	Hong Kong	-	01/10/2001	Porcine	JF968129	(Hui and Leung, 2012)
O/HKN/S09/2001	O/HKN/S09/01	Hong Kong	-	01/10/2001	Porcine	JF968130	(Hui and Leung, 2012)
O/HKN/S10/2001	O/HKN/S10/01	Hong Kong	-	01/10/2001	Porcine	JF968131	(Hui and Leung, 2012)
O/VIT/13/2002	O/VIT/13/02	Vietnam	-	01/01/2002	-	DQ165025	(Knowles et al., 2005)
O/HKN/S11/2002	O/HKN/S11/02	Hong Kong	-	01/01/2002	Porcine	JF968132	(Hui and Leung, 2012)
O/HKN/S12/2002	O/HKN/S12/02	Hong Kong	-	01/01/2002	Porcine	JF968133	(Hui and Leung, 2012)
O/HKN/S13/2002	O/HKN/S13/02	Hong Kong	-	01/01/2002	Porcine	JF968134	(Hui and Leung, 2012)
O/HKN/S14/2002	O/HKN/S14/02	Hong Kong	-	01/01/2002	Porcine	JF968135	(Hui and Leung, 2012)
O/HKN/1/2002	O/HKN/01/02	Hong Kong	Yuen Long	22/01/2002	Porcine	DQ164877	(Knowles et al., 2005)
O/HKN/3/2002	O/HKN/03/02	Hong Kong	Yuen Long	31/01/2002	Porcine	DQ164878	(Knowles et al., 2005)
O/HKN/2002	O/HKN/02	Hong Kong	-	01/02/2002	Porcine	AY317098	(Feng et al., 2004)
O/HKN/S15/2002	O/HKN/S15/02	Hong Kong	-	01/04/2002	Porcine	JF968136	(Hui and Leung, 2012)
O/HKN/S17/2002	O/HKN/S17/02	Hong Kong	-	01/04/2002	Porcine	JF968137	(Hui and Leung, 2012)
O/HKN/S18/2002	O/HKN/S18/02	Hong Kong	-	01/04/2002	Porcine	JF968138	(Hui and Leung, 2012)
O/HKN/S19/2002	O/HKN/S19/02	Hong Kong	-	01/04/2002	Porcine	JF968139	(Hui and Leung, 2012)
O/HKN/S20/2002	O/HKN/S20/02	Hong Kong	-	01/04/2002	Porcine	JF968140	(Hui and Leung, 2012)
O/HKN/S22/2002	O/HKN/S22/02	Hong Kong	-	01/05/2002	Porcine	JF968141	(Hui and Leung, 2012)
O/HKN/S24/2002	O/HKN/S24/02	Hong Kong	-	01/06/2002	Porcine	JF968142	(Hui and Leung, 2012)
O/HKN/S25/2002	O/HKN/S25/02	Hong Kong	-	01/06/2002	Porcine	JF968145	(Hui and Leung, 2012)
O/HKN/S32/2002	O/HKN/S32/02	Hong Kong	-	01/10/2002	Porcine	JF968143	(Hui and Leung, 2012)
O/HKN/S34/2002	O/HKN/S34/02	Hong Kong	-	01/10/2002	Porcine	JF968146	(Hui and Leung, 2012)
O/HKN/S44/2002	O/HKN/S44/02	Hong Kong	-	01/10/2002	Porcine	JF968147	(Hui and Leung, 2012)
O/HKN/S72/2003	O/HKN/S72/03	Hong Kong	-	01/01/2003	Porcine	JF968148	(Hui and Leung, 2012)
O/HKN/S73/2003	O/HKN/S73/03	Hong Kong	-	01/01/2003	Porcine	JF968148	(Hui and Leung, 2012)
O/HKN/S74/2003	O/HKN/S74/03	Hong Kong	-	01/01/2003	Porcine	JF968149	(Hui and Leung, 2012)
O/HKN/S75/2003	O/HKN/S75/03	Hong Kong	-	01/01/2003	Porcine	JF968150	(Hui and Leung, 2012)
O/HKN/S76/2003	O/HKN/S76/03	Hong Kong	-	01/01/2003	Porcine	JF968151	(Hui and Leung, 2012)
O/HKN/2/2003	O/HKN/02/03	Hong Kong	-	01/01/2003	Porcine	DQ164879	(Knowles et al., 2005)
O/HKN/3/2003	O/HKN/03/03	Hong Kong	-	01/01/2003	Porcine	DQ164880	(Knowles et al., 2005)
O/HKN/S78/2003	O/HKN/S78/03	Hong Kong	-	01/02/2003	Porcine	JF968152	(Hui and Leung, 2012)
O/HKN/S79/2003	O/HKN/S79/03	Hong Kong	-	01/02/2003	Porcine	JF968153	(Hui and Leung, 2012)

O/HKN/S80/2003	O/HKN/S80/03	Hong Kong	-	01/02/2003	Porcine	JF968154	(Hui and Leung, 2012)
O/HKN/S81/2003	O/HKN/S81/03	Hong Kong	-	01/02/2003	Porcine	JF968157	(Hui and Leung, 2012)
O/HKN/S83/2003	O/HKN/S83/03	Hong Kong	-	01/02/2003	Porcine	JF968155	(Hui and Leung, 2012)
O/HKN/S84/2003	O/HKN/S84/03	Hong Kong	-	01/02/2003	Porcine	JF968159	(Hui and Leung, 2012)
O/CHA/XJ1/03	O/CHA/XJ1/03	China	-	01/08/2003†	Bovine	AY373583	(Li et al., unpublished data)
O/HKN/3/2004	O/HKN/03/04	Hong Kong	-	28/01/2004	Porcine	DQ164881	(Knowles et al., 2005)
O/VIT/2/2004	O/VIT/02/04	Vietnam	Quang Nam	01/02/2004	Porcine	DQ165033	(Knowles et al., 2005)
O/HKN/4/2004	O/HKN/04/04	Hong Kong	-	11/02/2004	Porcine	DQ164882	(Knowles et al., 2005)
O/VIT/3/2004	O/VIT/03/04	Vietnam	Quang Nam	01/03/2004	Porcine	DQ165034	(Knowles et al., 2005)
O/HKN/6/2004	O/HKN/06/04	Hong Kong	-	02/03/2004	Porcine	DQ164883	(Knowles et al., 2005)
O/HKN/7/2004	O/HKN/07/04	Hong Kong	-	18/03/2004	Porcine	DQ164884	(Knowles et al., 2005)
O/HKN/0238/2004	O/HKN/0238/04	Hong Kong	-	01/06/2004	Porcine	JF968160	(Hui and Leung, 2012)
O/HKN/1738/2004	O/HKN/1738/04	Hong Kong	-	01/06/2004	Porcine	JF968161	(Hui and Leung, 2012)
O/HKN/2037/2004	O/HKN/2037/04	Hong Kong	-	01/06/2004	Porcine	JF968162	(Hui and Leung, 2012)
O/HKN/2038/2004	O/HKN/2038/04	Hong Kong	-	01/06/2004	Porcine	JF968163	(Hui and Leung, 2012)
O/HKN/2140/2004	O/HKN/2140/04	Hong Kong	-	01/06/2004	Porcine	JF968144	(Hui and Leung, 2012)
O/HKN/2228/2004	O/HKN/2228/04	Hong Kong	-	01/06/2004	Porcine	JF968164	(Hui and Leung, 2012)
O/HKN/2231/2004	O/HKN/2231/04	Hong Kong	-	01/06/2004	Porcine	JF968166	(Hui and Leung, 2012)
O/HKN/2235/2004	O/HKN/2235/04	Hong Kong	-	01/06/2004	Porcine	JF968165	(Hui and Leung, 2012)
O/HKN/2332/2004	O/HKN/2332/04	Hong Kong	-	01/06/2004	Porcine	JF968167	(Hui and Leung, 2012)
O/HKN/2822/2004	O/HKN/2822/04	Hong Kong	-	01/06/2004	Porcine	JF968169	(Hui and Leung, 2012)
O/HKN/2838/2004	O/HKN/2838/04	Hong Kong	-	01/06/2004	Porcine	JF968168	(Hui and Leung, 2012)
O/HKN/3039/2004	O/HKN/3039/04	Hong Kong	-	01/06/2004	Porcine	JF968170	(Hui and Leung, 2012)
O/HKN/S93/2004	O/HKN/S93/04	Hong Kong	-	01/07/2004	Porcine	JF968123	(Hui and Leung, 2012)
O/HKN/S95/2004	O/HKN/S95/04	Hong Kong	-	01/07/2004	Porcine	JF968124	(Hui and Leung, 2012)
O/HKN/S97/2004	O/HKN/S97/04	Hong Kong	-	01/07/2004	Porcine	JF968122	(Hui and Leung, 2012)
O/HKN/8/2004	O/HKN/08/04	Hong Kong	-	11/08/2004	Porcine	DQ164885	(Knowles et al., 2005)
O/HKN/9/2004	O/HKN/09/04	Hong Kong	-	11/08/2004	Porcine	DQ164886	(Knowles et al., 2005)
O/HKN/10/2004	O/HKN/10/04	Hong Kong	-	11/08/2004	Porcine	DQ164887	(Knowles et al., 2005)
O/HKN/11/2004	O/HKN/11/04	Hong Kong	-	11/08/2004	Porcine	DQ164888	(Knowles et al., 2005)
O/HKN/12/2004	O/HKN/12/04	Hong Kong	-	11/08/2004	Porcine	DQ164889	(Knowles et al., 2005)
O/HKN/13/2004	O/HKN/13/04	Hong Kong	-	21/12/2004	Porcine	KM243126	(Di Nardo et al., 2014)
O/HKN/P115/2005	O/HKN/P115/05	Hong Kong	-	01/01/2005	Porcine	JF968171	(Hui and Leung, 2012)
O/HKN/P125/2005	O/HKN/P125/05	Hong Kong	-	01/01/2005	Porcine	JF968172	(Hui and Leung, 2012)
O/VIT/1/2005	O/VIT/01/05	Vietnam	-	01/01/2005	Bovine	HQ116276	(Abdul-Hamid et al., 2011)
O/HKN/9/2005	O/HKN/09/05	Hong Kong	-	25/02/2005	Porcine	KM243129	(Di Nardo et al., 2014)
O/HKN/10/2005	O/HKN/10/05	Hong Kong	-	25/02/2005	Porcine	KM243130	(Di Nardo et al., 2014)
O/HKN/P179/2005	O/HKN/P179/05	Hong Kong	-	01/03/2005	Porcine	JF968173	(Hui and Leung, 2012)
O/HKN/12/2005	O/HKN/12/05	Hong Kong	-	11/03/2005	Porcine	KM243132	(Di Nardo et al., 2014)
O/HKN/14/2005	O/HKN/14/05	Hong Kong	-	14/03/2005	Porcine	KM243133	(Di Nardo et al., 2014)

O/HKN/15/2005	O/HKN/15/05	Hong Kong	-	14/03/2005	Porcine	KM243134	(Di Nardo et al., 2014)
O/HKN/P235/2005	O/HKN/P235/05	Hong Kong	-	01/05/2005	Porcine	JF968158	(Hui and Leung, 2012)
O/VIT/9/2005	O/VIT/09/05	Vietnam	Hai Duong	30/05/2005	Porcine	HQ116281	(Abdul-Hamid et al., 2011)
O/VIT/11/2005	O/VIT/11/05	Vietnam	Ha Giang	18/06/2005	Porcine	HQ116282	(Abdul-Hamid et al., 2011)
O/HKN/17/2005	O/HKN/17/05	Hong Kong	-	04/07/2005	Porcine	KM243135	(Di Nardo et al., 2014)
O/HKN/18/2005	O/HKN/18/05	Hong Kong	-	04/07/2005	Porcine	KM243136	(Di Nardo et al., 2014)
O/HKN/19/2005	O/HKN/19/05	Hong Kong	-	04/07/2005	Porcine	KM243137	(Di Nardo et al., 2014)
O/HKN/20/2005	O/HKN/20/05	Hong Kong	-	04/07/2005	Porcine	KM243138	(Di Nardo et al., 2014)
O/VIT/12/2005	O/VIT/12/05	Vietnam	Long An	28/07/2005	Porcine	KM243139	(Di Nardo et al., 2014)
O/HKN/22/2005	O/HKN/22/05	Hong Kong	-	15/11/2005	Porcine	KM243140	(Di Nardo et al., 2014)
O/HKN/23/2005	O/HKN/23/05	Hong Kong	-	15/11/2005	Porcine	KM243141	(Di Nardo et al., 2014)
O/HKN/24/2005	O/HKN/24/05	Hong Kong	-	21/11/2005	Porcine	KM243142	(Di Nardo et al., 2014)
O/HKN/25/2005	O/HKN/25/05	Hong Kong	-	21/11/2005	Porcine	KM243143	(Di Nardo et al., 2014)
O/TAI/5/2005	O/TAI/05/05	Thailand	-	26/11/2005	Porcine	HQ116235	(Abdul-Hamid et al., 2011)
O/TAI/6/2005	O/TAI/06/05	Thailand	-	27/11/2005	Porcine	HQ116236	(Abdul-Hamid et al., 2011)
O/HKN/P370/2005	O/HKN/P370/05	Hong Kong	-	01/12/2005	Porcine	JF968174	(Hui and Leung, 2012)
O/HKN/P371/2005	O/HKN/P371/05	Hong Kong	-	01/12/2005	Porcine	JF968175	(Hui and Leung, 2012)
O/HKN/P372/2005	O/HKN/P372/05	Hong Kong	-	01/12/2005	Porcine	JF968176	(Hui and Leung, 2012)
O/MAY/8/2005	O/MAY/08/05	Malaysia	Tanjong Sepat	02/12/2005	Porcine	HQ116202	(Abdul-Hamid et al., 2011)
O/VIT/1/2006	O/VIT/01/06	Vietnam	Long An	01/01/2006	Porcine	HQ116284	(Abdul-Hamid et al., 2011)
O/VIT/2/2006	O/VIT/02/06	Vietnam	Dong Thap	11/01/2006	Porcine	HQ116285	(Abdul-Hamid et al., 2011)
O/VIT/3/2006	O/VIT/03/06	Vietnam	Tien Giang	12/01/2006	Porcine	HQ116286	(Abdul-Hamid et al., 2011)
O/HKN/1/2006	O/HKN/01/06	Hong Kong	-	26/01/2006	Porcine	KM243144	(Di Nardo et al., 2014)
O/HKN/2/2006	O/HKN/02/06	Hong Kong	-	26/01/2006	Porcine	KM243145	(Di Nardo et al., 2014)
O/HKN/3/2006	O/HKN/03/06	Hong Kong	-	26/01/2006	Porcine	KM243146	(Di Nardo et al., 2014)
O/HKN/4/2006	O/HKN/04/06	Hong Kong	-	26/01/2006	Porcine	KM243147	(Di Nardo et al., 2014)
O/HKN/5/2006	O/HKN/05/06	Hong Kong	-	26/01/2006	Porcine	KM243148	(Di Nardo et al., 2014)
O/HKN/6/2006	O/HKN/06/06	Hong Kong	-	26/01/2006	Porcine	KM243149	(Di Nardo et al., 2014)
O/HKN/1/2007	O/HKN/01/07	Hong Kong	-	10/01/2007	Porcine	KM243150	(Di Nardo et al., 2014)
O/HKN/P389/2007	O/HKN/P389/07	Hong Kong	-	01/02/2007	Porcine	JF968177	(Hui and Leung, 2012)
O/HKN/P390/2007	O/HKN/P390/07	Hong Kong	-	01/02/2007	Porcine	JF968178	(Hui and Leung, 2012)
O/HKN/P391/2007	O/HKN/P391/07	Hong Kong	-	01/02/2007	Porcine	JF968179	(Hui and Leung, 2012)
O/HKN/P392/2007	O/HKN/P392/07	Hong Kong	-	01/02/2007	Porcine	JF968180	(Hui and Leung, 2012)
O/HKN/P393/2007	O/HKN/P393/07	Hong Kong	-	01/02/2007	Porcine	JF968181	(Hui and Leung, 2012)
O/HKN/2/2007	O/HKN/02/07	Hong Kong	-	23/03/2007	Porcine	KM243151	(Di Nardo et al., 2014)
O/HKN/3/2007	O/HKN/03/07	Hong Kong	-	25/10/2007	Porcine	KM243152	(Di Nardo et al., 2014)
O/HKN/4/2007	O/HKN/04/07	Hong Kong	-	25/10/2007	Porcine	KM243153	(Di Nardo et al., 2014)
O/VIT/1/2008	O/VIT/01/08	Vietnam	Ho Chi Minh	01/01/2008	Porcine	HQ116291	(Abdul-Hamid et al., 2011)
O/VIT/9/2008	O/VIT/09/08	Vietnam	Ho Chi Minh	04/02/2008	Porcine	KM243154	(Di Nardo et al., 2014)
O/HKN/1/2008	O/HKN/01/08	Hong Kong	-	10/11/2008	Porcine	KM243155	(Di Nardo et al., 2014)

O/HKN/2/2008	O/HKN/02/08	Hong Kong	-	10/11/2008	Porcine	KM243156	(Di Nardo et al., 2014)
O/HKN/3/2008	O/HKN/03/08	Hong Kong	-	10/11/2008	Porcine	KM243157	(Di Nardo et al., 2014)
O/HKN/4/2008	O/HKN/04/08	Hong Kong	-	10/11/2008	Porcine	KM243158	(Di Nardo et al., 2014)
O/HKN/P395/2008	O/HKN/P395/08	Hong Kong	-	01/12/2008	Porcine	JF968182	(Hui and Leung, 2012)
O/HKN/P397/2009	O/HKN/P397/09	Hong Kong	-	01/01/2009	Porcine	JF968183	(Hui and Leung, 2012)
O/HKN/P398/2009	O/HKN/P398/09	Hong Kong	-	01/01/2009	Porcine	JF968184	(Hui and Leung, 2012)
O/HKN/1/2009	O/HKN/01/09	Hong Kong	-	04/01/2009	Porcine	KM243159	(Di Nardo et al., 2014)
O/HKN/2/2009	O/HKN/02/09	Hong Kong	-	04/01/2009	Porcine	KM243160	(Di Nardo et al., 2014)
O/HKN/P399/2009	O/HKN/P399/09	Hong Kong	-	01/02/2009	Porcine	JF968185	(Hui and Leung, 2012)
O/TAW/1/2009	O/TAW/01/09	Taiwan	Mai-Liao	04/02/2009	Porcine	KM243161	(Di Nardo et al., 2014)
O-TW-257-2009	O/TAW/257/09	Taiwan	-	17/02/2009	Porcine	GQ292739	(Lin et al., 2010)
O-TW-258-2009	O/TAW/258/09	Taiwan	-	17/02/2009	Porcine	GQ292740	(Lin et al., 2010)
O/HKN/24/2010	O/HKN/24/10	Hong Kong	-	06/12/2010	Porcine	KM243162	(Di Nardo et al., 2014)
O/HKN/25/2010	O/HKN/25/10	Hong Kong	-	06/12/2010	Porcine	KM243163	(Di Nardo et al., 2014)
O/HKN/26/2010	O/HKN/26/10	Hong Kong	-	06/12/2010	Porcine	KM243164	(Di Nardo et al., 2014)
O/HKN/3/2011	O/HKN/03/11	Hong Kong	-	24/08/2011	Porcine	KM243165	(Di Nardo et al., 2014)
O/HKN/4/2011	O/HKN/04/11	Hong Kong	-	24/08/2011	Porcine	KM243166	(Di Nardo et al., 2014)
O/HKN/5/2011	O/HKN/05/11	Hong Kong	-	24/08/2011	Porcine	KM243167	(Di Nardo et al., 2014)
O/HKN/6/2011	O/HKN/06/11	Hong Kong	-	24/08/2011	Porcine	KM243168	(Di Nardo et al., 2014)
O/HKN/7/2011	O/HKN/07/11	Hong Kong	-	24/08/2011	Porcine	KM243169	(Di Nardo et al., 2014)
O/HKN/8/2011	O/HKN/08/11	Hong Kong	-	14/11/2011	Porcine	KM243170	(Di Nardo et al., 2014)
O/HKN/9/2011	O/HKN/09/11	Hong Kong	-	14/11/2011	Porcine	KM243171	(Di Nardo et al., 2014)
O/HKN/1/2013	O/HKN/01/13	Hong Kong	-	02/04/2013	Porcine	KM243172	(Di Nardo et al., 2014)

Appendix 3

Details of the full-genome sequences (n=39) processed from FMDV clinical samples collected during the UK 2001 FMD outbreak.

WRL No	IP No	Report Date	County	Location	Specie	GenBank No
UKG/11/2001	1	19/02/2001	Essex	Cheale Meats Abattoir	Porcine	DQ404180
UKG/126/2001	4	22/02/2001	Northumberland	Burnside Farm	Porcine	DQ404179
UKG/150/2001	6	23/02/2001	Northumberland	Prestwick Hall Farm	Bovine	DQ404176
UKG/173/2001	7	24/02/2001	Devon	Burdon Farm	Bovine	DQ404175
UKG/246/2001	14	25/02/2001	Durham	Sawmill Depot	Ovine	This study
UKG/220/2001	16	26/02/2001	Northamptonshire	Blunts Farm	Ovine	DQ404173
UKG/417/2001	27	28/02/2001	Cumbria	Smalmstown Farm	Bovine	FJ542365
UKG/621/2001	38	01/03/2001	Staffordshire	Hot Hill Farm	Bovine	DQ404172
UKG/1450/2001	104	08/03/2001	Cumbria	Drumburgh Castle	Bovine	FJ542366
UKG/1558/2001	133	09/03/2001	Cumbria	West End Farm	Bovine	FJ542367
UKG/1734/2001	191	10/03/2001	Cumbria	Bowness Hall	Bovine	FJ542368
UKG/2000/2001	201	12/03/2001	Cumbria	Northview Farm	Ovine	FJ542369
UKG/2085/2001	227	14/03/2001	Cumbria	Blackrigg Farm	Bovine	FJ542370
UKG/2526/2001	342	19/03/2001	Cumbria	Burnfoot	Bovine	FJ542371
UKG/2640/2001	348	19/03/2001	Cumbria	Old Sansfield Farm	Bovine	FJ542372
UKG/3952/2001	878	31/03/2001	Durham	Softley Farm	Ovine	EF552688
UKG/4014/2001	913	01/04/2001	Durham	Low Lands Farm	Bovine	EF552693
UKG/4141/2001	927	02/04/2001	Durham	Bucksfield Farm	Ovine	EF552689
UKG/4569/2001	1070	06/04/2001	Northumberland	Hexhamshire Common	Ovine	DQ404171
UKG/4998/2001	1182	10/04/2001	Durham	Paddock Mire Farm	Bovine	EF552694
UKG/5470/2001	1256	12/04/2001	Durham	High West Garth Farm	Bovine	EF552696
UKG/5681/2001	1378	13/04/2001	Durham	Cleatlam High Farm	Ovine	EF552697
UKG/7038/2001	1404	20/04/2001	Durham	No4 Middridges Farm	Ovine	DQ404169
UKG/7299/2001	1439	22/04/2001	Durham	Jubilee Wood Farm	Ovine	EF552692
UKG/7675/2001	1448	23/04/2001	Durham	East Farm	Ovine	DQ404170
UKG/8098/2001	1515	30/04/2001	Durham	Cliffe Bank Farm	Ovine	EU214601
UKG/9011/2001	1575	10/05/2001	North Yorkshire	Cowside Farm	Bovine	DQ404168
UKG/9161/2001	1583	11/05/2001	Durham	Keverstone Grange	Bovine	EF552691
UKG/9327/2001	1597	14/05/2001	Durham	Killerbay Hall Farm	Ovine	DQ404167
UKG/9443/2001	1619	17/05/2001	Durham	Burton House	Ovine	EF552695
UKG/9788/2001	1654	28/05/2001	Durham	The Grange	Bovine	DQ404166
UKG/9964/2001	1692	03/06/2001	Durham	New Moor Farm	Bovine	DQ404165
UKG/11676/2001	1757	17/06/2001	Somerset	Beardley Farm	Bovine	DQ404164
UKG/14339/2001	1945	11/08/2001	Powys	Rheld Farm	Bovine	DQ404163
UKG/14391/2001	1948	14/08/2001	Cumbria	Helton Head	Bovine	DQ404161
UKG/14476/2001	1956	16/08/2001	West Yorkshire	Chandlers Cote Farm	Ovine	DQ404162
UKG/14524/2001	1970	23/08/2001	Northumberland	Taylorburn	Bovine	DQ404160
UKG/14603/2001	1976	26/08/2001	Northumberland	The Hope	Bovine	DQ404159
UKG/15101/2001	2027	24/09/2001	Northumberland	Dukesfield Hall	Ovine	DQ404158

Appendix 4

Table A4-1. Epidemiological parameters estimated from the reconstructed transmission tree of the UK 2001 FMD epidemic according to the type of database used and the corresponding points in time of the control policies implemented.

Data	Parameter		Scenario	Average (95 PI)	Min-Max
2026 IPs	Number of Secondary Cases (R_t)		Full	0.99 (0 – 6)	0 – 27
			Before NMB	5.5 (0.1 – 18.5)	0 – 20
			After NMB	1.2 (0 – 7)	0 – 27
			After 24/48h IP/CP	0.8 (0 – 5)	0 – 20
	Generation Time (τ)		Full	7.2 (3 – 14)	0 – 20
			Before NMB	2.2 (0 – 4.9)	0 – 5
			After NMB	7.5 (3 – 14)	3 – 20
			After 24/48h IP/CP	6.9 (4 – 13)	3 – 19
	Transmission Distance		Full	27.6 (0.6 – 218.3)	0.1 – 543.2
			Before NMB	273.7 (1.5 – 464.7)	0.8 – 466.8
			After NMB	22.3 (0.4 – 172.2)	0.1 – 286.5
			After 24/48h IP/CP	30.5 (0.7 – 255.2)	0.1 – 473.9
	Time to cull interval		Full	9.1 (4 – 23)	5 – 16
			Before NMB	8.5 (6 – 11)	6.1 – 10.9
			After NMB	9.8 (5 – 23)	6 – 17
			After 24/48h IP/CP	8.8 (4 – 21)	5 – 16
	Incidence	I^{exp}	Full	8.9 (0 – 42)	0 – 52
			Before NMB	4.1 (0.3 – 8.7)	0 – 9
			After NMB	29.8 (12.1 – 51.1)	6 – 52
			After 24/48h IP/CP	5 (0 – 26)	0 – 27
		I^{les}	Full	8.7 (0 – 43.2)	0 – 47
			Before NMB	1.3 (0 – 3.7)	0 – 4
			After NMB	26.2 (5.9 – 47)	5 – 47
			After 24/48h IP/CP	5.8 (0 – 28.9)	0 – 47
		I^{rep}	Full	9 (0 – 42.4)	0 – 46
			Before NMB	1.5 (0.1 – 3.8)	0 – 4
			After NMB	23.3 (3.5 – 46)	0 – 46
			After 24/48h IP/CP	6.4 (0 – 34.5)	0 – 43
	Prevalence	P^{exp}	Full	88.3 (2 – 424.2)	1 – 442
			Before NMB	18.3 (3.3 – 46.5)	3 – 49
			After NMB	272.7 (63 – 437.6)	52 – 442
			After 24/48h IP/CP	56.9 (2 – 303)	1 – 384
		P^{les}	Full	46.2 (1 – 221)	0 – 230
			Before NMB	4.3 (1 – 12.2)	1 – 13
			After NMB	137.2 (22.9 – 229)	15 – 230
			After 24/48h IP/CP	31.2 (1 – 179.8)	0 – 217
		P^{rep}	Full	20.4 (0 – 114.2)	0 – 127
			Before NMB	0.4 (0 – 2)	0 – 2
			After NMB	68.8 (4 – 122.6)	4 – 127
			After 24/48h IP/CP	12.2 (0 – 76)	0 – 103
1616 IPs	Number of Secondary Cases (R_t)		Full	0.99 (0 – 6)	0 – 22
			Before NMB	5.5 (0.1 – 20.1)	0 – 22
			After NMB	1.2 (0 – 6)	0 – 15
			After 24/48h IP/CP	0.8 (0 – 5)	0 – 14
	Generation Time (τ)		Full	7.1 (4 – 13)	0 – 20
			Before NMB	1.8 (0 – 3.9)	0 – 4
			After NMB	7.5 (4 – 14)	3 – 20
			After 24/48h IP/CP	6.7 (3.8 – 13)	3 – 16
	Transmission Distance		Full	31.3 (0.6 – 255.2)	0.1 – 551.1
			Before NMB	363.3 (52 – 464.9)	8 – 466.8
			After NMB	20.8 (0.5 – 154.2)	0.1 – 271.6
			After 24/48h IP/CP	36 (0.7 – 302)	0.1 – 474.1
	Time to cull interval		Full	9 (4 – 22)	5 – 15.6
			Before NMB	9.5 (8 – 11)	8.1 – 10.9

			After NMB	9.7 (5 – 22)	6 – 16
			After 24/48h IP/CP	8.6 (4 – 21)	5 – 15
	Incidence	I^{exp}	Full	7.3 (0 – 31.5)	0 – 42
			Before NMB	4.1 (0.3 – 8.4)	0 – 9
			After NMB	23.2 (8 – 37.6)	8 – 42
			After 24/48h IP/CP	4.2 (0 – 16)	0 – 22
		I^{les}	Full	7.2 (0 – 31)	0 – 38
			Before NMB	1.2 (0 – 3)	0 – 3
			After NMB	20.9 (5 – 37.1)	5 – 38
			After 24/48h IP/CP	4.8 (0 – 21.2)	0 – 38
		I^{rep}	Full	7.4 (0 – 30)	0 – 41
			Before NMB	1.5 (0.1 – 3.8)	0 – 4
			After NMB	19.1 (3.5 – 38.4)	0 – 41
			After 24/48h IP/CP	5.2 (0 – 25)	0 – 30
	Prevalence	P^{exp}	Full	71.5 (3.6 – 323.3)	1 – 336
			Before NMB	17.5 (4 – 43.1)	4 – 45
			After NMB	217.2 (61 – 335.1)	52 – 336
			After 24/48h IP/CP	45.8 (3 – 211.7)	1 – 270
		P^{les}	Full	36.8 (1.6 – 167.1)	1 – 179
			Before NMB	4.3 (1 – 12.2)	1 – 13
			After NMB	109.1 (21.9 – 177)	14 – 179
			After 24/48h IP/CP	24.5 (2 – 125.1)	1 – 155
		P^{rep}	Full	16.6 (0 – 92)	0 – 100
			Before NMB	0.4 (0 – 2)	0 – 2
			After NMB	56 (4 – 99.1)	4 – 100
			After 24/48h IP/CP	9.7 (0 – 53.5)	0 – 73
1428 IPs	Number of Secondary Cases (R_t)		Full	0.99 (0 – 6)	0 – 19
			Before NMB	4.5 (0.1 – 17.1)	0 – 19
			After NMB	1.2 (0 – 6)	0 – 17
			After 24/48h IP/CP	0.8 (0 – 5)	0 – 13
	Generation Time (τ)		Full	7 (3 – 13)	0 – 23
			Before NMB	2.2 (0.1 – 4)	0 – 4
			After NMB	7.4 (4 – 13)	3 – 19
			After 24/48h IP/CP	6.7 (3 – 12.4)	2 – 16
	Transmission Distance		Full	32.3 (0.7 – 260.5)	0.1 – 551.1
			Before NMB	274.4 (2.7 – 464.9)	2.1 – 466.8
			After NMB	22.9 (0.6 – 154.1)	0.1 – 271.6
			After 24/48h IP/CP	36.8 (0.8 – 301.1)	0.2 – 469.6
	Time to cull interval		Full	8.9 (3 – 25)	5 – 15.3
			Before NMB	8.5 (7 – 10)	7.1 – 9.9
			After NMB	9.7 (4 – 25)	6 – 16
			After 24/48h IP/CP	8.4 (3 – 23)	5 – 15
	Incidence	I^{exp}	Full	6.5 (0 – 26.5)	0 – 31
			Before NMB	3.9 (0.3 – 9.7)	0 – 10
			After NMB	19.2 (5 – 29.2)	5 – 31
			After 24/48h IP/CP	4 (0 – 14.8)	0 – 17
		I^{les}	Full	6.3 (0 – 26)	0 – 32
			Before NMB	1.1 (0 – 2.7)	0 – 3
			After NMB	17.5 (5 – 30.2)	5 – 32
			After 24/48h IP/CP	4.4 (0 – 19)	0 – 28
		I^{rep}	Full	6.5 (0 – 26)	0 – 39
			Before NMB	1.5 (0.1 – 3.8)	0 – 4
			After NMB	16.4 (2.6 – 34.6)	0 – 39
			After 24/48h IP/CP	4.7 (0– 19.6)	0 – 24
	Prevalence	P^{exp}	Full	62.4 (3 – 263.7)	1 – 279
			Before NMB	15.2 (2.3 – 39.1)	2 – 41
			After NMB	181.8 (53.4 – 275)	49 – 279
			After 24/48h IP/CP	41.5 (3 – 158.9)	1 – 204
		P^{les}	Full	31.9 (1.6 – 140.3)	1 – 149
			Before NMB	4.2 (1 – 11.2)	1 – 12
			After NMB	91.9 (19.9 – 149)	12 – 149

		After 24/48h IP/CP	21.7 (2 – 90.9)	1 – 112
	P^{rep}	Full	14.7 (0 – 80)	0 – 88
		Before NMB	0.4 (0 – 2)	0 – 2
		After NMB	49.2 (4 – 88)	4 – 88
		After 24/48h IP/CP	8.8 (0 – 45.5)	0 – 60

Appendix 5

Table A5-1. Genetic parameters estimated from the simulated FMDV WGS data of the UK 2001 FMD epidemic according to the type of database used and the corresponding points in time of the control policies implemented.

Data	Parameter	Scenario	Average (95% PI)	Min-Max
2026 IPs	Nt Substitution/Transmission Link	Full	4.5 (0 – 21.4)	0 – 56
		Before NMB	6.2 (3.1– 13.1)	3 – 14
		After NMB	6.1 (0 – 31.7)	0 – 56
		After 24/48h IP/CP	3.3 (0 – 16.5)	0 – 31
	Evolutionary Duration (Δt)	Full	14.9 (10 – 24)	8 – 35
		Before NMB	11 (9.1 – 12)	9 – 12
		After NMB	14.9 (10 – 24)	8 – 35
		After 24/48h IP/CP	14.6 (10 – 23)	8 – 34
1616 IPs	Nt Substitution/Transmission Link	Full	1.4 (0 – 4)	0 – 7
		Before NMB	3.4 (2.1 – 4)	2 – 4
		After NMB	1.4 (0 – 4)	0 – 6
		After 24/48h IP/CP	1.3 (0 – 4)	0 – 7
	Evolutionary Duration (Δt)	Full	9.9 (6 – 18)	4 – 27
		Before NMB	19.4 (16 – 23.7)	16 – 24
		After NMB	9.5 (6 – 15.5)	4 – 21
		After 24/48h IP/CP	9.9 (5 – 18)	4 – 27
1428 IPs	Nt Substitution/Transmission Link	Full	4.1 (0 – 17)	0 – 36
		Before NMB	9.2 (3 – 14.9)	0 – 15
		After NMB	4.7 (0 – 20.8)	0 – 36
		After 24/48h IP/CP	3.7 (0 – 15)	0 – 22
	Evolutionary Duration (Δt)	Full	14.7 (10 – 23)	7 – 31
		Before NMB	11 (9.1 – 12)	9 – 12
		After NMB	14.7 (10 – 22)	7 – 26
		After 24/48h IP/CP	14.6 (10 – 23.5)	8 – 30

Appendix 6

A6.1 Scaled N_e formulation

A6.1.1 Epidemiological generation time τ

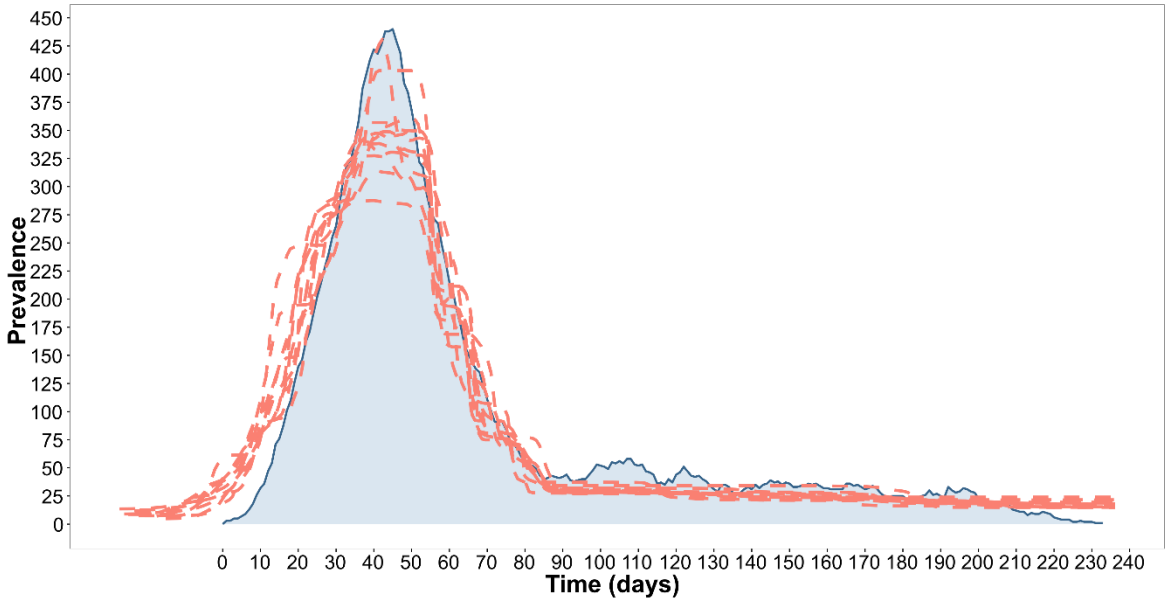

Figure A6-1. Scaled N_e estimated from 12 realisations of the UK 2001 FMDV simulated WGS data and reconstructed using the full IPs (n=2026) epidemic dataset. Epidemic curve was estimated from the P^{exp} (blue) prevalence data as defined in §3.2.2.2. Generation time is defined with the epidemiological τ formulation (§3.2.2.3).

Table A6-1. Overall and time specific number of infected cases (both incidence and prevalence) estimated under 12 realisations of the UK 2001 FMD full IPs (n=2026) epidemic dataset from the empirical epidemiological data and the scaled N_e recovered from the BSP analysis. Generation time is defined with the epidemiological τ formulation.

		Epidemic Phase				
		Overall	*Exponential*	*Peak*	*Decline*	*Plateau*
Generation Time	τ	7.16±0.07	7.59±0.12	-	6.48±0.09	7.18±0.09
Prevalence	P^{exp}	88.42±0.32	195.01±2.15	439.83±3.19	203.17±0.83	30.62±0.04
Effective Population Size	N_e	77.69±3.50	145.17±9.34	351.03±37.41	182.77±9.40	24.75±1.34

A6.1.2 Serial case interval τ_c

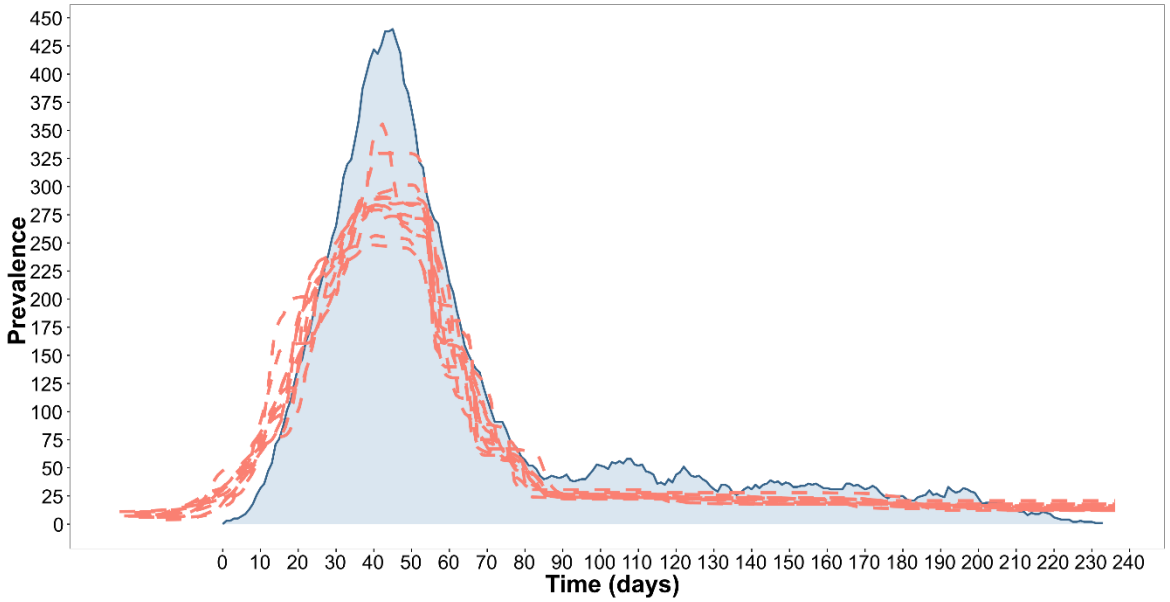

Figure A6-2. Scaled N_e estimated from 12 realisations of the UK 2001 FMDV simulated WGS data and reconstructed using the full IPs (n=2026) epidemic dataset. Epidemic curve was estimated from the P^{exp} (blue) prevalence data as defined in §3.2.2.2. Generation time is defined with the serial case interval τ_c formulation (§3.2.2.3).

Table A6-2. Overall and time specific number of infected cases (both incidence and prevalence) estimated under 12 realisations of the UK 2001 FMD full IPs (n=2026) epidemic dataset from the empirical epidemiological data and the scaled N_e recovered from the BSP analysis. Generation time is defined with the serial case interval τ_c formulation.

		Epidemic Phase				
		Overall	*Exponential*	*Peak*	*Decline*	*Plateau*
Serial Case Interval	τ_c	8.69±0.01	9.95±0.29	22.16±0.46	22.09±0.01	12.68±0.01
Prevalence	P^{exp}	88.42±0.32	195.01±2.15	439.83±3.19	203.17±0.83	30.62±0.04
Effective Population Size	N_e	64.47±2.16	120.45±6.26	291.22±28.72	151.69±6.44	20.54±1.08

A6.2 $var(R_t)$ scaling formulation

A6.2.1 Epidemiological generation time τ

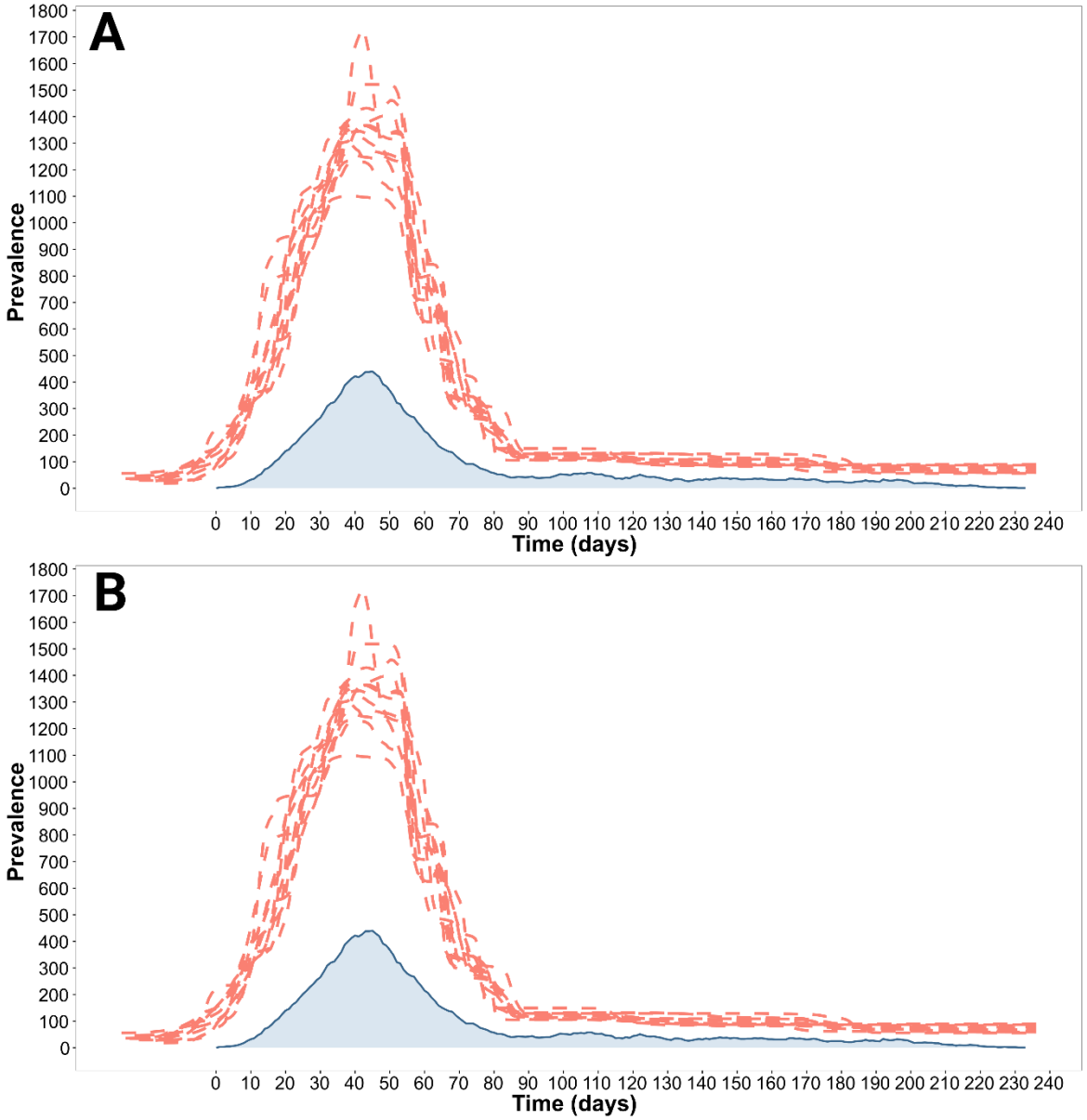

Figure A6-3. Infection prevalence N^* estimated from 12 realisations of the UK 2001 FMDV simulated WGS data and reconstructed using the full IPs (n=2026) epidemic dataset. The variance in the secondary cases per primary infection R_t was assumed a normal parameterisation of σ^2 (A) and using the Koelle and Rasmussen (2012) formulation (B) (§4.2.2.1). Generation time is defined with the epidemiological τ formulation (§3.2.2.3). Epidemic curve was estimated from the P^{exp} (blue) prevalence data as defined in §3.2.2.2.

Table A6-3. Overall and time specific number of infected cases (both incidence and prevalence) estimated under 12 realisations for the UK 2001 FMD full IPs (n=2026) epidemic dataset from the empirical epidemiological data and the scaled infection prevalence N^* estimated under the assumption of variance in R_t [σ^2 parameterisation (§4.2.2.1)]. Generation time is defined with the epidemiological τ formulation (§3.2.2.3).

		Epidemic Phase				
		Overall	*Exponential*	*Peak*	*Decline*	*Plateau*
Generation Time	τ	7.16±0.07	7.59±0.12	-	6.48±0.09	7.18±0.09
R_t Variance	σ^2	3.91±0.1	6.49±0.25	0.9±0.19	1.88±0.12	3.28±0.18
Prevalence	P^{exp}	88.42±0.32	195.01±2.15	439.83±3.19	203.17±0.83	30.62±0.04
Infection Prevalence	N^*	302.76±15.48	565.55±35.19	1368.77±157.52	712.17±37.69	96.44±5.87

Table A6-4. Overall and time specific number of infected cases (both incidence and prevalence) estimated under 12 realisations for the UK 2001 FMD full IPs (n=2026) epidemic dataset from the empirical epidemiological data and the scaled infection prevalence N^* estimated under the assumption of variance in R_t [Koelle and Rasmussen (2012) parameterisation (§4.2.2.1)]. Generation time is defined with the epidemiological τ formulation (§3.2.2.3).

		Epidemic Phase				
		Overall	*Exponential*	*Peak*	*Decline*	*Plateau*
Generation Time	τ	7.16±0.07	7.59±0.12	-	6.48±0.09	7.18±0.09
R_t Variance	$var(R_t)$	3.91±0.1	6.49±0.25	0.9±0.19	1.88±0.12	3.28±0.18
Prevalence	P^{exp}	88.42±0.32	195.01±2.15	439.83±3.19	203.17±0.83	30.62±0.04
Infection Prevalence	N^*	302.10±15.46	564.31±35.21	1365.73±157.14	710.59±37.56	96.24±5.86

A6.1.2 Serial case interval τ_c

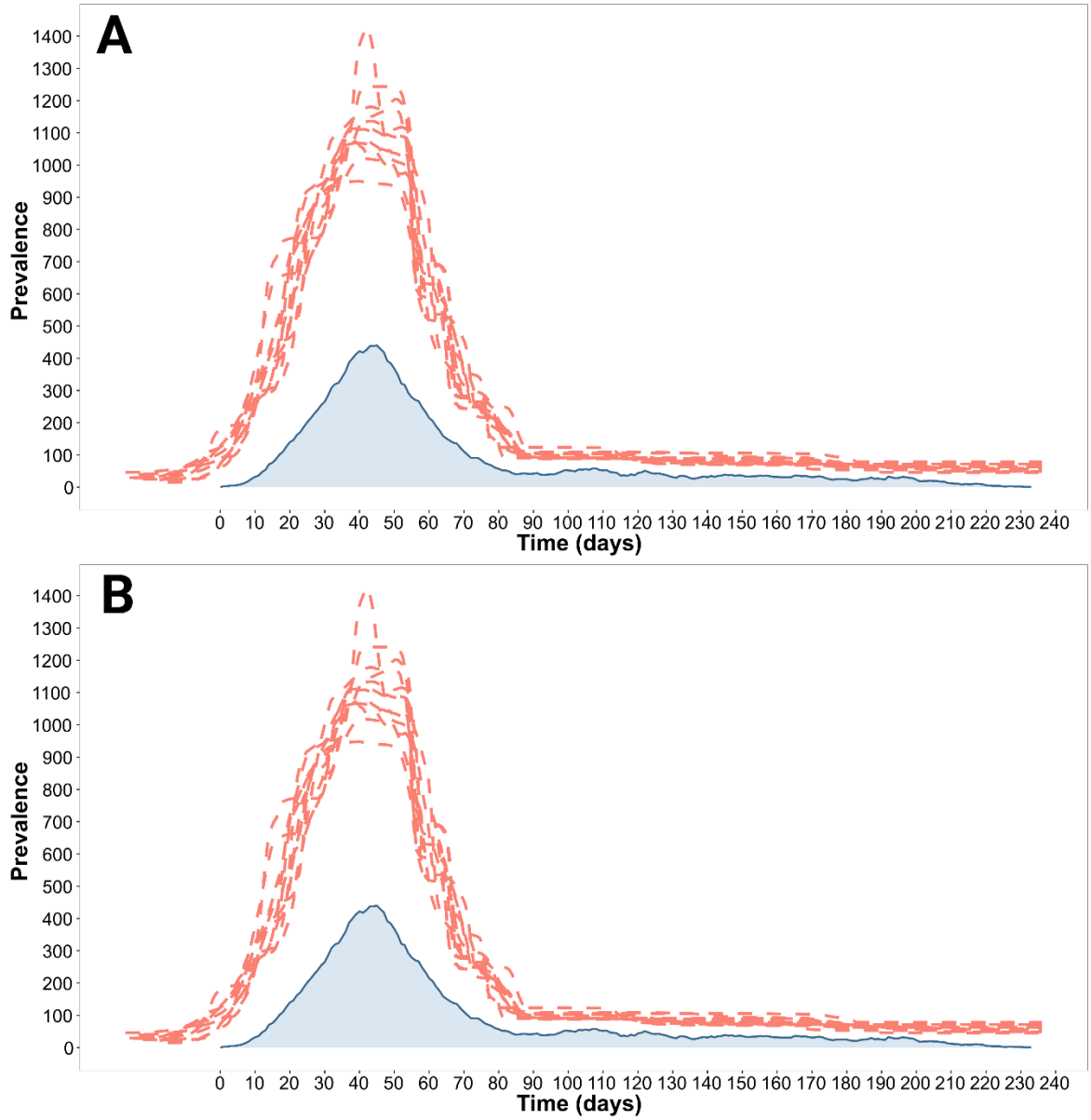

Figure A6-4. Infection prevalence N^* estimated from 12 realisations of the UK 2001 FMDV simulated WGS data and reconstructed using the full IPs (n=2026) epidemic dataset. The variance in the secondary cases per primary infection R_t was assumed a normal parameterisation of σ^2 (A) and using the Koelle and Rasmussen (2012) formulation (B) (§4.2.2.1). Generation time is defined with the serial case interval τ_c formulation (§3.2.2.3). Epidemic curve was estimated from the P^{exp} (blue) prevalence data as defined in §3.2.2.2.

Table A6-5. Overall and time specific number of infected cases (both incidence and prevalence) estimated under 12 realisations for the UK 2001 FMD full IPs (n=2026) epidemic dataset from the empirical epidemiological data and the scaled infection prevalence N^* estimated under the assumption of variance in R_t [σ^2 parameterisation (§4.2.2.1)]. Generation time is defined with the serial case interval τ_c formulation (§3.2.2.3).

		Epidemic Phase				
		Overall	*Exponential*	*Peak*	*Decline*	*Plateau*
Serial Case Interval	τ_c	8.69±0.01	9.95±0.29	22.16±0.46	22.09±0.01	12.68±0.01
Prevalence	P^{exp}	88.42±0.32	195.01±2.15	439.83±3.19	203.17±0.83	30.62±0.04
Infection Prevalence	N^*	251.18±9.44	469.08±22.00	1135.15±121.01	590.85±24.23	80.04±4.50

Table A6-5. Overall and time specific number of infected cases (both incidence and prevalence) estimated under 12 realisations for the UK 2001 FMD full IPs (n=2026) epidemic dataset from the empirical epidemiological data and the scaled infection prevalence N^* estimated under the assumption of variance in R_t [Koelle and Rasmussen (2012) parameterisation (§4.2.2.1)]. Generation time is defined with the serial case interval τ_c formulation (§3.2.2.3).

		Epidemic Phase				
		Overall	*Exponential*	*Peak*	*Decline*	*Plateau*
Serial Case Interval	τ_c	8.69±0.01	9.95±0.29	22.16±0.46	22.09±0.01	12.68±0.01
Prevalence	P^{exp}	88.42±0.32	195.01±2.15	439.83±3.19	203.17±0.83	30.62±0.04
Infection Prevalence	N^*	250.68±9.42	468.14±21.96	1132.88±120.76	589.67±24.18	79.88±4.49

A6.3 NLFT scaling formulation

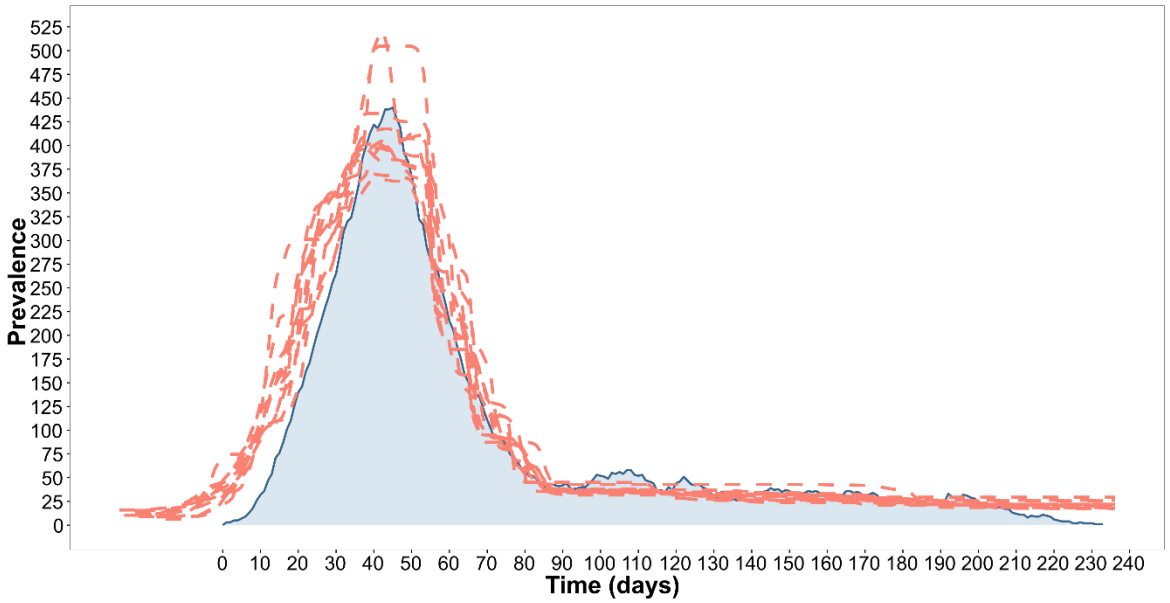

Figure A6-5. Infection prevalence N^* estimated from 12 realisations of the UK 2001 FMDV simulated WGS data and reconstructed using the full IPs (n=2026) epidemic dataset. Generation time is parameterised as the prevalence-to-incidence ratio τ_p (Frost and Volz, 2013) (§3.2.2.3, §4.2.2.2). Epidemic curve was estimated from the P^{exp} (blue) prevalence data as defined in §3.2.2.2.

Table A6-6. Overall and time specific number of infected cases estimated under 12 realisations for the UK 2001 FMD full IPs (n=2026) epidemic dataset from the empirical epidemiological data and the scaled infection prevalence N^* estimated by expressing the phylogenetic structure by NLFT. Generation time is defined with the prevalence-to-incidence ratio τ_p formulation (§3.2.2.3, §4.2.2.2).

		Epidemic Phase				
		Overall	*Exponential*	*Peak*	*Decline*	*Plateau*
Prevalence-to-Incidence Ratio	τ_p	12.15±0.40	7.81±1.15	11.85±2.71	15.33±0.97	12.82±0.52
Prevalence	P^{exp}	88.42±0.32	195.01±2.15	439.83±3.19	203.17±0.83	30.62±0.04
Infection Prevalence	N^*	92.87±5.14	173.53±12.55	419.61±47.58	218.50±13.66	29.58±1.92

Appendix 7

A7.1 Scaled N_e formulation

A7.1.1 Epidemiological generation time τ

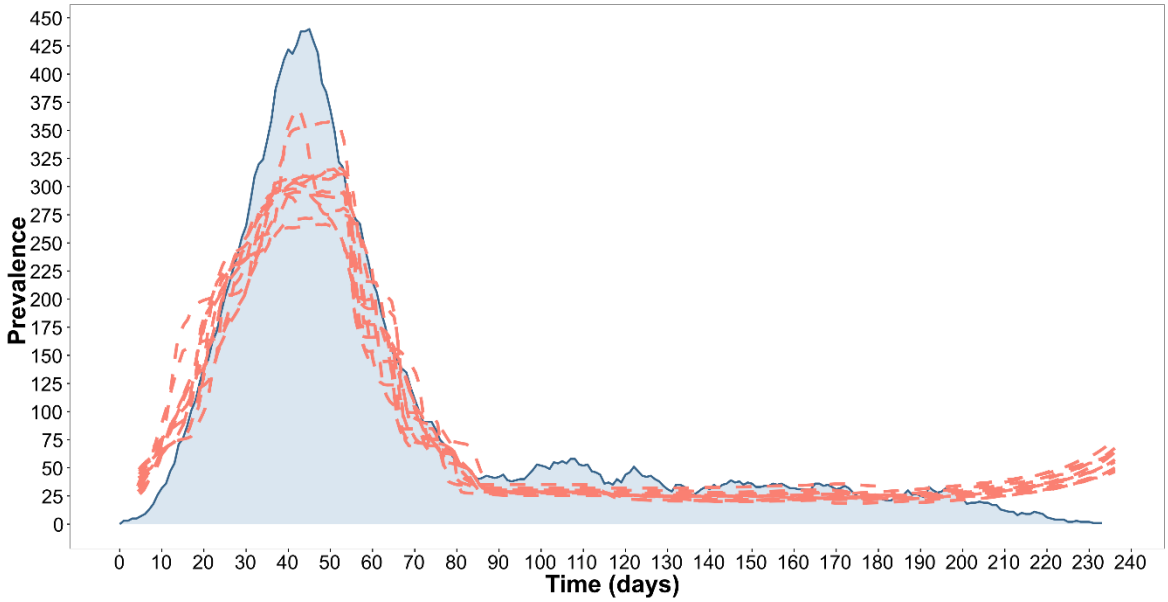

Figure A7-1. Scaled N_e estimated from 12 realisations of the UK 2001 FMDV simulated WGS data and reconstructed using the full IPs (n=2026) epidemic dataset. Epidemic curve was estimated from the P^{exp} (blue) prevalence data as defined in §3.2.2.2. Generation time is defined with the epidemiological τ formulation (§3.2.2.3).

Table A7-1. Overall and time specific number of infected cases estimated under 12 realisations of the UK 2001 FMD full IPs (n=2026) epidemic dataset from the empirical epidemiological data and the scaled N_e recovered from the BSP analysis. Generation time is defined with the epidemiological τ formulation.

		Epidemic Phase				
		Overall	*Exponential*	*Peak*	*Decline*	*Plateau*
Generation Time	τ	7.16±0.06	7.53±0.13	-	6.51±0.8	7.22±0.16
Prevalence	P^{exp}	88.42±0.32	195.01±2.15	439.83±3.19	203.17±0.83	30.62±0.04
Effective Population Size	N_e	78.92±2.68	188.91±9.70	309.98±29.78	166.68±7.46	29.60±1.59

A7.1.2 Serial case interval τ_c

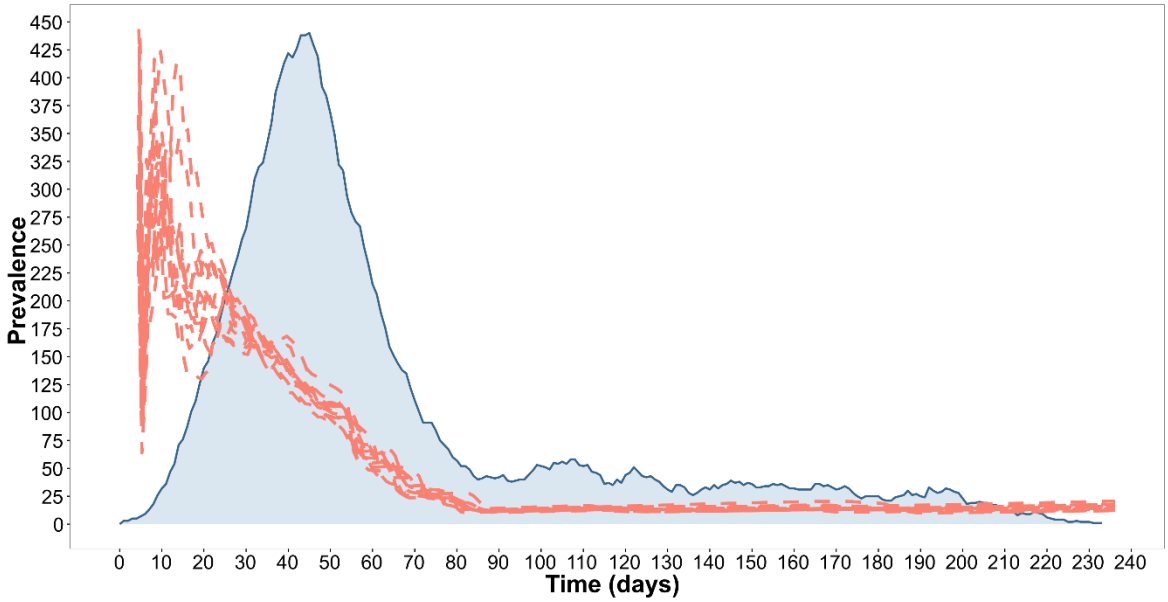

Figure A7-2. Scaled N_e estimated from 12 realisations of the UK 2001 FMDV simulated WGS data and reconstructed using the full IPs (n=2026) epidemic dataset. Epidemic curve was estimated from the P^{exp} (blue) prevalence data as defined in §3.2.2.2. Generation time is defined with the serial case intarval τ_c formulation (§3.2.2.3).

Table A7-2. Overall and time specific number of infected cases (both incidence and prevalence) estimated under 12 realisations of the UK 2001 FMD full IPs (n=2026) epidemic dataset from the empirical epidemiological data and the scaled N_e recovered from the BSP analysis. Generation time is defined with the serial case interval τ_c formulation.

		Epidemic Phase				
		Overall	*Exponential*	*Peak*	*Decline*	*Plateau*
Serial Case Interval	τ_c	5.91±0.1	7.57±0.11	5.91±0.1	6.93±0.07	5.35±0.67
Prevalence	P^{exp}	88.42±0.32	195.01±2.15	439.83±3.19	203.17±0.83	30.62±0.04
Effective Population Size	N_e	53.05±2.58	194.83±13.77	377.68±56.53	57.50±2.41	13.92±0.76

A7.2 $var(R_t)$ scaling formulation

A7.2.1 Epidemiological generation time τ

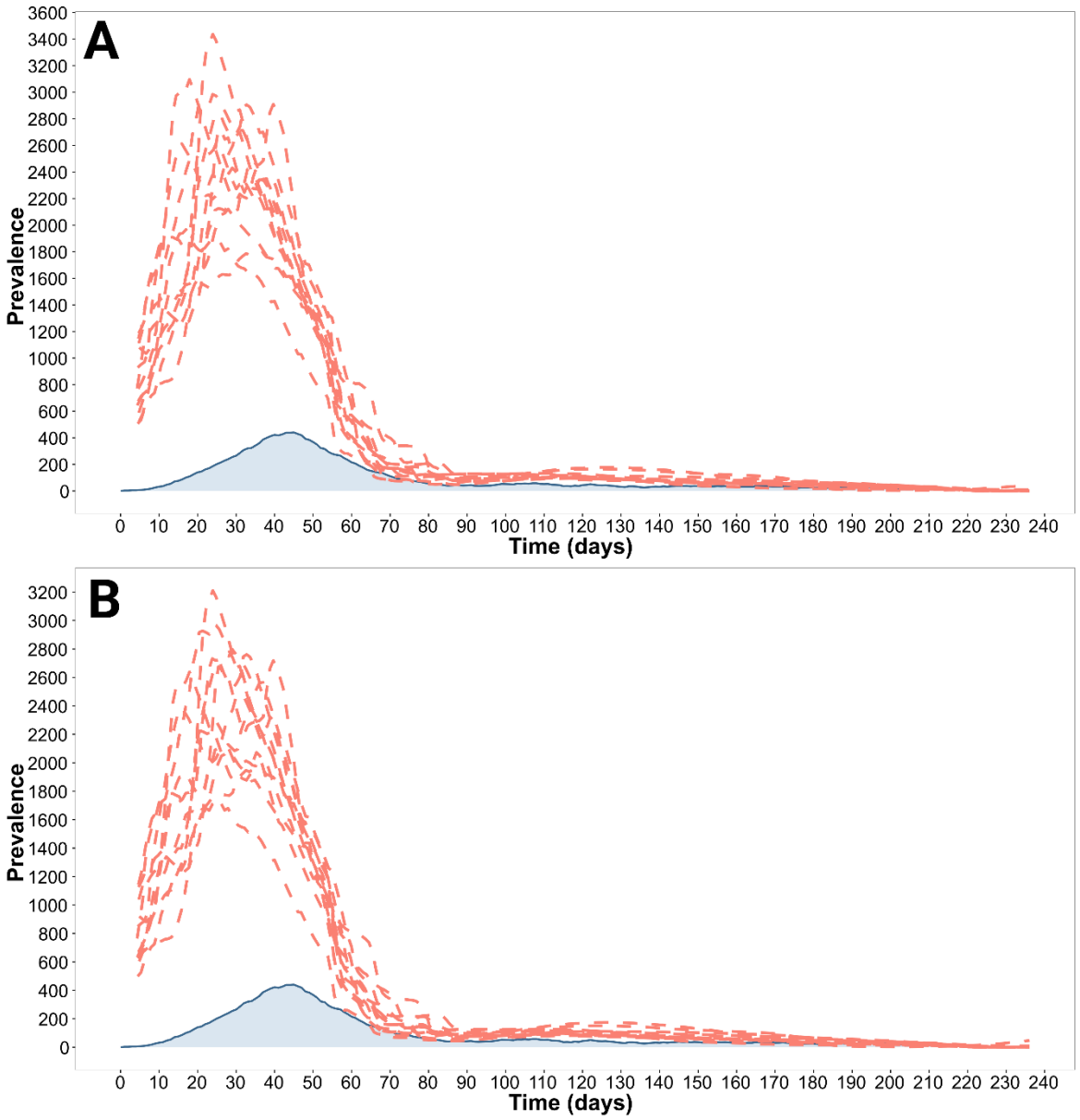

Figure A7-3. Infection prevalence N^* estimated from 12 realisations of the UK 2001 FMDV simulated WGS data and reconstructed using the full IPs (n=2026) epidemic dataset. The variance in the secondary cases per primary infection R_t was assumed a normal parameterisation of σ^2 (A) and using the Koelle and Rasmussen (2012) formulation (B) (§4.2.2.1). Generation time is defined with the epidemiological τ formulation (§3.2.2.3). Epidemic curve was estimated from the P^{exp} (blue) prevalence data as defined in §3.2.2.2.

Table A7-3. Overall and time specific number of infected cases (both incidence and prevalence) estimated under 12 realisations for the UK 2001 FMD full IPs (n=2026) epidemic dataset from the empirical epidemiological data and the scaled infection prevalence N^* estimated under the assumption of variance in R_t [σ^2 parameterisation (§4.2.2.1)]. Generation time is defined with the epidemiological τ formulation (§3.2.2.3).

		Epidemic Phase				
		Overall	*Exponential*	*Peak*	*Decline*	*Plateau*
Generation Time	τ	5.91±0.1	7.57±0.11	5.91±0.1	6.93±0.07	5.35±0.67
R_t Variance	σ^2	4.28±0.45	12.18±2.25	4.28±0.45	2.75±0.52	2.23±0.19
Prevalence	P^{exp}	88.42±0.32	195.01±2.15	439.83±3.19	203.17±0.83	30.62±0.04
Infection Prevalence	N^*	473.22±70.83	1909.05±342.34	2596.79±489.78	570.11±115.94	65.12±11.45

Table A7-4. Overall and time specific number of infected cases (both incidence and prevalence) estimated under 12 realisations for the UK 2001 FMD full IPs (n=2026) epidemic dataset from the empirical epidemiological data and the scaled infection prevalence N^* estimated under the assumption of variance in R_t [Koelle and Rasmussen (2012) parameterisation (§4.2.2.1)]. Generation time is defined with the epidemiological τ formulation (§3.2.2.3).

		Epidemic Phase				
		Overall	*Exponential*	*Peak*	*Decline*	*Plateau*
Generation Time	τ	7.16±0.06	7.53±0.13	-	6.51±0.08	7.22±0.16
R_t Variance	$var(R_t))$	3.91±0.1	6.49±0.25	0.9±0.19	1.88±0.12	3.28±0.18
Prevalence	P^{exp}	88.42±0.32	195.01±2.15	439.83±3.19	203.17±0.83	30.62±0.04
Infection Prevalence	N^*	457.15±64.73	1841.59±304.18	2502.47±427.95	553.17±120.88	63.10±11.60

A7.1.2 Serial case interval τ_c

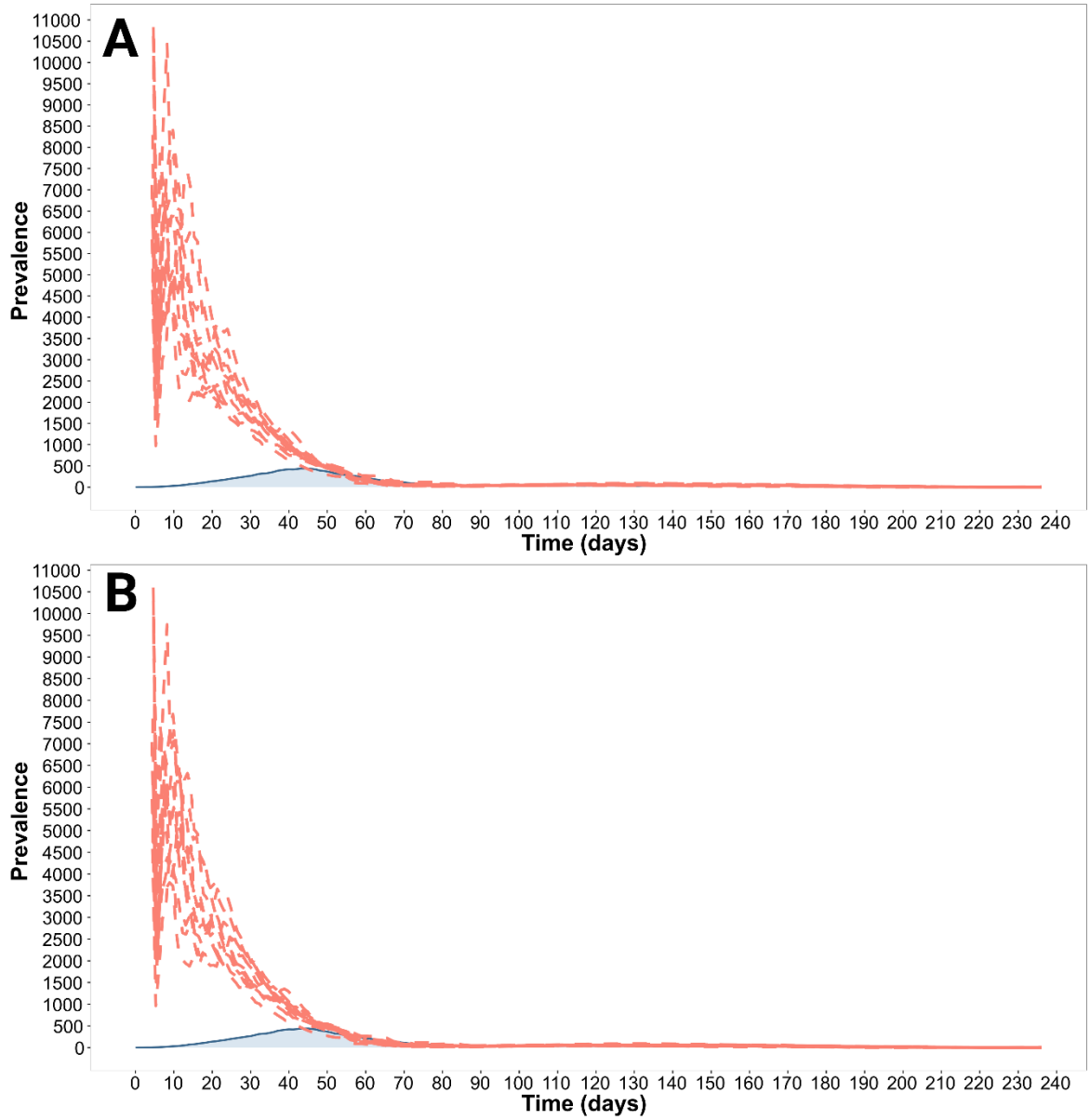

Figure A7-4. Infection prevalence N^* estimated from 12 realisations of the UK 2001 FMDV simulated WGS data and reconstructed using the full IPs (n=2026) epidemic dataset. The variance in the secondary cases per primary infection R_t was assumed a normal parameterisation of σ^2 (A) and using the Koelle and Rasmussen (2012) formulation (B) (§4.2.2.1). Generation time is defined with the serial case interval τ_c formulation (§3.2.2.3). Epidemic curve was estimated from the P^{exp} (blue) prevalence data as defined in §3.2.2.2.

Table A7-5. Overall and time specific number of infected cases (both incidence and prevalence) estimated under 12 realisations for the UK 2001 FMD full IPs (n=2026) epidemic dataset from the empirical epidemiological data and the scaled infection prevalence N^* estimated under the assumption of variance in R_t [σ^2 parameterisation (§4.2.2.1)]. Generation time is defined with the serial case interval τ_c formulation (§3.2.2.3).

		Epidemic Phase				
		Overall	*Exponential*	*Peak*	*Decline*	*Plateau*
Serial Case Interval	τ_c	5.91±0.1	7.57±0.11	5.91±0.1	6.93±0.07	5.35±0.67
Prevalence	P^{exp}	88.42±0.32	195.01±2.15	439.83±3.19	203.17±0.83	30.62±0.04
Infection Prevalence	N^*	525.52±102.25	2630.05±547.78	7709.00±2269.60	197.63±39.01	32.92±6.18

Table A7-6. Overall and time specific number of infected cases (both incidence and prevalence) estimated under 12 realisations for the UK 2001 FMD full IPs (n=2026) epidemic dataset from the empirical epidemiological data and the scaled infection prevalence N^* estimated under the assumption of variance in R_t [Koelle and Rasmussen (2012) parameterisation (§4.2.2.1)]. Generation time is defined with the serial case interval τ_c formulation (§3.2.2.3).

		Epidemic Phase				
		Overall	*Exponential*	*Peak*	*Decline*	*Plateau*
Serial Case Interval	τ_c	5.91±0.1	7.57±0.11	5.91±0.1	6.93±0.07	5.35±0.67
Prevalence	P^{exp}	88.42±0.32	195.01±2.15	439.83±3.19	203.17±0.83	30.62±0.04
Infection Prevalence	N^*	506.81±90.27	2534.95±482.26	7399.55±1999.10	191.84±41.39	31.91±6.26

A7.3 NLFT scaling formulation

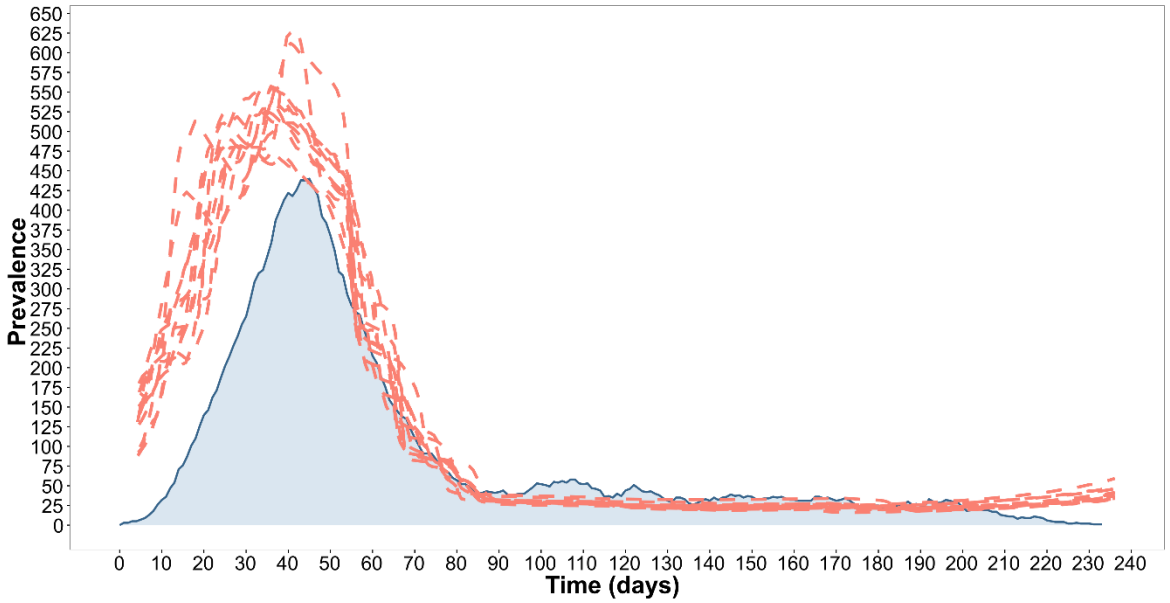

Figure A7-5. Infection prevalence N^* estimated from 12 realisations of the UK 2001 FMDV simulated WGS data and reconstructed using the full IPs (n=2026) epidemic dataset. Generation time is parameterised as the prevalence-to-incidence ratio τ_p (Frost and Volz, 2013) (§3.2.2.3, §4.2.2.2). Epidemic curve was estimated rom the P^{exp} (blue) prevalence data as defined in §3.2.2.2.

Table A7-7. Overall and time specific number of infected cases estimated under 12 realisations for the UK 2001 FMD full IPs (n=2026) epidemic dataset from the empirical epidemiological data and the scaled infection prevalence N^* estimated by expressing the phylogenetic structure by NLFT. Generation time is defined with the prevalence-to-incidence ratio τ_p formulation (§3.2.2.3, §4.2.2.2).

		Epidemic Phase				
		Overall	*Exponential*	*Peak*	*Decline*	*Plateau*
Prevalence-to-Incidence Ratio	τ_p	11.63±0.21	8.07±0.21	11.64±0.21	11.71±0.4	12.7±0.26
Prevalence	P^{exp}	88.42±0.32	195.01±2.15	439.83±3.19	203.17±0.83	30.62±0.04
Infection Prevalence	N^*	124.38±5.42	394.48±24.14	543.42±43.98	233.20±16.51	27.27±1.93

REFERENCES

ABAO, L. N., KONO, H., GUNARATHNE, A., PROMENTILLA, R. R. & GAERLAN, M. Z. 2014. Impact of foot-and-mouth disease on pork and chicken prices in Central Luzon, Philippines. *Prev Vet Med,* 113**,** 398-406.

ABDUL-HAMID, N. F., HUSSEIN, N. M., WADSWORTH, J., RADFORD, A. D., KNOWLES, N. J. & KING, D. P. 2011. Phylogeography of foot-and-mouth disease virus types O and A in Malaysia and surrounding countries. *Infect Genet Evol,* 11**,** 320-8.

AHMED, H. A., SALEM, S. A., HABASHI, A. R., ARAFA, A. A., AGGOUR, M. G., SALEM, G. H., GABER, A. S., SELEM, O., ABDELKADER, S. H., KNOWLES, N. J., MADI, M., VALDAZO-GONZALEZ, B., WADSWORTH, J., HUTCHINGS, G. H., MIOULET, V., HAMMOND, J. M. & KING, D. P. 2012. Emergence of foot-and-mouth disease virus SAT 2 in Egypt during 2012. *Transbound Emerg Dis,* 59**,** 476-81.

ALEXANDERSEN, S., ZHANG, Z., DONALDSON, A. I. & GARLAND, A. J. 2003. The pathogenesis and diagnosis of foot-and-mouth disease. *J Comp Pathol,* 129**,** 1-36.

AMARAL, A. R., BEHEREGARAY, L. B., BILGMANN, K., FREITAS, L., ROBERTSON, K. M., SEQUEIRA, M., STOCKIN, K. A., COELHO, M. M. & MOLLER, L. M. 2012. Influences of past climatic changes on historical population structure and demography of a cosmopolitan marine predator, the common dolphin (genus Delphinus). *Mol Ecol,* 21**,** 4854-71.

ANSELL, D. M., SAMUEL, A. R., CARPENTER, W. C. & KNOWLES, N. J. 1994. Genetic relationships between foot-and-mouth disease type Asia 1 viruses. *Epidemiol Infect,* 112**,** 213-24.

ATKINSON, Q. D., GRAY, R. D. & DRUMMOND, A. J. 2009. Bayesian coalescent inference of major human mitochondrial DNA haplogroup expansions in Africa. *Proc Biol Sci,* 276**,** 367-73.

BALINDA, S. N., SANGULA, A. K., HELLER, R., MUWANIKA, V. B., BELSHAM, G. J., MASEMBE, C. & SIEGISMUND, H. R. 2010a. Diversity and transboundary mobility of serotype O foot-and-mouth disease virus in East Africa: Implications for vaccination policies. *Infection Genetics and Evolution,* 10**,** 1058-1065.

BALINDA, S. N., SIEGISMUND, H. R., MUWANIKA, V. B., SANGULA, A. K., MASEMBE, C., AYEBAZIBWE, C., NORMANN, P. & BELSHAM, G. J. 2010b. Phylogenetic analyses of the polyprotein coding sequences of serotype O foot-and-mouth disease viruses in East Africa: evidence for interserotypic recombination. *Virol J,* 7**,** 199.

BARTON, N. H., DEPAULIS, F. & ETHERIDGE, A. M. 2002. Neutral evolution in spatially continuous populations. *Theor Popul Biol,* 61**,** 31-48.

BASTOS, A. D., HAYDON, D. T., FORSBERG, R., KNOWLES, N. J., ANDERSON, E. C., BENGIS, R. G., NEL, L. H. & THOMSON, G. R. 2001. Genetic heterogeneity of SAT-1 type foot-and-mouth disease viruses in southern Africa. *Arch Virol,* 146**,** 1537-51.

BASTOS, A. D., HAYDON, D. T., SANGARE, O., BOSHOFF, C. I., EDRICH, J. L. & THOMSON, G. R. 2003. The implications of virus diversity within the SAT 2 serotype for control of foot-and-mouth disease in sub-Saharan Africa. *J Gen Virol,* 84**,** 1595-606.

BATAILLE, A., VAN DER MEER, F., STEGEMAN, A. & KOCH, G. 2011. Evolutionary analysis of inter-farm transmission dynamics in a highly pathogenic avian influenza epidemic. *PLoS Pathog,* 7**,** e1002094.

BATISTA, G. E. A. P. A., KEOGH, E. J., TATAW, O. M. & DE SOUZA, V. M. A. 2014. CID: an efficient complexity-invariant distance for time series. *Data Mining and Knowledge Discovery,* 28**,** 634-669.

BEARD, C. W. & MASON, P. W. 2000. Genetic determinants of altered virulence of Taiwanese foot-and-mouth disease virus. *J Virol,* 74**,** 987-91.

BEDFORD, T., COBEY, S. & PASCUAL, M. 2011. Strength and tempo of selection revealed in viral gene genealogies. *BMC Evol Biol,* 11**,** 220.

BENNETT, S. N., DRUMMOND, A. J., KAPAN, D. D., SUCHARD, M. A., MUNOZ-JORDAN, J. L., PYBUS, O. G., HOLMES, E. C. & GUBLER, D. J. 2010. Epidemic dynamics revealed in dengue evolution. *Mol Biol Evol,* 27**,** 811-8.

BENSON, D. A., CAVANAUGH, M., CLARK, K., KARSCH-MIZRACHI, I., LIPMAN, D. J., OSTELL, J. & SAYERS, E. W. 2013. GenBank. *Nucleic Acids Res,* 41**,** D36-42.

BIEK, R., HENDERSON, J. C., WALLER, L. A., RUPPRECHT, C. E. & REAL, L. A. 2007. A high-resolution genetic signature of demographic and spatial expansion in epizootic rabies virus. *Proc Natl Acad Sci U S A,* 104**,** 7993-8.

BIENVENU, F. & LEGENDRE, S. 2015. A new approach to the generation time in matrix population models. *Am Nat,* 185**,** 834-43.

BOSKOVA, V., BONHOEFFER, S. & STADLER, T. 2014. Inference of epidemiological dynamics based on simulated phylogenies using birth-death and coalescent models. *PLoS Comput Biol,* 10**,** e1003913.

BOUCKAERT, R., HELED, J., KUHNERT, D., VAUGHAN, T., WU, C. H., XIE, D., SUCHARD, M. A., RAMBAUT, A. & DRUMMOND, A. J. 2014. BEAST 2: a software platform for Bayesian evolutionary analysis. *PLoS Comput Biol,* 10**,** e1003537.

CAO, Y. M., LU, Z. J., LI, D., FAN, P. J., SUN, P., BAO, H. F., FU, Y. F., LI, P. H., BAI, X. W., CHEN, Y. L., XIE, B. X. & LIU, Z. X. 2014. Evaluation of cross-protection against three topotypes of serotype O foot-and-mouth disease virus in pigs vaccinated with multi-epitope protein vaccine incorporated with poly(I:C). *Veterinary Microbiology,* 168**,** 294-301.

CARRILLO, C., LU, Z., BORCA, M. V., VAGNOZZI, A., KUTISH, G. F. & ROCK, D. L. 2007. Genetic and phenotypic variation of foot-and-mouth disease virus during serial passages in a natural host. *J Virol,* 81**,** 11341-51.

CARRILLO, C., TULMAN, E. R., DELHON, G., LU, Z., CARRENO, A., VAGNOZZI, A., KUTISH, G. F. & ROCK, D. L. 2005. Comparative genomics of foot-and-mouth disease virus. *J Virol,* 79**,** 6487-504.

CARRINGTON, C. V., FOSTER, J. E., PYBUS, O. G., BENNETT, S. N. & HOLMES, E. C. 2005. Invasion and maintenance of dengue virus type 2 and type 4 in the Americas. *J Virol,* 79**,** 14680-7.

CHARLESTON, B., BANKOWSKI, B. M., GUBBINS, S., CHASE-TOPPING, M. E., SCHLEY, D., HOWEY, R., BARNETT, P. V., GIBSON, D., JULEFF, N. D. & WOOLHOUSE, M. E. 2011. Relationship between clinical signs and transmission of an infectious disease and the implications for control. *Science,* 332**,** 726-9.

CHARLESWORTH, B. 2009. Effective population size and patterns of molecular evolution and variation. *Nat Rev Genet,* 10**,** 195-205.

CHENG, I. C., LIANG, S. M., TU, W. J., CHEN, C. M., LAI, S. Y., CHENG, Y. C., LEE, F., HUANG, T. S. & JONG, M. H. 2006. Study on the porcinophilic foot-and-mouth disease virus I. production and characterization of monoclonal antibodies against VP1. *J Vet Med Sci,* 68**,** 859-64.

CHIKHI, L., SOUSA, V. C., LUISI, P., GOOSSENS, B. & BEAUMONT, M. A. 2010. The confounding effects of population structure, genetic diversity and the sampling scheme on the detection and quantification of population size changes. *Genetics,* 186**,** 983-95.

CHIS STER, I. & FERGUSON, N. M. 2007. Transmission parameters of the 2001 foot and mouth epidemic in Great Britain. *PLoS One,* 2**,** e502.

CHIS STER, I., SINGH, B. K. & FERGUSON, N. M. 2009. Epidemiological inference for partially observed epidemics: the example of the 2001 foot and mouth epidemic in Great Britain. *Epidemics,* 1**,** 21-34.

CHITRAY, M., DE BEER, T. A., VOSLOO, W. & MAREE, F. F. 2014. Genetic heterogeneity in the leader and P1-coding regions of foot-and-mouth disease virus serotypes A and O in Africa. *Arch Virol,* 159**,** 947-61.

CHRISTENSEN, L. S., NORMANN, P., THYKIER-NIELSEN, S., SORENSEN, J. H., DE STRICKER, K. & ROSENORN, S. 2005. Analysis of the epidemiological dynamics during the 1982-1983 epidemic of foot-and-mouth disease in Denmark based on molecular high-resolution strain identification. *J Gen Virol,* 86**,** 2577-84.

CLEMENT, M., POSADA, D. & CRANDALL, K. A. 2000. TCS: a computer program to estimate gene genealogies. *Mol Ecol,* 9**,** 1657-9.

COCHRAN, W. G. 1977. *Sampling techniques,* New York, John Wiley & Sons, Inc.

COMAS, I., COSCOLLA, M., LUO, T., BORRELL, S., HOLT, K. E., KATO-MAEDA, M., PARKHILL, J., MALLA, B., BERG, S., THWAITES, G., YEBOAH-MANU, D., BOTHAMLEY, G., MEI, J., WEI, L., BENTLEY, S., HARRIS, S. R., NIEMANN, S., DIEL, R., ASEFFA, A., GAO, Q., YOUNG, D. & GAGNEUX, S. 2013. Out-of-Africa migration and Neolithic coexpansion of Mycobacterium tuberculosis with modern humans. *Nat Genet,* 45**,** 1176-82.

COTTAM, E. M., HAYDON, D. T., PATON, D. J., GLOSTER, J., WILESMITH, J. W., FERRIS, N. P., HUTCHINGS, G. H. & KING, D. P. 2006. Molecular epidemiology of the foot-and-mouth disease virus outbreak in the United Kingdom in 2001. *J Virol,* 80**,** 11274-82.

COTTAM, E. M., THEBAUD, G., WADSWORTH, J., GLOSTER, J., MANSLEY, L., PATON, D. J., KING, D. P. & HAYDON, D. T. 2008a. Integrating genetic and epidemiological data to determine transmission pathways of foot-and-mouth disease virus. *Proc Biol Sci,* 275**,** 887-95.

COTTAM, E. M., WADSWORTH, J., SHAW, A. E., ROWLANDS, R. J., GOATLEY, L., MAAN, S., MAAN, N. S., MERTENS, P. P., EBERT, K., LI, Y., RYAN, E. D., JULEFF, N., FERRIS, N. P., WILESMITH, J. W., HAYDON, D. T., KING, D. P., PATON, D. J. & KNOWLES, N. J. 2008b. Transmission pathways of foot-and-mouth disease virus in the United Kingdom in 2007. *PLoS Pathog,* 4**,** e1000050.

DARRIBA, D., TABOADA, G. L., DOALLO, R. & POSADA, D. 2012. jModelTest 2: more models, new heuristics and parallel computing. *Nat Methods,* 9**,** 772.

DE BRUYN, M., HALL, B. L., CHAUKE, L. F., BARONI, C., KOCH, P. L. & HOELZEL, A. R. 2009. Rapid response of a marine mammal species to holocene climate and habitat change. *PLoS Genet,* 5**,** e1000554.

DE CARVALHO, L. M., SANTOS, L. B., FARIA, N. R. & DE CASTRO SILVEIRA, W. 2013. Phylogeography of foot-and-mouth disease virus serotype O in Ecuador. *Infect Genet Evol,* 13**,** 76-88.

DE KOEIJER, A. A., BOENDER, G. J., NODELIJK, G., STAUBACH, C., MEROC, E. & ELBERS, A. R. 2011. Quantitative analysis of transmission parameters for bluetongue virus serotype 8 in Western Europe in 2006. *Vet Res,* 42**,** 53.

DE SILVA, E., FERGUSON, N. M. & FRASER, C. 2012. Inferring pandemic growth rates from sequence data. *J R Soc Interface,* 9**,** 1797-808.

DEFRA 2002. Origins of the UK foot-and-mouth disease epidemic in 2001. London: Department for Environment, Food & Rural Affairs.

DI NARDO, A., KNOWLES, N. J. & PATON, D. J. 2011. Combining livestock trade patterns with phylogenetics to help understand the spread of foot and mouth disease in sub-Saharan Africa, the Middle East and Southeast Asia. *Rev Sci Tech,* 30**,** 63-85.

DI NARDO, A., KNOWLES, N. J., WADSWORTH, J., HAYDON, D. T. & KING, D. P. 2014. Phylodynamic reconstruction of O CATHAY topotype foot-and-mouth disease virus epidemics in the Philippines. *Veterinary Research,* 45**,** 90.

DIDELOT, X., GARDY, J. & COLIJN, C. 2014. Bayesian inference of infectious disease transmission from whole-genome sequence data. *Mol Biol Evol,* 31**,** 1869-79.

DOMINGO, E., ESCARMIS, C., BARANOWSKI, E., RUIZ-JARABO, C. M., CARRILLO, E., NUNEZ, J. I. & SOBRINO, F. 2003. Evolution of foot-and-mouth disease virus. *Virus Res,* 91**,** 47-63.

DOMINGO, E., GONZALEZ-LOPEZ, C., PARIENTE, N., AIRAKSINEN, A. & ESCARMIS, C. 2005. Population dynamics of RNA viruses: the essential contribution of mutant spectra. *Arch Virol Suppl***,** 59-71.

DONALDSON, A., LEE, R., WARD, N. & WILKINSON, K. 2006. Foot and mouth - five years on: the legacy of the 2001 foot and mouth disease crisis for farming and the British countryside *Center for Rural Economy Discussion Paper Series No 6.* Newcastle upon Tyne: University of Newcastle upon Tyne.

DONNELLY, P. & TAVARE, S. 1995. Coalescents and genealogical structure under neutrality. *Annu Rev Genet,* 29**,** 401-21.

DRAKE, J. W. 1993. Rates of spontaneous mutation among RNA viruses. *Proc Natl Acad Sci U S A,* 90**,** 4171-5.

DRUMMOND, A. J., HO, S. Y., PHILLIPS, M. J. & RAMBAUT, A. 2006. Relaxed phylogenetics and dating with confidence. *PLoS Biol,* 4**,** e88.

DRUMMOND, A. J., NICHOLLS, G. K., RODRIGO, A. G. & SOLOMON, W. 2002. Estimating mutation parameters, population history and genealogy simultaneously from temporally spaced sequence data. *Genetics,* 161**,** 1307-20.

DRUMMOND, A. J., PYBUS, O. G., RAMBAUT, A., FORSBERG, R. & RODRIGO, A. G. 2003. Measurably evolving populations. *Trends Ecol Evol,* 18**,** 481-88.

DRUMMOND, A. J. & RAMBAUT, A. 2007. BEAST: Bayesian evolutionary analysis by sampling trees. *BMC Evol Biol,* 7**,** 214.

DRUMMOND, A. J., RAMBAUT, A., SHAPIRO, B. & PYBUS, O. G. 2005. Bayesian coalescent inference of past population dynamics from molecular sequences. *Mol Biol Evol,* 22**,** 1185-92.

DRUMMOND, A. J. & SUCHARD, M. A. 2010. Bayesian random local clocks, or one rate to rule them all. *BMC Biol,* 8**,** 114.

DRUMMOND, A. J., SUCHARD, M. A., XIE, D. & RAMBAUT, A. 2012. Bayesian phylogenetics with BEAUti and the BEAST 1.7. *Mol Biol Evol,* 29**,** 1969-73.

DUFFY, S., SHACKELTON, L. A. & HOLMES, E. C. 2008. Rates of evolutionary change in viruses: patterns and determinants. *Nat Rev Genet,* 9**,** 267-76.

EL-SHEHAWY, L. I., ABU-ELNAGA, H. I., RIZK, S. A., ABD EL-KREEM, A. S., MOHAMED, A. A. & FAWZY, H. G. 2014. Molecular differentiation and phylogenetic analysis of the Egyptian foot-and-mouth disease virus SAT2. *Arch Virol,* 159**,** 437-43.

FAO 2011. *World livestock 2011 - livestock in food security,* Rome, Italy, Food and Agriculture Organization of the United Nations.

FELSENSTEIN, J. 1971. Inbreeding and variance effective numbers in populations with overlapping generations. *Genetics,* 68**,** 581-97.

FELSENSTEIN, J. 2004. *Inferring phylogenies,* Sunderland, Mass., Sinauer Associates.

FENG, Q., YU, H., LIU, Y., HE, C., HU, J., SANG, H., DING, N., DING, M., FUNG, Y. W., LAU, L. T., YU, A. C. & CHEN, J. 2004. Genome comparison of a novel foot-and-mouth disease virus with other FMDV strains. *Biochem Biophys Res Commun,* 323**,** 254-63.

FERRIS, N. P., KING, D. P., REID, S. M., SHAW, A. E. & HUTCHINGS, G. H. 2006. Comparisons of original laboratory results and retrospective analysis by real-time reverse transcriptase-PCR of virological samples collected from confirmed cases of foot-and-mouth disease in the UK in 2001. *Vet Rec,* 159**,** 373-8.

FINE, P. E. M. 2003. The interval between successive cases of an infectious disease. *American Journal of Epidemiology,* 158**,** 1039-1047.

FINLAY, E. K., GAILLARD, C., VAHIDI, S. M., MIRHOSEINI, S. Z., JIANLIN, H., QI, X. B., EL-BARODY, M. A., BAIRD, J. F., HEALY, B. C. & BRADLEY, D. G. 2007. Bayesian inference of population expansions in domestic bovines. *Biol Lett,* 3**,** 449-52.

FISHER, R. A. S. 1930. *The genetical theory of natural selection,* Oxford, Clarendon Press.

FORMAN, S., LE GALL, F., BELTON, D., EVANS, B., FRANCOIS, J. L., MURRAY, G., SHEESLEY, D., VANDERSMISSEN, A. & YOSHIMURA, S. 2009. Moving towards the global control of foot and mouth disease: an opportunity for donors. *Rev Sci Tech,* 28**,** 883-96.

FORSS, S., STREBEL, K., BECK, E. & SCHALLER, H. 1984. Nucleotide sequence and genome organization of foot-and-mouth disease virus. *Nucleic Acids Res,* 12**,** 6587-601.

FROST, S. D. & VOLZ, E. M. 2010. Viral phylodynamics and the search for an 'effective number of infections'. *Philos Trans R Soc Lond B Biol Sci,* 365**,** 1879-90.

FROST, S. D. & VOLZ, E. M. 2013. Modelling tree shape and structure in viral phylodynamics. *Philos Trans R Soc Lond B Biol Sci,* 368**,** 20120208.

FU, Y. X. 2006. Exact coalescent for the Wright-Fisher model. *Theor Popul Biol,* 69**,** 385-94.

GARSKE, T. & RHODES, C. J. 2008. The effect of superspreading on epidemic outbreak size distributions. *J Theor Biol,* 253**,** 228-37.

GIBBENS, J. C., SHARPE, C. E., WILESMITH, J. W., MANSLEY, L. M., MICHALOPOULOU, E., RYAN, J. B. & HUDSON, M. 2001. Descriptive epidemiology of the 2001 foot-and-mouth disease epidemic in Great Britain: the first five months. *Vet Rec,* 149**,** 729-43.

GIGNOUX, C. R., HENN, B. M. & MOUNTAIN, J. L. 2011. Rapid, global demographic expansions after the origins of agriculture. *Proc Natl Acad Sci U S A,* 108**,** 6044-9.

GILL, M. S., LEMEY, P., FARIA, N. R., RAMBAUT, A., SHAPIRO, B. & SUCHARD, M. A. 2013. Improving Bayesian population dynamics inference: a coalescent-based model for multiple loci. *Mol Biol Evol,* 30**,** 713-24.

GLEESON, L. J. 2002. A review of the status of foot and mouth disease in South-East Asia and approaches to control and eradication. *Rev Sci Tech,* 21**,** 465-75.

GLOSTER, J., CHAMPION, H. J., MANSLEY, L. M., ROMERO, P., BROUGH, T. & RAMIREZ, A. 2005. The 2001 epidemic of foot-and-mouth disease in the United Kingdom: epidemiological and meteorological case studies. *Vet Rec,* 156**,** 793-803.

GLOSTER, J., CHAMPION, H. J., SORENSEN, J. H., MIKKELSEN, T., RYALL, D. B., ASTRUP, P., ALEXANDERSEN, S. & DONALDSON, A. I. 2003. Airborne transmission of foot-and-mouth disease virus from Burnside Farm, Heddon-on-the-Wall, Northumberland, during the 2001 epidemic in the United Kingdom. *Vet Rec,* 152**,** 525-33.

GORDO, I. & CAMPOS, P. R. 2007. Patterns of genetic variation in populations of infectious agents. *BMC Evol Biol,* 7**,** 116.

GRAY, R. R., PYBUS, O. G. & SALEMI, M. 2011. Measuring the Temporal Structure in Serially-Sampled Phylogenies. *Methods Ecol Evol,* 2**,** 437-445.

GRENFELL, B. T., PYBUS, O. G., GOG, J. R., WOOD, J. L., DALY, J. M., MUMFORD, J. A. & HOLMES, E. C. 2004. Unifying the epidemiological and evolutionary dynamics of pathogens. *Science,* 303**,** 327-32.

GRIFFITHS, R. C. & TAVARE, S. 1994a. Ancestral inference in population genetics. *Statistical Science,* 9**,** 307-319.

GRIFFITHS, R. C. & TAVARE, S. 1994b. Sampling theory for neutral alleles in a varying environment. *Philos Trans R Soc Lond B Biol Sci,* 344**,** 403-10.

GRUBMAN, M. J. & BAXT, B. 2004. Foot-and-mouth disease. *Clin Microbiol Rev,* 17**,** 465-93.

GUILLOT, E. G., TUMONGGOR, M. K., LANSING, S. J., SUDOYO, H. & COX, M. P. 2013. Climate change influenced fenale population sizes through time across the Indonesian Archipelago. *Human Biology,* 85**,** 135-152.

GUINDON, S., DUFAYARD, J. F., LEFORT, V., ANISIMOVA, M., HORDIJK, W. & GASCUEL, O. 2010. New algorithms and methods to estimate maximum-likelihood phylogenies: assessing the performance of PhyML 3.0. *Syst Biol,* 59**,** 307-21.

GUINDON, S. & GASCUEL, O. 2003. A simple, fast, and accurate algorithm to estimate large phylogenies by maximum likelihood. *Syst Biol,* 52**,** 696-704.

HALL, M. & RAMBAUT, A. 2014. Epidemic reconstruction in a phylogenetics framework: transmission trees as partitions. *ArXiv e-prints,* 1406.0428.

HALL, M. D., KNOWLES, N. J., WADSWORTH, J., RAMBAUT, A. & WOOLHOUSE, M. E. 2013. Reconstructing geographical movements and host species transitions of foot-and-mouth disease virus serotype SAT 2. *mBio,* 4**,** e00591-13.

HARRELL, F. E. 2001. *Regression modeling strategies: with applications to linear models, logistic regression, and survival analysis,* London, Springer.

HASEGAWA, M., KISHINO, H. & YANO, T. 1985. Dating of the human-ape splitting by a molecular clock of mitochondrial DNA. *J Mol Evol,* 22**,** 160-74.

HAYDON, D. T., BASTOS, A. D. & AWADALLA, P. 2004. Low linkage disequilibrium indicative of recombination in foot-and-mouth disease virus gene sequence alignments. *J Gen Virol,* 85**,** 1095-100.

HAYDON, D. T., CHASE-TOPPING, M., SHAW, D. J., MATTHEWS, L., FRIAR, J. K., WILESMITH, J. & WOOLHOUSE, M. E. 2003. The construction and analysis of epidemic trees with reference to the 2001 UK foot-and-mouth outbreak. *Philos Trans R Soc Lond B Biol Sci,* 270**,** 121-7.

HAYDON, D. T., SAMUEL, A. R. & KNOWLES, N. J. 2001. The generation and persistence of genetic variation in foot-and-mouth disease virus. *Prev Vet Med,* 51**,** 111-24.

HAYDON, D. T., WOOLHOUSE, M. E. & KITCHING, R. P. 1997. An analysis of foot-and-mouth-disease epidemics in the UK. *IMA J Math Appl Med Biol,* 14**,** 1-9.

HEATH, L., VAN DER WALT, E., VARSANI, A. & MARTIN, D. P. 2006. Recombination patterns in aphthoviruses mirror those found in other picornaviruses. *J Virol,* 80**,** 11827-32.

HELED, J. & DRUMMOND, A. J. 2008. Bayesian inference of population size history from multiple loci. *BMC Evol Biol,* 8**,** 289.

HEMADRI, D., TOSH, C., SANYAL, A. & VENKATARAMANAN, R. 2002. Emergence of a new strain of type O foot-and-mouth disease virus: Its phylogenetic and evolutionary relationship with the PanAsia pandemic strain. *Virus Genes,* 25**,** 23-34.

HICKS, A. L. & DUFFY, S. 2011. Genus-specific substitution rate variability among picornaviruses. *J Virol,* 85**,** 7942-7.

HO, S. Y. & SHAPIRO, B. 2011. Skyline-plot methods for estimating demographic history from nucleotide sequences. *Mol Ecol Resour,* 11**,** 423-34.

HOLLATZ, C., VILACA, S. T., REDONDO, R. A. F., MARMONTEL, M., BAKER, C. S. & SANTOS, F. R. 2011. The Amazon River system as an ecological barrier driving genetic differentiation of the pink dolphin (Inia geoffrensis). *Biol J Linn Soc,* 102**,** 812-27.

HUI, R. K. & LEUNG, F. C. 2012. Evolutionary trend of foot-and-mouth disease virus in Hong Kong. *Vet Microbiol,* 159**,** 221-9.

HYNDMAN, R. J. & KOEHLER, A. B. 2006. Another look at measures of forecast accuracy. *International Journal of Forecasting,* 22**,** 679-688.

JACKSON, A. L., O'NEILL, H., MAREE, F., BLIGNAUT, B., CARRILLO, C., RODRIGUEZ, L. & HAYDON, D. T. 2007. Mosaic structure of foot-and-mouth disease virus genomes. *J Gen Virol,* 88**,** 487-92.

JACKSON, T., KING, A. M., STUART, D. I. & FRY, E. 2003. Structure and receptor binding. *Virus Res,* 91**,** 33-46.

JAMAL, S. M., FERRARI, G., AHMED, S., NORMANN, P. & BELSHAM, G. J. 2011a. Genetic diversity of foot-and-mouth disease virus serotype O in Pakistan and Afghanistan, 1997-2009. *Infection Genetics and Evolution,* 11**,** 1229-1238.

JAMAL, S. M., FERRARI, G., AHMED, S., NORMANN, P. & BELSHAM, G. J. 2011b. Molecular characterization of serotype Asia-1 foot-and-mouth disease viruses in Pakistan and Afghanistan; emergence of a new genetic Group and evidence for a novel recombinant virus. *Infect Genet Evol,* 11**,** 2049-62.

JAMAL, S. M., FERRARI, G., AHMED, S., NORMANN, P., CURRY, S. & BELSHAM, G. J. 2011c. Evolutionary analysis of serotype A foot-and-mouth disease viruses circulating in Pakistan and Afghanistan during 2002-2009. *Journal of General Virology,* 92**,** 2849-2864.

JENKINS, G. M., RAMBAUT, A., PYBUS, O. G. & HOLMES, E. C. 2002. Rates of molecular evolution in RNA viruses: a quantitative phylogenetic analysis. *J Mol Evol,* 54**,** 156-65.

JOMBART, T., CORI, A., DIDELOT, X., CAUCHEMEZ, S., FRASER, C. & FERGUSON, N. 2014. Bayesian reconstruction of disease outbreaks by combining epidemiologic and genomic data. *PLoS Comput Biol,* 10**,** e1003457.

JOMBART, T., EGGO, R. M., DODD, P. J. & BALLOUX, F. 2011. Reconstructing disease outbreaks from genetic data: a graph approach. *Heredity (Edinb),* 106**,** 383-90.

JULEFF, N., VALDAZO-GONZÁLEZ, B., WADSWORTH, J., WRIGHT, C. F., CHARLESTON, B., PATON, D. J., KING, D. P. & KNOWLES, N. J. 2013. Accumulation of nucleotide

substitutions occurring during experimental transmission of foot-and-mouth disease virus. *J Gen Virol,* 94**,** 108-19.

KAJ, I. & KRONE, S. M. 2003. The coalescent process in a population with stochastically varying size. *J Appl Prob,* 40**,** 33-48.

KAO, R. R. 2002. The role of mathematical modelling in the control of the 2001 FMD epidemic in the UK. *Trends Microbiol,* 10**,** 279-86.

KAO, R. R., HAYDON, D. T., LYCETT, S. J. & MURCIA, P. R. 2014. Supersize me: how whole-genome sequencing and big data are transforming epidemiology. *Trends Microbiol,* 22**,** 282-91.

KEELING, M. 2005. The implications of network structure for epidemic dynamics. *Theor Popul Biol,* 67**,** 1-8.

KEELING, M. J. & ROHANI, P. 2008. *Modeling infectious diseases in humans and animals,* Princeton, N.J. ; Woodstock, Princeton University Press.

KEELING, M. J., WOOLHOUSE, M. E., MAY, R. M., DAVIES, G. & GRENFELL, B. T. 2003. Modelling vaccination strategies against foot-and-mouth disease. *Nature,* 421**,** 136-42.

KENAH, E., LIPSITCH, M. & ROBINS, J. M. 2008. Generation interval contraction and epidemic data analysis. *Math Biosci,* 213**,** 71-9.

KIMURA, M. & CROW, J. F. 1963. The measurement of effective population number. *Evolution,* 17**,** 279-288.

KINGMAN, J. F. 1982a. The coalescent. *Stochast Proc Appl,* 13**,** 235-48.

KINGMAN, J. F. 1982b. On the genealogy of large population. *J Appl Prob,* 19A**,** 27-43.

KITCHING, R. P. 2002. Clinical variation in foot and mouth disease: cattle. *Rev Sci Tech,* 21**,** 499-504.

KITCHING, R. P. & ALEXANDERSEN, S. 2002. Clinical variation in foot and mouth disease: pigs. *Rev Sci Tech,* 21**,** 513-8.

KITCHING, R. P. & HUGHES, G. J. 2002. Clinical variation in foot and mouth disease: sheep and goats. *Rev Sci Tech,* 21**,** 505-12.

KLEIN, J., HUSSAIN, M., AHMAD, M., NORMANN, P., AFZAL, M. & ALEXANDERSEN, S. 2007. Genetic characterisation of the recent foot-and-mouth disease virus subtype A/IRN/2005. *Virol J,* 4**,** 122.

KLEIN, J., PARLAK, U., OZYORUK, F. & CHRISTENSEN, L. S. 2006. The molecular epidemiology of foot-and-mouth disease virus serotypes A and O from 1998 to 2004 in Turkey. *BMC Vet Res,* 2**,** 35.

KNOWLES, N. J., BACHANEK-BANKOWSKA, K. & WADSWORTH, J. 2015. WRLFMD/2015/00007 Genotyping Report - Sultanate of Oman. World Reference Laboratory for Foot-and-Mouth Disease.

KNOWLES, N. J., DAVIES, P. R., HENRY, T., O'DONNELL, V., PACHECO, J. M. & MASON, P. W. 2001a. Emergence in Asia of foot-and-mouth disease viruses with altered host range: characterization of alterations in the 3A protein. *J Virol,* 75**,** 1551-6.

KNOWLES, N. J., HE, J., SHANG, Y., WADSWORTH, J., VALDAZO-GONZÁLEZ, B., ONOSATO, H., FUKAI, K., MORIOKA, K., YOSHIDA, K., CHO, I. S., KIM, S. M., PARK, J. H., LEE, K. N., LUK, G., BORISOV, V., SCHERBAKOV, A., TIMINA, A., BOLD, D., NGUYEN, T., PATON, D. J., HAMMOND, J. M., LIU, X. & KING, D. P. 2012. Southeast Asian foot-and-mouth disease viruses in Eastern Asia. *Emerg Infect Dis,* 18**,** 499-501.

KNOWLES, N. J., HOVI, T., HYYPIÄ, T., KING, A. M. Q., LINDBERG, A. M., PALLANSCH, M. A., PALMENBERG, A. C., SIMMONDS, P., SKERN, T., STANWAY, G., YAMASHITA, T. & ZELL, R. 2011. Picornaviridae. *In:* KING, A. M. Q., LEFKOWITZ, E. J., ADAMS, M. J. & CARSTENS, E. B. (eds.) *Virus Taxonomy. Classification and Nomenclature of Viruses: Ninth Report of the International Committee on Taxonomy of Viruses.* San Diego: Elsevier.

KNOWLES, N. J., NAZEM SHIRAZI, M. H., WADSWORTH, J., SWABEY, K. G., STIRLING, J. M., STATHAM, R. J., LI, Y., HUTCHINGS, G. H., FERRIS, N. P., PARLAK, U., OZYORUK, F., SUMPTION, K. J., KING, D. P. & PATON, D. J. 2009. Recent spread of a new strain (A-Iran-05) of foot-and-mouth disease virus type A in the Middle East. *Transbound Emerg Dis,* 56**,** 157-69.

KNOWLES, N. J. & SAMUEL, A. R. 2003. Molecular epidemiology of foot-and-mouth disease virus. *Virus Res,* 91**,** 65-80.

KNOWLES, N. J., SAMUEL, A. R., DAVIES, P. R., KITCHING, R. P. & DONALDSON, A. I. 2001b. Outbreak of foot-and-mouth disease virus serotype O in the UK caused by a pandemic strain. *Vet Rec,* 148**,** 258-9.

KNOWLES, N. J., SAMUEL, A. R., DAVIES, P. R., MIDGLEY, R. J. & VALARCHER, J. F. 2005. Pandemic strain of foot-and-mouth disease virus serotype O. *Emerg Infect Dis,* 11**,** 1887-93.

KNOWLES, N. J., WADSWORTH, J., HAMMOND, J. M. & KING, D. P. 2010. Foot-and-mouth disease virus geontype definitions and nomenclature. Open Session of the

European Commission for the Control of Foot-and-Mouth Disease Standing Technical Committee, 28 September - 1 October 2010a Vienna, Austria.

KNOWLES, N. J., WADSWORTH, J., PARLAK, U., OZYORUK, F., NAZEM SHIRAZI, M. H., FERRIS, N. P., HUTCHINGS, G. H., STIRLING, J. M., HAMMOND, J. M. & KING, D. P. Recent events in the evolution of foot-and-mouth disease in the Middle East. Open Session of the European Commission for the Control of Foot-and-Mouth Disease Standing Technical Committee, 28 September - 1 October 2010b Vienna.

KOBLMULLER, S., WAYNE, R. K. & LEONARD, J. A. 2012. Impact of Quaternary climatic changes and interspecific competition on the demographic history of a highly mobile generalist carnivore, the coyote. *Biol Lett,* 8**,** 644-7.

KOELLE, K. & RASMUSSEN, D. A. 2012. Rates of coalescence for common epidemiological models at equilibrium. *J R Soc Interface,* 9**,** 997-1007.

KONIG, G. A., COTTAM, E. M., UPADHYAYA, S., GLOSTER, J., MANSLEY, L. M., HAYDON, D. T. & KING, D. P. 2009. Sequence data and evidence of possible airborne spread in the 2001 foot-and-mouth disease epidemic in the UK. *Vet Rec,* 165**,** 410-1.

KONIG, G. A., PALMA, E. L., MARADEI, E. & PICCONE, M. E. 2007. Molecular epidemiology of foot-and-mouth disease virus types A and O isolated in Argentina during the 2000-2002 epizootic. *Vet Microbiol,* 124**,** 1-15.

KOUYOS, R. D., ALTHAUS, C. L. & BONHOEFFER, S. 2006. Stochastic or deterministic: what is the effective population size of HIV-1? *Trends Microbiol,* 14**,** 507-11.

KUHNER, M. K. 2006. LAMARC 2.0: maximum likelihood and Bayesian estimation of population parameters. *Bioinformatics,* 22**,** 768-70.

KUHNERT, D., STADLER, T., VAUGHAN, T. G. & DRUMMOND, A. J. 2014. Simultaneous reconstruction of evolutionary history and epidemiological dynamics from viral sequences with the birth-death SIR model. *J R Soc Interface,* 11**,** 20131106.

KUHNERT, D., WU, C. H. & DRUMMOND, A. J. 2011. Phylogenetic and epidemic modeling of rapidly evolving infectious diseases. *Infect Genet Evol,* 11**,** 1825-41.

LAW, G. R., FELTBOWER, R. G., TAYLOR, J. C., PARSLOW, R. C., GILTHORPE, M. S., BOYLE, P. & MCKINNEY, P. A. 2008. What do epidemiologists mean by 'population mixing'? *Pediatr Blood Cancer,* 51**,** 155-60.

LEE, K. N., OEM, J. K., PARK, J. H., KIM, S. M., LEE, S. Y., TSERENDORJ, S., SODNOMDARJAA, R., JOO, Y. S. & KIM, H. 2009. Evidence of recombination in a

new isolate of foot-and-mouth disease virus serotype Asia 1. *Virus Res,* 139**,** 117-21.

LEMEY, P., RAMBAUT, A., DRUMMOND, A. J. & SUCHARD, M. A. 2009a. Bayesian phylogeography finds its roots. *PLoS Comput Biol,* 5**,** e1000520.

LEMEY, P., RAMBAUT, A., WELCH, J. J. & SUCHARD, M. A. 2010. Phylogeography takes a relaxed random walk in continuous space and time. *Mol Biol Evol,* 27**,** 1877-85.

LEMEY, P., SUCHARD, M. & RAMBAUT, A. 2009b. Reconstructing the initial global spread of a human influenza pandemic: A Bayesian spatial-temporal model for the global spread of H1N1pdm. *PLoS Curr,* 1**,** RRN1031.

LEVENTHAL, G. E., KOUYOS, R., STADLER, T., WYL, V., YERLY, S., BONI, J., CELLERAI, C., KLIMKAIT, T., GUNTHARD, H. F. & BONHOEFFER, S. 2012. Inferring epidemic contact structure from phylogenetic trees. *PLoS Comput Biol,* 8**,** e1002413.

LEWIS, F., HUGHES, G. J., RAMBAUT, A., POZNIAK, A. & LEIGH BROWN, A. J. 2008. Episodic sexual transmission of HIV revealed by molecular phylodynamics. *PLoS Med,* 5**,** e50.

LI, D., SHANG, Y. J., LIU, Z. X., LIU, X. T. & CAI, X. P. 2007. Molecular relationships between type Asia 1 new strain from China and type O Panasia strains of foot-and-mouth-disease virus. *Virus Genes,* 35**,** 273-9.

LIEBERMAN, E., HAUERT, C. & NOWAK, M. A. 2005. Evolutionary dynamics on graphs. *Nature,* 433**,** 312-6.

LIN, Y. L., JONG, M. H., HUANG, C. C., SHIEH, H. K. & CHANG, P. C. 2010. Genetic and antigenic characterization of foot-and-mouth disease viruses isolated in Taiwan between 1998 and 2009. *Veterinary Microbiology,* 145**,** 34-40.

LIPPOLD, S., MATZKE, N. J., REISSMANN, M. & HOFREITER, M. 2011. Whole mitochondrial genome sequencing of domestic horses reveals incorporation of extensive wild horse diversity during domestication. *BMC Evol Biol,* 11**,** 328.

LLOYD-SMITH, J. O. 2007. Maximum likelihood estimation of the negative binomial dispersion parameter for highly overdispersed data, with applications to infectious diseases. *PLoS One,* 2**,** e180.

LLOYD-SMITH, J. O., SCHREIBER, S. J., KOPP, P. E. & GETZ, W. M. 2005. Superspreading and the effect of individual variation on disease emergence. *Nature,* 438**,** 355-9.

LOGAN, G., FREIMANIS, G. L., KING, D. J., VALDAZO-GONZALEZ, B., BACHANEK-BANKOWSKA, K., SANDERSON, N. D., KNOWLES, N. J., KING, D. P. & COTTAM, E. M. 2014. A universal protocol to generate consensus level genome sequences

for foot-and-mouth disease virus and other positive-sense polyadenylated RNA viruses using the Illumina MiSeq. *BMC Genomics,* 15**,** 828.

LOHR, S. L. 2010. *Sampling: design and analysis,* London, Duxbury Press.

LORENZEN, E. D., NOGUES-BRAVO, D., ORLANDO, L., WEINSTOCK, J., BINLADEN, J., MARSKE, K. A., UGAN, A., BORREGAARD, M. K., GILBERT, M. T., NIELSEN, R., HO, S. Y., GOEBEL, T., GRAF, K. E., BYERS, D., STENDERUP, J. T., RASMUSSEN, M., CAMPOS, P. F., LEONARD, J. A., KOEPFLI, K. P., FROESE, D., ZAZULA, G., STAFFORD, T. W., JR., AARIS-SORENSEN, K., BATRA, P., HAYWOOD, A. M., SINGARAYER, J. S., VALDES, P. J., BOESKOROV, G., BURNS, J. A., DAVYDOV, S. P., HAILE, J., JENKINS, D. L., KOSINTSEV, P., KUZNETSOVA, T., LAI, X., MARTIN, L. D., MCDONALD, H. G., MOL, D., MELDGAARD, M., MUNCH, K., STEPHAN, E., SABLIN, M., SOMMER, R. S., SIPKO, T., SCOTT, E., SUCHARD, M. A., TIKHONOV, A., WILLERSLEV, R., WAYNE, R. K., COOPER, A., HOFREITER, M., SHER, A., SHAPIRO, B., RAHBEK, C. & WILLERSLEV, E. 2011. Species-specific responses of Late Quaternary megafauna to climate and humans. *Nature,* 479**,** 359-64.

LOTH, L., OSMANI, M. G., KALAM, M. A., CHAKRABORTY, R. K., WADSWORTH, J., KNOWLES, N. J., HAMMOND, J. M. & BENIGNO, C. 2011. Molecular characterization of foot-and-mouth disease virus: implications for disease control in Bangladesh. *Transbound Emerg Dis,* 58**,** 240-6.

LUIKART, G., RYMAN, N., TALLMON, D. A., SCHWARTZ, M. K. & ALLENDORF, F. W. 2010. Estimation of census and effective population sizes: the increasing usefulness of DNA-based approaches. *Conserv Genet,* 11**,** 355-73.

MAGIORKINIS, G., SYPSA, V., MAGIORKINIS, E., PARASKEVIS, D., KATSOULIDOU, A., BELSHAW, R., FRASER, C., PYBUS, O. G. & HATZAKIS, A. 2013. Integrating phylodynamics and epidemiology to estimate transmission diversity in viral epidemics. *PLoS Comput Biol,* 9**,** e1002876.

MAHAPATRA, M., YUVARAJ, S., MADHANMOHAN, M., SUBRAMANIAM, S., PATTNAIK, B., PATON, D. J., SRINIVASAN, V. A. & PARIDA, S. 2015. Antigenic and genetic comparison of foot-and-mouth disease virus serotype O Indian vaccine strain, O/IND/R2/75 against currently circulating viruses. *Vaccine,* 33**,** 693-700.

MANSLEY, L. M., DONALDSON, A. I., THRUSFIELD, M. V. & HONHOLD, N. 2011. Destructive tension: mathematics versus experience--the progress and control of the 2001 foot and mouth disease epidemic in Great Britain. *Rev Sci Tech,* 30**,** 483-98.

MANSLEY, L. M., DUNLOP, P. J., WHITESIDE, S. M. & SMITH, R. G. 2003. Early dissemination of foot-and-mouth disease virus through sheep marketing in February 2001. *Vet Rec,* 153**,** 43-50.

MARDONES, F., PEREZ, A., SANCHEZ, J., ALKHAMIS, M. & CARPENTER, T. 2010. Parameterization of the duration of infection stages of serotype O foot-and-mouth disease virus: an analytical review and meta-analysis with application to simulation models. *Vet Res,* 41**,** 45.

MARTINEZ, M. A., DOPAZO, J., HERNANDEZ, J., MATEU, M. G., SOBRINO, F., DOMINGO, E. & KNOWLES, N. J. 1992. Evolution of the capsid protein genes of foot-and-mouth disease virus: antigenic variation without accumulation of amino acid substitutions over six decades. *J Virol,* 66**,** 3557-65.

MASON, P. W., GRUBMAN, M. J. & BAXT, B. 2003. Molecular basis of pathogenesis of FMDV. *Virus Res,* 91**,** 9-32.

MCWILLIAM, H., LI, W., ULUDAG, M., SQUIZZATO, S., PARK, Y. M., BUSO, N., COWLEY, A. P. & LOPEZ, R. 2013. Analysis Tool Web Services from the EMBL-EBI. *Nucleic Acids Res,* 41**,** W597-600.

MININ, V. N., BLOOMQUIST, E. W. & SUCHARD, M. A. 2008. Smooth skyride through a rough skyline: Bayesian coalescent-based inference of population dynamics. *Mol Biol Evol,* 25**,** 1459-71.

MOHAPATRA, J. K., SUBRAMANIAM, S., PANDEY, L. K., PAWAR, S. S., DE, A., DAS, B., SANYAL, A. & PATTNAIK, B. 2011. Phylogenetic structure of serotype A foot-and-mouth disease virus: global diversity and the Indian perspective. *J Gen Virol,* 92**,** 873-9.

MOLLENTZE, N., NEL, L. H., TOWNSEND, S., LE ROUX, K., HAMPSON, K., HAYDON, D. T. & SOUBEYRAND, S. 2014. A Bayesian approach for inferring the dynamics of partially observed endemic infectious diseases from space-time-genetic data. *Proc Biol Sci,* 281**,** 20133251.

MOOERS, A. O. & HEARD, S. B. 1997. Inferring evolutionary process from phylogenetic tree shape. *Q Rev Biol,* 72**,** 31-54.

MORATORIO, G., COSTA-MATTIOLI, M., PIOVANI, R., ROMERO, H., MUSTO, H. & CRISTINA, J. 2007. Bayesian coalescent inference of hepatitis A virus populations: evolutionary rates and patterns. *J Gen Virol,* 88**,** 3039-42.

MORELLI, M. J., THEBAUD, G., CHADŒUF, J., KING, D. P., HAYDON, D. T. & SOUBEYRAND, S. 2012. A bayesian inference framework to reconstruct transmission trees using epidemiological and genetic data. *PLoS Comput Biol,* 8**,** e1002768.

NEE, S., HOLMES, E. C., RAMBAUT, A. & HARVEY, P. H. 1995. Inferring population history from molecular phylogenies. *Philos Trans R Soc Lond B Biol Sci,* 349**,** 25-31.

O'FALLON, B. D. & FEHREN-SCHMITZ, L. 2011. Native Americans experienced a strong population bottleneck coincident with European contact. *Proc Natl Acad Sci U S A,* 108**,** 20444-8.

OIE 2014. Animal Health Data (Handistatus II). World Organisation for Animal Health.

OPGEN-RHEIN, R., FAHRMEIR, L. & STRIMMER, K. 2005. Inference of demographic history from genealogical trees using reversible jump Markov chain Monte Carlo. *BMC Evol Biol,* 5**,** 6.

ORTON, R. J., WRIGHT, C. F., MORELLI, M. J., JULEFF, N., THEBAUD, G., KNOWLES, N. J., VALDAZO-GONZÁLEZ, B., PATON, D. J., KING, D. P. & HAYDON, D. T. 2013. Observing micro-evolutionary processes of viral populations at multiple scales. *Philos Trans R Soc Lond B Biol Sci,* 368**,** 20120203.

PALACIOS, J. A. & MININ, V. N. Integrated nested laplace approximation for bayesian nonparametric phylodynamics. Conference on Uncertainity in Artificial Intelligence, August 15-17 2012 2012 Catalina Island, CA, USA.

PATON, D. J., SUMPTION, K. J. & CHARLESTON, B. 2009. Options for control of foot-and-mouth disease: knowledge, capability and policy. *Philos Trans R Soc Lond B Biol Sci,* 364**,** 2657-67.

PATTNAIK, B., VENKATARAMANAN, R., TOSH, C., SANYAL, A., HEMADRI, D., SAMUEL, A. R., KNOWLES, N. J. & KITCHING, R. P. 1998. Genetic heterogeneity of Indian field isolates of foot-and-mouth disease virus serotype O as revealed by partial sequencing of 1D gene. *Virus Res,* 55**,** 115-27.

PETER, B. M., WEGMANN, D. & EXCOFFIER, L. 2010. Distinguishing between population bottleneck and population subdivision by a Bayesian model choice procedure. *Mol Ecol,* 19**,** 4648-60.

POMEROY, L. W., BJORNSTAD, O. N. & HOLMES, E. C. 2008. The evolutionary and epidemiological dynamics of the paramyxoviridae. *J Mol Evol,* 66**,** 98-106.

POPINGA, A., VAUGHAN, T., STADLER, T. & DRUMMOND, A. J. 2015. Inferring epidemiological dynamics with Bayesian coalescent inference: the merits of deterministic and stochastic models. *Genetics,* 199**,** 595-607.

POSADA, D. & BUCKLEY, T. R. 2004. Model selection and model averaging in phylogenetics: advantages of akaike information criterion and bayesian approaches over likelihood ratio tests. *Syst Biol,* 53**,** 793-808.

PYBUS, O. G., DRUMMOND, A. J., NAKANO, T., ROBERTSON, B. H. & RAMBAUT, A. 2003. The epidemiology and iatrogenic transmission of hepatitis C virus in Egypt: a Bayesian coalescent approach. *Mol Biol Evol,* 20**,** 381-7.

PYBUS, O. G. & RAMBAUT, A. 2009. Evolutionary analysis of the dynamics of viral infectious disease. *Nat Rev Genet,* 10**,** 540-50.

PYBUS, O. G., RAMBAUT, A. & HARVEY, P. H. 2000. An integrated framework for the inference of viral population history from reconstructed genealogies. *Genetics,* 155**,** 1429-37.

PYBUS, O. G., SUCHARD, M. A., LEMEY, P., BERNARDIN, F. J., RAMBAUT, A., CRAWFORD, F. W., GRAY, R. R., ARINAMINPATHY, N., STRAMER, S. L., BUSCH, M. P. & DELWART, E. L. 2012. Unifying the spatial epidemiology and molecular evolution of emerging epidemics. *Proc Natl Acad Sci U S A,* 109**,** 15066-71.

QU, Y., LUO, X., ZHANG, R., SONG, G., ZOU, F. & LEI, F. 2011. Lineage diversification and historical demography of a montane bird Garrulax elliotii--implications for the Pleistocene evolutionary history of the eastern Himalayas. *BMC Evol Biol,* 11**,** 174.

R CORE TEAM 2015. R: A language and environment for statistical computing. *R Foundation For Statistical Computing.* Vienna, Austria.

RAMBAUT, A., PYBUS, O. G., NELSON, M. I., VIBOUD, C., TAUBENBERGER, J. K. & HOLMES, E. C. 2008. The genomic and epidemiological dynamics of human influenza A virus. *Nature,* 453**,** 615-9.

RANDOLPH, T. F., PERRY, B. D., BENIGNO, C. C., SANTOS, I. J., AGBAYANI, A. L., COLEMAN, P., WEBB, R. & GLEESON, L. J. 2002. The economic impact of foot and mouth disease control and eradication in the Philippines. *Rev Sci Tech,* 21**,** 645-61.

RASMUSSEN, D. A., BONI, M. F. & KOELLE, K. 2014a. Reconciling phylodynamics with epidemiology: the case of dengue virus in southern Vietnam. *Mol Biol Evol,* 31**,** 258-71.

RASMUSSEN, D. A., RATMANN, O. & KOELLE, K. 2011. Inference for nonlinear epidemiological models using genealogies and time series. *PLoS Comput Biol,* 7**,** e1002136.

RASMUSSEN, D. A., VOLZ, E. M. & KOELLE, K. 2014b. Phylodynamic inference for structured epidemiological models. *PLoS Comput Biol,* 10**,** e1003570.

RIOS INSUA, D., RUGGERI, F. & WIPER, M. P. 2012. Discrete Time Markov Chains and Extensions. *Bayesian Analysis of Stochastic Process Models.* John Wiley & Sons, Ltd.

RODRIGO, A. G. & FELSENSTEIN, J. 1999. Coalescent approach to HIV population genetics. *In:* CRANDALL, K. A. (ed.) *Molecular evolution of HIV.* Baltimore: Johns Hopkins University Press.

ROEDER, P. L. & KNOWLES, N. J. Foot-and-mouth disease virus type C situation: the first target for eradication? Open Session of the European Commission for the Control of Foot-and-Mouth Disease Standing Technical Committee, 14-17 October 2008 Erice, Italy.

ROSENBERG, N. A. & NORDBORG, M. 2002. Genealogical trees, coalescent theory and the analysis of genetic polymorphisms. *Nat Rev Genet,* 3**,** 380-90.

RUE, H., MARTINO, S. & CHOPIN, N. 2009. Approximate Bayesian inference for latent Gaussian models by using integrated nested Laplace approximations. *J Roy Stat Soc Ser B (Stat Method),* 71**,** 319-92.

RWEYEMAMU, M., ROEDER, P., MACKAY, D., SUMPTION, K., BROWNLIE, J., LEFORBAN, Y., VALARCHER, J. F., KNOWLES, N. J. & SARAIVA, V. 2008. Epidemiological patterns of foot-and-mouth disease worldwide. *Transbound Emerg Dis,* 55**,** 57-72.

SAMUEL, A. R. & KNOWLES, N. J. 2001. Foot-and-mouth disease type O viruses exhibit genetically and geographically distinct evolutionary lineages (topotypes). *J Gen Virol,* 82**,** 609-21.

SAMUEL, A. R., KNOWLES, N. J., KITCHING, R. P. & HAFEZ, S. M. 1997. Molecular analysis of foot-and-mouth disease type O viruses isolated in Saudi Arabia between 1983 and 1995. *Epidemiol Infect,* 119**,** 381-9.

SANGULA, A. K., BELSHAM, G. J., MUWANIKA, V. B., HELLER, R., BALINDA, S. N., MASEMBE, C. & SIEGISMUND, H. R. 2010. Evolutionary analysis of foot-and-mouth disease virus serotype SAT 1 isolates from east Africa suggests two independent introductions from southern Africa. *BMC Evol Biol,* 10**,** 371.

SANJUAN, R. 2012. From molecular genetics to phylodynamics: evolutionary relevance of mutation rates across viruses. *PLoS Pathog,* 8**,** e1002685.

SIEBENGA, J. J., LEMEY, P., KOSAKOVSKY POND, S. L., RAMBAUT, A., VENNEMA, H. & KOOPMANS, M. 2010. Phylodynamic reconstruction reveals norovirus GII.4 epidemic expansions and their molecular determinants. *PLoS Pathog,* 6**,** e1000884.

SIEVERS, F., WILM, A., DINEEN, D., GIBSON, T. J., KARPLUS, K., LI, W., LOPEZ, R., MCWILLIAM, H., REMMERT, M., SODING, J., THOMPSON, J. D. & HIGGINS, D. G. 2011. Fast, scalable generation of high-quality protein multiple sequence alignments using Clustal Omega. *Mol Syst Biol,* 7**,** 539.

SINNOTT, R. W. 1984. Virtues of the Haversine. *Sky and Telescope,* 68**,** 159-59.

SJODIN, P., KAJ, I., KRONE, S., LASCOUX, M. & NORDBORG, M. 2005. On the meaning and existence of an effective population size. *Genetics,* 169**,** 1061-70.

SLATKIN, M. & HUDSON, R. R. 1991. Pairwise comparisons of mitochondrial DNA sequences in stable and exponentially growing populations. *Genetics,* 129**,** 555-62.

SOUBEYRAND, S. 2014. Construction of semi-Markov genetic-space-time SEIR models and inference *HAL,* 01090675.

SPADA, E., SAGLIOCCA, L., SOURDIS, J., GARBUGLIA, A. R., POGGI, V., DE FUSCO, C. & MELE, A. 2004. Use of the minimum spanning tree model for molecular epidemiological investigation of a nosocomial outbreak of hepatitis C virus infection. *J Clin Microbiol,* 42**,** 4230-6.

ST ONGE, K. R., PALME, A. E., WRIGHT, S. I. & LASCOUX, M. 2012. Impact of sampling schemes on demographic inference: an empirical study in two species with different mating systems and demographic histories. *G3 (Bethesda),* 2**,** 803-14.

STACK, J. C., WELCH, J. D., FERRARI, M. J., SHAPIRO, B. U. & GRENFELL, B. T. 2010. Protocols for sampling viral sequences to study epidemic dynamics. *J R Soc Interface,* 7**,** 1119-27.

STADLER, T. 2009. On incomplete sampling under birth-death models and connections to the sampling-based coalescent. *J Theor Biol,* 261**,** 58-66.

STADLER, T. 2010. Sampling-through-time in birth-death trees. *J Theor Biol,* 267**,** 396-404.

STADLER, T. & BONHOEFFER, S. 2013. Uncovering epidemiological dynamics in heterogeneous host populations using phylogenetic methods. *Philos Trans R Soc Lond B Biol Sci,* 368**,** 20120198.

STADLER, T., HAUBOLD, B., MERINO, C., STEPHAN, W. & PFAFFELHUBER, P. 2009. The impact of sampling schemes on the site frequency spectrum in nonequilibrium subdivided populations. *Genetics,* 182**,** 205-16.

STADLER, T., KOUYOS, R., VON WYL, V., YERLY, S., BONI, J., BURGISSER, P., KLIMKAIT, T., JOOS, B., RIEDER, P., XIE, D., GUNTHARD, H. F., DRUMMOND, A. J. & BONHOEFFER, S. 2012. Estimating the basic reproductive number from viral sequence data. *Mol Biol Evol,* 29**,** 347-57.

STADLER, T., KUHNERT, D., BONHOEFFER, S. & DRUMMOND, A. J. 2013. Birth-death skyline plot reveals temporal changes of epidemic spread in HIV and hepatitis C virus (HCV). *Proc Natl Acad Sci U S A,* 110**,** 228-33.

STADLER, T., KUHNERT, D., RASMUSSEN, D. A. & DU PLESSIS, L. 2014. Insights into the early epidemic spread of ebola in sierra leone provided by viral sequence data. *PLoS Curr,* 6.

STADLER, T., VAUGHAN, T. G., GAVRYUSHKIN, A., GUINDON, S., KUHNERT, D., LEVENTHAL, G. E. & DRUMMOND, A. J. 2015. How well can the exponential-growth coalescent approximate constant-rate birth-death population dynamics? *Philos Trans R Soc Lond B Biol Sci,* 282**,** 20150420.

STEINER, U. K., TULJAPURKAR, S. & COULSON, T. 2014. Generation time, net reproductive rate, and growth in stage-age-structured populations. *Am Nat,* 183**,** 771-83.

STREICKER, D. G., ALTIZER, S. M., VELASCO-VILLA, A. & RUPPRECHT, C. E. 2012. Variable evolutionary routes to host establishment across repeated rabies virus host shifts among bats. *Proceedings of the National Academy of Sciences of the United States of America,* 109**,** 19715-19720.

STRIMMER, K. & PYBUS, O. G. 2001. Exploring the demographic history of DNA sequences using the generalized skyline plot. *Mol Biol Evol,* 18**,** 2298-305.

SUMPTION, K., DOMENECH, J. & FERRARI, G. 2012. Progressive control of FMD on a global scale. *Vet Rec,* 170**,** 637-9.

SVENSSON, A. 2007. A note on generation times in epidemic models. *Math Biosci,* 208**,** 300-11.

TAMURA, K. & NEI, M. 1993. Estimation of the number of nucleotide substitutions in the control region of mitochondrial DNA in humans and chimpanzees. *Mol Biol Evol,* 10**,** 512-26.

TAMURA, K., STECHER, G., PETERSON, D., FILIPSKI, A. & KUMAR, S. 2013. MEGA6: Molecular Evolutionary Genetics Analysis version 6.0. *Mol Biol Evol,* 30**,** 2725-9.

TAVARE, S., BALDING, D. J., GRIFFITHS, R. C. & DONNELLY, P. 1997. Inferring coalescence times from DNA sequence data. *Genetics,* 145**,** 505-18.

TAYLOR, N. M. 2012. *RE: Foot-and-mouth disease UK 2001 outbreak database.* Type to DI NARDO, A.

TEMPLETON, A. R., CRANDALL, K. A. & SING, C. F. 1992. A cladistic analysis of phenotypic associations with haplotypes inferred from restriction endonuclease mapping and DNA sequence data. III. Cladogram estimation. *Genetics,* 132**,** 619-33.

TILLE, Y. 2006. *Sampling algorithms,* New York, Springer.

TOSH, C., HEMADRI, D. & SANYAL, A. 2002. Evidence of recombination in the capsid-coding region of type A foot-and-mouth disease virus. *J Gen Virol,* 83**,** 2455-60.

TRUSCOTT, J., GARSKE, T., CHIS-STER, I., GUITIAN, J., PFEIFFER, D., SNOW, L., WILESMITH, J., FERGUSON, N. M. & GHANI, A. C. 2007. Control of a highly pathogenic H5N1 avian influenza outbreak in the GB poultry flock. *Philos Trans R Soc Lond B Biol Sci,* 274**,** 2287-95.

TSAI, C. P., PAN, C. H., LIU, M. Y., LIN, Y. L., CHEN, C. M., HUANG, T. S., CHENG, I. C., JONG, M. H. & YANG, P. C. 2000. Molecular epidemiological studies on foot-and-mouth disease type O Taiwan viruses from the 1997 epidemic. *Vet Microbiol,* 74**,** 207-16.

TULLY, D. C. & FARES, M. A. 2008. The tale of a modern animal plague: tracing the evolutionary history and determining the time-scale for foot and mouth disease virus. *Virology,* 382**,** 250-6.

UPADHYAYA, S., AYELET, G., PAUL, G., KING, D. P., PATON, D. J. & MAHAPATRA, M. 2014. Genetic basis of antigenic variation in foot-and-mouth disease serotype A viruses from the Middle East. *Vaccine,* 32**,** 631-8.

VALARCHER, J. F., KNOWLES, N. J., ZAKHAROV, V., SCHERBAKOV, A., ZHANG, Z., SHANG, Y. J., LIU, Z. X., LIU, X. T., SANYAL, A., HEMADRI, D., TOSH, C., RASOOL, T. J., PATTNAIK, B., SCHUMANN, K. R., BECKHAM, T. R., LINCHONGSUBONGKOCH, W., FERRIS, N. P., ROEDER, P. L. & PATON, D. J. 2009. Multiple origins of foot-

and-mouth disease virus serotype Asia 1 outbreaks, 2003-2007. *Emerg Infect Dis,* 15**,** 1046-51.

VALDAZO-GONZÁLEZ, B., KIM, J. T., SOUBEYRAND, S., WADSWORTH, J., KNOWLES, N. J., HAYDON, D. T. & KING, D. P. 2015. The impact of within-herd genetic variation upon inferred transmission trees for foot-and-mouth disease virus. *Infect Genet Evol,* 32**,** 440-8.

VALDAZO-GONZÁLEZ, B., KNOWLES, N. J., HAMMOND, J. & KING, D. P. 2012a. Genome Sequences of SAT 2 Foot-and-Mouth Disease Viruses from Egypt and Palestinian Autonomous Territories (Gaza Strip). *J Virol,* 86**,** 8901-2.

VALDAZO-GONZÁLEZ, B., KNOWLES, N. J., WADSWORTH, J., KING, D. P., HAMMOND, J. M., OZYORUK, F., FIRAT-SARAC, M., PARLAK, U., POLYHRONOVA, L. & GEORGIEV, G. K. 2011. Foot-and-mouth disease in Bulgaria. *Vet Rec,* 168**,** 247.

VALDAZO-GONZÁLEZ, B., POLIHRONOVA, L., ALEXANDROV, T., NORMANN, P., KNOWLES, N. J., HAMMOND, J. M., GEORGIEV, G. K., OZYORUK, F., SUMPTION, K. J., BELSHAM, G. J. & KING, D. P. 2012b. Reconstruction of the transmission history of RNA virus outbreaks using full genome sequences: foot-and-mouth disease virus in Bulgaria in 2011. *PLoS One,* 7**,** e49650.

VALDAZO-GONZÁLEZ, B., TIMINA, A., SCHERBAKOV, A., ABDUL-HAMID, N. F., KNOWLES, N. J. & KING, D. P. 2013. Multiple introductions of serotype O foot-and-mouth disease viruses into East Asia in 2010-2011. *Vet Res,* 44**,** 76.

VAN BALLEGOOIJEN, W. M., VAN HOUDT, R., BRUISTEN, S. M., BOOT, H. J., COUTINHO, R. A. & WALLINGA, J. 2009. Molecular sequence data of hepatitis B virus and genetic diversity after vaccination. *Am J Epidemiol,* 170**,** 1455-63.

VAUGHAN, T. G., KÜNERTH, D., POPINGA, A., WELCH, D. & DRUMMOND A. J. 2014. Efficient Bayesian inference under the structured coalescent. *Bioinformatics*, 30, 2272-9.

VIJAYKRISHNA, D., BAHL, J., RILEY, S., DUAN, L., ZHANG, J. X., CHEN, H., PEIRIS, J. S., SMITH, G. J. & GUAN, Y. 2008. Evolutionary dynamics and emergence of panzootic H5N1 influenza viruses. *PLoS Pathog,* 4**,** e1000161.

VOLZ, E. & POND, S. 2014. Phylodynamic analysis of ebola virus in the 2014 sierra leone epidemic. *PLoS Curr,* 6.

VOLZ, E. M. 2012. Complex population dynamics and the coalescent under neutrality. *Genetics,* 190**,** 187-201.

VOLZ, E. M. & FROST, S. D. W. 2014. Sampling through time and phylodynamic inference with coalescent and birth-death models. *ArXiv e-prints,* 1408.6694.

VOLZ, E. M., KOSAKOVSKY POND, S. L., WARD, M. J., LEIGH BROWN, A. J. & FROST, S. D. 2009. Phylodynamics of infectious disease epidemics. *Genetics,* 183**,** 1421-30.

VRANCKEN, B., RAMBAUT, A., SUCHARD, M. A., DRUMMOND, A., BAELE, G., DERDELINCKX, I., VAN WIJNGAERDEN, E., VANDAMME, A. M., VAN LAETHEM, K. & LEMEY, P. 2014. The genealogical population dynamics of HIV-1 in a large transmission chain: bridging within and among host evolutionary rates. *PLoS Comput Biol,* 10**,** e1003505.

WANG, J. 2005. Estimation of effective population sizes from data on genetic markers. *Philos Trans R Soc Lond B Biol Sci,* 360**,** 1395-409.

WELCH, D., BANSAL, S. & HUNTER, D. R. 2011. Statistical inference to advance network models in epidemiology. *Epidemics,* 3**,** 38-45.

WHITE, P. J., WARD, H. & GARNETT, G. P. 2006. Is HIV out of control in the UK? An example of analysing patterns of HIV spreading using incidence-to-prevalence ratios. *AIDS,* 20**,** 1898-901.

WICKHAM, H. 2009. *Ggplot2: elegant graphics for data analysis,* New York, Springer.

WILSON, I. J. & BALDING, D. J. 1998. Genealogical inference from microsatellite data. *Genetics,* 150**,** 499-510.

WRIGHT, C. F., KNOWLES, N. J., DI NARDO, A., PATON, D. J., HAYDON, D. T. & KING, D. P. 2013. Reconstructing the origin and transmission dynamics of the 1967-68 foot-and-mouth disease epidemic in the United Kingdom. *Infect Genet Evol,* 20**,** 230-8.

WRIGHT, C. F., MORELLI, M. J., THEBAUD, G., KNOWLES, N. J., HERZYK, P., PATON, D. J., HAYDON, D. T. & KING, D. P. 2011. Beyond the consensus: dissecting within-host viral population diversity of foot-and-mouth disease virus by using next-generation genome sequencing. *J Virol,* 85**,** 2266-75.

WRIGHT, S. 1931. Evolution in Mendelian Populations. *Genetics,* 16**,** 97-159.

WRIGHT, S. 1938. Size of a population and breeding structure in relation to evolution. *Science,* 87**,** 430-431.

WU, Z. Y., HE, C. Q., LIU, Y. Y., FENG, Q., TENG, J. L. & CHEN, J. G. 2009. A study of homologous recombination in foot-and-mouth disease virus in china. *Progr Biochem Biophys,* 36**,** 689-95.

YANG, P. C., CHU, R. M., CHUNG, W. B. & SUNG, H. T. 1999. Epidemiological characteristics and financial costs of the 1997 foot-and-mouth disease epidemic in Taiwan. *Vet Rec,* 145**,** 731-4.

YOON, S. H., LEE, K. N., PARK, J. H. & KIM, H. 2011a. Molecular epidemiology of foot-and-mouth disease virus serotypes A and O with emphasis on Korean isolates: temporal and spatial dynamics. *Arch Virol,* 156**,** 817-26.

YOON, S. H., PARK, W., KING, D. P. & KIM, H. 2011b. Phylogenomics and molecular evolution of foot-and-mouth disease virus. *Mol Cells,* 31**,** 413-21.

YPMA, R. J., BATAILLE, A. M., STEGEMAN, A., KOCH, G., WALLINGA, J. & VAN BALLEGOOIJEN, W. M. 2012. Unravelling transmission trees of infectious diseases by combining genetic and epidemiological data. *Philos Trans R Soc Lond B Biol Sci,* 279**,** 444-50.

YPMA, R. J., VAN BALLEGOOIJEN, W. M. & WALLINGA, J. 2013. Relating phylogenetic trees to transmission trees of infectious disease outbreaks. *Genetics,* 195**,** 1055-62.

ZEHENDER, G., BERNINI, F., DELOGU, M., CUSI, M. G., REZZA, G., GALLI, M. & CICCOZZI, M. 2009. Bayesian skyline plot inference of the Toscana virus epidemic: a decline in the effective number of infections over the last 30 years. *Infect Genet Evol,* 9**,** 562-6.

ZHANG, Q., LIU, X., FANG, Y., PAN, L., LV, J., ZHANG, Z., ZHOU, P., DING, Y., CHEN, H., SHAO, J., ZHAO, F., LIN, T., CHANG, H., ZHANG, J., WANG, Y. & ZHANG, Y. 2015. Evolutionary analysis of structural protein gene VP1 of foot-and-mouth disease virus serotype Asia 1. *The Scientific World Journal,* 2015**,** 734253.